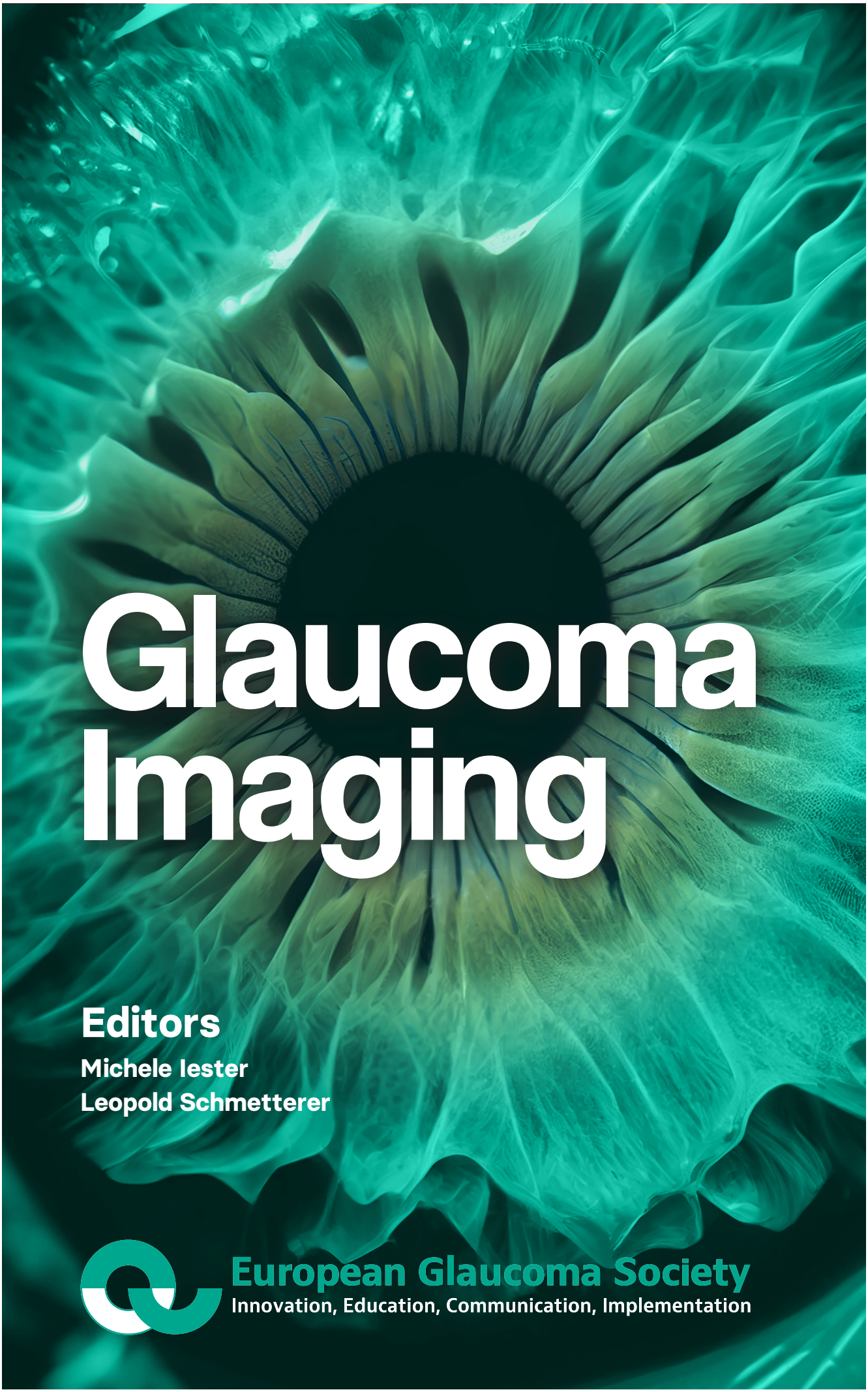
Glaucoma Imaging
Editors
Michele Iester
Leopold Schmetterer
European Glaucoma Society
Innovation, Education, Communication, Implementation

Glaucoma Imaging

Editors

Michele Iester
Leopold Schmetterer

European Glaucoma Society

Foreword

Fotis Topouzis
President, European Glaucoma Society (EGS)

The vision of the EGS is to promote the best possible well-being for Individuals with glaucoma and the minimal glaucoma induced visual disability within an affordable healthcare system.

The mission of the EGS Education Theme and related activities is to promote evidence-based practice and life-long learning through systematic, comprehensive and often renewed training.

The 3rd edition of Glaucoma Imaging Book (2024) is an important addition to the EGS training materials to complement the EGS Guidelines currently in their 5th Edition (2020). In EGS Guidelines evaluation of imaging and its role in Glaucoma management is included. However, besides Guidelines the EGS leadership considers that a book focusing on Glaucoma Imaging would provide with valuable in-depth knowledge and comprehensive assessment of the pivotal role of Imaging in Glaucoma management. The effort and high quality work put in place by experts in the field to create the 3rd edition of Glaucoma Imaging book has been considerable and the EGS leadership would like to thank the Editors and all contributors.

An accurate glaucoma diagnosis, including the identification (and quantification) of progression, is required to build a solid basis for cost effective care. The updated EGS Glaucoma Imaging book gives concise information and up-dates for the practical use of the imaging devices in everyday clinical work and also looks to the future technological developments. Integration of Imaging is an established mainstay of clinical practice while there are great expectations towards upcoming developments in Artificial Intelligence field providing further support to the use of Imaging towards better screening, diagnosis and individualized management.

Overall, acknowledging the current advantages and limitations of the imaging devices make this a must-read book for every clinician.

ISBN: 979-12-80718-23-5

Platform Network Srl
24/6 piazzetta di Brera
20121 Milano
17/7 via Pietro Paleocapa
17100 Savona

Printed in May 2024

Preface

Michele Iester and Leopold Schmetterer

As a leading cause of irreversible blindness worldwide, early detection and monitoring of glaucoma are paramount for effective management and preservation of vision. Ocular imaging is an invaluable tool in glaucoma management, providing a non-invasive and quantitative means to assess the structural changes associated with the disease.

In recent years, technological advancements in ocular imaging have revolutionized the understanding and management of glaucoma. From traditional techniques like fundus photography and optic nerve head examination to more sophisticated modalities such as optical coherence tomography (OCT) and OCT angiography, ocular imaging offers clinicians a comprehensive evaluation of the optic nerve head, retinal nerve fiber layer, and macular region. These imaging modalities provide high-resolution, cross-sectional images of ocular tissues, enabling precise assessment of structural abnormalities, progression monitoring, and guiding therapeutic interventions.

Furthermore, the integration of artificial intelligence and machine learning algorithms with ocular imaging has unlocked new frontiers in glaucoma diagnosis and management. These computational approaches facilitate the automated analysis of vast imaging datasets, aiding in the early detection of subtle structural changes indicative of glaucomatous damage. Additionally, they enable the development of predictive models for disease progression, personalized risk stratification, and optimization of treatment strategies tailored to individual patients.

Despite these advancements, challenges persist in the realm of ocular imaging in glaucoma. Standardization of imaging protocols, interpretation of complex datasets, and integration of multimodal imaging findings remain areas of ongoing research and clinical refinement. Moreover, accessibility to advanced imaging technologies and cost-effectiveness in resource-limited settings pose significant hurdles to widespread implementation.

In this introduction to ocular imaging in glaucoma, we delve into the principles, applications, and emerging trends shaping the field. Through a comprehensive exploration of various imaging modalities, computational techniques, and clinical implications, we aim to elucidate the pivotal role of ocular imaging in the early diagnosis, precise monitoring, and personalized management of glaucoma. By harnessing the power of ocular imaging, it is the ultimate goal of preserving vision and enhancing the quality of life for individuals affected by this sight-threatening disease.

Acknowledgements

Michele Iester and Leopold Schmetterer

This book would not have been made possible without the contribution and dedication of the authors listed below.

Luca Agnifili
Alfonso Anton
João Barbosa-Breda
Paola Cassottana
Balwantray C Chauhan
Alina Popa Cherecheanu
Jacqueline Chua
David P Crabb
José Ignacio Fernández-Vigo
Antonio Ferreras
Michele Figus
Panayiota Founti
Julián García-Feijóo
Sara Giammaria
Noemí Güemes-Villahoz
Ruben Hemelings
Michele Iester
Munirah Ismail
Andreas Katsanos
Maroun Khreish
Cristina Maltese
Christian Y Mardin
Leonardo Mastropasqua
Manuele Michelessi
Giovanni Montesano
Dhakshi Muhundhakumar
Francesco Oddone
Marta Pazos
Natalia Porporato
Chiara Posarelli
Leopold Schmetterer
Joel S Schuman
Ingeborg Stalmans
Jorge Vila-Arteaga
Ananth Viswanathan
Gadi Wollstein

Scientific committee
Michele Iester
Manuele Michelessi
Francesco Oddone
Marta Pazos
Leopold Schmetterer

History of imaging in glaucoma

Leopold Schmetterer

The history of ocular imaging is a fascinating journey through technological advancements and medical discoveries that have revolutionized our understanding and management of eye diseases. From rudimentary observational techniques to sophisticated imaging modalities, each milestone has contributed to improved diagnosis, treatment, and monitoring of ocular conditions.

The earliest recorded attempts at ocular imaging date back to ancient civilizations. Egyptian papyri and Mesopotamian clay tablets contain descriptions of eye diseases and their treatments. Greek and Roman physicians such as Hippocrates and Galen made significant contributions to ophthalmology through observations and rudimentary sketches of the eye.

During the Renaissance period, artists and scientists began to depict the human anatomy with greater accuracy. Leonardo da Vinci's anatomical drawings, including detailed renderings of the eye, provided invaluable insights into ocular structure and function.

The invention of the ophthalmoscope in the 19th century marked a milestone in ocular imaging. German physician Hermann von Helmholtz developed the first direct ophthalmoscope in 1851, allowing for the visualization of the eye's interior structures, such as the retina and optic nerve head. This revolutionary device transformed the practice of ophthalmology and enabled the diagnosis of various retinal diseases.

The advent of photography in the late 19th century facilitated the documentation and sharing of ocular findings. Fundus cameras, equipped with specialized lenses and film, were developed to capture high-quality images of the retina. These images became essential for diagnosing and monitoring conditions such as diabetic retinopathy, age-related macular degeneration, and glaucoma.

Fluorescein angiography emerged as a powerful tool for evaluating retinal blood flow and vascular abnormalities. By injecting fluorescein dye intravenously and capturing sequential images of its passage through the retinal vasculature, one could diagnose conditions such as retinal vascular occlusions, diabetic macular edema, and choroidal neovascularization.

Ultrasound imaging, initially developed for non-ocular applications, was later adapted for ophthalmic use. A-scan and B-scan ultrasound allowed for the visualization of intraocular structures, particularly in cases where optical media were opaque, such as cataracts or vitreous hemorrhage.

This modality proved invaluable for diagnosing retinal detachment, intraocular tumors, and ocular trauma.

The introduction of optical coherence tomography (OCT) revolutionized ocular imaging in the late 20th century. OCT employs low-coherence interferometry to generate high-resolution, cross-sectional images of the retina, optic nerve head, and anterior segment. This non-invasive imaging modality quickly became indispensable for diagnosing and managing retinal diseases, glaucoma, and corneal pathologies.

In recent years, retinal imaging technologies have continued to evolve, with innovations such as spectral-domain OCT (SD-OCT), swept-source OCT (SS-OCT), and adaptive optics imaging. These modalities offer enhanced resolution, depth penetration, and visualization of cellular structures, paving the way for early detection and monitoring of subtle retinal changes in diseases like macular degeneration and inherited retinal dystrophies.

Anterior segment imaging has also seen significant advancements, with techniques such as specular microscopy, confocal microscopy, and anterior segment OCT (AS-OCT) providing detailed visualization of corneal morphology, endothelial cells, and angle structures. These modalities play a crucial role in diagnosing and managing corneal diseases, glaucoma, and anterior segment anomalies.

The future of ocular imaging holds promise for further innovation and integration of artificial intelligence (AI) and machine learning algorithms. AI-driven image analysis tools have the potential to improve diagnostic accuracy, streamline workflow, and facilitate personalized treatment strategies in ophthalmology.

In conclusion, the history of ocular imaging is a testament to human ingenuity and scientific progress. From ancient observations to cutting-edge technologies, each milestone has expanded our understanding of ocular anatomy and pathology, ultimately improving patient care and outcomes in ophthalmology. As technology continues to advance, the future of ocular imaging holds boundless possibilities for further innovation and discovery.

Contents

Part I

Chapter 1

Principles of OCT imaging and existing platforms

Maroun Khreish
Joel S Schuman
Gadi Wollstein

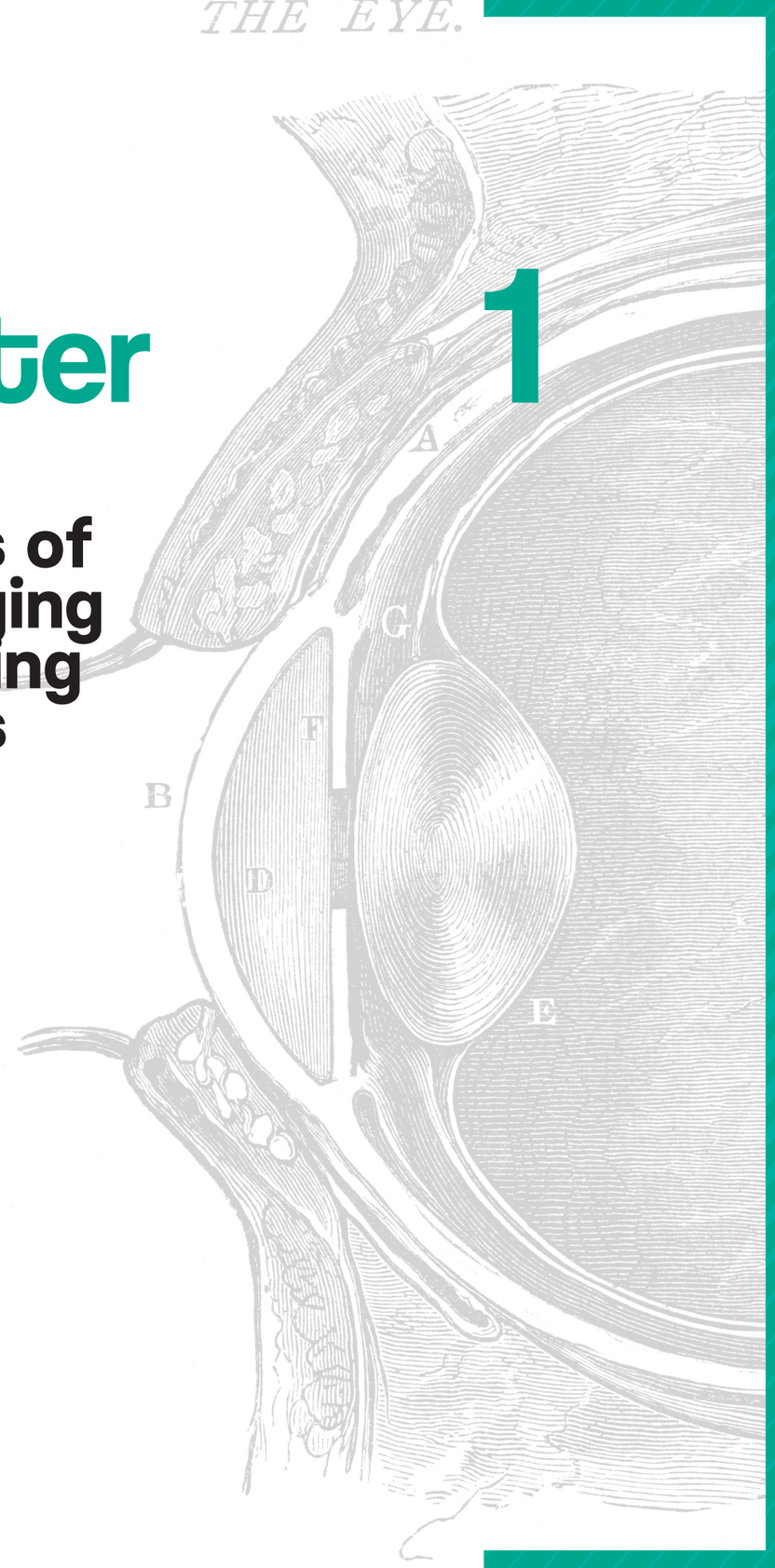

Principles of OCT imaging and existing platforms

Maroun Khreish,[1] Joel S Schuman,[2-5] Gadi Wollstein[2,3]

[1]Department of Ophthalmology, NYU School of Medicine, New York, NY
[2]Wills Eye Hospital, Philadelphia, PA
[3]Vickie and Jack Farber Vision Research Center, Philadelphia, PA
[4]School of Biomedical Engineering, Science and Health Studies, Drexel University, Philadelphia, PA
[5]Sidney Kimmel Medical College, Thomas Jefferson University, Philadelphia, PA

Optical coherence tomography (OCT) is a non-invasive and non-contact technique for cross-sectional tissue imaging. OCT was introduced in 1991,[1] and has evolved through multiple iterations, from time-domain OCT, to spectral-domain OCT, to swept-source OCT, all of which improved the resolution and speed of scans. New advancements in the technology, such as OCT-angiography, visible-light OCT, and adaptive optics, have further enhanced the use of OCT in glaucoma management.

The working principle of OCT is based on low coherence interferometry. Low coherence light is projected toward a beam splitter and divided into two paths: one toward the eye and the other toward a reference mirror. The back reflected light from both paths reach a spectrometer or photodetector (depending on the OCT iteration) to create axial (A-) scan profile representing the depth of the tissue.[2] A sequence of A-scans in the transverse plane produces a B-scan (2-dimensional image).[3]

OCT technology has evolved over the years with meaningful improvements in the outcome information (Table 1). Below we summarize the main features of several iterations of the technology.

Time-domain OCT (TD-OCT) was the first generation of OCT that became available in the 1990s. TD-OCT light source emits near-infra red (center wavelength around 850 nm) light and a reference arm which includes an oscillating mirror. Light reflected from both arms is detected and the signal from the eye is matched with corresponding signal from the reference arm.

Table 1

Evolution and specifications of OCTs used in glaucoma evaluation

OCT Technology	Year introduced	Axial resolution in tissue (µm)	Lateral resolution in tissue (µm)	Maximum scanning rates (A-scans per second)
TD-OCT	1991	10-15	20	400
SD-OCT	2001	5-8	20	100,000
SS-OCT	2012	8-9	20	200,000
OCT-A	2015	5	20	200,000

OCT=Optical coherence tomography; TD-OCT=Time domain OCT; SD-OCT=Spectral domain OCT; SS-OCT=Swept source OCT; OCT-A=OCT angiography.

Maroun Khreish, Joel S Schuman, Gadi Wollstein

By recording the location of the mirror that generated the specific signal the depth of the tissue is determined. TD-OCT, produces cross-sectional images with a scanning speed of 400 A-scans per second, with an axial resolution of 8 to 10 µm and a transverse resolution of approximately 20 µm.[3] The scanning speed of this iteration was limited by the oscillation of the mirror which was overcome in subsequent iterations allowing faster scanning speed. A circle with a 3.4 mm diameter centered on the optic nerve head became the standard sampling location from this version onward allowing quantification of all retinal ganglion cell axons as they transit from the retina toward the optic nerve. An automated software delineates the margins of the retinal nerve fiber layer (RNFL) to quantify the thickness of the ganglion cell axons. Global and sectoral circumpapillary RNFL thickness has been shown to enable detection and monitoring of glaucoma progression with high accuracy.[4]

Spectral-domain OCT (SD-OCT) was the next iteration of the OCT technology. This iteration included a stationary mirror in the reference arm and a spectrometer (Fig. 1). A Fourier transformation is used to match the signals from the eye and the reference arm to determine the depth of the structures. SD-OCT is using a near infrared light source, offers higher scanning speed (up to 100,000 A-scans per second) and improved axial resolution (5-6 µm) compared to TD-OCT while maintaining similar transverse resolution (20 µm). The faster scanning speed enables new scanning patterns such as raster scans with a dense sequence of B-scans, to allow thorough sampling of regions of interest, such as the optic nerve head and the surrounding peripapillary region. Some devices have incorporated eye motion tracking system to reduce motion artifacts. Another approach was to determine the angle between the optic nerve head and the fovea to correct torsional movement and improve reliability of sectoral measurement. Taken together along with the improved resolution, this iteration has been shown to provide highly reliable RNFL thickness measurements for improved disease detection and monitoring and became a corner stone in clinical glaucoma evaluation.[4,5]

Figure 1
Schematic diagram of Spectral Domain OCT system. Light is projected from a low coherence source to a beam splitter which projects the light to the eye and static reference mirror. Light returning from both arms is detected by the spectrometer and the similar signal is matched for resolving the location of each point.

Figure 1

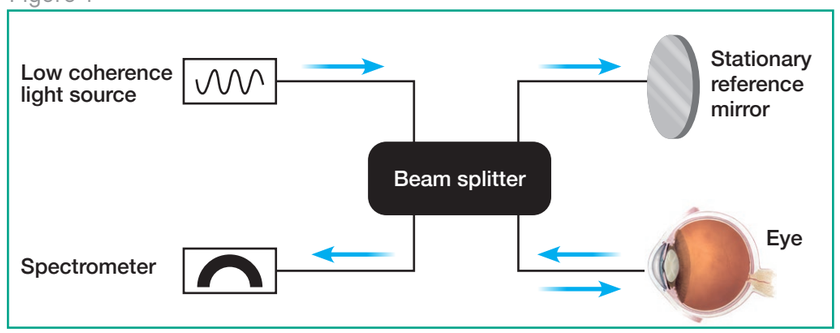

Swept-source OCT (SS-OCT), is based on a fast-sweeping pattern through bandwidth of the light source. A photodetector is used to capture the interference pattern, and by Fourier transformation, matched with the signal from the eye and the reference arm. Because each signal pattern originating from the reference arm is associated with a known wavelength there is no need for the use of a spectrometer, as it is done with SD-OCT, and thus enabling faster scanning speed up to 2,000,000 A-scans per second. The axial resolution of this iteration is 7-8 µm with lateral resolution of 20 µm. The center wavelength of the light source of SS-OCT devices is at 1,050 nm allowing greater axial depth imaging and better visualization of deeper ophthalmologic structures like the choroid and lamina cribrosa (LC). Also, the signal to noise and resolution drop-off are less depth-dependent with SS-OCT, and scan quality is improved.[6] Some of these devices also offer eye motion tracking system and correction for the optic nerve to fovea angle. The main scanning patterns used by the machine include line, circular and raster scans that were described above (Fig. 2). An important advantage of the raster scan its capability to generate a 3-dimensional cube of data that allows post-hoc analysis. The spoke scan pattern consists of a series of B-scans at regular angular intervals taken at radial orientation. This pattern provides dense sampling at and near the crossing point of the radial scans but further away from that point, the large gap between the radial lines is filled with interpolations.[7]

OCT Angiography (OCT-A) is an OCT version which provides mapping of the vascular network of the eye without the need of dye. The underlying principle of this system is to highlight locations with moving signal, such as those originating from blood flow, and to suppress all stationary signals. There are two main methods used for generating OCT-A: 1. split-spectrum amplitude-decorrelation angiography (SSADA) and 2. Optical micro angiography complex (OMAG).[8] OCT-A provides depth resolved detailed mapping of blood vessels network. However, an important limitation is that

Figure 2
OCT common scanning patterns: (a) Circular (b) Raster and (c) Radial scanning protocols.

Figure 2

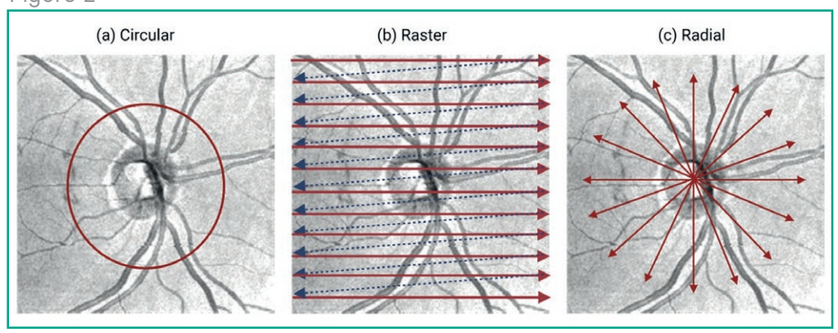

blood leaks cannot be detected with OCT-A because the blood in these locations is stationary. Furthermore, the system cannot determine changes in the blood flow as long as there is an active flow inside a vessel, which is within the system's detection range, it will be highlighted. The system capability to automatically quantify blood vessel density is important for disease detection because a reduction in density, particularly in the inner plexus, has been shown to be associated with glaucomatous damage.[9]

When evaluating OCT results, it is important to also examine image quality. All devices provide a scan quality indicator that primarily reflect the signal level. However, artifacts that could compromise the reliability and the outcome of the automated analysis are not included in the image quality indictor. These artifacts include situations such as motion artifacts, blinks or shadowing from floaters. Examining the enface OCT image is often sufficient to identify those artifacts. The effect of some of these artifacts can be reduced by using the eye tracking feature when available in newer OCT versions.[10]

Glaucoma is typically a slowly progressing disease, making it difficult to monitor by clinical evaluation alone. The incorporation of OCT into routine clinical care has transformed this capability due to its micron scale resolution and high test-to-test reproducibility.[11] This allows detection of a small changes with high reliability that could be used to subsequently adjust the treatment plan. A number of advanced OCT technologies are currently being developed. Among the various iterations we will briefly introduce some of the devices which are currently at the most advanced stage of development including Visible-Light OCT (Vis-OCT), Adaptive Optics OCT (AO-OCT) and Polarization-sensitive OCT (PS-OCT).

Visible-Light OCT (Vis-OCT) relies on visible light broadband light source, compared to narrow near infrared light in previous OCT iterations, which allows acquisition of higher resolution images.[12] Another potential advantage of this iteration is the possibility of extracting specific wavelengths which contain new information such as the oxygenation of the blood.

Adaptive Optics OCT (AO-OCT) is based on the use of a deformable mirror that corrects wavefront and ocular aberrations, thus improving OCT image quality, most particularly in the transverse direction.[13] The device has been shown to resolve the photoreceptor mosaic, ganglion cells and lamina cribrosa microstructure.[14]

Polarization-sensitive OCT (PS-OCT) uses polarized light which alters the tissue polarization state revealing tissue-specific features. By utilizing the polarization information, it is able to determine tissue birefringence and enhance image contrast sensitivity and dynamic changes within the tissue.[15]

In conclusion, OCT is an invaluable tool for assessing glaucoma and monitoring its progression. This must be combined with a clinical examination and visual field analysis to determine the appropriate management for the patient.

References

1. Huang D, Swanson EA, Lin CP, et al. Optical coherence tomography. Science. 1991;254(5035):1178-81.
2. Popescu DP, Choo-Smith LP, Flueraru C, et al. Optical coherence tomography: fundamental principles, instrumental designs and biomedical applications. Biophys Rev. 2011;3(3):155.
3. Dong ZM, Wollstein G, Schuman JS. Clinical Utility of Optical Coherence Tomography in Glaucoma. Invest Ophthalmol Vis Sci. 2016 Oct;57(9):556-67.
4. Kotowski J, Wollstein G, Folio LS, et al. Clinical use of OCT in assessing glaucoma progression. Ophthalmic Surg Lasers Imaging. 2011;42 Suppl(0):S6-S14.
5. de Boer JF, Cense B, Park BH, et al. Improved signal-to-noise ratio in spectral-domain compared with time-domain optical coherence tomography. Opt Lett. 2003;28(21):2067-69.
6. Mrejen S, Spaide RF. Optical coherence tomography: imaging of the choroid and beyond. Surv Ophthalmol. 2013;58(5):387-429.
7. Rahimy E, Rayess N, Maguire JI, et al. Radial versus raster spectral-domain optical coherence tomography scan patterns for detection of macular pathology. Am J Ophthalmol. 2014;158(2):345-353.e342.
8. Spaide RF, Fujimoto JG, Waheed NK, et al. Optical coherence tomography angiography. Prog Retin Eye Res. 2018;64:1-55.
9. Moghimi S, Bowd C, Zangwill LM, et al. Measurement Floors and Dynamic Ranges of OCT and OCT Angiography in Glaucoma. Ophthalmology. 2019;126(7):980-88.
10. Giani A, Cigada M, Esmaili DD, et al. Artifacts in automatic retinal segmentation using different optical coherence tomography instruments. Retina. 2010;30(4):607-16.
11. Schuman JS, Hee MR, Arya AV, et al. Optical coherence tomography: a new tool for glaucoma diagnosis. Curr Opin Ophthalmol. 1995;6(2):89-95.
12. Zhang T, Kho AM, Yiu G, et al. Visible Light Optical Coherence Tomography (OCT) Quantifies Subcellular Contributions to Outer Retinal Band 4. Transl Vis Sci Technol. 2021;10(3):30.
13. Miller DT, Kocaoglu OP, Wang Q, et al. Adaptive optics and the eye (super resolution OCT). Eye (Lond). 2011;25(3):321-30.
14. Dong ZM, Wollstein G, Wang B, et al. Adaptive optics optical coherence tomography in glaucoma. Prog Retin Eye Res. 2017;57:76-88.
15. Pircher M, Hitzenberger CK, Schmidt-Erfurth U. Polarization sensitive optical coherence tomography in the human eye. Prog Retin Eye Res. 2011;30(6):431-51.

Part I

Chapter 2

Normal and pathologic posterior segment OCT

Cristina Maltese
Paola Cassottana
Michele Iester

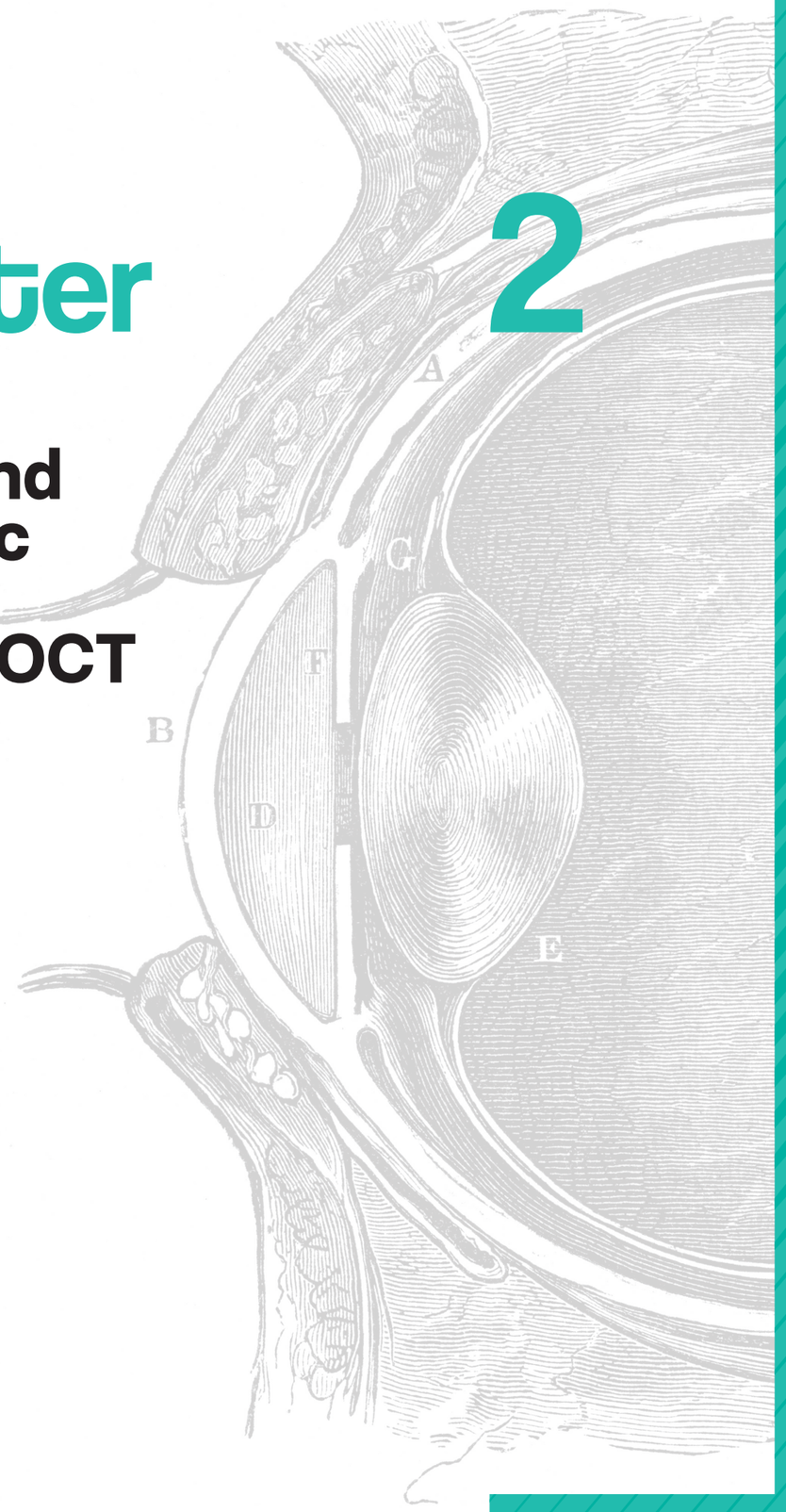

Normal and pathologic posterior segment OCT

Cristina Maltese, Paola Cassottana, Michele Iester

Clinica Oculistica, Department of Neurosciences, Rehabilitation, Ophthalmology, Genetics, Maternal and Child Health (DiNOGMI), University of Genoa, IRCCS Ospedale Policlinico San Martino, Genoa, Italy

Optical Coherence Tomography (OCT) has significantly advanced our understanding of normal ocular anatomy and pathology. OCT, with its high-resolution imaging capabilities, provides clinicians with the means to detect, monitor, and manage various ocular conditions, ranging from glaucoma to macular degeneration.[1-4] The advantages of OCT are numerous and vital in the context of glaucoma diagnosis and management. It delivers reproducible, reliable results that can be compared with later images, making it an indispensable aid in monitoring the progression of the disease. OCT is user-friendly and non-invasive with a relatively short learning curve for clinicians, further enhancing its accessibility.

The technique is highly sensitive as a diagnostic technique for detecting anatomical damage in glaucomatous eyes, which is clinically relevant particularly in the early stages of the disease. It allows clinicians to visualize structural changes in the optic nerve head, retinal nerve fiber layer, and other critical anatomical structures, facilitating timely intervention. However, it is important to acknowledge the potential limitations of OCT. Conditions involving media opacities, such as dense cataracts or vitreous hemorrhage,[5] can hinder the accuracy of imaging. Additionally, there is the possibility of OCT results leading to false-positive or false-negative identifications of glaucoma. Therefore, OCT should always be supplemented with a comprehensive clinical examination, and the diagnosis should not rely solely on the findings of one diagnostic technique.[6]

The new generations of spectral-domain OCT have significantly enhanced sensitivity in detecting structural changes in retinal nerve fiber layer (RNFL) thickness, optic nerve head (ONH) morphology, macular ganglion cell complex (GCC), and the lamina cribrosa (LC). OCT of the optic nerve enables the detection of retinal nerve fiber damage and allows for follow up by statistical comparison of different OCT images from the same patient. The three major sites of the posterior pole examined by SD-OCT, are peripapillary RNFL, the ONH, and the macula. In most machines optic nerve head region and macular region are acquired sequentially although modern wide field devices are capable of imaging both areas in one scan. They must be considered to be indissociable because they constitute different and complementary sources of information that must be interpreted according to each clinical form of glaucoma. There are various components that collectively provide a comprehensive assessment of the optic nerve and surrounding structures, aiding in the diagnosis and monitoring of various ocular conditions, including glaucoma.[7]

Cristina Maltese, Paola Cassottana, Michele Iester

Figure 1
Analysis of the three sites.

Figure 1

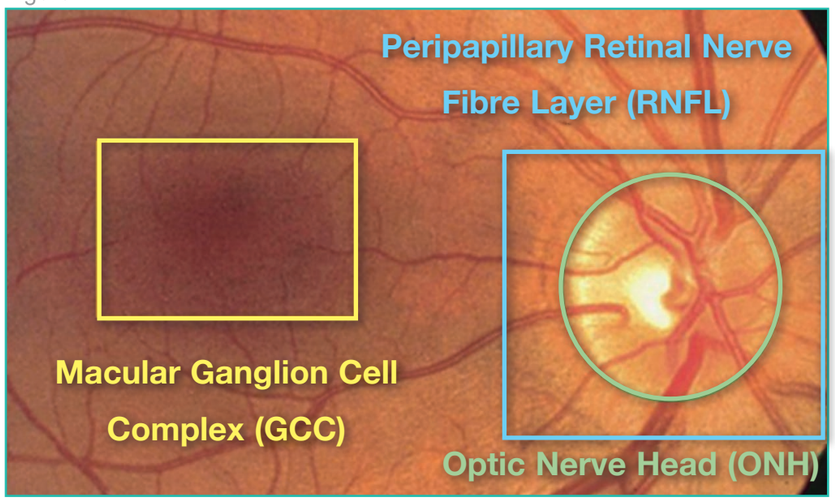

The OCT examination print-out consists of various parts:

1. Table of parameters compared with a normative database
2. Topographic map of retinal nerve fiber layer (RNFL) thickness
3. Map of RNFL deviation from normal values
4. Neuroretinal rim thickness
5. RNFL TSNIT or NSTIN graph of measurements in the area analyzed
6. Mean RNFL thickness in each quadrant or sector
8. Calculation of RNFL thickness in the circle of interest

1. Optic Nerve Head Analysis (ONH)

The initial challenge in optic nerve imaging is the precise definition of the optic nerve's contours and the beginning of the cup. It is crucial to establish accurate definitions for these parameters because, in cases of uneven disc morphology, erroneous identification of the reference plane can lead to distorted measurements. In the context of OCT investigations, a standardised reference plane is arbitrarily set between 120 and 150 µm above the level of the peripapillary pigment epithelium, or or between the Bruch membrane opening (BMO) and the internal limiting membrane or the vitreoretinal interface.
This approach allows measurement of papillary dimensions such as:

- The width and area of the neuroretinal rim at different meridians
- The size of the disc and cup
- The cup/disc ratio

Of the ONH parameters examined, those that revealed progressive changes in the manifestations of glaucoma were the vertical thickness of the neuroretinal rim, the overall area of the rim, and the vertical C/D ratio.[8]

2. Retinal Nerve Fiber Layer

RNFL thickness is measured at a distance of 3.4 mm from the centre of the optic disc[9].This distance is chosen to strike a balance between the thickness of the retinal nerve fiber layer (RNFL) and individual variability. Measurements taken farther from the disc show less variability across individuals but are less sensitive to small changes in RNFL thickness. While measurements at 3.4 mm from the disc's center may not reveal the earliest signs of disease, they provide a compromise that allows for reliable follow-up assessments.

Figure 2

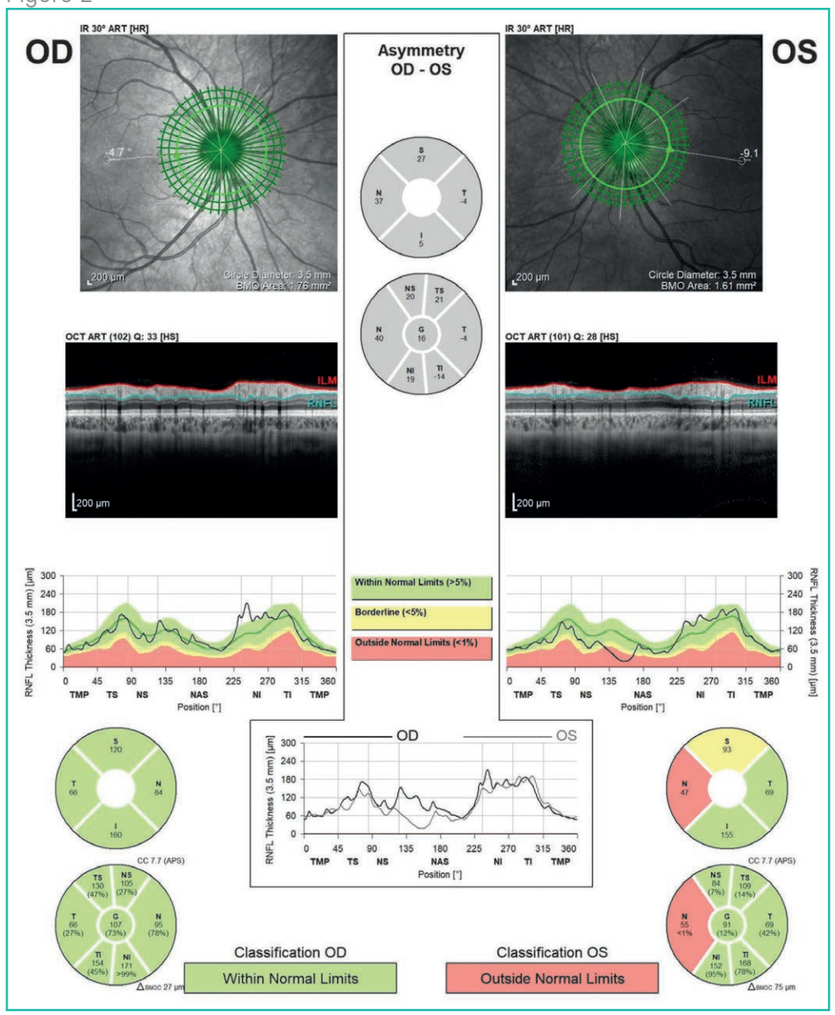

Figure 2
Print-out of ONH and RNFL analysis. On the top the image of the OHN with the green line where the RNFLanalysis was calculated, below the segmentation analysis of peripapillary RNFL scan. The TSNIT graph, the quadrant and the sector analysis with colour code. In the middle there is the assessment of the asymmetry (above) and the comparison of the two TSNIT graphs.

Cristina Maltese, Paola Cassottana, Michele Iester

RNFL thickness is visualized using a color code that ranges from white to green, yellow, and red. The color scheme serves to represent specific attributes in different visual elements, such as the position of the A-scan in the graph, quadrant mean values, clock positions in circular graphs, and columns for right and left eye data in the table. In the context of an age-matched normal population, the percentiles associated with each RNFL thickness measurement are interpreted as follow:

- *Measurements of less than 1 % of the normative values are represented in the red area (considered outside normal limits)*
- *Measurements falling between 1 % to 5 % of the normative values are depicted in or below the yellow area (considered suspect)*
- *Measurements ranging from 5 % to 95 % of the normative values are displayed in the green area (considered within the normal range)*
- *Measurements of more than 95 % of the normative values are shown in the white area*[6]

Figure 3

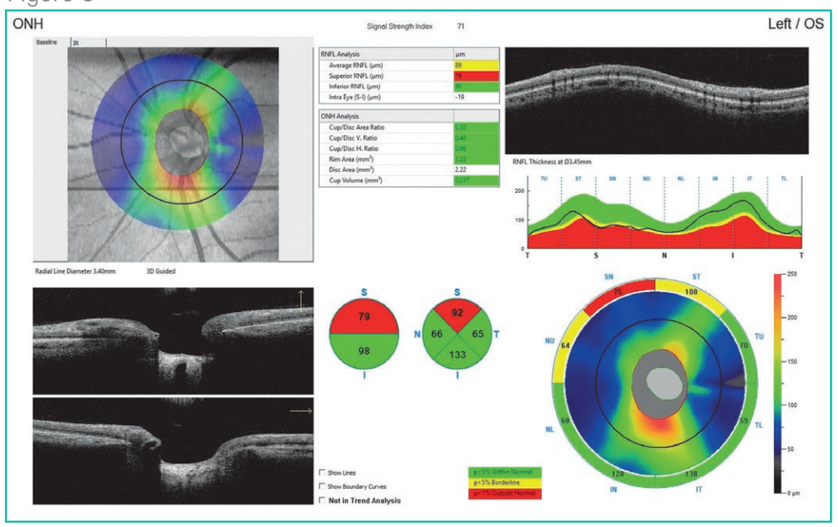

Figure 3
ONH scan with a colour RNFL rappresentation (warm colour means thick area, cold colour thin area). Below ONH trasversal scan; cup and lamina cribrosa can be visualized. On the right top, there are RNFL and ONH parameters in two tables, RNFL scan with below the TSNIT analysis graph, and belo RNFL analysys with sector analysis. Colour code is used to show if the measurement is in the normal, borderline or outside range.

In the early stages of glaucoma structural changes in the retina and optic nerve may be detectable using OCT before the condition becomes clinically apparent with visual field impairment.[10]
Parameters that have been proposed for early detection of glaucoma include:

- The vertical thickness of the neuroretinal rim
- The overall area of the neuroretinal rim
- The vertical cup-to-disc (C/D) ratio

While these parameters are valuable for detecting the presence of glaucoma, they exhibit limitations when it comes to distinguishing early-stage glaucoma from moderate cases.[11]

In the context of RNFL measurements, the OCT parameters that prove most effective in distinguishing between normal subjects and those with early-stage glaucoma are:

- RNFL thickness in the lower temporal zone
- RNFL thickness in the lower quadrant
- Average RNFL thickness

There is also evidence suggesting that measurements in the upper temporal sector could be as effective in discriminating between individuals with and without glaucoma as measurements in the lower temporal quadrant.[12]

Figure 4

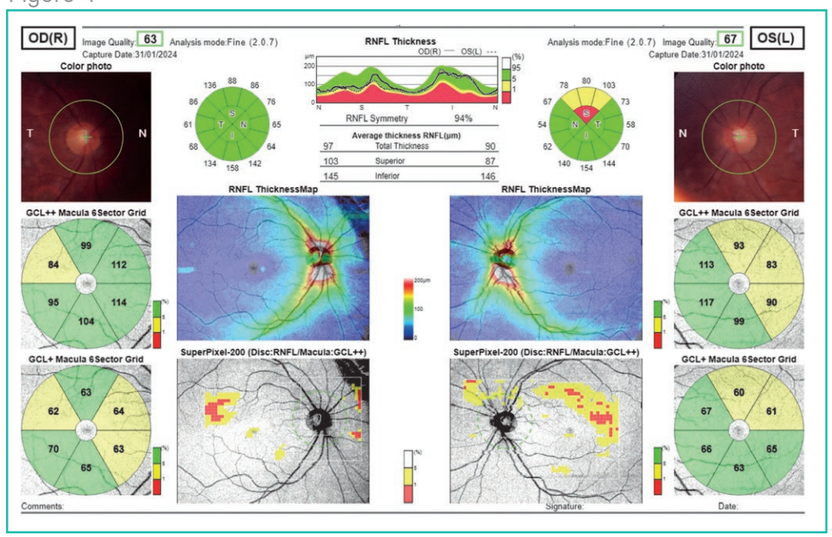

Figure 4
Colour photos of the ONH with the green line that shows the RNFL scan position, RNFL thincknes graph, the sector analysis of the RNFL and GCC. In the center there are two images tha show the ganglion cells thickenss on the poterior pole by using colour code (warm colour means thick area, cold colour thin area). Below the statistcal analysis of this area: coloured clusters show statistical significant changes.

Although diagnosis and follow-up assessments of glaucoma are based on anatomical and functional damage, the relationship between the two has is complex. Studies seeking a connection between the visual field and anatomical damage have resulted in glaucomatous structure/function relationships. An understanding of the relation between structure and function in glaucoma facilitates early diagnosis of glaucoma damage and its accurate staging.
Anatomical variations in the optic nerve head may lead to erroneous OCT classifications due to the wide variability of presentation, furthermore relatively small database used by OCT software can not help the capacity to distinguish healthy from statistically abnormal ONH. This may lead to the classification of abnormal RNFL parameters for normal subjects. Longitudinal investigations proof that some statistically abnormal ONH and RNFL could be glaucomatous in the absence of visual field changes, the disease is called preperimetric glaucoma.

Cristina Maltese, Paola Cassottana, Michele Iester

At the stage when structural damage gets associated with functional visual field damage, it can be defined as early glaucoma.[6] When the severity of glaucoma increases to the stage of moderate, it can be present with a greater OCT evidence of structural damage than functional visual field damage. In this case, anatomical damage can provide important indications of how functional damage could evolve. Another possible presentation shows greater concordance of structural ONH damage and RNFL thickness with visual field damage.
Structural damage to RNFL thickness does not go below approximately 40-50 µm, called floor effect. In these late stages of glaucoma, the concordance between anatomical and functional damage gets weaker, and the visual field is the most important parameter in monitoring progression.[13]

3. Macular Ganglion Cell Complex (GCC)

The thickness of the ganglion cell layer is another parameter that is frequently used for diagnosing and monitoring glaucoma, but it is difficult to segment. Hence, the Ganglion Cell Complex (GCC) which consists of three layers (the nerve fiber layer, the ganglion cell layer, and the inner plexiform layer), is typically used in glaucoma. The GCC has the advantage of relatively invariable imaging of the central retina, avoiding the confounding effect of optic disc variability.[14]
The GCC measures the entire neural transmission system for the retinal visual impulse in the macular area, including ganglion cell bodies, their dendrites (inner plexiform layer), and the thickness of ganglion cell axons passing above them (RNFL).[15]

Figure 5
The three GCC layers measured with OCT.

Figure 5

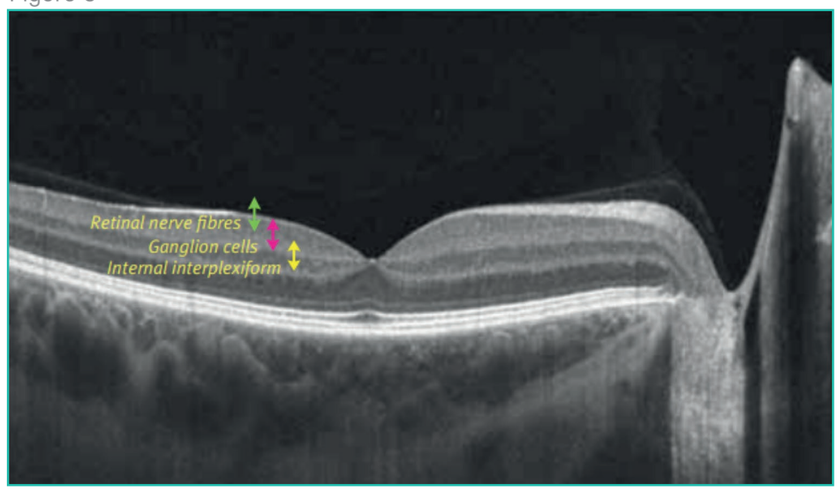

Different OCT use different methods to distinguish these different layers and different retinal layers can be included in the analysis. In this way the thickness of the ganglion cell layer can be different for the method of measurements and for the retinal layers included.
As previously described for RNFL and ONH, the data are initially compared with a normative database in the form of colorimetric maps, graphs, and tables, as we described above.
For the evaluation of glaucoma, several studies have suggested that in the early stages, GCC analysis, particularly the thickness of the inferior and inferotemporal GCC layers, is a more sensitive examination compared to the peripapillary RNFL (pRNFL).[16] Another strategy for detecting glaucoma is to identify any asymmetry of the ganglion cell–inner plexiform layers (GCIPL) between the two macular hemifields.
Furthermore, in some studies it has been found that GCC can be associated with other structural changes, such as tilted disc or atrophy around the optic nerve, where pRNFL cannot be properly determined using OCT. However, similar to pRNFL, changes in GCC are nonspecific and can be altered in other ocular diseases such as multiple sclerosis, ocular ischemia, diabetes mellitus, and toxic syndrome.[18]

What anatomical area can better detect Glaucoma?

Anatomical variability, the simultaneous presence of other local or systemic pathologies, or the entity of sight defects can influence structural measurements, such as RNFL and GCC thickness. Both parameterts are useful to follow glaucomatous patients.
Hood et al. conducted a study that concluded that there is an asymmetry between the inferior and superior fields in OCT macular scans, with greater GCC damage located inferiorly in glaucoma patients.[19] Furthermore, this study highlighted that GCC thinning was more pronounced on the temporal side of the fovea. This study, along with other recent studies, describes the existence of a sensitive pRNFL region on the optic disc, extending from 7 o'clock to 8 o'clock, which is suscettible to glaucoma damage. Clinically, disc hemorrhages in this region of pRNFL have been described and functionally as an arcuate defect found in the upper macular VF. The loss of pRNFL is associated with a decrease in the GCC thickness in the inferior temporal region of the macula, referred to as the "macular vulnerability zone" (MVZ). The strategy for glaucoma detection is to identify the asymmetry between the superior and inferior sectors of the macula. This begins with the anatomical asymmetry in the distribution of retinal fibers, as demonstrated by several studies showing that the temporal part of the horizontal raphe does not strictly follow the horizontal meridian, with an average slope of approximately 10 degrees above the horizontal meridian.[20] The reason for the initial inferior loss of GCC and subsequently the inferior RNFL compared to the superior area is related to the greater vulnerability of the inferior lamina cribrosa

and the higher fiber density in the inferior segment compared to the superior segment.[21,22] In particular, in preperimetric and suspected glaucoma patients, GCC and pRNFL exhibit better specificity and outperform visual field testing. The asymmetry of the ganglion cell complex is considered by some authors as a valuable indicator for preperimetric glaucoma, superior to RNFL thickness or the absolute thickness parameters of GCIPL.
In early glaucomatous patients there are strong evidences that the thickness of the inferior temporal sector could be useful to detect glaucoma as Jonas introduced when published the "ISNT rule".[3]

Many studies have analyzed the GCC and RNFL diagnostic capacity with completely different results, probably due to the stage of the disease of the included patients, the race, the refractive error, the age, and other reasons. Furthermore the discordance between the OCT and visual field data can be also attributed to the substantial reserve of ganglion cells for different areas of the visual field,or the different receptor fields leading.
Until now, OCT analysis in advanced glaucoma is not suggested for both pRNFL and GCC due to the "floor effect". Therefore, in this stage, it is more useful to assess the visual field for monitoring glaucoma progression.
In conclusion, GCC and pRNFL are parameters that can be used for glaucoma diagnosis and monitoring disease progression, the higher the damage of the disease, the better the accuracy of classification until the advanced stages when the thickness of the layer is below 40 µm.[18] In the following table there is a summary of the GCC, RNFL and VF parameters in different glaucoma stages, reported in a recent review, published in 2023 by Ghita et al.[1]

Table 1

PARAMETERS	GLAUCOMA STAGE			
		Early	**Moderate**	**Advanced**
	Ganglion Cell Complex (GCC)	Inferior and inferotemporal quadrant thickness are the most sensitive parameters	Same as early-stage glaucoma	Superior quadrant thickness best correlated to MD value
	Retinal Nerve Fiber Layer (RNFL)	Inferior quadrant thickness is a sensitive parameter	Inferior quadrant thickness has a stronger correlation to MD value onVF	Not very reliable (reaches the floor effect before GCC)
	Mean Deviation (from the visual field)	Less sensitive than RNFL and GCC	Some studies show correlation with parameters of the RNFL and GCC	Superior RNFL and slightly superior or similar with GCC

Modified from Ghita 2023

Figure 6

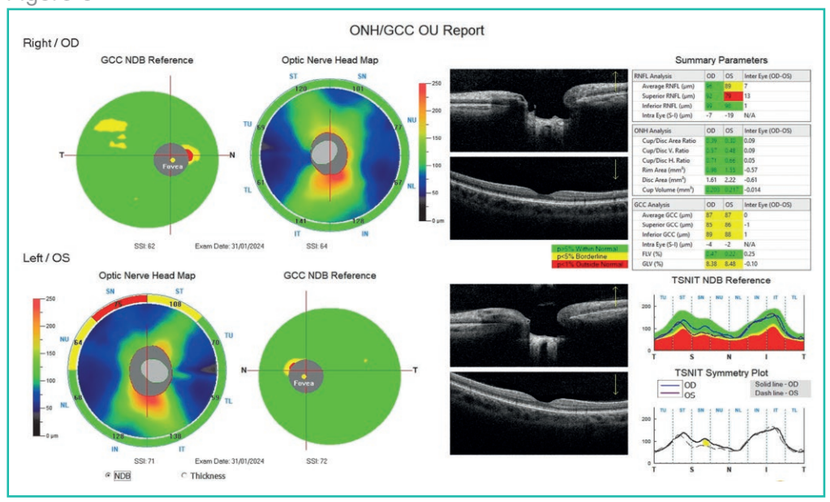

Figure 6
GCC and RNFL analysis on the left of the image warm colour means thick area, cold colour thin area. ONH and macular scan in the centre. On the top-right RNFL, ONH and GCC parameters layers measured with OCT, while on the botton-right TSNIT graph, both tables and graphes use the colour code to show in the measurement is in the normal, borderline or outside range.

4. Lamina Cribrosa (LC)

The recent Enhanced Depth Imaging (EDI) technique allows for improved visualization of deeper structures, such as the choroid and lamina cribrosa (LC), which are probably involved in the physiopathology of glaucoma,[23] but until now they are not used in clinical routine.
More details are in other chapters.

References

1. Aumann S, Donner S, Fischer J, Müller F. Optical Coherence Tomography (OCT): principle and tech- nical realization. In: Bille JF, editor. High resolution imaging in microscopy and ophthalmology: new frontiers in biomedical optics. Cham: Springer. 2019;59–85.
2. Kanamori A, Nakamura M, Escano MF, Seya R, Maeda H, Negi A. Evaluation of the glaucomatous damage on retinal nerve fiber layer thickness measured by optical coherence tomography. Am J Ophthalmol. 2003;135(4):513–20.
3. Yuksel Elgin C, Chen D, Al-Aswad LA. Ophthalmic imaging for the diagnosis and monitoring of glaucoma: A review. Clinical Exper Ophthalmology. 2022;50(2):183-97. doi:10.1111/ceo.14044
4. Aumann S, Donner S, Fischer J, Müller F. Optical Coherence Tomography (OCT): principle and tech- nical realization. In: Bille JF, editor. High resolution imaging in microscopy and ophthalmology: new frontiers in biomedical optics. Cham: Springer. 2019;59–85.
5. Zhang L, Van Dijk EHC, Borrelli E, Fragiotta S, Breazzano MP. OCT and OCT Angiography Update: Clinical Application to Age-Related Macular Degeneration, Central Serous Chorioretinopathy, Macular Telangiectasia, and Diabetic Retinopathy. Diagnostics. 2023;13(2):232. doi:10.3390/diagnostics13020232
6. Park KH, Kim TW, eds. OCT Imaging in Glaucoma: A Guide for Practitioners. Springer Singapore. 2021. doi:10.1007/978-981-16-1178-0

7. Paunescu LA, Schuman JS, Price LL, et al. Reproducibility of nerve fiber thickness, macular thickness, and optic nerve head measurements using Stratus OCT. Invest Ophthalmol Vis Sci. 2004;45(6):1716–24.
8. Oddone F, Lucenteforte E, Michelessi M, et al. Macular versus retinal nerve fiber layer parameters for diag- nosing manifest glaucoma: a systematic review of diagnostic accuracy studies. Ophthalmology. 2016;123(5):939–49.
9. Gür Güngör S, Akman A, Küçüködük A, Çolak M. Retinal Nerve Fiber Layer Thicknesses in Three Different Optic Nerve Head Size Groups Measured by Cirrus Spectral Domain Optical Coherence Tomography. Turk J Ophthalmol. 2016;Apr;46(2):58-61.
10. Klamann MK, Grünert A, Maier AK, Gonnermann J, Joussen AM, Huber KK. Comparison of functional and morphological diagnostics in glaucoma patients and healthy subjects. Ophthalmic Res. 2013;49:192-98.
11. Mawanza JC, Oakley JD, Budens, DL, Anderson DR. Ability of Cirrus HD-OCT Optic nerve head parameters to discriminates normal from glaucomatous eyes. Ophthalmology. 2011;118:241-48.
12. Lisboa R, Leite MT, Zangwill LM, Tafreshi A, Weinreb RN, Medeiros FA. Diagnosing premerimetric glaucoma with Spectral Domain OCT. Ophthalmology. 2012;119:2161-69.
13. Rao HL, Zangwill LM, Weinreb RN, Leite MT, Sample PA, Medeiros FA. Structurefunction relationship in glaucoma using spectral-domain optical coherence tomography. Arch Ophthalmol 2011;129:864–71.
14. Renard, JP, Fénolland, JR, Giraud, JM. Glaucoma Progression Analysis by Spectral-Domain Optical Coherence Tomography (SD-OCT). J. Fr. Ophtalmol. 2019;42:499-516.
15. Hou H, Moghimi S, Kamalipour A, et al. Macular Thickness and Microvasculature Loss in Glaucoma Suspect Eyes. Ophthalmology Glaucoma. 2022;5(2):170-78. doi:10.1016/j.ogla.2021.07.009
16. Moreno PAM, Konno B, Lima VC, Castro DPE, Castro LC, Leite MT, Mendes Pacheco MAM, Lee JM, Prata TS. Spectral-Domain Optical Coherence Tomography for Early Glaucoma Assessment: Analysis of Macular Ganglion Cell Complex versus Peripapillary Retinal Nerve Fiber Layer. Can. J. Ophthalmol. 2011;46:543-47.
17. Choi JA, Shin HY, Park HYL, Park CK. The Pattern of Retinal Nerve Fiber Layer and Macular Ganglion Cell-Inner Plexiform Layer Thickness Changes in Glaucoma. J. Ophthalmol. 2017;6078365.
18. Ghita AM, Iliescu DA, Ilie LA, Otobic A. Ganglion Cell Complex Analysis: Correlations with Retinal Nerve Fiber Layer on Optical Coherence Tomography. Diagnostics. 2023;13(2):266. doi:10.3390/diagnostics13020266
19. Hood DC, Raza AS, De Moraes CGV, Liebmann JM, Ritch R. Glaucomatous damage of the macula. Progress in Retinal and Eye Research. 2013;32:1-21. doi:10.1016/j.preteyeres.2012.08.003
20. Huang G, Luo T, Gast TJ, Burns SA, Malinovsky VE, Swanson WH. Imaging Glaucomatous Damage Across the Temporal Raphe. Invest Ophthalmol Vis Sci. 2015;56(6):3496. doi:10.1167/iovs.15-16730
21. Hood DC, Raza AS, De Moraes CGV, Johnson CA, Liebmann JM, Ritch R. The Nature of Macular Damage in Glaucoma as Revealed by Averaging Optical Coherence Tomography Data. Trans Vis Sci Tech. 2012;1(1):3. doi:10.1167/tvst.1.1.3
22. Choi JA, Park HYL, Jung KI, Hong KH, Park CK. Difference in the Properties of Retinal Nerve Fiber Layer Defect Between Superior and Inferior Visual Field Loss in Glaucoma. Invest Ophthalmol Vis Sci. 2013;54(10):6982. doi:10.1167/iovs.13-12344
23. Ferreras A, ed. Glaucoma Imaging. Springer International Publishing. 2016. doi:10.1007/978-3-319-18959-8

Part I

Chapter 3

Quantitative assessment of posterior-segment Optical Coherence Tomography in Glaucoma

Giovanni Montesano
David P Crabb

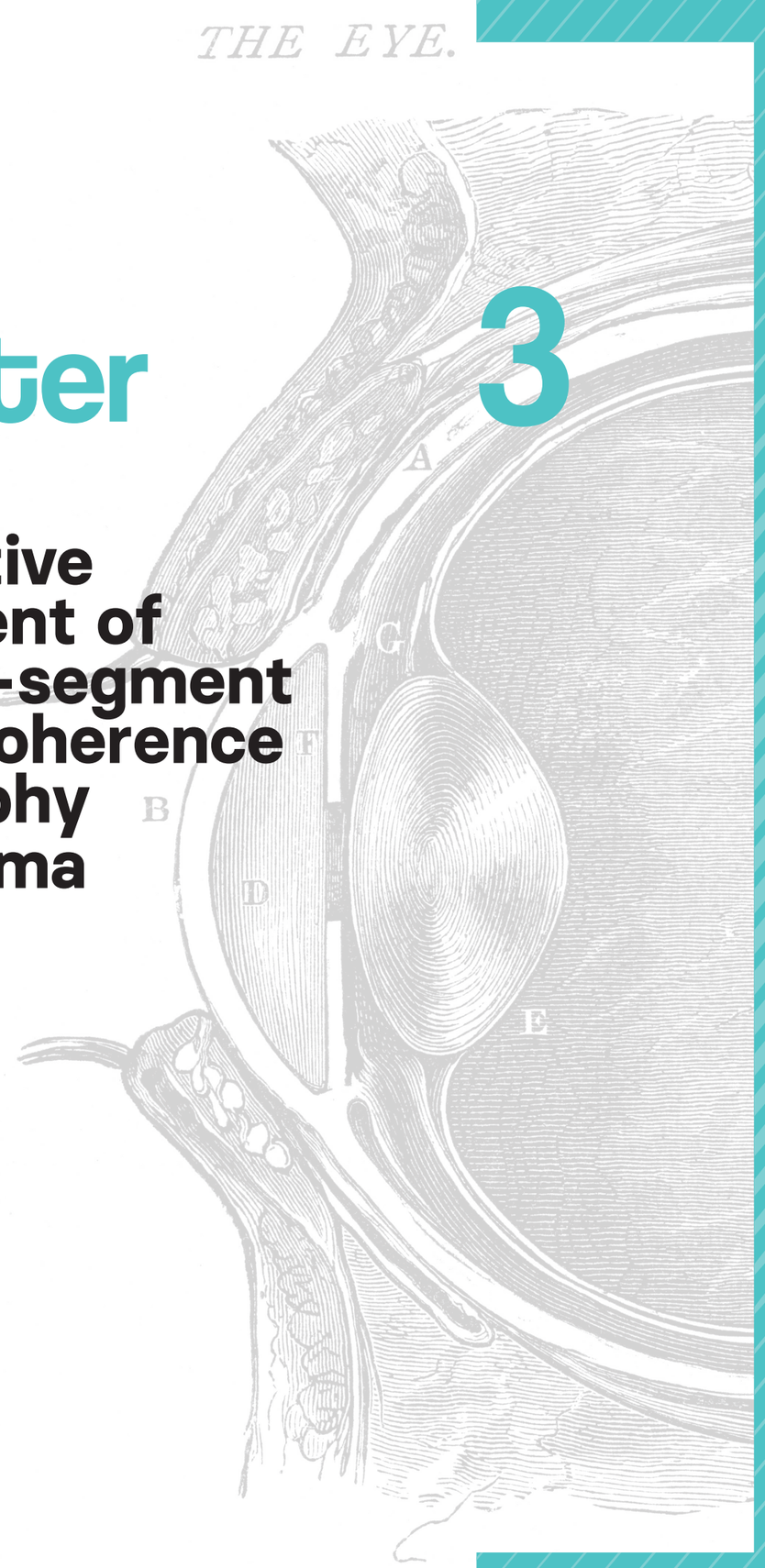

3
Part I

Quantitative assessment of posterior-segment Optical Coherence Tomography in Glaucoma

Giovanni Montesano,[1,2] David P Crabb[1]

[1] City, University of London, Optometry and Visual Sciences, London, United Kingdom
[2] NIHR Biomedical Research Centre, Moorfields Eye Hospital NHS Foundation Trust and UCL Institute of Ophthalmology, London, United Kingdom

Introduction

Optical Coherence Tomography (OCT) is often used in glaucoma to image structures of the optic nerve head (ONH) and the macula. This imaging assessment provides clinicians with quantitative values that can be used to assess structural changes from glaucoma.

In clinical practice, structural metrics are generally used to either help with diagnosing glaucoma or assessing progression of damage. Diagnosis is usually helped by detecting deviation from expected "healthy" anatomy, whereas progression tries to identify changes over time. Naturally, there is overlap between these two, because progression is a defining (and potentially diagnostic) feature of glaucoma in patients who are glaucoma suspects or ocular hypertensives. Most commercial software packages provide automated statistical tools and printouts providing quantitative analyses. It is important for clinicians to understand the basics of how these tools operate, together with caveats and pitfalls around their use, so that they can be effectively incorporated in patients' care.

DIAGNOSIS

Normative databases and ranges

Normative limits are reference values used by software and clinicians to define a range within which the majority of the values from "healthy" people are expected to be found. Glaucoma clinicians are mostly interested in loss of tissue and therefore common thresholds for these limits are the 5th and 1st percentiles. This means that 95% of the values from a healthy cohort will be above (thicker) the 5th percentile and 99% above the 1st percentile. However, this also means that 5% and 1% of healthy eyes will have values below these limits, respectively.

Normative values can be affected by multiple factors, most notably age, race, and eye axial length[1]. Normative databases are generally composed of a few hundred eyes that are representative of the general population.

Optic nerve head

The imaging of the ONH has a prominent role in glaucoma management. Most clinicians are familiar with circular OCT scans of the peripapillary tissue at a fixed distance around ONH, used to segment and measure the thickness of the Retinal Nerve Fibre Layer (RNFL). This profile is extended and reported over normative reference limits, usually colour-coded (green above the 5% limit, yellow below the 5% limit, red below the 1% limit) to visualise localised loss in the tissue. Most devices also report summary thickness measures, such as the global average or by individual sectors. These are also usually colour-coded to indicate their relationship with normative limits.

Some devices, such as the Spectralis (Heidelberg Engineering, Heidelberg, Germany) or the Cirrus (Zeiss Meditec, Dublin, CA) provide normative values "adjusted" according to patients' characteristics, most commonly age and disc size. In its simplest form, this correction is performed through linear regression, whereby a line is fitted to predict the average thickness for any given value of the predictor (see Fig. 1). When more than one predictor is used (i.e. age and disc area), their combined effect is modelled through a multivariable linear regression. However, this type of linear regression only predicts the change in the mean value, assuming constant variability around that mean. This is often not the case.[2] A very practical solution is to perform a quantile regression. This regression technique models any arbitrary quantile (such as the 5th or the 1st percentile) according to a set of predictors.
This means, for example, that in a univariable relationship (such as with age) the line representing the relationship with the 5th percentile is not assumed to be parallel to the line representing the mean (see Fig. 1), modelling the non-constant variability. These techniques are applied differently by various manufacturers and might be used for some or all of their ONH metrics.
It should be noted that sector and global averages might hide localised loss, for example when focal defects spread over two adjacent sectors (Fig. 2).
Similar calculations are performed on other metrics such as the neuro-retinal rim (NRR on Topcon and Zeiss devices) or Bruch's membrane opening – minimum rim width (BMO-MRW on the Spectralis), with analogous interpretations.

Figure 1

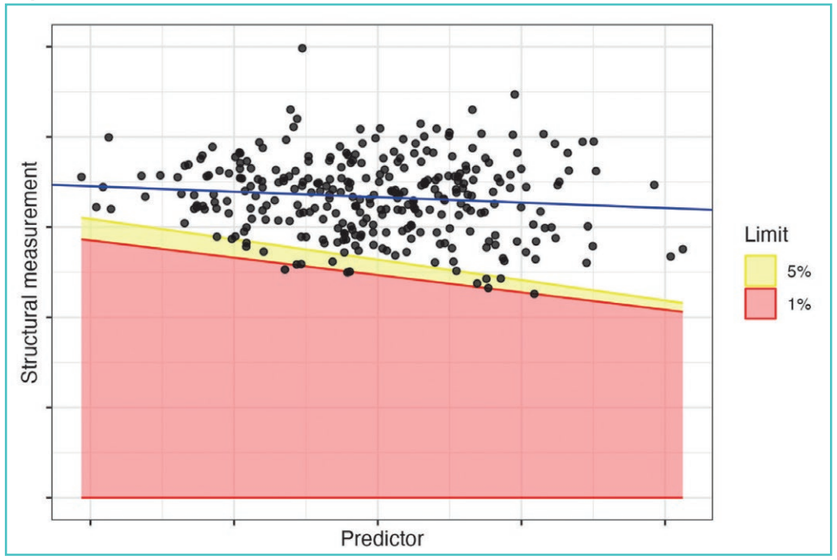

Figure 1
Example of how the normative mean and percentiles are calculated with standard linear regression (blue line) and quantile regression (yellow and red shaded areas). Note how the 5% and 1% limits obtained by quantile regression are not parallel to the blue line and to each other, indicating a non-constant variability. Illustrative example, not real data.

Figure 2

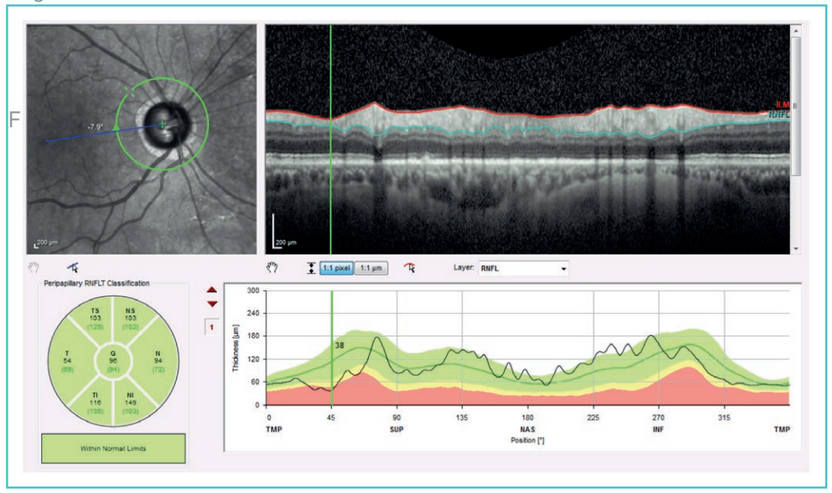

Figure 2
Example of how a clear localised defect (profile) can be missed by the sector averages (on the bottom left), because the average value is still within the normative limits.

Macula

OCT devices can provide macular volumes of variable density with quantification of different macular layers. For glaucoma, the inner retinal layers are usually of interest. Thickness values for these layers can also be summarised by global averages or sectors, in a similar fashion as the ONH. However, dense scans also offer the opportunity to investigate the spatial patterns of tissue loss in detail. This is usually achieved by presenting deviation maps of superpixels (i.e. local averages of a set of nearby pixels in the image), colour-coded to indicate which areas are below a certain normative limit, similarly to the peripapillary scans (Fig. 3). Some devices also use dense cube scans of the ONH to reconstruct the circular peripapillary profiles. These scans can also provide detailed two-dimensional deviation maps of the area around the ONH, identical to those used for the macular region.

Figure 3

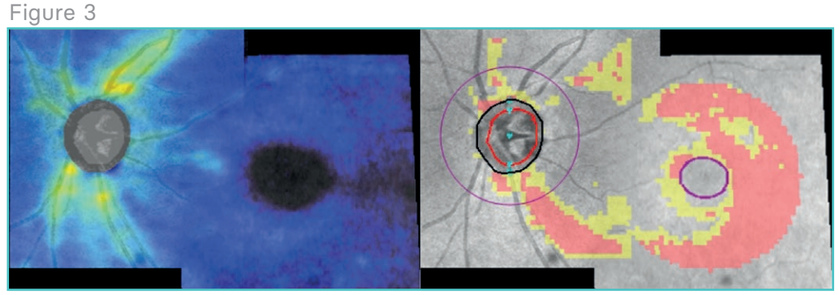

Figure 3
Combined macular and ONH RNFL thickness map (right) and RNFL and Ganglion Cell Layer + Inner Plexiform Layer deviation maps (right).

Caveats

Normative limits give the probability that a normal subject will produce values that are below that limit, not the probability that a subject has tissue loss. Therefore, profiles or values that fall in the "red" or "yellow" regions do not necessarily indicate disease.

Normative databases, by their nature, cannot encompass the full range of variability of the entire population. For example, they often exclude eyes with extreme refractive errors and are unlikely to contain extreme values of disc area size.

Normative models are constructed assuming that their predictors, such as age and disc area, are measured without errors. While this is approximately true for a variable like age, it is certainly not for quantities like the disc area, which is also quantified by the device using the OCT scans and can be subject to segmentation errors. It is useful to remember that the measurement of disc area is also affected by ocular magnification and can be imprecise when the axial length for the eye being tested is not provided.[3]

Normative models do not account for all possible sources of variability. For example, in the Cirrus, many other predictors were excluded from the final model because of their small contribution to the overall prediction. However, even the strongest predictor (disc area) only accounted for 40% of the variability, with age explaining less than 5%.[4] Another major source of variability for the RNFL profile is the position of the major blood vessels in the retina (see example in Fig. 4).[5,6] Successful efforts have been made to account for these additional sources of variability with more complex modelling approaches that include other factors such as vessel location and ethnicity[1,5], but these have not yet made their way into commercial software.

Figure 4

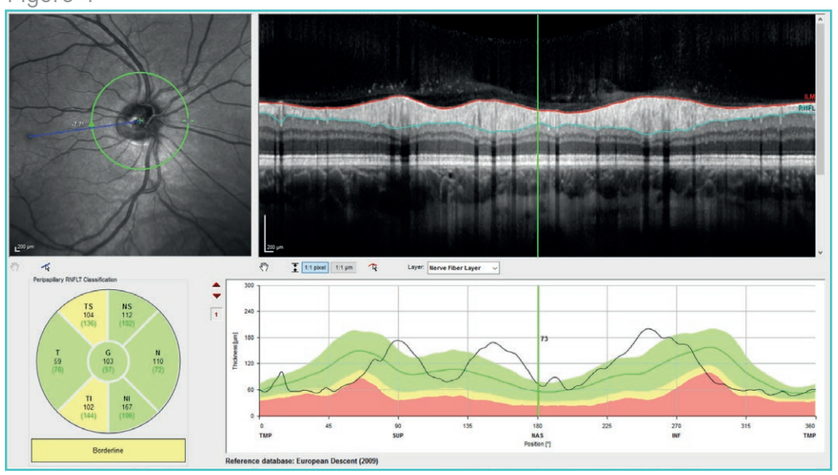

Figure 4
Healthy RNFL profile flagged as "borderline" because the position of the blood vessels causes the "humps" to be displaced compared to the average profile from the normative database.

Deviation maps are particularly prone to detecting false abnormalities, simply because the chance of at least one measurement being outside the normative limits increases the more measurements we make. Approaches to address this problem have been proposed for other imaging techniques used in glaucoma.[7] This is a well-studied problem in statistics and finds particular application in fields like functional magnetic resonance imaging. Particularly illuminating in this regard is the short paper by Bennet et al. reporting on the brain activity of a dead salmon.[8] Clinicians can improve specificity by considering the location and spatial arrangement of the "abnormal" superpixels, looking for patterns characteristic of glaucoma.[9]

Progression

Event-based progression

Event-based progression is concerned with detecting changes from an established baseline. This concept has been borrowed from the Guided Progression Analysis (GPA) implemented for visual field progression on the Humphrey Field Analyzer (Zeiss Meditec, Dublin, CA) and is available for the Cirrus. The method uses the average of two scans as a baseline. Pixels in the OCT cube (or A-scans for the circular profiles) are compared to baseline and marked as progressed if the change exceeds the 97.5% test-retest variability limits in one (yellow) or two (red) consecutive exams. This method is applied to peripapillary scans, ONH and macular cube scans (Ganglion Cell + Inner Plexiform Layers) and ONH average cup-to-disc ratio (Fig. 5). This method compares multiple superpixels (or A-scans) to a baseline and therefore the likelihood of false detection of change is high. This is mitigated by requiring that a certain amount of neighbouring superpixels (A-scans) show progression to define a "possible progression" (one follow-up) or a "likely progression" (two consecutive follow-ups) event.[10]

Trend-based progression

Trend-based methods assess progression by estimating the rate of structural loss with a linear regression of the structural measurement over time. This can be performed for a global metric (such as the average RNFL thickness) or by individual sectors (Fig. 6). The rate is reported as µm/year. Its statistical significance is assessed by either a 95%-confidence interval (95%-CI) of the slope or a p-value. Most software requires at least 4 measurements to produce these values. The 95%-CI is an estimate of the precision of the estimate of the slope. The narrower 95%-CI, the better the precision of the estimate. A p-value is the probability of measuring that rate of progression if there was no actual change (i.e. if the rate of progression was 0 µm/year). If the 95%-CI does not include 0 µm/year, the p-value will be < 0.05. In general, a 95%-CI is more informative than a p-value. For example, we know that some RNFL loss is expected from

Figure 5
Examples of event-based progression for the RNFL (top) and the Ganglion Cell + Inner Plexiform macular layers (different patients). Images courtesy of Dr G. De Moraes and Dr E. Tsamis, Columbia University, New York, USA.

Figure 5

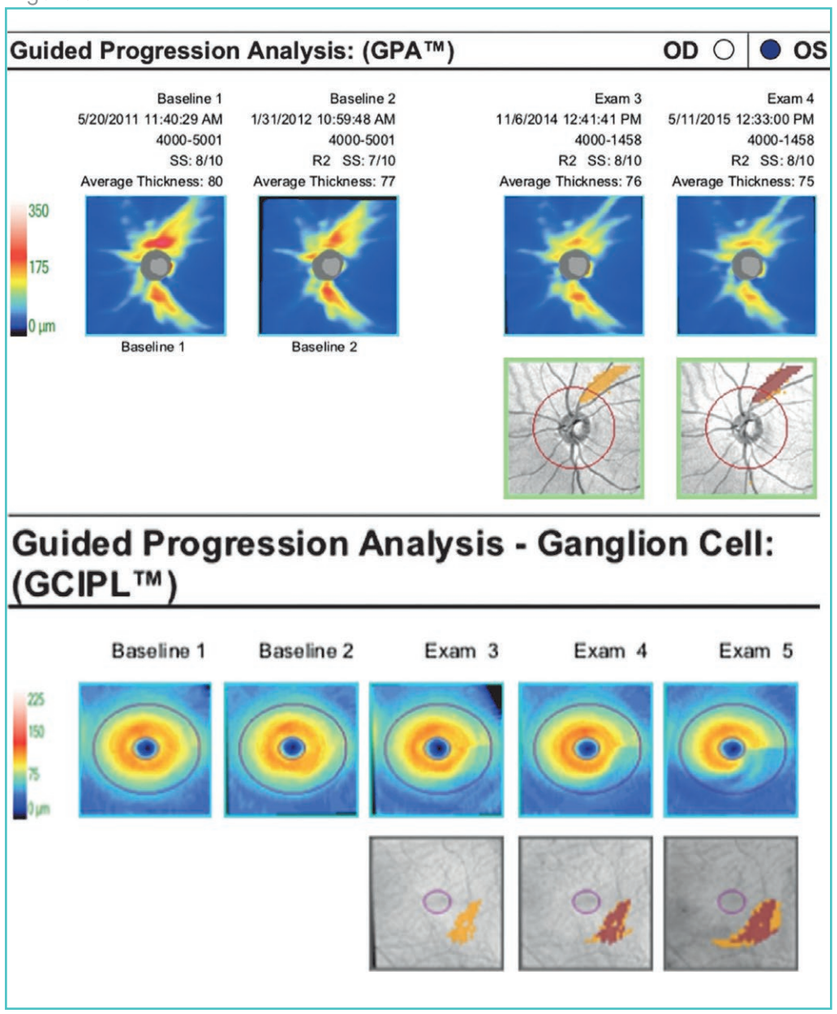

ageing (approximately -0.2 µm/year).[11] While a p-value would simply tell if the observed rate is significantly different from 0 µm/year, a 95%-CI would allow to verify if the estimated rate is compatible with an age-related decline, even if statistically significant (i.e. if the 95%-CI contains -0.2 µm/year). Another aspect to keep in mind is that, as the damage progresses, structural metrics approach a measurement floor.[12] Therefore, the measurements appear to "stabilise" and the measured slopes tend to become less steep, underestimating the rate of progression of the disease.

Figure 6

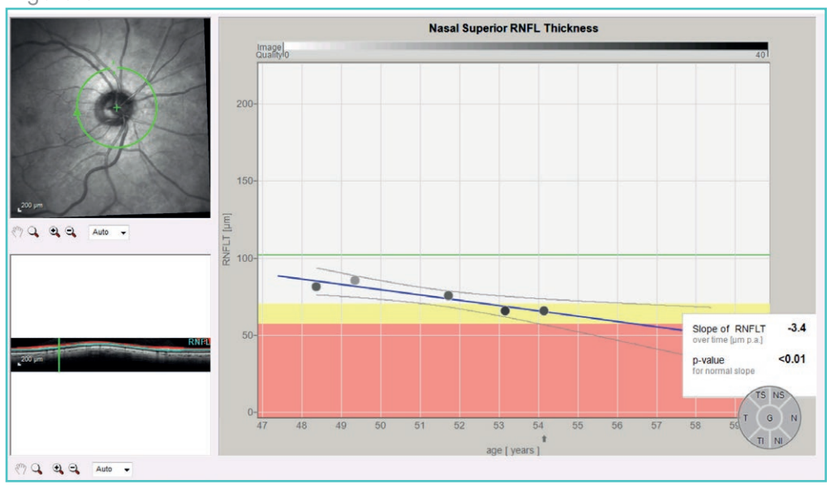

Figure 6
Trend based progression for one sector. The p-value indicates statistically significant progression. The band around the main trend line represents the 95% prediction intervals (not to be confused with the 95%-CI of the slope), an indicator of the estimated variability of the observations around the predicted trend.

References

1. Chua J, Schwarzhans F, Wong D, et al. Multivariate Normative Comparison, a Novel Method for Improved Use of Retinal Nerve Fiber Layer Thickness to Detect Early Glaucoma. Ophthalmol Glaucoma. 2022;5(3):359-68.
2. Artes PH, Crabb DP. Estimating normative limits of Heidelberg Retina Tomograph optic disc rim area with quantile regression. Invest Ophthalmol Vis Sci. 2010;51(1):355-61.
3. Garway-Heath DF, Rudnicka AR, Lowe T, et al. Measurement of optic disc size: equivalence of methods to correct for ocular magnification. Br J Ophthalmol. 1998;82(6):643-49.
4. Knight OJ, Girkin CA, Budenz DL, et al. Effect of race, age, and axial length on optic nerve head parameters and retinal nerve fiber layer thickness measured by Cirrus HD-OCT. Arch Ophthalmol. 2012;130(3):312-18.
5. Chua J, Schwarzhans F, Nguyen DQ, et al. Compensation of retinal nerve fibre layer thickness as assessed using optical coherence tomography based on anatomical confounders. Br J Ophthalmol 2020;104(2):282-90.
6. Rho S, Sung Y, Kang T, et al. Improvement of diagnostic performance regarding retinal nerve fiber layer defect using shifting of the normative database according to vessel position. Invest Ophthalmol Vis Sci. 2014;55(8):5116-24.
7. Patterson AJ, Garway-Heath DF, Strouthidis NG, Crabb DP. A New Statistical Approach for Quantifying Change in Series of Retinal and Optic Nerve Head Topography Images. Investigative Ophthalmology & Visual Science. 2005;46(5):1659-67.
8. Bennett CM, Baird AA, Miller MB, Wolford GL. of Serendipitous and Unexpected Results Neural Correlates of Interspecies Perspective Taking in the Post-Mortem Atlantic Salmon: An Argument For Proper Multiple Comparisons Correction. 2010.
9. La Bruna S, Rai A, Mao G, et al. The OCT RNFL Probability Map and Artifacts Resembling Glaucomatous Damage. Transl Vis Sci Technol. 2022;11(3):18.
10. Hood DC, Melchior B, Tsamis E, et al. Did the OCT Show Progression Since the Last Visit? J Glaucoma. 2021;30(4):e134-e45.
11. Patel NB, Lim M, Gajjar A, et al. Age-associated changes in the retinal nerve fiber layer and optic nerve head. Invest Ophthalmol Vis Sci. 2014;55(8):5134-43.
12. Hood DC, Kardon RH. A framework for comparing structural and functional measures of glaucomatous damage. Prog Retin Eye Res. 2007;26(6):688-710.

Part I

Chapter 4

OCT: Limitations and pitfalls

Francisco Javier Goñi

Vertical Section

4
Part I

OCT: Limitations and pitfalls

Francisco Javier Goñi

Chief of the Ophthalmology Dept. Hospital Universitari de Mollet. Mollet del Vallès. Barcelona, Spain
Glaucoma consultant. CTIG. Hospital Quiron Teknon. Barcelona, Spain

Introduction

OCT is an imaging technology that uses a laser beam and the principles of low coherence interferometry to scan ocular tissues in a cross-sectional way, obtaining thousands of tomograms reconstructed in 2-dimensional or 3-dimensional images, employing a computer software.

Image quality refers to the level of accuracy with which different imaging systems capture, process, store, compress, transmit and display the signals that form an image[1] The images obtained by an instrument should depict as accurately as possible the characteristics of the object that the technology aims to represent, according to its methodology and limitations. In the case of OCT used in glaucoma diagnosis, the objects imaged are the anterior segment, the retina, choroid, vessels, and the optic nerve head (ONH). Errors are differences between the observed representation of these structures and their true characteristics, mainly in thickness, shape, and optical properties. Images are then inaccurate or misleading and can misrepresent the structure. Sources of error may come from any potential interference in one or more of the different steps of the whole procedure, and are related to the instrument itself, the operator, and the patient. Artifacts are errors leading to a misrepresentation of the structure imaged. Artifacts in OCT come usually from the operation of image capture and from the procedure of delimitation of image landmark boundaries, mainly retinal and optic nerve segmentation. On the other hand, limitations of measurement are restrictions linked to the instrument and patient's characteristics, mainly those related to the eye features.

Artifacts

Image artifacts are more frequently produced during image capture and processing. They are produced by the instrument, the operator, and the patient.
Instrument-related artifacts. A well-functioning OCT must provide a robust signal strength (SS). The SS index (SSI) is determined from the intensity of the reflected light across the entire scan, and each instrument has specific SSI values. The observation of an unexplained, persistently low SSI suggests contacting the technical service of the instrument. Software-related artifacts appear during processing of OCT scans. Segmentation errors are misidentifications of retinal layers and ONH boundaries. (Fig. 1). Mirror artifacts arise from the Fourier transformation used in SD and swept-source OCT and are more frequently seen in moderate and high myopia.[2]
Operator-related artifacts. Image capture requires sufficient illumination, sharp focus and a correct centring (Fig. 2) and completeness of the structure to be imaged, to avoid cut edge artifacts or out-of-register artifacts. (Fig. 3) Failure to meet any of these results in poor image acquisition, producing degraded images. The role of the operator is very relevant, since he/she must ensure the best possible quality of the acquired image.

Figure 1
Interrupted delimitation of the internal limiting membrane, erroneously displaced to the edge of the RNFL circular tomogram window due to signal loss, resuming when the signal is recovered.

Figure 2
Unreliable image results due to poor signal quality capture related to inadequate illumination, focus, and centering.

Figure 1

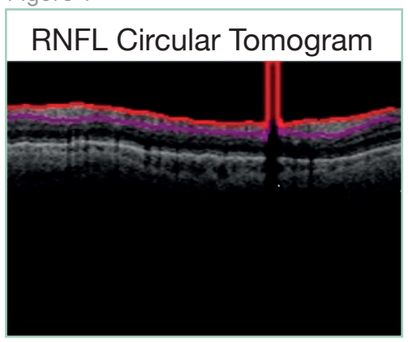

Figure 2

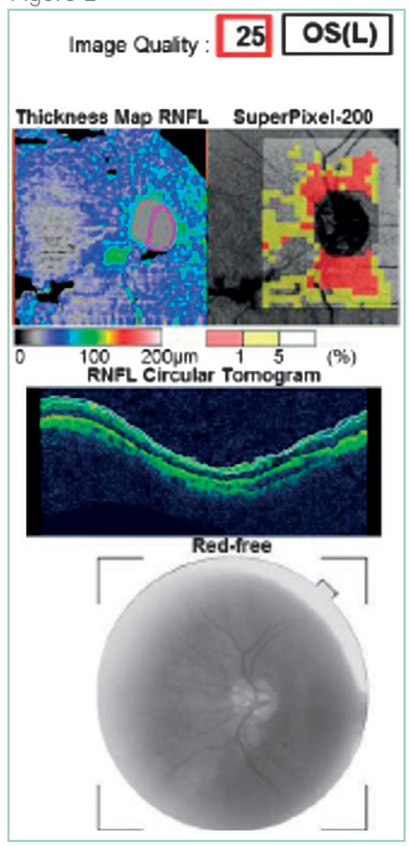

In case of doubt, the operator should obtain a new image. If image quality cannot be finally improved, the operator should note it in the patient's medical record.

Patient-related artifacts. During image acquisition, the patient may lose concentration, showing voluntary or involuntary eye movements losing and resuming fixation, (Fig. 4) or blinking. (Fig. 5). During fixation, there are three main types of involuntary eye motions: tremor, drifts and microsaccades. The object's image on the retina can move up to several hundred photoreceptors during microsaccades, with a duration about 25 milliseconds.[3] Saccades may produce wider image movements, that can lead to significant data loss. On the other hand, retinal axial motions are due to head movements caused by the heart rate.[4] Heavy breathing can also cause axial motion artifacts, compromising the acquisition of true curvature of the retina thus producing curve-shaped artifacts. In the case of OCT angiography (OCTA), specific artifacts like doubling of retinal vessels are also associated with eye movement.[5]

Media opacities can attenuate SS, reducing quality image and increasing inter-test variability.[6] Cortical cataracts have the most significant impact followed by posterior subcapsular opacities.[7]
A study using optical density filters in normal subjects has reported an underestimation of both RNFL thickness and macular inner retina

Figure 3

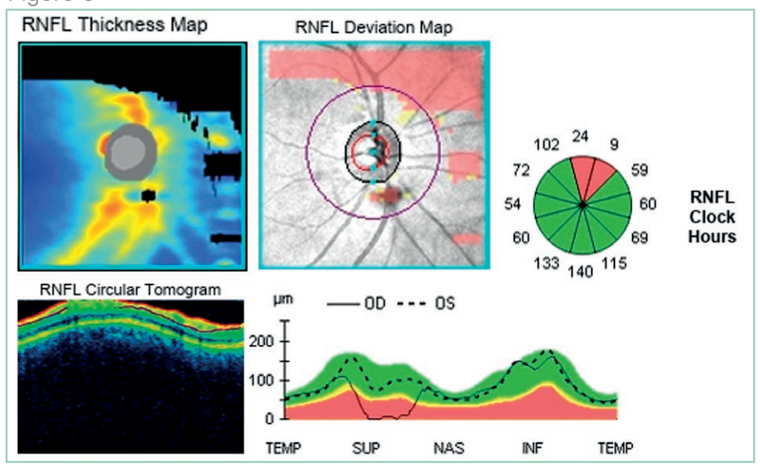

Figure 3
Out-of-register artifact. The image is displaced vertically, and the inner retina is partially out of range of scan. The RNFL circular tomogram is interrupted at the level of temporal and nasal superior aspects, dropping to zero values on TSNIT map.

Figure 4

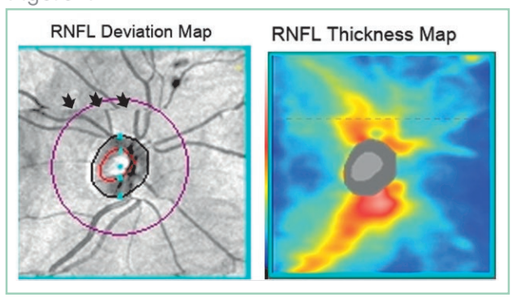

Figure 4
A quick eye movement losing and resuming fixation produces a sectoral image displacement. The retinal vessels' trajectory is interrupted and retaken in a different position. (black arrows). If the RNFL circular tomogram is affected, results may not be reliable and image capture should be repeated.

Figure 5

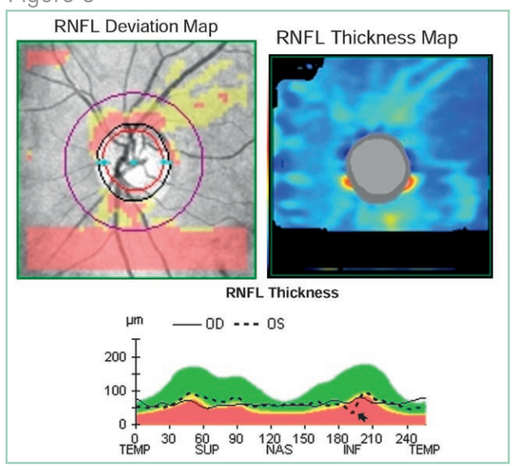

Figure 5
A blink usually produces a loss of image capture, appearing as a black longitudinal band on the RNFL thickness map. The artifact affects the RNFL circular tomogram, depicting a wrong thinning on the TSNIT map (black arrows).

Figure 6
A vitreous floater interferes with the laser beam, creating a shadow across the entire retinal thickness of the RNFL circular tomogram and dropping to zero values on TSNIT map. One sector on RNFL clock hours map is flagged as abnormal, masquerading as a typical glaucoma loss. This artifact reflects the importance of checking all maps of an OCT printout before making a diagnostic decision.

Figure 6

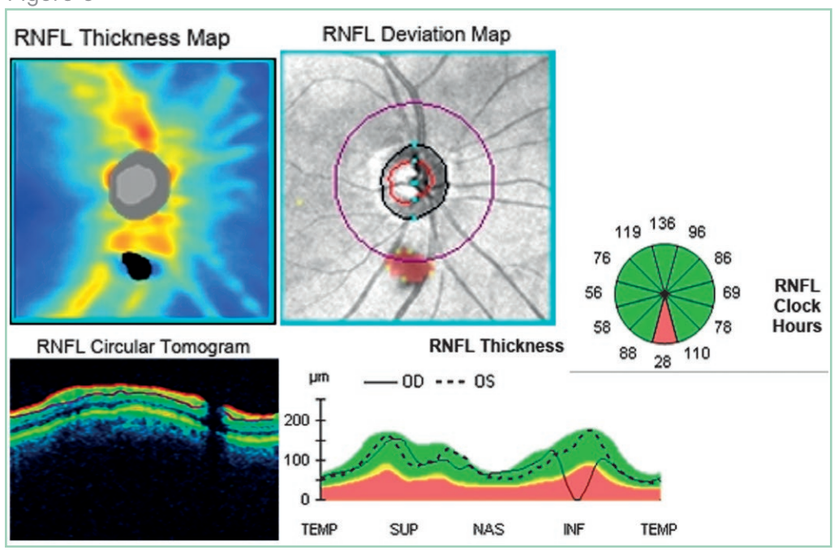

layer (MIRL) thickness, caused by a shift of retinal layer boundary placement.[8] In cases with cataract-related low SS, after cataract surgery RNFL thickness and signal strength increase by 9.3% and 24.1% respectively, regardless of the presence of glaucoma.[9]
Vitreous floaters may interfere with the laser beam, reducing the SS on the shaded area. Dense vitreous focal opacities produce shadow artifacts and may drive RNFL or MIRL measurements to zero, affecting areas relevant for analysis. (Fig. 6) In OCTA, it can masquerade as regional perfusion loss.[10]

Limitations of measurement

Normative database-related limitations. Normative databases (NDB) allow for comparison of tissue quantification to normal ranges. They include adult subjects with ethnically diverse backgrounds, but NDB currently available may not correspond to the actual physiological variation in thickness measurements due to demographic disparities within populations.[11] In fact, results cannot be strictly compared across the different instruments.
High myopia is underrepresented in most NDB, producing false positive results in a number of these patients. Specific NDB developed for high myopic eyes look promising for a more specific detection of myopic glaucoma, but they aren't commercially available yet, to the best of the author's knowledge. Similarly, a NDB is lacking for the paediatric population. On this matter, a review of paediatric normative values published in the literature has been reported.[12]

Figure 7

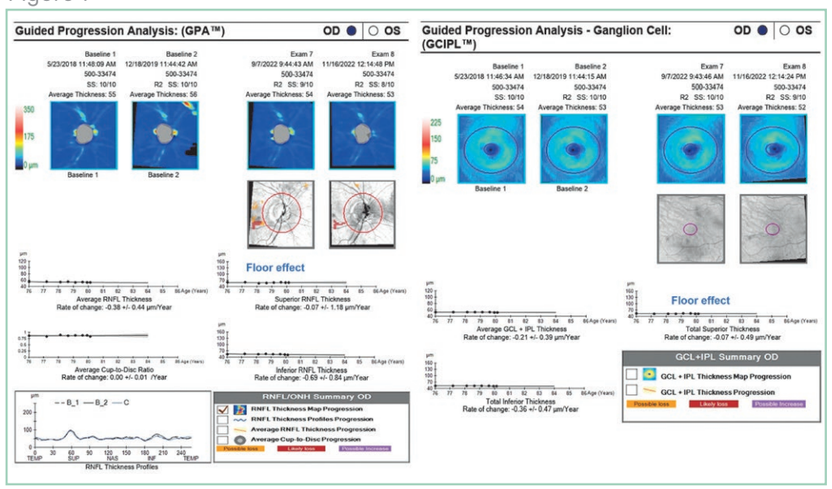

Figure 7
Floor effect on a RNFL (left) and MIRL (right) analysis after 4-year follow-up. The rate of change of superior RNFL and MIRL thickness is close to zero, due to the deep thinning of tissues already present at baseline. The rate of progression of inferior RNFL and MIRL is still quantifiable.

Anatomical and pathological pitfalls

OCT is used mainly to measure the thickness of the ocular structures under study. Glaucoma is a progressive disease, and structural thickness is reduced due to the disease itself and concomitantly, also due to ageing. Unlike perimetry, NDBs don't correct data in relation to the age of the patient. A normal subject will show a thinning of their RNFL and MIRL due to ageing. Furthermore, it has been reported a significant interaction between age and mean IOP and the rate of RNFL loss. In other words, older patients may be more susceptible to glaucomatous progression than younger patients at the same level of IOP.[13] On the long-term follow-up, normal subjects will show an estimated average RNFL thickness change of -0.54 ± 0.23 µm/year.[14] This aspect is relevant, because a glaucoma patient will accumulate a rate of progression due to the disease, to the age and their interaction. Current instruments do not allow establishing an estimation of the amount of each component in structural thinning of glaucoma patients. On the other hand, when the tissue loss is extreme, and only architectural elements like glia cells and blood vessels remain, the so-called floor effect is observed, where the limit of the OCT to measure further changes is reached beyond the variability of the instrument. This happens sooner in some regions of the RNFL and MIRL than in others, so OCT may continue to be useful for measuring changes in areas that still show some tissue sparing. (Fig. 7)
In some cases, an anatomical variation of normality can manifest itself as a suspicious change of glaucomatous value, like the split RNFL. (Fig. 8) In respect of this and other normal variations, glaucoma-like artifacts as seen on RNFL probability maps have been defined, masquerading as arcuate, widespread, and/or temporal damage.

Figure 8
Illustration of a bilateral, temporal superior split RNFL. Thinning is depicted as clusters of yellow superpixels on RNFL deviation maps of both eyes. The RNFL circular tomogram is not significantly affected, as seen in TSNIT map (black arrows). In extreme cases, these anatomical variations can masquerade as glaucoma loss.

Figure 8

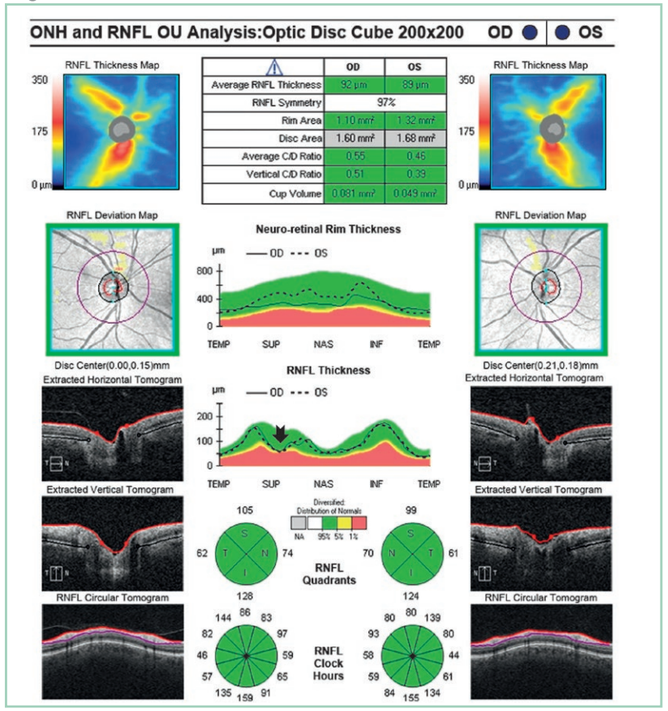

Figure 9
Illustration of myopic shifted RNFL peak. The right eye of a myopic subject shows a temporal displacement of inferior temporal peak of the RNFL, as seen on TSNIT map (black arrow). The displacement produces an apparent loss of fibers, flagged as red superpixels and red sectors in all maps, resembling glaucoma defects.

Figure 9

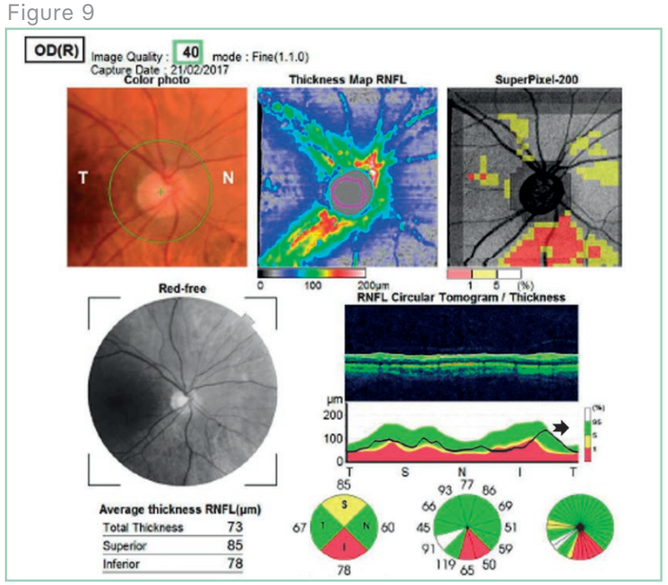

As a useful clue, these artifacts usually fail to cross the vertical midline, differently than true glaucoma defects.[15] In sum, an OCT examination should not be evaluated in a vacuum, but rather in relation to its full clinical context.

As said above, myopia may represent another tricky challenge. The myopic structures may show specific anatomical features, like a global RNFL thinning, adding uncertainty to the interpretation of OCT results. A feature associated with myopic discs is the shifted RNFL peaks. The superior and inferior temporal humps of the RNFL circle are displaced temporally compared to the NDB anatomical reference in the TSNIT map, generating an apparent loss of fibers in these areas, typically related to glaucoma. (Fig. 9) Even so, training to read OCT scans to exclude myopia related OCT artifacts and segmentation errors allows for an accurate diagnosis of glaucoma in most myopic patients.[16]

Macular pathology may interfere with glaucoma when interpreting MIRL. Over time, an increasing number of glaucoma patients show macular changes like age-related macular degeneration (AMD) or an epiretinal membrane (ERM). (Fig. 10) Any suspicious finding at MIRL must be evaluated in the context of patient's retinal examination and macular retinal thickness results to check for specific changes, mainly at the level of the outer retinal layers (AMD) and the internal limiting membrane (ERM). Finally, any other pathology affecting the retina, ONH or the visual pathways may sometimes produce puzzling findings in cases where glaucoma must be ruled out. (Fig. 11) Here it is essential to take a careful history, also performing a detailed clinical examination, to consider any pathologies that may have gone unnoticed and that could explain OCT results.

Figure 10

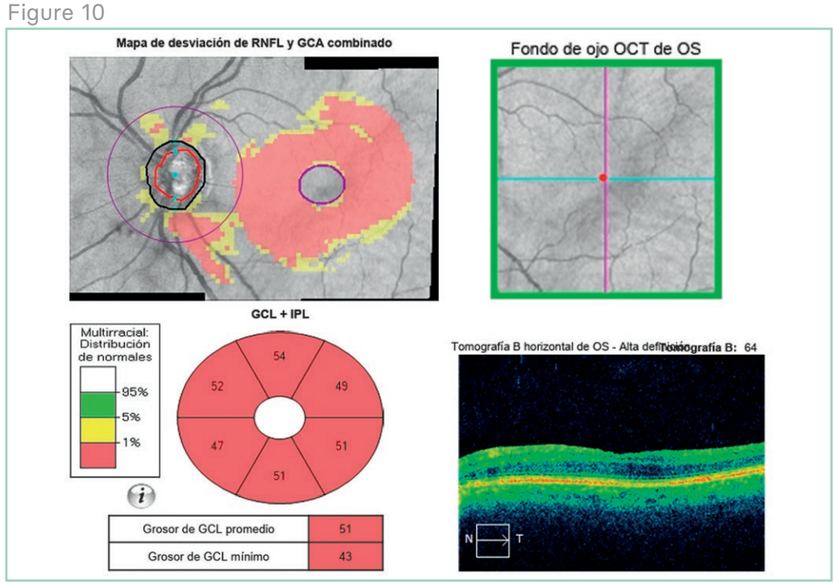

Figure 10
Combined RNFL and MIRL analysis of the left eye in a patient with temporal inferior glaucomatous loss and diffuse macular thinning, mainly due to a previous surgery of an epiretinal membrane, as seen on macular tomography.

Figure 11
Bilateral, combined RNFL and MIRL analysis in a patient with glaucomatous loss and a right homonymous hemi-macular loss related to an old posterior cerebral artery stroke.

Figure 11

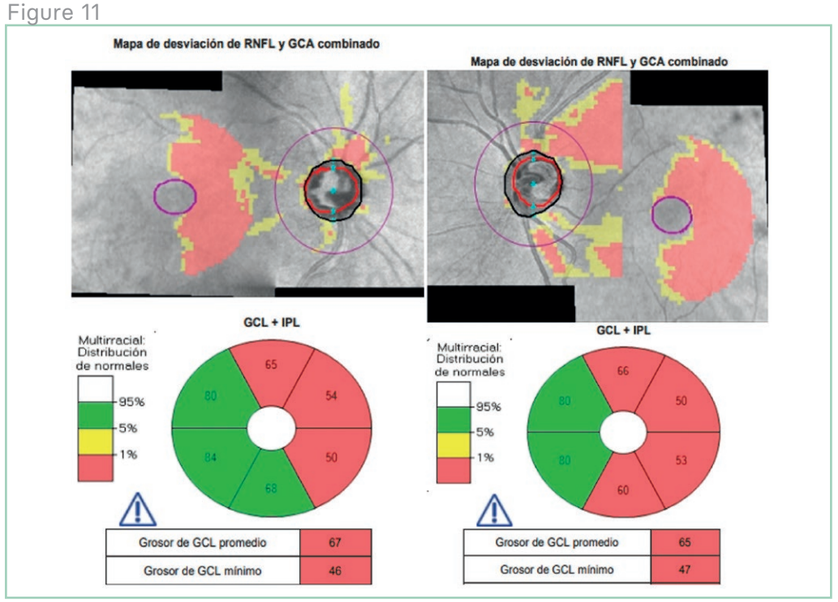

References

1. In: https://en.wikipedia.org/wiki/Image_quality#Image_quality_factors.
2. Ho J, Castro DP, Castro LC, Chen Y, Liu J, Mattox C, Krishnan C, Fujimoto JG, Schuman JS, Duker JS. Clinical assessment of mirror artifacts in spectral-domain optical coherence tomography. Invest Ophthalmol Vis Sci. 2010;Jul;51(7):3714-20. doi: 10.1167/iovs.09-4057. Epub 2010 Feb 24. PMID: 20181840; PMCID: PMC2904018.
3. Baghaie A, Yu Z, D'Souza RM. Involuntary Eye Motion Correction in Retinal Optical Coherence Tomography: Hardware or Software Solution? Med Image Anal. 2017 Apr;37:129-45. doi:10.1016/j.media.2017.02.002
4. de Kinkelder R, Kalkman J, Faber DJ, Schraa O, Kok PH, Verbraak FD, van Leeuwen TG. Heartbeat-induced axial motion artifacts in optical coherence tomography measurements of the retina. Invest Ophthalmol Vis Sci. 2011 Jun 1;52(6):3908-13. doi: 10.1167/iovs.10-6738. PMID: 21467182.
5. Anvari P, Ashrafkhorasani M, Habibi A, Falavarjani KG. Artifacts in Optical Coherence Tomography Angiography. J Ophthalmic Vis Res. 2021 Apr 29;16(2):271-86. doi:10.18502/jovr.v16i2.9091. PMID: 34055264; PMCID: PMC8126744.
6. Vizzeri G, Bowd C, Medeiros FA, Weinreb RN, Zangwill LM. Effect of signal strength and improper alignment on the variability of stratus optical coherence tomography retinal nerve fiber layer thickness measurements. Am J Ophthalmol. 2009 Aug;148(2):249-55.e1. doi:10.1016/j.ajo.2009.03.002. Epub 2009 May 9. PMID: 19427621; PMCID: PMC2848173.
7. Lee DW, Kim JM, Park KH, Choi CY, Cho JG. Effect of media opacity on retinal nerve fiber layer thickness measurements by optical coherence tomography. J Ophthalmic Vis Res. 2010 Jul;5(3):151-57. PMID: 22737349; PMCID: PMC3379912.
8. Darma S, Kok PH, van den Berg TJ, Abràmoff MD, Faber DJ, Hulsman CA, Zantvoord F, Mourits MP, Schlingemann RO, Verbraak FD. Optical density filters modeling media opacities cause decreased SD-OCT retinal layer thickness measurements with inter- and intra-individual variation. Acta Ophthalmol. 2015 Jun;93(4):355-61. doi: 10.1111/aos.12596. Epub 2014 Dec 8. PMID: 25487761.
9. Mwanza JC, Bhorade AM, Sekhon N, McSoley JJ, Yoo SH, Feuer WJ, Budenz DL. Effect of cataract and its removal on signal strength and peripapillary retinal nerve fiber layer optical coherence tomography measurements. J Glaucoma. 2011 Jan;20(1):37-43. doi:10.1097/IJG.0b013e3181ccb93b. PMID: 20179622.
10. Camino A, Jia Y, Yu J, Wang J, Liu L, Huang D. Automated detection of shadow artifacts in optical coherence tomography angiography. Biomed Opt Express. 2019 Feb 28;10(3):1514-31. doi:10.1364/BOE.10.001514. PMID: 30891364; PMCID: PMC6420267.
11. Mehta N, Waheed NK. Diversity in optical coherence tomography normative databases: moving beyond race. Int J Retin Vitr 2020 Mar 5:6:5. doi:10.1186/s40942-020-0208-5
12. Banc A, Ungureanu MI. Normative data for optical coherence tomography in children: a systematic review. Eye (Lond). 2021 Mar;35(3):714-38. doi:10.1038/s41433-020-01177-3. Epub 2020 Sep 14. PMID: 32929184; PMCID: PMC8027201.
13. Jammal AA, Berchuck SI, Thompson AC, Costa VP, Medeiros FA. The Effect of Age on Increasing Susceptibility to Retinal Nerve Fiber Layer Loss in Glaucoma. Invest Ophthalmol Vis Sci. 2020 Nov 2;61(13):8. doi:10.1167/iovs.61.13.8. PMID: 33151281; PMCID: PMC7645210.
14. Wu Z, Saunders LJ, Zangwill LM, Daga FB, Crowston JG, Medeiros FA. Impact of Normal Aging and Progression Definitions on the Specificity of Detecting Retinal Nerve Fiber Layer Thinning. Am J Ophthalmol. 2017;Sep;181:106-113. doi:10.1016/j.ajo.2017.06.017. Epub 2017 Jun 29. PMID: 28669780. Zemborain ZZ, Jarukasetphon R, Tsamis E, De Moraes CG, Ritch R, Hood DC. Optical Coherence Tomography Can Be Used to Assess Glaucomatous Optic Nerve Damage in Most Eyes With High Myopia. J Glaucoma. 2020 Oct;29(10):833-45. doi:10.1097/IJG.0000000000001631. PMID: 33006872; PMCID: PMC7534586.
15. La Bruna S, Rai A, Mao G, Kerr J, Amin H, Zemborain ZZ, Leshno A, Tsamis E, De Moraes CG, Hood DC. The OCT RNFL Probability Map and Artifacts Resembling Glaucomatous Damage. Transl Vis Sci Technol. 2022 Mar 2;11(3):18. doi:10.1167/tvst.11.3.18. PMID: 35289836; PMCID: PMC8934545.
16. Zemborain ZZ, Jarukasetphon R, Tsamis E, De Moraes CG, Ritch R, Hood DC. Optical Coherence Tomography Can Be Used to Assess Glaucomatous Optic Nerve Damage in Most Eyes With High Myopia. J Glaucoma. 2020 Oct;29(10):833-45. doi:10.1097/IJG.0000000000001631. PMID: 33006872; PMCID: PMC7534586.

Part I

Chapter 5

Optic Nerve Imaging

Francesco Oddone
Sara Giammaria

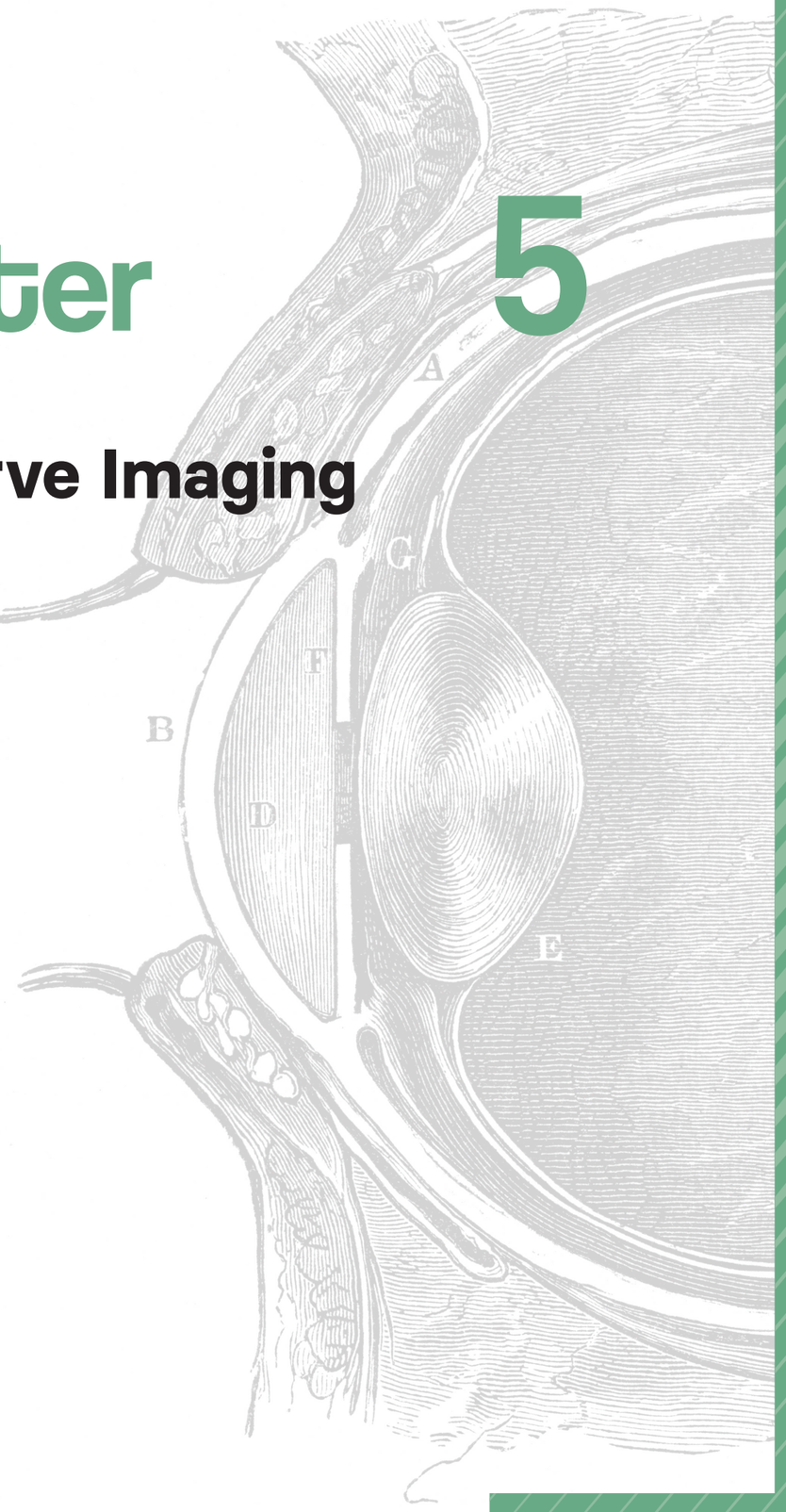

Vertical Section

5
Part I

Optic Nerve Imaging

Francesco Oddone, Sara Giammaria

Glaucoma Unit - IRCCS Fondazione Bietti, Rome, Italy
The work of the Authors is partially suported by Fondazione Roma

Optic nerve head (ONH) examination is the cornerstone of glaucoma patient examination and its imaging with OCT, together with analysis of the RNFL and macula allows for a comprehensive structural assessment and enhanced diagnosis. Compared to previous imaging technologies used to evaluate the ONH, OCT offers a more detailed, reliable, and reproducible analysis of anatomical structures, thus providing a series of parameters that can be objectively quantified.

ONH Anatomy

With ophthalmoscopy, fundus photographs and laser scanning tomography, is it difficult to consistently evaluate the disc margin. With these techniques, the disc margin is usually arbitrarily identified with the inner edge of the scleral ring, named the peripapillary ring of Elschnig, where the retinal pigmented epithelium terminates and the connective tissue of Elsching (which originates from the sclera and connects to the Bruch's membrane, BM) delimits the choriocapillaris defining the optic nerve margin. However, by comparing the clinical evaluation of the disc margin with the OCT scans of the ONH, it has been shown that a consistent anatomical structure corresponding to the disc margin could not be identified.[1] The reason for this mismatch lies in the anatomical variability around the optic disc, which depends on which of these structures protrudes most into the scleral canal, the orientation of the rim tissue and the position of the optic nerve head in relation to the macula (described by the orientation of the axis connecting the ONH and the fovea, the Fovea-to-disc axis). The OCT scans allow to reliably identify anatomical structures including the retinal pigmented epithelium (RPE) and the BM opening (BMO) in the b-scans. In particular, the latter has recently emerged as a consistent landmark within the optic nerve, thus allowing the OCT technology to consistently estimate the neuroretinal rim, using it to define the disc margin. (Fig. 1)

ONH parameters

All the OCT devices have ONH scan protocols which differ in software algorithms and dimensions of the scanned area. The existing algorithms identify the ONH margin mainly by two methods: through 3D volume scans (e.g., Cirrus, Optovue RTVue-100, Canon HS-100 OCTs) or radial scans (e.g., Spectralis OCT, Nidek RS-3000 OCT). Thereafter the reference plane to subsequently define the ONH parameters is identified: the edges of the RPE (e.g., Optovue RTVue-100, 3D Topcon OCTs) or the BMO (e.g., Cirrus and Spectralis OCTs). From the reference plane, different methods exist to estimate ONH parameters by defining: (I) the area between a parallel line set at arbitrary distance above the RPE edges (e.g, 150 µm for the Optovue RTVue-100 OCT and 120 µm of the 3D Topcon OCT), (II) the

minimum area of a surface measured between the BMO to the vitreoretinal interface (VRI) (e.g., Cirrus OCT), (III) the minimum width measured between the BMO and the internal limiting membrane (e.g. Spectralis OCT). Despite the differences in the algorithms, most of the analysis of the ONH parameters are consistently reported among the devices, with some peculiar features depending on the manufacturers. The main parameters include the rim area, the disc area, the average and vertical and horizontal cup-to-disc (C/D) ratio and cup volume and area. The values of the parameters are generally reported in summary tables (e.g., Cirrus, 3D Topcon, Optovue RTVue-100, Nidek RS-3000, Canon HS-100 OCTs). In some devices the values are compared with the reference database of the instrument thanks to a color code (green: "within normal limits", yellow: "borderline", red: "outside normal limits" and white: "above normal limits") and the values of both eyes can be displayed side by side (Fig. 2).

The neuroretinal rim thickness is reported in a Temporal-Superior-Nasal-Inferior-Temporal (TSNIT) plot (similar to the TSNIT plot of the RNFL), which also allows comparison with the reference database and between the two eyes (e.g., Cirrus OCT and Spectralis OCT) (Fig. 2A and Fig. 3). In addition, the ONH analysis of the Spectralis OCT includes the global and sectorial analyses of the neuroretinal rim and considers the inter-individual variability by adjusting the sector analysis to the Fovea-to-disc axis orientation (determined by the axis connecting the fovea to the BMO center) and splitting the superior and inferior sectors in their respective nasal and temporal portions (Garway-Heath sectors: T, TS, NS, N, NI, TI) to enhance the detection of smaller defects in these locations where most frequently the glaucoma damage occurs (Fig. 3).

Figure 1

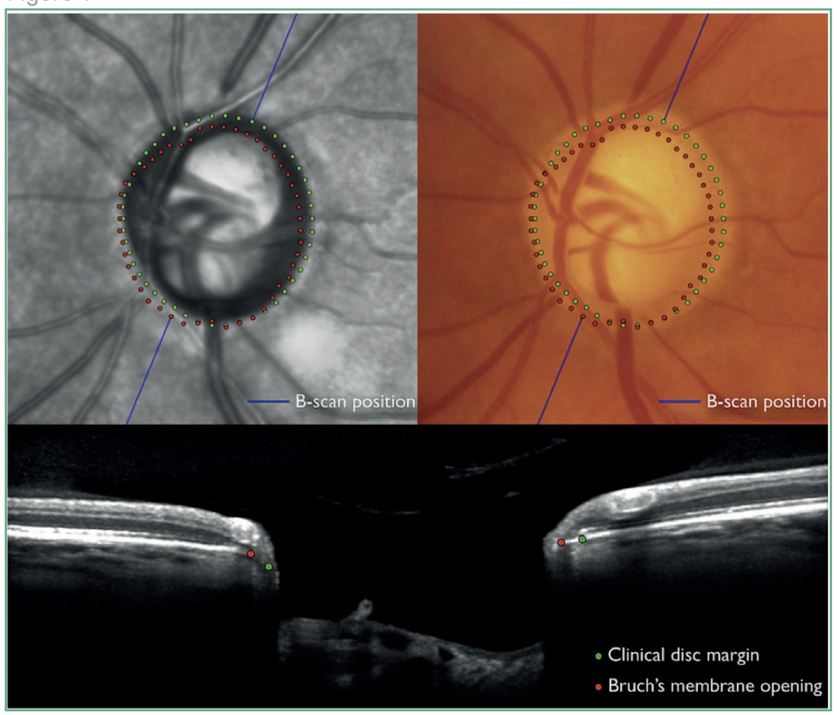

Figure 1
Mismatch between the clinical and the OCT based evaluation of the optic nerve head margin. Green dots reported on the OCT infrared (IR) image (top left) and the optic disc photograph (top right) represent the margin of the optic nerve head ophthalmoscopically determined by clinical evaluation, whereas the red dots represent the Bruch's membrane opening (BMO) evaluated by OCT. The blue line top two image represent the position of the b-scan (bottom) where the mismatch between the clinical disc margin and the BMO is also indicated. Figure reproduced with permission from Chauhan and Burgoyne 2013[13]

Figure 2

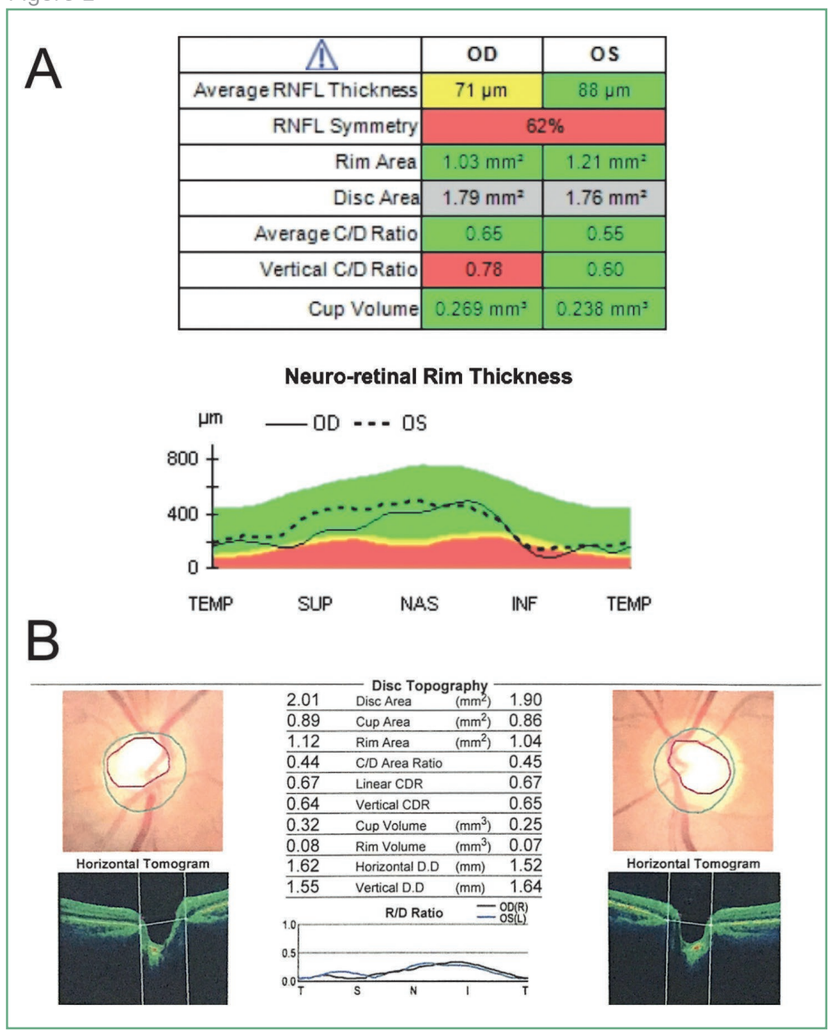

Figure 2
Examples of summary table of the ONH parameters from different devices. Comparisons of summary tables of the ONH parameters of the right and left eyes of glaucoma patients from Cirrus OCT (A) and 3D Topcon OCT (B). Both devices report common ONH parameters (e.g., Rim Area, Disc Area, Cup Volume, Vertical Cup-to-Disc Ratio). Specific ONH parameters can be found in each report (e.g., the Average C/D Ratio of the Cirrus OCT and the Horizontal and Vertical Disc Diameter of the 3D Topcon OCT). Furthermore, Cirrus displays the TSNIT plot of the neuroretinal rim thickness whereas the 3D Topcon OCT displays the TSNIT plot of the Rim-to-Cup (R/D) Ratio.

Besides the advantages offered from the OCT technology, the clinicians should be aware of the hardware and software differences existing between different devices which may give reason to differences in the reproducibility and in the diagnostic accuracy and limit the interchangeability of results from different devices. Furthermore, each device has its own reference database which differs for age, gender, ethnicity, range of refractive error and number of subjects included. Therefore, color code classifications may disagree from device to device. Finally, the quality of the acquired images and the possible presence of segmentation artifacts or anatomical abnormalities of the optic nerve (e.g., vitreopapillary tractions) should never be underestimated, as they can potentially lead to erroneous classifications and misdiagnosis.

Identifying glaucoma damage of the ONH

In the landscape of available ONH parameters, the rim area and the vertical C/D ratio perform considerably better than other ONH parameters (e.g., disc area, cup volume) and are comparable to the RNFL and the inner macular layers thickness in detecting glaucoma, with increasing diagnostic ability with increasing severity of the disease.[2–4]

Furthermore, the rim area has also shown to have the highest diagnostic accuracy, compared to average and vertical C/D and cup volume, independently from the disc size.[5]

The neuroretinal rim measurements are characterized by high reproducibility[6] and an excellent structure-function relationship.[7,8] The neuroretinal rim has shown diagnostic accuracy similar to or even higher than the RNFL in patients with glaucoma. In the early stage of the disease, the neuroretinal rim may perform better than the RNFL both in the global and sectoral analysis,[9,10] with the infero-temporal sector showing the highest diagnostic ability.[10] Similar to other ONH parameters, the diagnostic performance of the neuroretinal rim increases as the glaucoma becomes more advanced.

The neuroretinal rim analysis may also be particularly helpful in analyzing myopic eyes in which the tilting of the disc or the presence of peripapillary atrophy may hinder the RNFL evaluation. In these cases, evidence exists that the neuroretinal rim has better diagnostic performance than RNFL in early detection of glaucoma in myopic eyes and has fewer false-positive results when evaluating tilted optic discs.[11] However, the influence of the disc size should not be underestimated in these cases, since it has also been shown that for discs with a BMO area >2.5 mm^2 the diagnostic accuracy of the BMO becomes comparable to that of the RNFL.[12]

Conclusions

Thanks to the high-resolution imaging of the optic nerve head, OCT improved the assessment and accurate measurement of anatomical structures crucial to glaucoma diagnosis. Despite the evidence of the remarkable ability of the ONH parameters to correctly discriminate between glaucoma and healthy subjects, this type of analysis still has some limitations. Therefore, the integrative use of the ONH parameters with the RNFL and macular layers remains advisable.

Figure 3

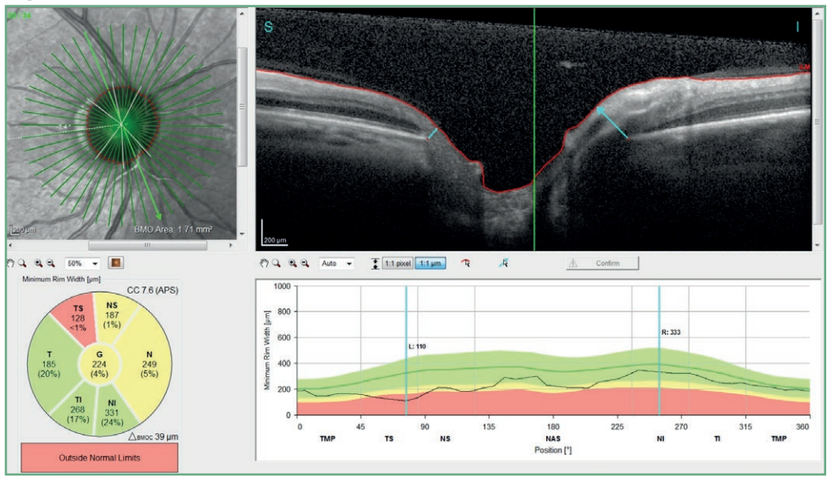

Figure 3
Analysis of the neuroretinal rim with Spectralis OCT of the right eye of a glaucoma patient. The Infrared image of the optic nerve head with the radial scan protocol (green lines and the Bruch's membrane opening (BMO) (red dots) is shown in the top left panel. In the top right panel, the b-scan is shown. The red line represents the internal limiting membrane (ILM) and the two red dots the position of the BMO margin. The cyan arrows represent the minimum rim width (MRW), namely the neuroretinal rim thickness. In the bottom the sectorial (temporal-superior: TS, temporal: T, temporal-inferior: TI, nasal-inferior: NI, nasal: N and nasal-superior: NS) and global (G) values of the BMO-MRW are shown with the color code and the T, TS, NS, N, NI, TI thickness plot.
The analysis shows a reduction of the neuroretinal rim in the temporal-superior portion of the ONH in this patient.

References

1. Strouthidis NG, Yang H, Reynaud JF, et al. Comparison of clinical and spectral domain optical coherence tomography optic disc margin anatomy. Invest Ophthalmol Vis Sci. 2009;50(10):4709-18. doi:10.1167/iovs.09-3586
2. Sung KR, Na JH, Lee Y. Glaucoma diagnostic capabilities of optic nerve head parameters as determined by Cirrus HD optical coherence tomography. J Glaucoma. 2012;21(7):498-504. doi:10.1097/IJG.0b013e318220dbb7
3. Shin HY, Park HYL, Jung Y, Choi JA, Park CK. Glaucoma diagnostic accuracy of optical coherence tomography parameters in early glaucoma with different types of optic disc damage. Ophthalmology. 2014;121(10):1990-97. doi:10.1016/j.ophtha.2014.04.030
4. Michelessi M, Lucenteforte E, Oddone F, et al. Optic nerve head and fibre layer imaging for diagnosing glaucoma. Cochrane Database Syst Rev. 2015;2015(11):CD008803. doi:10.1002/14651858.CD008803.pub2
5. Sato S, Ukegawa K, Nitta E, Hirooka K. Influence of Disc Size on the Diagnostic Accuracy of Cirrus Spectral-Domain Optical Coherence Tomography in Glaucoma. J Ophthalmol. 2018;2018:5692404. doi:10.1155/2018/5692404
6. Reis ASC, Zangalli CES, Abe RY, et al. Intra- and interobserver reproducibility of Bruch's membrane opening minimum rim width measurements with spectral domain optical coherence tomography. Acta Ophthalmol. 2017;95(7):e548-e555. doi:10.1111/aos.13464

7. Danthurebandara VM, Sharpe GP, Hutchison DM, et al. Enhanced structure-function relationship in glaucoma with an anatomically and geometrically accurate neuroretinal rim measurement. Invest Ophthalmol Vis Sci. 2014;56(1):98-105. doi:10.1167/iovs.14-15375
8. Pollet-Villard F, Chiquet C, Romanet JP, Noel C, Aptel F. Structure-function relationships with spectral-domain optical coherence tomography retinal nerve fiber layer and optic nerve head measurements. Invest Ophthalmol Vis Sci. 2014;55(5):2953-62. doi:10.1167/iovs.13-13482
9. Chauhan BC, O'Leary N, AlMobarak FA, et al. Enhanced detection of open-angle glaucoma with an anatomically accurate optical coherence tomography-derived neuroretinal rim parameter. Ophthalmology. 2013;120(3):535-43. doi:10.1016/j.ophtha.2012.09.055
10. Michelessi M, Riva I, Martini E, et al. Macular versus nerve fibre layer versus optic nerve head imaging for diagnosing glaucoma at different stages of the disease: Multicenter Italian Glaucoma Imaging Study. Acta Ophthalmol. 2019;97(2):e207-e215. doi:10.1111/aos.13930
11. Rebolleda G, Casado A, Oblanca N, Muñoz-Negrete FJ. The new Bruch's membrane opening – minimum rim width classification improves optical coherence tomography specificity in tilted discs. Clin Ophthalmol. 2016;10:2417-25. doi:10.2147/OPTH.S120237
12. Park DH, Kook KY, Kang YS, Piao H, Sung MS, Park SW. Clinical Utility of Bruch Membrane Opening-Minimum Rim Width for Detecting Early Glaucoma in Myopic Eyes. J Glaucoma. 2021;30(11):971-80. doi:10.1097/IJG.0000000000001934
13. Chauhan BC, Burgoyne CF. From clinical examination of the optic disc to clinical assessment of the optic nerve head: a paradigm change. Am J Ophthalmol. 2013;156(2):218-227.e2. doi:10.1016/j.ajo.2013.04.016

Part I

Chapter 6

Peripapillary RNFL

Marta Pazos

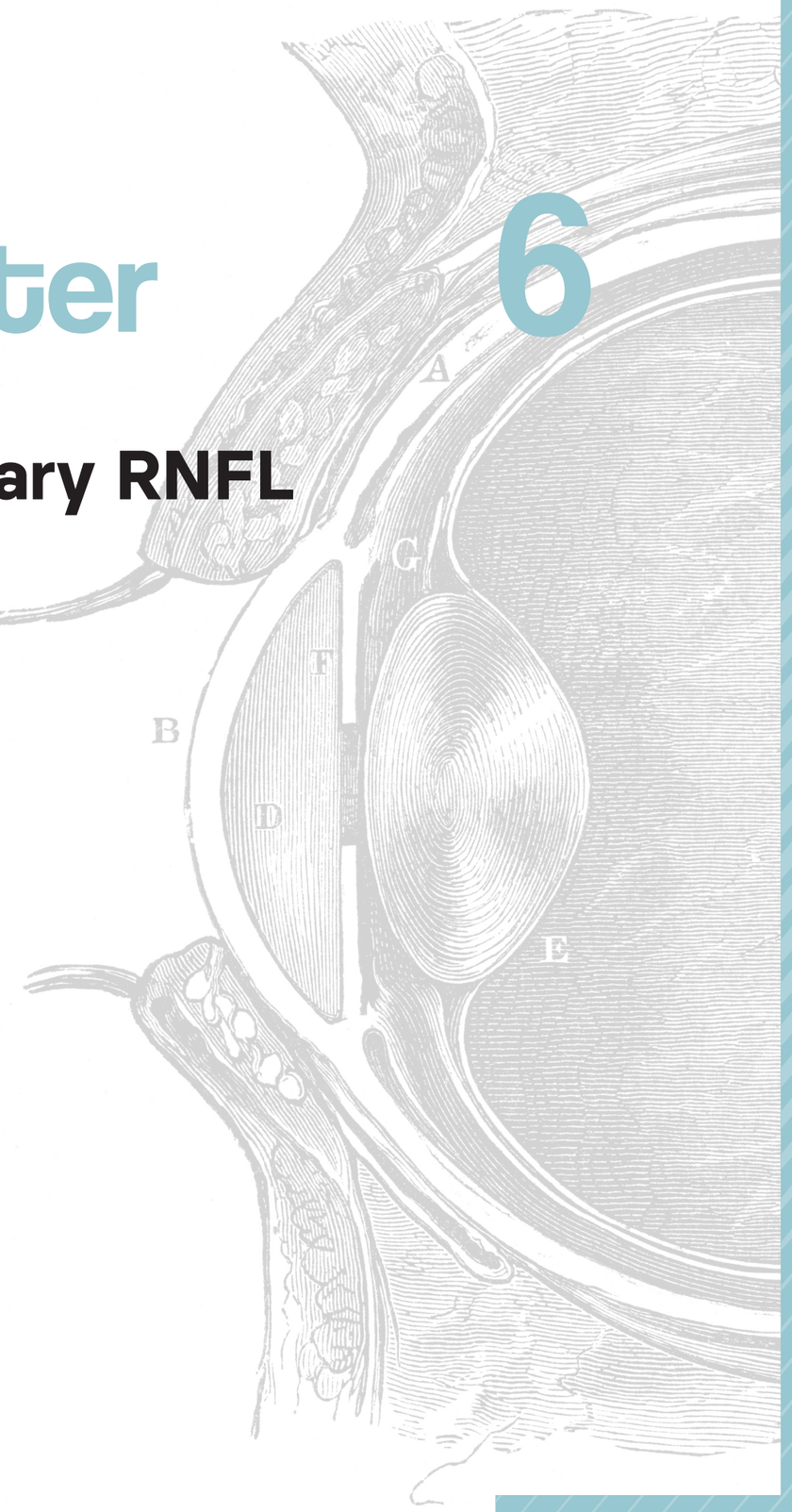

Vertical Section

Peripapillary RNFL

Marta Pazos

Glaucoma consultant & Head of the Ophthalmic Surgery Section
Institute of Ophthalmology. Hospital Clínic Barcelona
Barcelona, Spain

Anatomy of the OCT pRNFL target structures relevant to glaucoma care

The anatomy of the retinal nerve fiber layer (Henle's layer) has a characteristic arcuate pattern (see Fig. 1). Retinal ganglion cells (RGCs) in the temporal retina project their axons to the superior and inferior quadrants of the optic disc so as to bypass the central macula. As a result, neighboring RGCs on either side of the temporal horizonal raphe project to opposite poles of the optic nerve head, explaining the pattern of many common glaucomatous visual field defects. Due to structural characteristics of the lamina cribrosa, the inferior temporal and superior temporal poles of the optic disc are the most susceptible to damage, explaining why the corresponding regions of the peripapillary retinal nerve fiber layer (pRNFL) are often affected earliest in glaucoma.[1]

Statistic behind the databases

Normal databases

Reference normative databases include normal subjects of different age ranges and are different for each instrument. Actually, most of these databases are built with less than 300 patients and have a limited representation of refractive errors, extreme optic discs, ethnical groups or age distribution. It is important to take into account the characteristics of the patients included in each of them so as to ensure its clinical application in a specific patient. For more details of the normative databases of the most used OCT instruments see table 1.

Figure 1

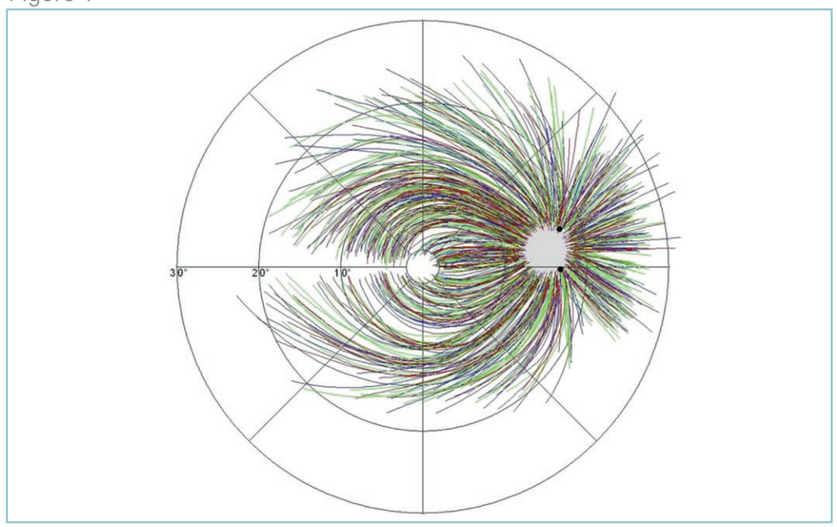

Figure 1
Schematic diagram of the retinal nerve fiber layer anatomy (reprinted from Jansonius et al).

Color-coded classification

The color-coded classification values of pRNFL are obtained from a comparison with the built-in age-adjusted normative database. OCT imaging instruments typically provide three potential outcomes depending on their probability of significance limits: 1) "within normal limits", or green (between the 95thand 5th normative percentile); 2) "borderline" or yellow (between 5th-1st percentile); and 3) "outside normal limits", or red (below the 1st percentile). No imaging device provides a clinical diagnosis but just a statistical result, based on comparison with the corresponding reference database of healthy eyes. Therefore, an interpretation of the result in the context of all clinical data is mandatory.

Red and green disease

Glaucoma imaging results can be easily misunderstood without a good understanding of the underlying technology limitations. This can lead to false positive results and diagnosis in which OCT mistakenly indicates that something is abnormal (red disease).[2] Similarly, apparently "normal" results do not always necessarily mean "healthy", and sometimes OCT data shows no signs of abnormality, despite clinical evidence of disease (green disease).

Table 1

Instrument	Spectralis (Heidelberg)	Cirrus (Zeiss)	RTVue (Optovue)	Triton (Topcon)
System	SD-OCT	SD-OCT	SD-OCT	SS-OCT
Recommended Signal Strength (SS)	>15/40	> 6/10	>30/100	>60/160
Scan speed	4*104 scans/seg	2,7*104 scans/seg	2,6*104 scans/seg	1,8*104 scans/seg
Normative database	330 subjects with ethnic composition representative of US population Age range: 20-90 yo Refraction: +6D to – 6D	≅ 280 subjects, predominantly european descent Age range: only 31> 70 yo; only 3 patients >80 yo Refraction: +8D to – 12D	≅ 250 subjects european descent	399 subjects, different ethnicities
pRNFL measurements • **How?** • **Best parameter**	4 sect//6 sect[#] + Avg Avg> I > S	4 sect//12 sect[&] + Avg Avg > I > S	2 sect//8 sect[$] + Avg Avg > I > S	4 sect//12 sect[&] + Avg Avg > I > S

Table 1
Technical characteristics of the most used commercially available OCT instruments and the RNFL parameters measured. D: Diopters; SD-Spectral Domain; SS-Swept source, Avg: average thicknesss; I: inferior thickness; S: superior thickness; yo: years old; pRNFL: peripapillary retinal nerve fiber layer. [#]Spectralis divides peripapillary area in 4 (ISNT) and 6 sectors (superior temporal, superior nasal, inferior temporal, inferior-nasal, temporal and nasal; [$]RTVue divides de same área in two (superior and inferior) o in 8 sectors (divides in two also the temporal and nasal regions). [&]Cirrus and Triton, although with different protocols have the same 4 and 12 sectors (hourly distribution).

Working principles and image acquisition

OCT is based on interferometry. Most OCT platforms provide RNFL thickness values at a fixed distance away from the optic nerve (3.46 -mm-diameter, circular, cross-sectional thickness centered around the optic nerve). This circle is then "unrolled" and showed as a horizontal scan, in which the different layers are displayed in a single shot. Based on the amount of light reflected between the outer edge of the RNFL and the internal limiting membrane (ILM), the thickness of the RNFL is measured. Thickness measurements are often shown in a TSNIT (temporal, superior, nasal, inferior, temporal) orientation and are compared to age-matched controls. In a healthy eye, the RNFL thickness profile presents a characteristic "double hump" configuration. Current instruments are spectral domain (SD) and Swept-source (SS) systems. Their technical, software and reference database characteristics vary; for this reason, values measured with different OCT systems are not interchangeable. For exemple, RNFL average thickness can vary between 90.8 -105.5 microns among different manufacturers.[3] See Table 1 for a summary of the technical characteristics of the most widely used OCT instruments.

Image quality

The clinician should assess the quality of the image and segmentation analysis and judge whether the reference database is relevant for the particular patient. Quality is crucial to obtain reliable measurements of the different structures.

Signal strength (SS)

Signal strength is one of the most important ways of assessing quality. Each instrument has its own minimal recommended signal strength values (see table 1 for specific information for the most used OCT instruments). There are several situations that can reduce SS, like low visual acuity, presence of lens opacities and/or underlying myopia.[4] Low SS has an impact in the measurements obtained, often leading to thinner thickness values.[5] The lower the SS, the lower the thickness and this has shown to have greater impact in advanced glaucoma.[6] For all this reasons, images with insufficient SS should be disregarded.

Figure 2

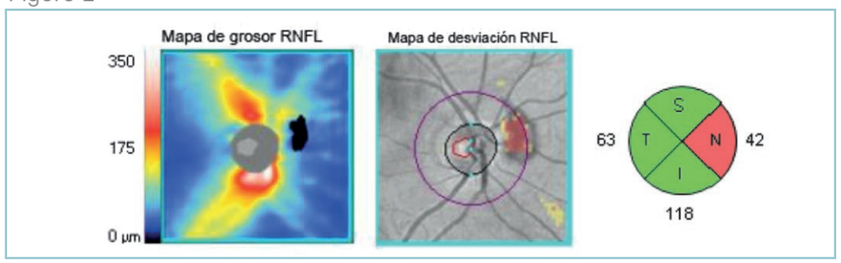

Figure 2
Example of an artifact in a pRNFL capture. In this case a posterior vitreous detachment is causing a posterior shadow in the measurement circle that induces a false thinning of the nasal sector.

Artifacts

Imaging artifacts and software errors when measuring pRNFL are quite common (between 15 and 46% depending on the studies),[7,8] and appear more often in eyes that are highly myopic or have tilted nerves. Even images with significant artifacts can have normal SS. The most frequent artifacts are: decentration, posterior vitreous detachment, anterior RNFL misidentification, peripapillary atrophy associated error, incomplete segmentation, motion artifacts or cut-edge images.

Deviation and thickness maps are very useful to check a correct segmentation and rule out artifacts. In cases of areas of RNFL of 0 or close to 0 or in when black areas are present in the deviation map, an artifact is very likely and needs to be suspected. When occurring at the level of the scan circle, they can have a dramatic impact in RNFL measurements, therefore images with artifacts must not be considered (see Fig. 2).

OCT pRNFL in diagnosis

Peripapillary RNFL has still not been overcome by any other isolated OCT parameter. Typically changes in this layer appear years before functional damage as detected by visual field testing:[9] this, together with its excellent diagnostic accuracy (Area under the curve greater than 0.9)[10] helps detecting glaucoma at an earlier stage. However, OCT pRNFL doesn't always agree with clinical examination in diagnosing glaucoma,[11] and has only moderate agreement with visual field testing. It is important to have in mind that OCT on its own does not provide a clinical diagnosis of glaucoma, but a statistical deviation from a reference database.[12] Careful interpretation and combination with other clinical data is mandatory to make a proper diagnosis. See Figure 3 for an OCT report of a patient with glaucoma showing the most important aspects.

OCT pRNFL parameters

Peripapillary RNFL discriminative ability is especially good in mild to moderate glaucoma,[13] and the best diagnostic parameters are average and inferior pRNFL thickness. Its diagnostic performance is not as good in advanced glaucoma. Changes in the temporal inferior area of the RNFL thickness profile (TSNIT profile) are very suggestive of glaucoma.

OCT pRNFL deviation/thickness maps

RNFL wedge defects have been shown to be very characteristic of glaucoma. The gold standard test for its evaluation is red-free retinography,[14] but it requires pupilar dilation and clear media. On the other hand, OCT deviation or probability maps are infrared *en face* images in which yellow or red super pixels are superposed after comparing the patient pRNFL to the reference database (see Fig. 3 C and D and Fig. 4)[15] without necessarily needing dilation. When this comparison is made, the superpixels distribution (or the colder colors in the thickness map) has the characteristic wedged-shape, with the vertex at the disc level following the RNFL trajectory, towards the macula. They are more frequently seen inferior temporally followed by the superior temporal area of the disc. In the optic nerve, these maps have achieved the same diagnostic ability than pRNFL thickness, showing glaucomatous damage can be overlooked if we only look at sectors or global indices.[16] Additionally, this topographical analysis can help distinguishing glaucomatous damage in myopes or tilted discs.[17]

Figure 3

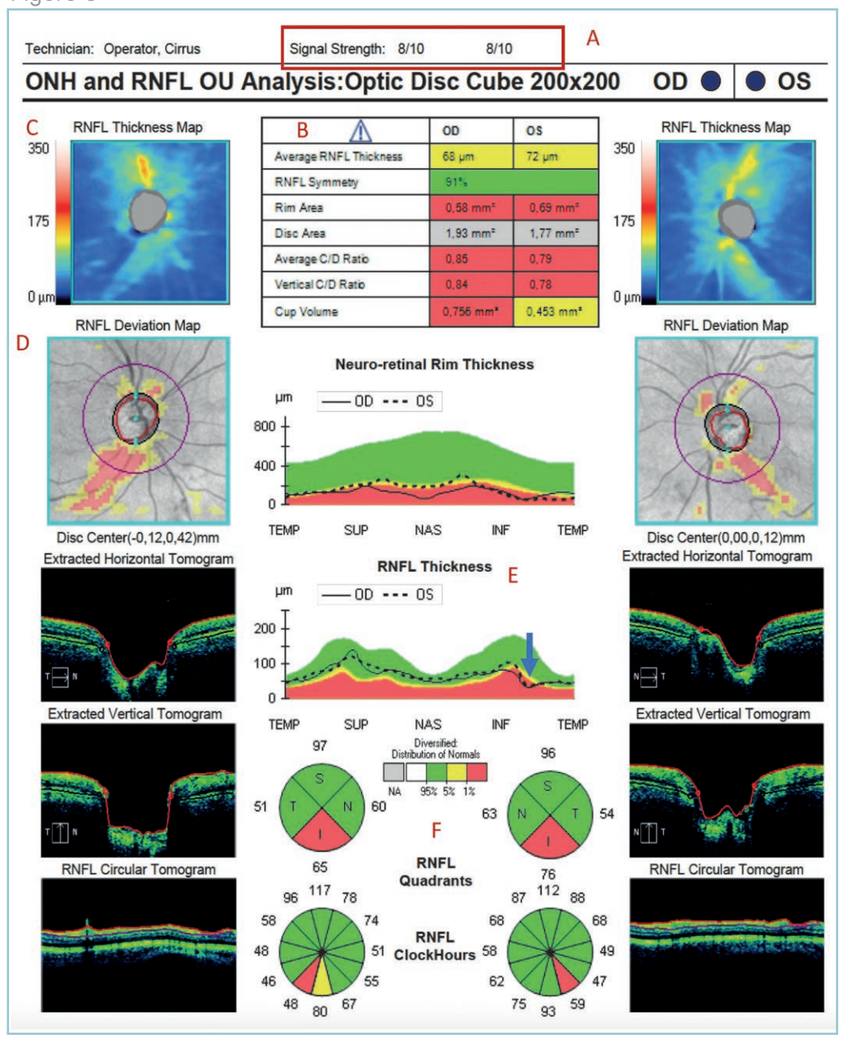

Figure 3
OCT report showing disc and pRNFL parameters in a glaucomatous patient. A: Signal Strength (SS); B: Global indices and its comparison with a normal database showing a borderline average RNFL thinning in both eyes (yellow) C: RNFL Thickness map showing an inferior wedge defect; D: RNFL Deviation map (or probability map) showing the same inferior thinning in red. E: RNFL Thickness profile in which there is a clear thinning in the temporal inferior region (blue arrow); F: RFNL quadrant analysis showing an statistically significant characteristic thinning of the inferior quadrant of both eyes.

Combining OCT RNFL with GCL parameters

Although pRNFL measurements are the most used parameters, OCT macular parameters can be better in certain situations (see macular OCT chapter for further information). Currently, evidence suggests that pRNFL and macular measurements are complimentary, and that using multiple parameters in combination enhances the sensitivity diagnosing the disease.[18] For this reason, and considering that recent instruments can acquire images in less than 30 seconds, it is recommended to take peripapillary and macular imaging in every glaucomatous patient undergoing OCT. Some commercially available instruments can even make compositions showing peripapillary and macular images and measurements at the same time.

OCT pRNFL in progression

Glaucoma is a progressive disease. Although visual field testing remains the gold standard for assessing deterioration of the glaucomatous neuropathy, the functional evaluation has several limitations like the longer duration of the test and its subjective nature. Additionally, changes in structure occur normally earlier in time, which could potentially lead to earlier detection.

Significant amount of change in OCT RNFL parameters

It is important to assess reproducibility of a determined device and parameter before assessing what is a significant variation. Any instrument variability is defined as the changes in the measuring device that might account for normal differences in two or more measurements. For OCT RNFL variability, changes up to 5 microns for average thickness, 7 microns for temporal, superior and inferior quadrants, and 8 microns in the inferior region are considered normal[19,20] (Table 2).

Table 2
Normal variability and changes related to aging of the most used OCT pRNFL parameters.

Table 2

Signficant amount of change	Change related to aging
- 5 microns (global)	- 0.52 microns /year (global)
- 7 microns (temporal, superior, inferior)	- 1.35 microns/year (superior)
- 8 microns (nasal)	- 1.25 microns/year (inferior)

Changes related to aging

Even in healthy patients, there is a normal decline in pRNFL thickness over time, secondary to the physiological loss of ganglion cells and its axons with aging. For average pRNFL, this normal change related to aging is approximately -0.52 microns per year. In the superior and inferior quadrants this normal thinning is larger, of -1.35 microns/year and -1.25 microns/year, respectively[19] (Table 2).

Detecting OCT pRNFL change over time

OCT pRNFL is the most used parameter to evaluate structural progression. It has high sensitivity in detecting progression in early glaucoma but not so much in advanced glaucoma, because of the instrument "floor effect" (see below). In general, the most recommended way to assessing change over time is using linear regression or "trend analysis". This approach is intuitive and simple, and is able to detect most eyes with clinically significant progression, being the most important parameter to start treatment. It is important to have enough test to obtain a reliable rate of progression, normally it is recommended to have at least 5 tests in 2 years.
Most commercial imaging devices have specific software for quantifying glaucomatous progression, including rate of progression (see Fig. 5). These results may serve as additional tools for the assessment of glaucomatous progression but need careful interpretation in conjunction with other tests and patient circumstances. High quality baseline images are important, as well as checking the quality of the test series before including the software output in the assessment of the patient. Most commercially available software does not compensate for aging, therefore statistically significant slopes do not necessarily represent true glaucomatous progression.

Figure 4

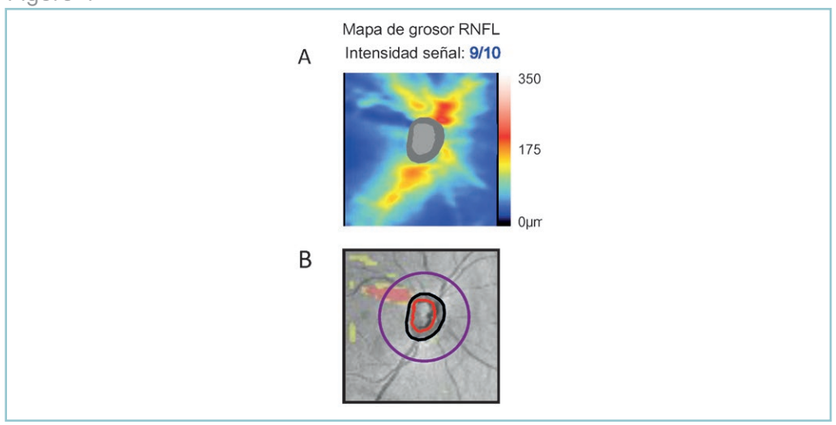

Figure 4
Deviation map and B) Probability map of the same patient showing a characteristic wedge shape of a supero-temporal glaucomatous defect.

Because of the physiological decline in pRNFL thickness, and the absence of age-compensation, if we wait enough time eventually all our patients will have a significant negative slope (false positives). Studies with different cut-outs for definition of clinically significant progression have suggested that rates of structural progression faster than -1 micron per year for pRNFL average thickness (which corresponds to the significant negative slope relative to the 5% lower limit) are probably clinically significant. See figure 5 for a clinical case showing significant structural progression.

Future directions for OCT pRNFL

Artificial intelligence (AI) in ophthalmology has been a fast-expanding field of interest in Ophthalmology and there are already several algorithms using OCT pRNFL. In the future, AI will facilitate not only diagnosis of glaucoma, but also the detection of disease progression and even estimate those patients at highest risk of visual deterioration.

OCT-based deep learning (DL) models using conventional 2D B scans and 3D volumetric scans have yielded excellent accuracy.[21] Interesting research has also been able to estimate visual field appearance directly from OCT imaging, without the actual need of performing a functional testing.[22] Other groups have published models to accurately identify glaucoma progression from longitudinal OCT dada (2 visits) with good performance.[23]

Figure 5

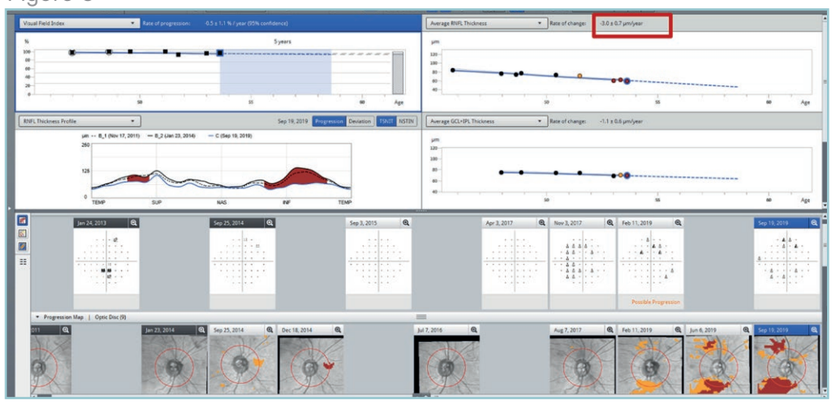

Figure 5
Glaucoma Progression analysis evaluation report over time of a 53 year-old female with ocular hypertension and escalation of hypotensive drops over time and IOP of 22 mmHg in the last visit. During the follow up, there is a clinically significant structural rate of change of -3 microns per year of the average rate of progression (see red square in the top right), due to a significant thinning of the inferior and superior regions (see deviation maps at the botton right).

References

1. Jansonius NM, et al. Exp Eye Res. 2012.
2. Chong GT, Lee RK. Glaucoma versus red disease: imaging and glaucoma diagnosis. Curr Opin Ophthalmol. 2012 Mar;23(2):79-88. doi: 10.1097/ICU.0b013e32834ff431. PMID: 22262083.
3. Pierro L, et al. Invest Ophthalmol Vis Sci. 2012;53:5912-20.
4. Lee R, Tham YC, Cheung CY, et al. Factors affecting signal strength in spectral-domain optical coherence tomography. Acta Ophthalmol. 2018;96(1):e54-e58.
5. Samarawickrama C, Pai A, Huynh SC, Burlutsky G, Wong TY, Mitchell P. Influence of OCT signal strength on macular, optic nerve head, and retinal nerve fiber layer parameters. Invest Ophthalmol Vis Sci. 2010;51(9):4471-75.
6. Yohannan J, Cheng M, Da J, et al. Evidence-Based Criteria for Determining Peripapillary OCT Reliability. Ophthalmology. 2020;127(2):167-76.
7. Liu Y, Simavli H, Que C, Rizzo JL et al. Patient characteristics associated with artifacts in Spectralis Optical Coherence Tomography Imaging of the Retinal Nerve Fiber Layer in glaucoma. Am J ophthalmol. 2015 Mar;159(3):565-76.
8. Asrani S, Essaid L, Alder BD, Santiago-Turla C. Artifacts in Spectral-Domain optical coherence tomography mesurements in glaucoma. JAMA Ophthalmology. 2014 Apr 1;132(4).
9. Kuang TM, et al. Ophthalmology 2015.
10. Ervin AM, et al. 2012.
12. European Glaucoma Society Guidelines. 5th Edition.
13. Bussel I, BJO 2013.
14. Park JH, Yoo C, Kim YY. Localized Retinal Nerve Fiber Layer Defect Location among Red-free Fundus Photographs, en Face Structural Images, and Cirrus HD-OCT Maps. J Glaucoma. 2019;28(12):1054-60.
15. Kim H, Park HM, Jeong HC, et al. Wide-field optical coherence tomography deviation map for early glaucoma detection. British Journal of Ophthalmology. 2021;107(1):49-55.
16. Hood DC, Merchior B, Tsamis E, Liebmann, JM, De Moraes CG. Did the OCT Show progression since de te last visit? J Glaucoma 2021;30(4):E134-145.
17. Baek SU, Kim KE, Kim YK, Prk KH, Jeoung JV. Development of Topographic scoring system for identifying glaucoma in myopic eyes: a spectral-domain OCT sgudy. Ophthalmology. 2018;125(11):1710-19.
18. Mwanza JC, Warren JL, Budenz DL. Utility of combining spectral domain coherence tomography structural parameters for the diagnosis of early glaucoma: a mini-review. Eye Vis. 2018;51(1):9.
19. Leung CK, et al. Ophthalmology 2009;116(7):1257-63.
20. Mwanza JC, Invest Ophthal Vis Sci 2010;51(1):5724-30.
21. Wu JH, Nishida T, Weinreb RN, Lin JW. Performances of machine learning in detecting glaucoma using fundus and retinal optical coherence tomography images: a meta-analysis. Am J ophthalmol 2022;237:1-12.
22. Hemmelings R, Elen B, Barbosa-Breda J, Bellon B, Blaschko MB, De Boever P, Stalmans I. Pointwise visual field estimation from optical coherence tomography in glaucoma using deep learning. Trans Vis Sci Tech 2022;11(8):22.
23. Mariottoni EB, Datta S, Shigueoka LS, Jammal AA, Tavares IM, Henao R, et al. Deep learning-assisted detection of glaucoma progression in spectral-domain OCT. Ophthalmol Glaucoma 2023;6(3):228-38.

Part I

Chapter 7

Macular Optical Coherence Tomography

Chiara Posarelli
Michele Figus

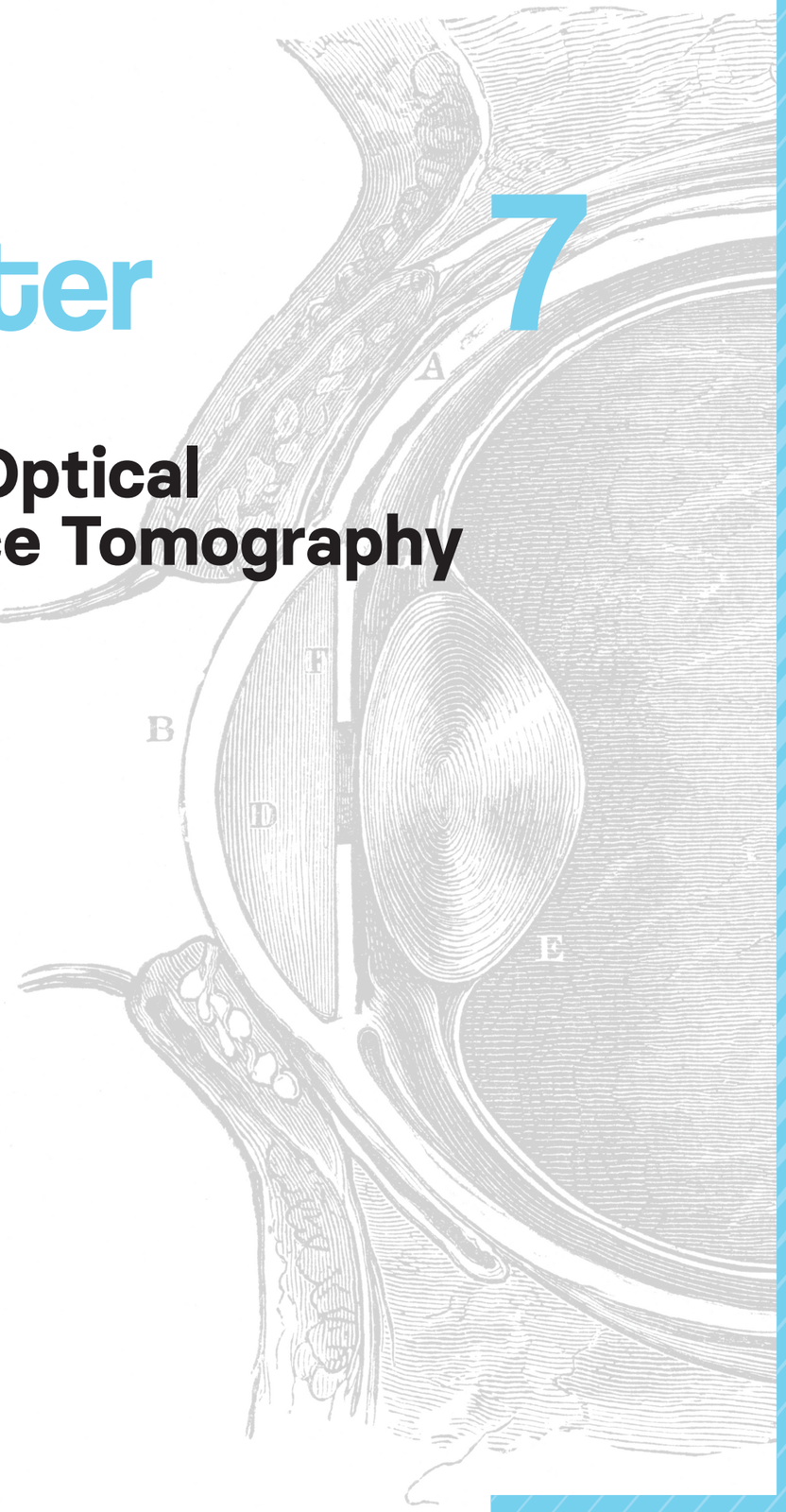

Vertical Section

Macular Optical Coherence Tomography

Chiara Posarelli, Michele Figus

Department of Surgical, Medical, Molecular Pathology and Critical Care Medicine, University of Pisa, Pisa, Italy
Azienda Ospedaliero Universitaria Pisana, U.O. Oculistica Universitaria, Pisa, Italy

Introduction

Timely detection and management of glaucoma stand as pivotal endeavors to safeguard visual health. In this pursuit, advanced imaging technologies have emerged as useful allies for clinicians, and among them, Macular Optical Coherence Tomography (OCT) excels as a beacon of precision and insight. Macular OCT has evolved into a versatile imaging modality with applications extending beyond its initial scope. In the context of glaucoma, abnormalities in the retinal nerve fiber layer (RNFL) may indicate the early stages of disease before other observable changes manifest. Nevertheless, alterations in the appearance during examinations may not consistently be evident or may lack specificity.[1]

Macular OCT operates on the principles of low-coherence interferometry, it employs a near-infrared light source, and analyzes their back-scattering patterns to construct high-resolution cross-sectional images of the retina and optic nerve. This method enables swift imaging of living tissue with micron-level precision, reaching depths of several millimeters, visualizing individual retinal layers with exceptional clarity. In addition, with the introduction of spectral domain modalities, OCT utilizes a spectrometer to enhance scanning speed, offering the advantage of quicker image acquisition compared to time domain OCT. Finally, Swept-Source OCT (SS-OCT) scans through a narrow range of wavelengths, delivering the greatest axial depth, rapid image capture, and optimal signal-to-noise ratios. These recent techniques enable more detailed imaging within a shorter time. This precision is particularly relevant when assessing the macula in the context of glaucoma, where subtle structural changes may hold crucial diagnostic information.[2]

Anatomy of the Macula in Glaucoma

Glaucoma diagnosis mostly relays on ONH appearance, but overall macular thickness (the macular region contains a high concentration of more than 50% of retinal ganglion cells), asymmetry between the eyes, and changes over time can serve as valuable indicators. Additionally, observable arcuate patterns of RNFL loss may extend from the macula towards the optic nerve head.[2]
Early in the progression of glaucoma, damage to the ganglion cell complex (GCC) can occur, leading to identifiable variations in its thickness.[2,3] GCC and inner plexiform layers (IPL) represent respectively the sites of the retinal ganglion cell bodies and dendrites.
Precisely delineating individual macular layers, still represents a challenge (Fig. 1); consequently, OCT measurements for macular analysis are typically presented either as the combined ganglion cell and inner plexiform layers (GCIPL) or as the ganglion cell complex, which additionally encompasses the retinal nerve fiber layer.[3,4] Combining multiple layers enhances the stability or reproducibility of segmentation performance. However, this

amalgamation may concurrently decrease sensitivity to glaucomatous damage, as it includes a structure, namely the inner plexiform layer, that is not the primary site of glaucomatous damage.[4]
In contrast to earlier time domain OCT generations newer spectral domain and swept source OCTs enable this refined level of examination. Currently, all OCT machines can generate maps illustrating total macular thickness and cross-sectional images. Furthermore, the majority of devices offer maps specifically delineating ganglion cell analysis.[3,5]

Macular OCT performance in glaucoma assessment

Glaucoma diagnosis using GCC and/or GCIPL compared to conventional circumpapillary retinal nerve fiber layer (cpRNFL) thickness measurement deserved equally effectiveness for glaucoma detection and disease progression.[5,6] Obviously, diagnosis it's easier in advanced cases.[7]

Figure 1
Example of retinal layer segmentation, with thickness values map of a right eye.

Figure 1

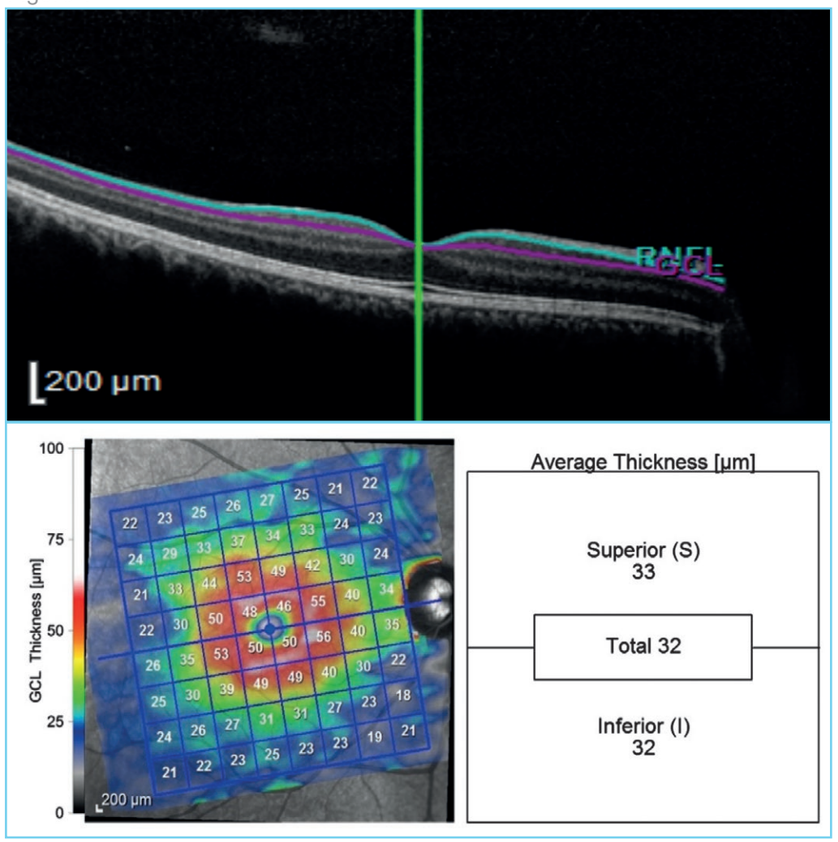

But alterations in the macula might manifest earlier and with greater consistency in glaucoma compared to cpRNLF changes. This implies that utilizing macular OCT could potentially enhance sensitivity in glaucoma screening.[6,8–10] Interestingly, in the initial stages of the disease, assessing changes over time may prove to be beneficial for diagnosing glaucoma, offering advantages compared to the classification of eyes using cross-sectional normative databases.[11]

At present, there is a consensus that combining analysis of the retinal nerve fiber layer and ganglion cells represents the most effective approach for OCT-based glaucoma assessment.[7,9,10] In a particular study, a composite index, incorporating factors such as GCC volume loss, inferior RNFL thickness, age, and visual field loss, outperformed individual factors in predicting the development of glaucoma over a six-year period.[6] Several studies have explored deeper into this perspective, employing multivariable analysis to construct predictive models for the early detection of glaucoma.[11]
Quantifying the reproducibility of measurements is crucial, as the timely detection of progression relies on the capacity to distinguish genuine changes from the noise of test-retest variability. The confidence in detecting genuine change can be enhanced by obtaining two or more baseline measurements and confirming changes in subsequent scans.[10]

Correlation with visual field testing

Visual field test represents the primary method to identify glaucomatous damage and progression. Sometimes visual field chances anticipate detectable structural changes. The stage of disease is crucial to detect progression: eyes with earlier disease are more likely to be identified as progressing by OCT but not by perimetry. Conversely, eyes with more advanced disease have a higher likelihood of being recognized as progressing by perimetry but not by OCT.[12]
Moreover, the simultaneous detection of change in structure and function is rare.[13] Information from OCT can be integrated with visual field evidence through either the Bayesian probability theorem or by converting the measurements to a standardized scale that reflects neural losses. The results can then be presented as an index.[14,15] Integrating data from both structural and functional tests, or from different structural measurements, offers a chance to simplify the collected evidence and present them concurrently.

Future Directions and Research

The use of deep learning (DL) and machine learning algorithms in OCT for glaucoma assessment has demonstrated efficiency, accuracy, and promising outcomes.[16,17] However, some challenges should be addressed before further employing DL in OCT for glaucoma assessment, including its application in computer-aided triage, screening, and diagnosis settings.

First, creating infrastructure powered by deep learning for real-word implementation, then assessing generalizability through prospective evaluations in unfamiliar datasets, conducting cost-effectiveness analyses, and finally addressing the "black box" explanation problem associated with artificial intelligence.[16]

Conclusion

Macular OCT represents a valid tool for the current management of glaucoma patients, aiding physicians in early diagnosis of disease and in identifying progression.

Promisingly, multimodal imaging together with artificial intelligence will implement our possibilities to avoid visual function impairment in glaucoma patients.

References

1. Salmon JF. Glaucoma. Kanski's Clinical Ophthalmology. A systematic approach. 9 ed. Elsevier, 2020.
2. Gupta D, Asrani S. Macular thickness analysis for glaucoma diagnosis and management. Taiwan J Ophthalmol 2016;6:3-7.
3. Sung MS, Yoon JH, Park SW. Diagnostic Validity of Macular Ganglion Cell-Inner Plexiform Layer Thickness Deviation Map Algorithm Using Cirrus HD-OCT in Preperimetric and Early Glaucoma. J Glaucoma 2014;23:e144-e151.
4. Ishikawa H, Stein DM, Wollstein G, et al. Macular Segmentation with Optical Coherence Tomography. Invest Opthalmol Vis Sci 2055;46:2012.
5. Kim NR, Lee ES, Seong GJ, et al. Structure–Function Relationship and Diagnostic Value of Macular Ganglion Cell Complex Measurement Using Fourier-Domain OCT in Glaucoma. Invest Opthalmol Vis Sci 2010;51:4646.
6. Zhang X, Loewen N, Tan O, et al. Predicting Development of Glaucomatous Visual Field Conversion Using Baseline Fourier-Domain Optical Coherence Tomography. Am J Ophthalmol 2016;163:29-37.
7. Suda K, Hangai M, Akagi T, et al. Comparison of Longitudinal Changes in Functional and Structural Measures for Evaluating Progression of Glaucomatous Optic Neuropathy. Invest Opthalmol Vis Sci 2015;56:5477.
8. Oddone F, Lucenteforte E, Michelessi M, et al. Macular versus Retinal Nerve Fiber Layer Parameters for Diagnosing Manifest Glaucoma. Ophthalmology 2016;123:939-49.
9. Na JH, Sung KR, Baek S, et al. Macular and Retinal Nerve Fiber Layer Thickness: Which Is More Helpful in the Diagnosis of Glaucoma? Invest Opthalmol Vis Sci 2011;52:8094.
10. Mwanza JC, Warren JL, Budenz DL. Combining Spectral Domain Optical Coherence Tomography Structural Parameters for the Diagnosis of Glaucoma With Early Visual Field Loss. Invest Opthalmol Vis Sci 2013;54:8393.
11. Tatham AJ, Medeiros FA. Detecting Structural Progression in Glaucoma with Optical Coherence Tomography. Ophthalmology 2017;124:S57-S65.
12. Abe RY, Diniz-Filho A, Zangwill LM, et al. The Relative Odds of Progressing by Structural and Functional Tests in Glaucoma. Invest Opthalmol Vis Sci 2016;57:OCT421.
13. Medeiros FA, Lisboa R, Weinreb RN, et al. A combined index of structure and function for staging glaucomatous damage. Arch Ophthalmol 2012;130:1107-16.
14. Meira-Freitas D, Lisboa R, Tatham A, et al. Predicting Progression in Glaucoma Suspects With Longitudinal Estimates of Retinal Ganglion Cell Counts. Invest Opthalmol Vis Sci 2013;54:4174.
15. Russell RA, Malik R, Chauhan BC, et al. Improved Estimates of Visual Field Progression Using Bayesian Linear Regression to Integrate Structural Information in Patients with Ocular Hypertension. Invest Opthalmol Vis Sci 2012;53:2760.
16. Ran AR, Tham CC, Chan PP, et al. Deep learning in glaucoma with optical coherence tomography: a review. Eye 2021;35:188-201.
17. Hood DC, La Bruna S, Tsamis E, et al. Detecting glaucoma with only OCT: Implications for the clinic, research, screening, and AI development. Prog Retin Eye Res 2022;90:101052.

Part I

Chapter 8

Imaging of the lamina cribrosa of the optic nerve in glaucomas

Christian Y Mardin

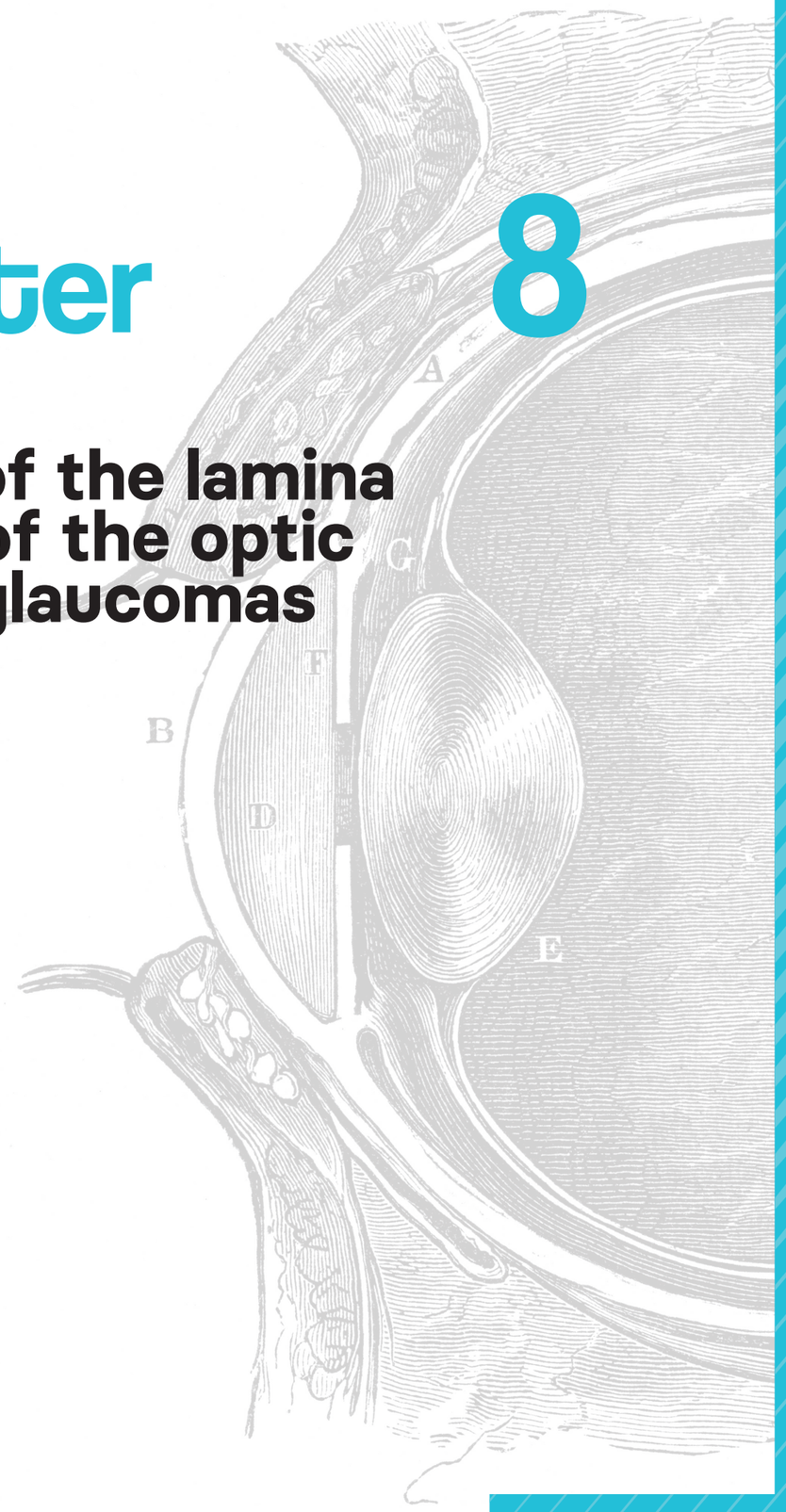

Vertical Section

Imaging of the lamina cribrosa of the optic nerve in glaucomas

Christian Y Mardin

Department of Ophthalmology, University Erlangen-Nuremberg, Germany

The lamina cribrosa in the posterior sclera, the site of entrance and exit of the retinal vessels and nerve fibers, respectively, is believed to help preserve a pressure gradient between the extraocular and intraocular space. Related on its inner surface to intrapapillary structures of the optic nerve head, the optic cup and the neuroretinal rim, e.g., the retinal nerve fibers emerging from its outer surface, become myelinated by oligodendrocytes to form the retrobulbar part of the optic nerve. The lamina cribrosa is condensed[1] in glaucomatous eyes, with increased intraocular pressure leading to an abnormally elevated trans-lamina-cribrosa pressure gradient. Based on morphologic studies and investigations of the rapid axoplasmatic transport in eyes with artificially raised intraocular pressure, the lamina cribrosa has been labeled the site at which the damage in glaucoma occurs.[2]

Anatomically the lamina cribrosa is a sieve-like perforation in the posterior part of the sclera with differing pore sizes with smaller pores situated nasally and temporally and larger pores inferiorly and superiorly (Figs 1; 3).
Consisting of collagen and elastin optic nerve head (ONH) biomechanical properties have been shown to alter with the occurrence of glaucoma and are regarded as a potential biomarker for glaucoma diagnosis and prognosis. The stiffness of the sclera has been found to increase with age and with exposure to chronic intraocular pressure (IOP) elevation in monkey and human eyes.[4]

Figure 1

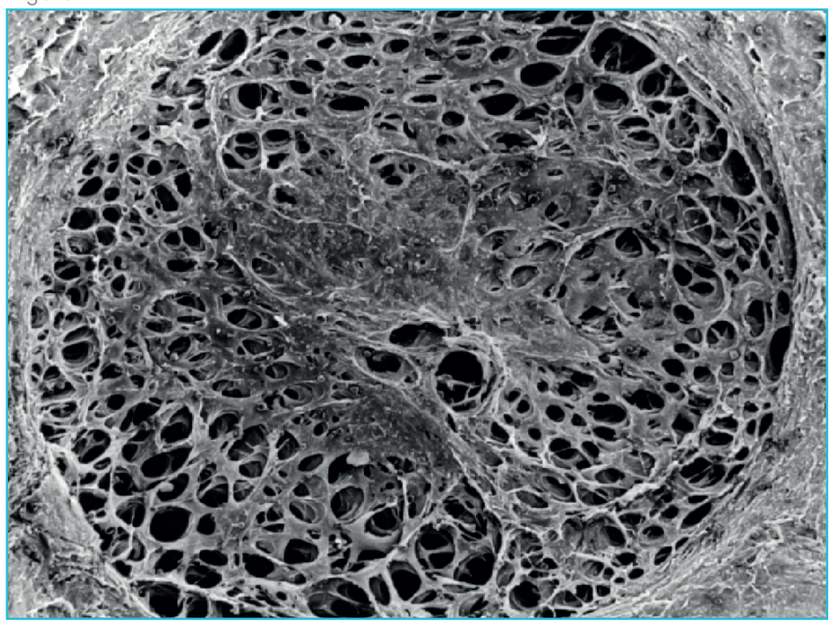

Figure 1
Electron-microscopy image of the anterior surface of trypsin digested ex-vivo human specimen of the lamina cribrosa. Note that larger pores are found superiorly and inferiorly and smaller pores temporally and nasally. Central in-/outlet for retinal vessel stem.

Christian Y Mardin

Thus, the lamina cribrosa becomes a key structure in glaucoma. It has been traditionally difficult to evaluate it in vivo. Pores adjacent to the scleral rim are covered by tissue of the neuroretinal rim (NRR) and only pores belonging to the excavation can be evaluated on fundus photography or with ophthalmoscopy. Heidelberg Retina tomograph (HRT; Heidelberg Engineering, Heidelberg) was the first semi-automated Scanning-Laser instrument to image lamina cribrosa surface and offer information of cup-depth, cup-volume dependent and steepness of the cup walls with Third-Moment and GPS being independent of a reference plane (Fig. 2). HHRT delivered information only about the surface contour of the lamina cribrosa, but lacked to deliver depth information. Axial and lateral resolution was limited to 300 µm and 10 µm respectively

However, recent advances in imaging technologies, such as Scanning Laser Ophthalmoscopy (SLO) (Fig. 2), optical coherence tomography (OCT) (Fig. 3), Enhanced Depth Imaging (EDI) and experimental adaptive optics scanning laser ophthalmoscopy (AOSLO), have enabled the visualization of the lamina cribrosa in glaucomatous eyes.[5,6,7] OCT imaging using spectral-domain and swept-source techniques have significantly elevated axial and lateral resolution to 5 µm and 7 µm respectively.

Figure 2

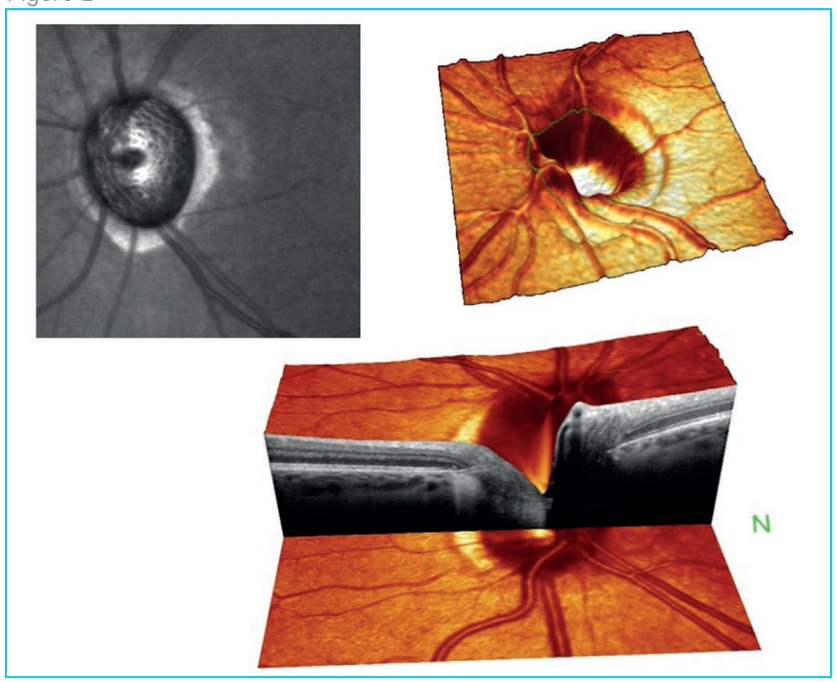

Figure 2
SLO image on the left of a glaucomatous optic disc with near-infrared imaging. Parapapillary atrophy of RPE and choriocapillaris, pores and loss of neuroretinal rim can easily be appreciated. HRT in the middle was able to visualize lamina cribrosa surface and could analyze changes in the course of progression using variables as cup-depth, cup-volume and third moment. OCT images cross sections of the lamina with higher details and depth information of its tissue.

Figure 3

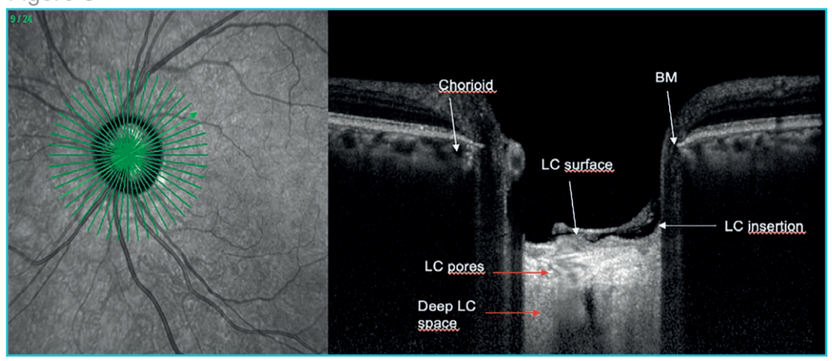

Figure 3
Horizontal cross section SD-OCT scan through the center of the optic disc with a good visibility of the anterior face of the lamina cribrosa, lateral temporal insertion, ending of Bruch's membrane. Note shadowing by the temporal retinal vessels and light attenuation at the posterior part of the lamina cribrosa making it difficult observe details nasally (24 Scans, 48 measuring points every 7.5°).

High scan-speeds to more than 100,000 A-scans/sec enabling three-dimensional reconstruction in volume scans (Table 1). Using swept-source technique and laser wavelength in the infrared spectrum (e.g. Triton, Topcon 1050nm; Table 1) increase OCT penetration depth, improving lamina cribrosa visibility in the deeper layers.

Table 1

Device	RTVueXR Avanti	Spectralis OCTII	Plex Elite 9000	Triton	RS-3000 Advance
Manufacturer	Optovue	Heidelberg Engineering	Zeiss	Topcon	Nidek
SD/SS	SD	SD	SD	SS	SD
Algorithm	SSADA	Full Spec-trum prob-abilistic ap-proach	OMAG	OCTARA	CODAA
Scan speed (A-scans/sec)	70,000	85,000	100,000	100,000	53,000
Wave length (nm)	840	870	1,000	1,050	880
Axial/Lateral resolution (µm)	5/15	3.9/5.7	6,3/-20	8/20	7/20
Eye tracking	Motion Cor-rection Technology	Dual beam life eye tracking	Tracking by SLO	SMART Track	Tracking by SLO
Enhanced depth imaging (EDI)	Built in	Built in	Built in	Depth range imaging (DRI)	Built in

Table 1
Selected OCT Devices in comparison. (8; Modified from Hagag AM et al Taiwan J Ophthalmol 2017)

Imaging of the lamina cribrosa of the optic nerve in glaucomas

Christian Y Mardin

Light attenuation and shadowing by larger retinal vessels at the disc present a challenge for high-resolution imaging of the deeper lamina cribrosa (Fig. 3). A range of studies have explored methods to enhance the imaging depth of spectral-domain optical coherence tomography (SD-OCT). Wang[9] proposed a pixel shift technique to double the spectral sampling rate and improve image contrast in areas with large depths. Ravichandran[10] developed a bidirectional imaging modality to increase the ability to characterize depth-enhanced images. Li et al (11) demonstrated a 1050-nm SD-OCT system with a 12 mm imaging depth, while Yu et al[12] reported on depth-enhanced 2-D OCT using complex wavefront shaping. These studies collectively highlight the potential for various techniques to enhance the imaging depth of SD-OCT (enhanced imaging depth; EDI). Girard et al's[13] results indicated that adaptive compensation (AC) was superior to EDI in terms of improving general LC visibility, although combining EDI with AC generated the optimal visibility. They concluded that anterior LC surface was the most consistently detectable feature of the LC, followed by the LC insertions.

Still the posterior part of the lamina cribrosa and its boundary stays poorly imageable with OCT.[13]

Kim et al[6] could show, that by applying experimental compensation algorithms to OCT images and adaptive optics technology, visualization of the beams and pores and neural pathways of the LC and the scleral insertion sites could substantially be improved. Figure 4 illustrates how visibility of LC details can be improved using EDI mode in high-resolution OCT.

Figure 4

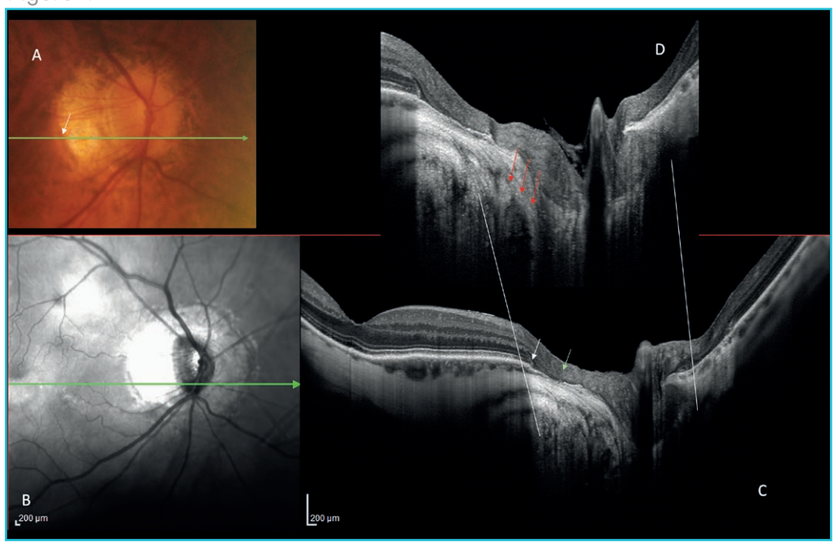

Figure 4
High-resolution image in EDI mode of the LC of a myopic optic disc. Fundus photo (A) and IR image (B) show the temporal scleral flange with white reflection. OCT-scan in C shows transition (white, green arrows) of the scleral flange into LC with columns of axonal bundles in the superficial part of LC (D), marked with red arrows.

MR imaging presents an alternative method to visualize optic nerve structures, especially in the area of the posterior scleral canal and in the retrobulbar space. 7 Tesla MRI imaging is able, to visualize retrobulbar space with highly defined details, but images are still not comparable to OCT in terms of resolution. Thus, MR imaging is still not sufficient for clinical assessment when visualization of the optic nerve head is possible with light-based OCT. Krueger et al[14] correlated histology images with ex-vivo 7 Tesla MRI. Although images were taken ex vivo without eye movement and perfusion artefacts, they still lack the details of OCT images.[14]

OCT imaging techniques have revealed changes in the lamina cribrosa in glaucomas, including posterior displacement, altered thickness, and focal defects, which are associated with glaucomatous retinal ganglion cell loss and focal retinal nerve fiber (RNF) loss.[5]

In a review paper Abe et al[5] could show from the literature that OCT imaging identified general and localized configurational changes in the lamina of glaucomatous eyes, including posterior laminar displacement and altered laminar thickness. This finding reflects ex vivo findings in histology showing backward bowing and sintering of the multilayer structure with progressing glaucomatous disease. Park et al found posterior bowing and sliding of the laminar insertion, with localized deformation of the lamina cribrosa in those with glaucoma. This presents a substantial re-modelling of optic nerve head tissue visible in vivo leading to potential mechanical stress of RNF. Aquired optic pits inf fundus imaging in glaucoma are equivalent to focal LC defects with structure OCT (Fig. 5).

Figure 5

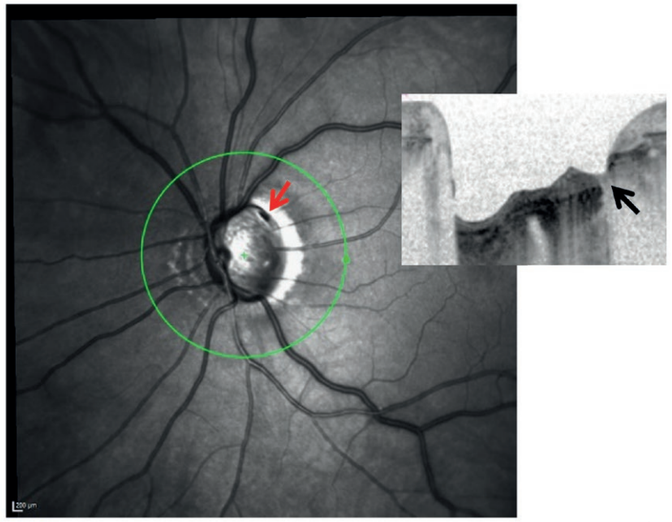

Figure 5
Infrared SLO fundus image showing an acquired optic pit temporally superior on LC border (red arrow) in a progressed glaucomatous optic disc. This corresponds to an insertion defect of the LC (black arrow).

Imaging of the lamina cribrosa of the optic nerve in glaucomas

Christian Y Mardin

Takayama et al[15] could show from their work that focal lamina cribrosa defects corresponded with neuroretinal rim thinning, concurrent or previous disc hemorrhages, abnormal circumpapillary RNF layer thickness, ganglion cell loss and visual field defects.
Furthermore, three-dimensional imaging using swept-source OCT has allowed visualization of lamina cribrosa defects, which are more prevalent in eyes with longer axial length and are associated with disc hemorrhages.[15]
The ability to visualize these changes has significant clinical implications, as they can serve as biomarkers for glaucoma diagnosis and progression.[5,6]
But there are still no available parameters to measure lamina cribrosa changes or optic nerve head cupping with standard OCT software. So, in this perspective HRT is still indispensable to show changes of cup and lamina cribrosa bowing with its reference independent GPS parameter and Topographic Change Analysis (TCA) (Fig. 6a, b).

Deepening of the cup and sintering of the lamina cribrosa is an indicator for glaucoma progression. One way to measure cup depth is to measure the distance of the surface to a plane defined by the ending of Bruch's membrane opening.[16] KKim et al could show with manual segmentation of structure OCT images that even in early-to-moderate glaucoma, the cup surface depth changed faster than did the RNFL thickness.

Figure 6

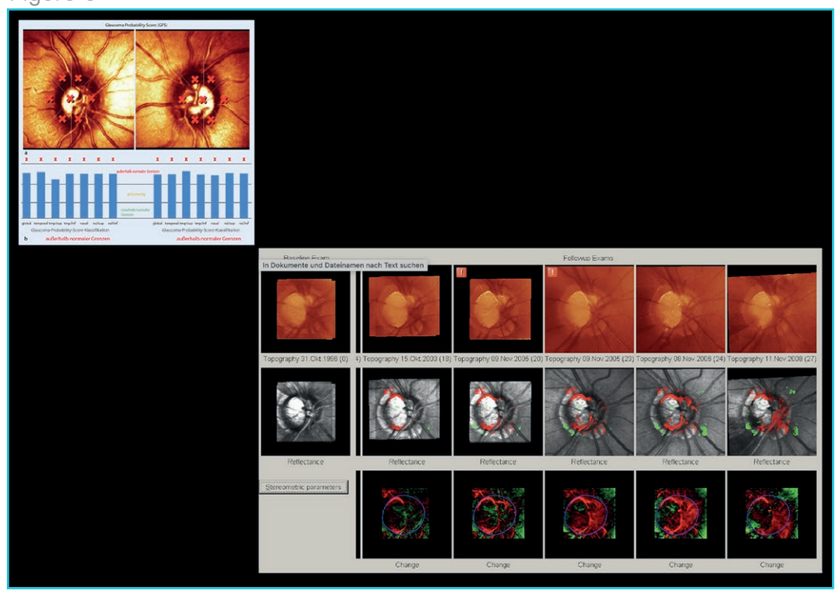

Figure 6
HRT variables to analyze change of lamina cribrosa and cup change in glaucomas. 6a shows GPS analysis to evaluate the slope of the cup on the surface of lamina cribrosa, 6b TCA analysis showing in red in a sub-cluster analysis tissue loss. Green indicates elevation in the course of observation.

Marques et al[17] discussed in a review that manual segmentation of structure OCT images is time consuming and user dependent procedure which is often necessary to retrieve important biomarkers for disease diagnosis and/or progression. Combination of automated disc and lamina cribrosa segmentation with AI and Deep-Learning could contribute to progression analysis, especially in progressed cases where few rim tissue is left and increasing lamina cribrosa depth could give more readily available information on tissue re-modelling processes in the optic disc.[17]

The latest commercially available application of OCT technique is OCT-Angiography (OCT-A). It allows visualization also of smaller perfused retinal and choroidal vessels even at the level of capillaries. Numa et al[18] could demonstrate in an OCT-A study in normals and glaucomas using en-face OCTA images flow signals on or areas immediately adjacent to lamina beams, but not inside lamina pores. Glaucomatous eyes had a sectoral reduction in lamina cribrosa microvasculature blood flow that was not detected in normal eyes in typical areas of the superior and inferior lamina cribrosa. The authors discuss that previous OCTA studies have shown peripapillary and macular microvasculature reduction in glaucomatous eyes. However, considering that the lamina cribrosa is the origin of glaucomatous optic nerve damage, the lamina cribrosa circulation could be directly associated with glaucoma pathophysiology.[18] Circulation dropouts in the lamina cribrosa could even probably precede structural defects in the lamina cribrosa, NRR or RNF layer (Fig. 7).

These findings highlight the potential of lamina cribrosa imaging in glaucoma diagnosis and monitoring in future.

Figure 7

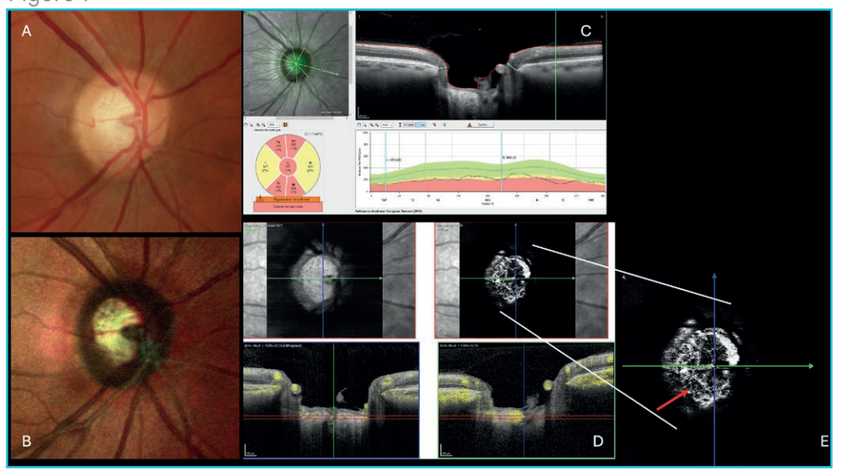

Figure 7
Right eye with intermediate glaucomatous optic atrophy showing elongation of cup and thinning of neuroretinal rim superiorly and inferiorly in fundus (A) and multicolor (B) image. Structure OCT (C) shows details of anterior LC with shadowing effect nasally by larger retinal vessel. Anterior LC slab of OCT angiography shows enface LC pore details left and perfusion on LC beams right. E highlights magnified LC OCT-A slab with reduced perfusion temporally inferior where loss of neuroretinal rim is present, although LC pores do not seem larger than temporally superior.

Christian Y Mardin

References

1. Quigley HA, Hohmann RM, Addicks EM, Massof RW, Green RW. Morphologic changes in the lamina cribrosa correlated with neural loss in open-angle glaucoma. Am J Ophthalmol 1983;95:673.
2. Anderson DR, Hendrickson A. Effect of intraocular pres- No. 2 MORPHOMETRY OF THE HUMAN LAMINA CRIBROSA SURFACE / Jonos er ol 405 sure on rapid axoplasmatic transport in monkey optic nerve. Invest Ophthalmol Vis Sci 1974;13:771.
3. Jonas JB, Mardin CY, Schlötzer-Schrehardt U, Naumann GO. Morphometry of the human lamina cribrosa surface. Investigative ophthalmology & visual science 1991;32(2):401-405.
4. Zhang L, Beotra MR, Baskaran M, et al. In vivo measurements of prelamina and lamina cribrosa biomechanicalproperties in humans. InvestOphthalmol Vis Sci 2020;61(3):27.
5. Abe RY, Gracitelli CPB, Diniz-Filho A, Tatham AJ, Medeiros FA. Curr Ophthalmol Rep 2015;3:74-84.
6. Kim TW, Kagemann L, Girard MJ, Strouthidis N, Sung K, Leung C, Schumann J, Wollnstein G. Imaging of the Lamina Cribrosa in Glaucoma: Perspectives of Pathogenesis and Clinical Applications. Cur Eye Research 2013;38:903-909.
7. Vilupuru AS, Rangaswamy NV, LJ Frishman, EL Smith III, RS Harwerth, A Roorda. Adaptive optics scanning laser ophthalmoscopy for in vivo imaging of lamina cribrosa. J Opt Soc Am A Opt Image Sci Vis 2007;24(5):1417–25.
8. Hagag AM, Gao SS, Jia Y, Huang D. Optical coherence tomography angiography: Technical principles and clinical applications in ophthalmology. Taiwan J Ophthalmol 2017;7:115-29.
9. Zhenguo Wang, Zhijia Yuan, Hongyu Wang, Yingtian Pan. Increasing the imaging depth of spectral-domain OCT by using interpixel shift technique. Opt Express 2016 Aug 7;14(16):7014-23.
10. Ravichandran N, RE Wijesinghe RE, Shirazi MF, Park K, Jeon M, Jung W, et al. Depth enhancement in spectral domain optical coherence tomography using bidirectional imaging modality with a single spectrometer. J Biomed Opt 2016 Jul 1;21(7):76005.
11. Li P, An L, Lan G, Johnstone M, Malchow D, Wang RK. Extended imaging depth to 12 mm for 1050-nm spectral domain optical coherence tomography for imaging the whole anterior segment of the human eye at 120-kHz A-scan rate. J Biomed Opt 2013; 18(1):16012.
12. Yu H, Jang J, Lim J, Park JH, Jang W, Kim JY, et al. Depth-enhanced 2-D optical coherence tomography using complex wavefront shaping. Opt Express 2014 Apr 7;22(7):7514-23.
13. Girard MJA, Tun TA, Husain R, et al. Lamina cribrosa visibility using optical coherence tomography: comparison of devices and effects of image enhancement techniques. Invest Ophthalmol Vis Sci 2015;56:865–874.
14. Krueger PC, Stachs O, Hadlich S, Falke K, Erbersdobler A, Hosten N, Langner S. MR Microscopy of the human eye at 7.1 T and correlation with histopathology-proof of principle. Orbit. 2012;31(6):390-3.
15. Takayama K, Hangai M, Kimura Y, Morooka S, Nukada M, Akagi T, Ikeda H, et al. Three-dimensional imaging of lamina cribrosa defects in glaucoma using swept-source optical coherence tomography. Invest Ophthalmol Vis Sci 2013 Jul 18;54(7):4798-807.
16. Kim YK, Ha A, Lee WJ, Jeoung JW, Park KH. Measurement of Optic Disc Cup Surface Depth Using Cirrus HD-OCT. Journal of Glaucoma 2017;26(12):1072-1080.
17. Marques R, De Jesus DA, Barbosa-Breda J, et al. Comput Methods Programs Biomed 2022;220:106801.
18. Numa S, Akagi T, Uji A, Suda K, Nakanishi H, Kameda T, Ikeda HO, Tsujikawa A. Visualization of the Lamina Cribrosa Microvasculature in Normal and Glaucomatous Eyes: A Swept-source Optical Coherence Tomography Angiography Study. J Glaucoma 2018;27:1032–1035.

Part I

Chapter 9

Choroidal Imaging

Manuele Michelessi

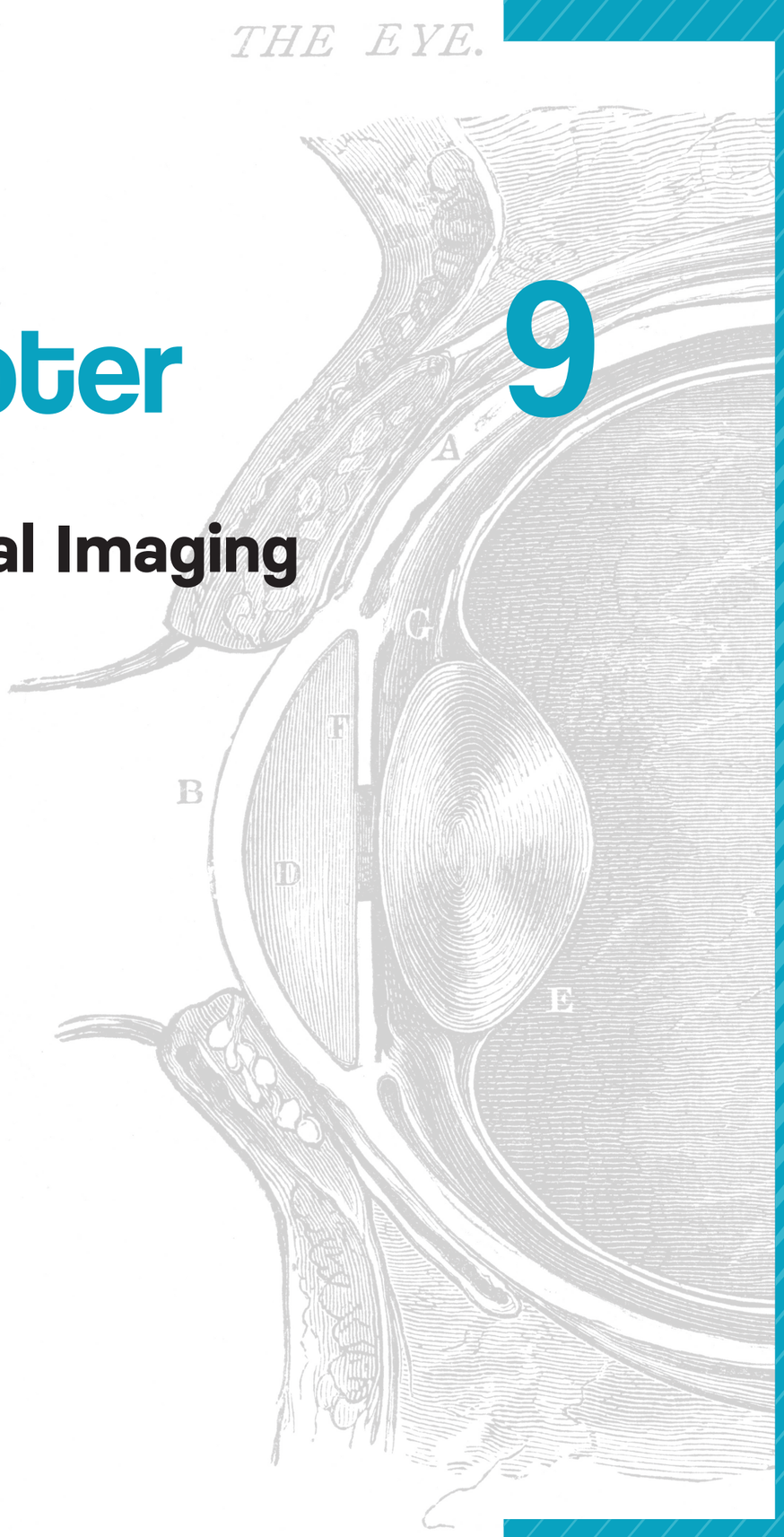

Vertical Section

Choroidal Imaging

Manuele Michelessi

IRCCS - Fondazione Bietti, Rome, Italy

The choroid is a vascular tissue located between the inner retina and sclera, from the optic nerve head (ONH) to the ora serrata. Choroidal maximum thickness is around 0.2 mm at the posterior pole and it is commonly divided in five layers: the Bruch's membrane, separating the choroid from the retinal pigment epithelium (RPE); the choriocapillaris (consisted of high diameter capillaries); the outer Haller's layer and the inner Sattler's layer, composed respectively of large and medium arteries and veins; and the suprachoroidal space.[1]
The choroid is a highly perfused membrane supply by the perforating anterior ciliary arteries and both the long and short posterior ciliary arteries. In turn, choroid nourishes the outer portion of retina and the ONH through direct vessels of posterior ciliary arteries and the circle of Zinn-Haller.[2]
Structural or functional damages to the choroid, with a consequent reduced blood supply to the ONH, can be implicated in the development of ONH ischemic damages and it has long been advocated as involved in the pathogenesis of glaucoma.[3]

However, the complex nature of choroid and its deep position have always made it difficult to properly evaluate and visualize it in vivo. Blood flow of choroidal circulation has been indirectly measured in the past by indocyanine green angiography, laser speckle flowgraphy, laser doppler flowmetry, and scanning laser doppler flowmetry. With such methods of measurement, glaucomatous eyes showed ONH filling defects and delayed parapapillary choroidal filling when compared with healthy controls.[4]
The recent developments of optical coherence tomography (OCT) such as enhanced-depth imaging OCT (EDI-OCT), swept-source OCT (SS-OCT), and OCT angiography (OCT-A) have significantly changed the ability to visualize the choroidal structure.
With spectral domain OCT (SD-OCT), the scattering of light from RPE layer and the decreased resolution with increasing displacement from zero-delay line, impede to identifies the outer limits of choroid. With EDI-OCT the peak sensitivity is placed posteriorly toward the sclera and the zero-line is settled adjacent to the choroid, allowing a deeper visualization of choroid and the choroid sclera-interface, as well as measurements of choroidal thickness (CT).[5]

Although the improvement in comparison with SD-OCT, the visualization of the choriocapillaris and choroidal microvasculature, close to RPE, remains challenging also with EDI-OCT.
SS-OCT uses a long wavelength (1050nm), a tunable laser and a photodetector. By using a high imaging speed and a high penetration rate, SS-OCT is less subject to shadow effect of RPE and lens opacities, allowing a better light penetration throughout the RPE and a better visualization of deeper layers of the choroid and choroid-sclera interface.[6]

Choroidal Imaging

Manuele Michelessi

OCT-A is a non-invasive in vivo imaging of the retinal microvasculature, without the need for injection of intravascular agent. OCT-A captures and analyzes consecutive images of the same tissue and allow a reconstruction of the microvascular network of the retina and choroid, exploding the fact that the only element that changes in a tissue over a brief time of period is the blood flowing through the vessels.[7-8]
OCT-A provides a detailed visualization of vascular layer at different depths, however, the visualization of the deeper layers of the choroid is still challenging due to scattering by the pigment in the RPE and by the vessels in the choriocapillaris (signal attenuation effect). In addition, OCT-A does not provide a direct measurement of the actual blood flow and it is subject to artifacts: segmentation errors (affecting the en-face OCT-A images); projection artifacts (affecting the visualization of the deeper vascular layers); and shadowing artifacts (attenuating of blocking the transition of the OCT beam to the deeper layer).

Despite these limitations, the latest advance of choroid OCT analysis contributed to renewing interest of research on the weight of vascular and structural choroidal integrity to the glaucomatous process, as well as on the potential applicability of choroidal imaging in clinical practice. The question is: the choroidal features detected with OCT and OCT-A can be regarded as a biomarker for the diagnosis and progression of glaucoma?

Figure 1
Meta-analysis of subfoveal choroidal thickness between open-angle glaucoma and controls. CI (confidence interval; WMD (weighted mean difference).[11]

Figure 1

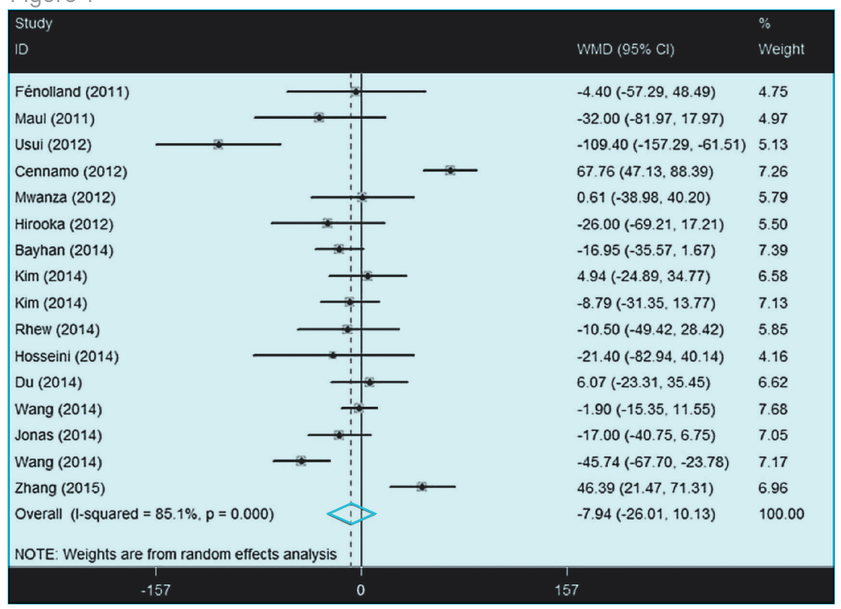

The first characteristics that has been largely studied in association with glaucoma, is the CT, as indicator of structural and functional choroidal integrity. Some studies reported that glaucoma is associated with a thinner choroid, but other studies have shown no differences in CT between healthy and glaucomatous eyes.[9-10]
In 2016, Zhang et al. conducted a meta-analysis including studies evaluating the association between CT (as measured by EDI-OCT) and glaucoma and found no significant differences between primary open-angle glaucoma (POAG) eyes and controls, for both sub-foveal CT (pooled weighted mean difference (WMD) of −7.36 μm (95% confidence interval [CI]: −24.39 to 9.67, p = 0.397) (Fig. 1) and peripapillary CT (pooled weighted mean difference of 6.67 μm (95% CI: −2.45 to 15.79, p = 0.152) (Fig. 2). They found a substantial heterogeneity between studies, primary referred to differences in study design, sample sizes and characteristics, methods of measurement of CT, and methods of analysis.[11]

With the development of OCT-A, attention has been focused on the choroidal vascularization. The choroidal vasculature in the parapapillary area may reflect the perfusion status of the ONH and may be considered a prognostic factor across the disease process.

Figure 2

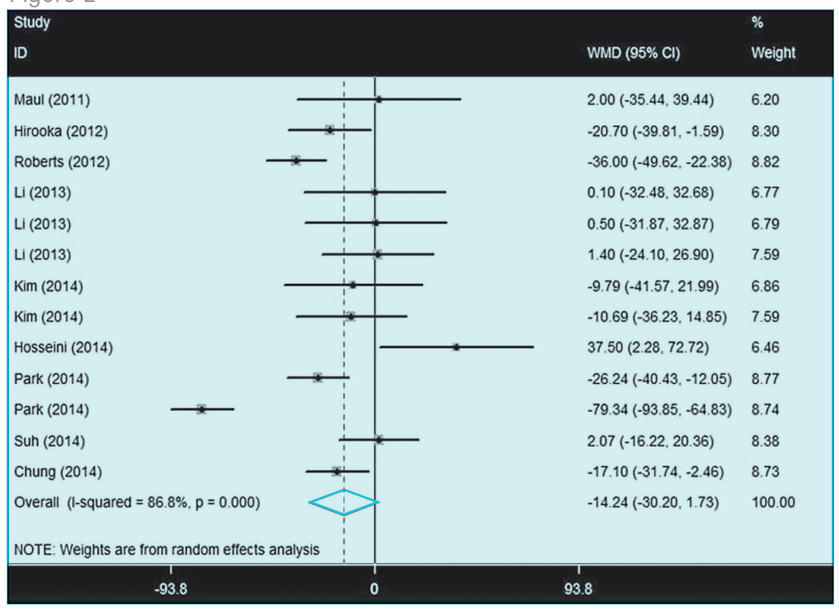

Figure 2
Meta-analysis of average peripapillary choroidal thickness between open-angle glaucoma and controls. CI (confidence interval; WMD (weighted mean difference).[11]

OCT-A analysis allowed us to characterize a new ocular finding on the choroidal layer vessel density map, within area of paripapillary atrophy (β and γ) of glaucoma patients. A complete focal loss of the choriocapillaris or the microvasculature within the scleral flange on both horizontal and en-face choroidal layer vessel density maps, called choroidal microvasculare dropout (CmVD) (Fig. 3).[12]
In 2016, Lee et all, showed that area of microvascular parapapillary choroidal dropout visible on OCT-A correspond to area of perfusion defect visible with indocyanine angiography, suggesting that OCT-A can detect vascular damages that are well correlated to that visible with indocyanine angiography.[13] The association of CmVD and glaucoma has been investigated in numerous studies.

Deep layer microvasculature dropout was more frequently located in the infero-temporal and the supero-temporal sectors. In POAG, CmVD is associated with the presence of focal lamina cribrosa defects, thinner retinal nerve fiber layers (RNFL) thickness, worse visual field, reduced RNFL vessel density, thinner CT, and lower diastolic blood pressure.[12]
CmVDs are topographically associated with the location of focal lamina cribrosa defects, RNFL defects and parafoveal visual field defects.[14]
Further, glaucoma eyes with CmVD were significantly more myopic than eyes without CmVD.[15]
The association between CmVD and ONH damages has been evaluated in primary angle closure glaucoma (PACG) as well. Eyes with CmVD showed thinner average RNFL, more advanced glaucoma, and lower paripapillary vessel density, compared with eye without CmVD. CmvD and RNFL defects, showed good topographic correlation.[16]
In a 2019 study, Park et al, have shown that choroidal vasculature impairment at baseline was associated with glaucoma progression in the follow up as measured by visual field but OCT structural analysis did not show statistically significant progression. The authors suggested that CmVD could be clinically relevant in the estimation of functional progression, even when structural progression is not present in glaucoma.[17]

Figure 3

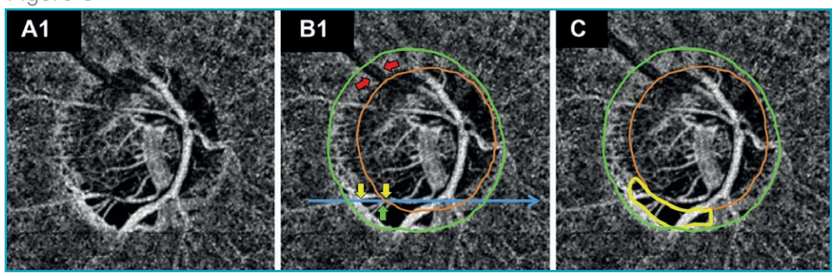

Figure 3
Choroidal vessel density map of optic nerve head optical coherence tomography angiography. Yellow outline marks the Deep-layer microvasculature dropout, within the β parapapillary atrophy (green outline), adjacent the disc margin (orange outline).[12]

In another study, the association between disc hemorrhages (DH), CmVD and RNFL thinning has been studied prospectively, showing that CmVD was more frequent in POAG with DH compared with eyes without. DH eyes with corresponding CmVD showed a faster rate of RNFL thinning than eyes with DH or CmVD alone, suggesting that the presence of CmVD is associated with progressive RNFL thinning and this prognostic factor is stronger when associated with corresponding DH.[18] Taken together, these data suggest that OCT-A parameters of the choroidal microvasculature could represent a valuable vascular factor, potentially applicable in clinical practice, however the overall scenario still remains unclear.

The key point is the temporal relationship between structural and vascular changes: is the structural damages secondary to the primary vascular perfusion defect or is the vascular defect secondary to structural primary damages, with a consequent reduction of the nutritional needed and bloody supply? Longitudinal and well powered studies, to investigate the vascular deep layer as primary endpoint outcome, are needed. Reference databases for choroidal structural and vascular features that consider factors such as race, gender, age, axial length, refractive error, IOP, systemic blood flow, are needed as well. Although the unclear scenario, vascular choroidal defect is associated with more advanced disease, it topographically correlates with RNFL and lamina cribrosa defects, and it is more frequently associated with fast progression. OCT and OCT-A choroidal imaging is a promising biomarker for glaucoma, and reasonably, the future developments of OCT technology (such as High-Resolution OCT) will improve our understanding of the role of vascular impairment in the glaucoma onset and progression.

References

1. Kur J, Newman EA, Chan-Ling T. Cellular and physiological mechanisms underlying blood flow regulation in the retina and choroid in health and disease. Prog Retin Eye Res. 2012;31:377-406.
2. Nickla DL, Wallman J. The multifunctional choroid. Prog Retin Eye Res. 2010;29:144-68.
3. Hayreh SS. Blood supply of the optic nerve head and its role in optic atrophy, glaucoma, and oedema of the optic disc. Br J Ophthalmol 1969;53:721-48.
4. Plange N, Kaup M, Weber A, et al. Fluorescein filling defects and quantitative morphologic analysis of the optic nerve head in glaucoma. Arch Ophthalmol. 2004;122(2):195e201.
5. Margolis R, Spaide RF. A pilot study of enhanced depth imaging optical coherence tomography of the choroid in normal eyes. Am J Ophthalmol. 2009;147:811-15.
6. Choma MA, Sarunic MV, Yang C, Izatt JA. Sensitivity advantage of swept source and Fourier domain optical coherence tomography. Opt Express. 2003;11:2183e9.

7. Jia Y, Morrison JC, Tokayer J, et al. Quantitative OCT angiography of optic nerve head blood flow. Biomed Opt Express 2012;3:3127-37.
8. Jia Y, Wei E, Wang X, et al. Optical coherence tomography angiography of optic disc perfusion in glaucoma. Ophthal- mology. 2014;121(7):1322-32.
9. Lee KM, Lee EJ, Kim TW. Juxtapapillary choroid is thinner in normal-tension glaucoma than in healthy eyes. Acta Ophthalmol. 2016;94:e697-e708.
10. Mwanza, JC, Hochberg JT, Banitt MR, Feuer WJ, Budenz DL. Lack of association between glaucoma and macular choroidal thickness measured with enhanced depth-imaging optical coherence tomography. Investig. Ophthalmol. Vis. Sci. 2011;52:3430-35.
11. Zhang Z, Yu M, Wang F, Dai Y, Wu Z. Choroidal Thickness and Open-Angle Glaucoma: A Meta-Analysis and Systematic Review. J. Glaucoma 2016;25:e446–e454.
12. Suh MH, Zangwill LM, Manalastas PIC, et al. Deep Retinal Layer Microvasculature Dropout Detected by the Optical Coherence Tomography Angiography in Glaucoma. Ophthalmology. 2016;123(12)2509-18.
13. Lee EJ, Lee SH, Kim JA, Kim TW. Parapapillary deep-layer microvasculature dropout in glaucoma: topographic association with glaucomatous damage. Invest Ophthalmol Vis Sci. 2017;58(7):3004e3010.
14. Kwon J, Shin JW, Lee J, et al. Choroidal Microvasculature Dropout Is Associated With Parafoveal Visual Field Defects in Glaucoma. AM J Ophthalmology. 2018;188:141-154.
15. Micheletti E, El-Nimri N, Nishida T, et al. Central visual field damage in glaucoma eyes with choroidal microvasculature dropout with and without high axial myopia. Br J Ophthalmol. 2023;bjo-2022-322234.
16. Tan L, Ma D, He J, et al. The Topographic Relationship Between Choroidal Microvascular Dropout and Glaucomatous Damage in Primary Angle-Closure Glaucoma. Trans Vis Sci Technol. 2022;11(10):20.
17. Park HY, Shin DY, Jeon SJ, et al. Association Between Parapapillary Choroidal Vessel Density Measured With Optical Coherence Tomography Angiography and Future Visual Field Progression in Patients With Glaucoma. JAma Ophthalmol. 2019;136(6):681-88.
18. Park HY, Kim JW, Park CK. Choroidal Microvasculature Dropout Is Associated with Progressive Retinal Nerve Fiber Layer Thinning in Glaucoma with Disc Hemorrhage. Ophtalmology. 2018;125(7):1003-13.

Manuele Michelessi

9
Part I

Part I

Chapter 10

Evaluation of Progression using OCT

Sara Giammaria
Balwantray C Chauhan

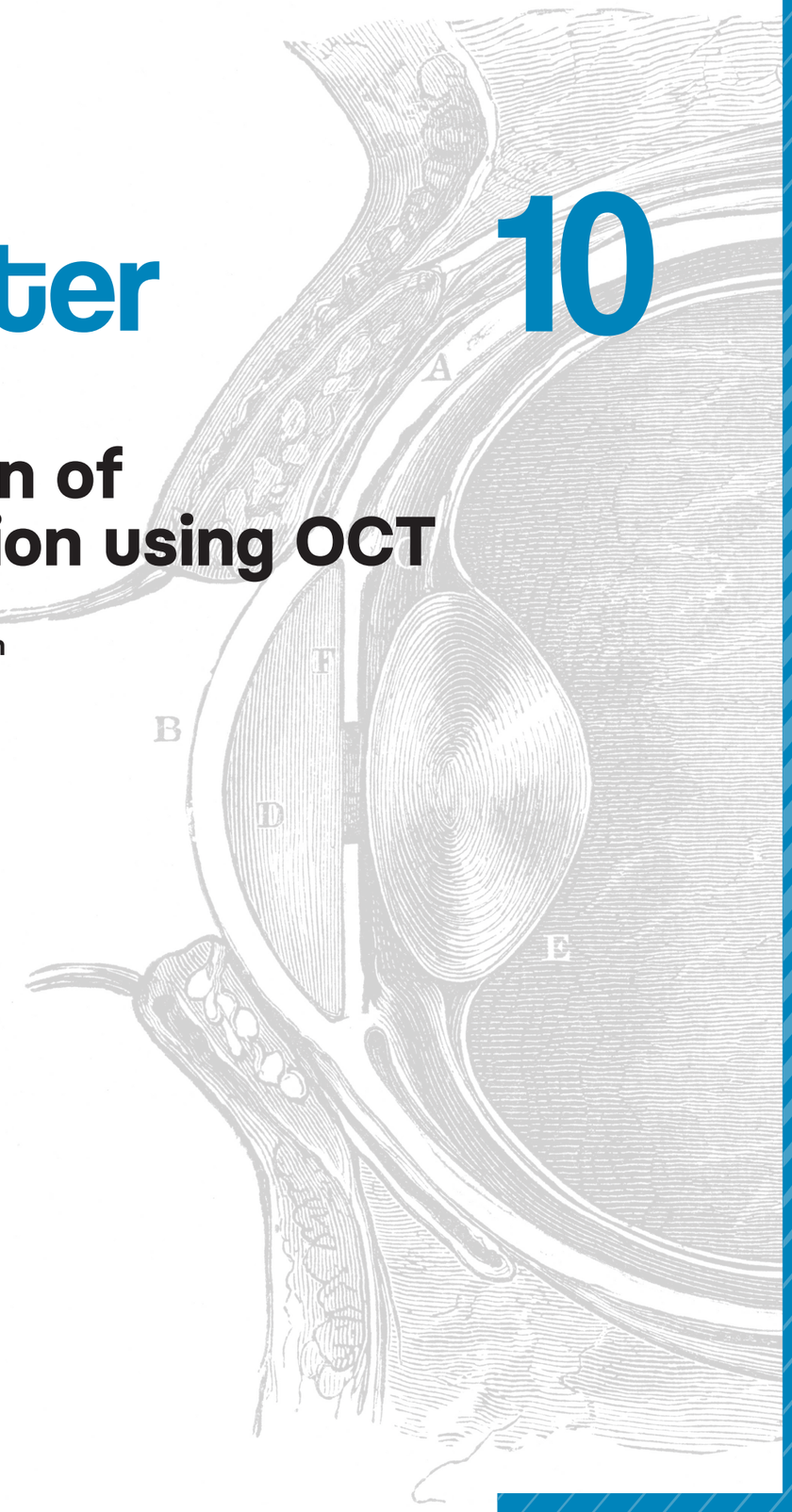

Vertical Section

Evaluation of Progression using OCT

Sara Giammaria,[1] Balwantray C Chauhan[2]

[1] IRCCS - Fondazione Bietti, Rome, Italy
[2] Department of Ophthalmology and Visual Sciences, Dalhousie University, Halifax, Nova Scotia, Canada

Optical coherence tomography (OCT) is widely and routinely employed for detecting structural damage and its progression in glaucoma. However, it can be challenging to distinguish between structural changes caused by glaucoma progression and those that can be attributed to: (1) test-retest variability and (2) effect of age which leads to neural losses that impact OCT measurements. In the first case, estimating test-retest variability may help distinguish clinically significant change (signal) from artefactual changes caused by variability (noise). Continual technological improvements have increased OCT imaging resolution and the reproducibility of the parameters measured. For this reason, OCT has become a reliable tool for the detection of structural progression in glaucoma, able to replace other imaging technologies in clinical practice over time. In the second case, aging induces a progressive and physiological reduction of all OCT parameters.[1,2]

Progression analyses provided by several OCT devices do not account for aging effects, therefore, it is important to be aware that only changes beyond these physiological structural changes can be attributed to glaucoma. However, a simulation study showed that up to 18% of normal eyes could be falsely diagnosed as progressing with OCT over 5 years of follow-up.[3] Each OCT device has different imaging protocols and age-adjusted normative databases. Therefore, direct comparison of results from different devices, or combining examinations from different devices to extend follow-up to detect long-term progression of glaucomatous damage should be avoided. As with visual field examinations, an adequate number of OCT images should be acquired to ensure early detection of structural progression. Recent estimates propose that glaucoma patients should undergo OCT testing at 6-month intervals to improve the detection of progression against a reasonable allocation of health care resources.[4,5]

Retinal Nerve Fiber Layer (RNFL) and Minimum Rim Width (MRW) progression

RNFL and MRW are two of the main OCT parameters used for the structural follow-up of glaucoma. Both parameters can be monitored over time by global or sectorial thickness measurements. Circumpapillary RNFL thickness (cpRNFLT) is one of the parameters most widely studied, and reports suggest that global, and inferior and infero-temporal sectors are the most clinically relevant for detecting glaucoma progression.[5] Fewer studies exist on progression assessment with MRW. Recently, Shi et al., reported that showed faster rates of progression in MRW in the temporal sector, followed by the supero-nasal and supero-temporal sectors.[6] Comparing cpRNFLT and MRW also shows that while the MRW rate of progression may be informative in different sectors with increasing severity of the disease, cpRNFLT in the infero-temporal sector showed the fastest rate of progression over the full range of disease severity.[7] Different patterns

of RNFL progression have been documented. Specifically, progressive RNFL loss manifests more frequently as widening of the defect followed by deepening of the defect and development of newer defects.[8]

Macular progression

Macular changes can be studied by full macular thickness, by single layer or combinations of the inner macular layers, depending on device. Recent evidence shows that the damage of the macular inner layers occurs at a different rate compared to cpRNFLT, with the latter being faster.[9] However, monitoring macular layer thickness has been shown to be particularly valuable for detection of progression in advanced stages of glaucoma. In these cases, it can be possible to detect significant macular thinning when no further significant RNFL change can be detected because the floor of the dynamic range of measurements with cRNFLT is thought to be reached.[9,10]

Nevertheless, in these cases, attention should be paid to the increasing chance of segmentation errors with increasing macular layer thinning. Finally, in highly myopic eyes, where RNFL thickness and MRW evaluation could be challenging because of the altered anatomy and potential segmentation errors, monitoring macular thickness may be more useful for determining progression.[11] Similar to the RNFL, in the macula, defects become wider before deepening, with new defects developing at a later stage.[12]

Figure 1

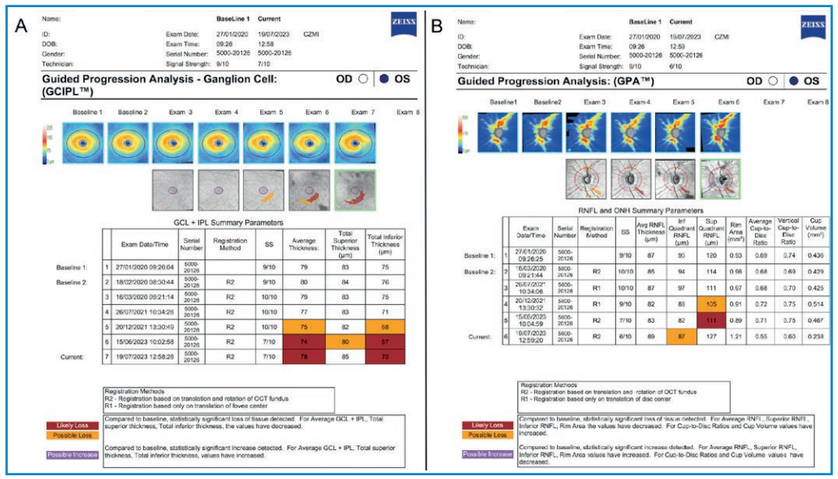

Figure 1
Event analysis of the Ganglion Cell – Inner Plexiform Layer (GCIPL) (A) and Retinal Nerve Fiber Layer (RNFL) and rim parameters (B) with Cirrus OCT. For both parameters, the first two tests are set as baseline for comparison with the following tests. In the upper half of the report, the thickness maps and the deviation maps are displayed. Progression is flagged by orange or red superpixels (4x4 pixels), indicating "Possible Loss" (progression detected in one test) and "Likely Loss" (progression detected in two or more tests), respectively, if the change exceeds the test-retest variability. A "Possible Increase" in the measurement is flagged in lavender. In the lower half of the report, a summary table is reported. In this table, the global and sectorial thicknesses of the GCIPL and the RNFL (e.g., Total superior and Total inferior thickness of the GCIPL and Inferior and Superior Quadrant of the RNFL) and optic nerve head parameters (Rim area, cup-to-disc ratios, and Cup Volume) measured at each examination are summarized. The changes are flagged with the same color code used in the maps.

Event and trend analysis

Every OCT device has its own progression analysis software for detecting changes. Two statistical methods are mainly used to evaluate glaucoma progression with OCT: event or trend analysis. In event analysis baseline is established using the first (or the first two test, according to the type of instrument) and used for comparison with following examinations. The variability of the tests set as baseline reference is important in event analysis, as it can influence the sensitivity and specificity of progression detection. When a follow-up measurement exceeds a predetermined threshold, progression is flagged.

For instance, if the variability of the first two tests is high, a higher threshold for progression results, increasing specificity but reducing sensitivity. Event analysis can be applied to regional changes such as RNFL or macula thickness (Fig. 1), or to global and sectorial parameters like average RNFL thickness or rim measurements (Fig. 1 and Fig. 2). In trend analysis, a regression analysis is performed on follow-up measurements, providing a rate of change over time, with the assumption that the change is linear. In trend-based analysis, the slope is estimated in µm/year with 95% confidence intervals (Fig. 3 and Fig. 4). This analysis has the advantage of being less influenced by outliers among consecutive measurements (caused for example by test-retest variability or segmentation artifacts), especially when a large number of observations is avaiable.

Figure 2

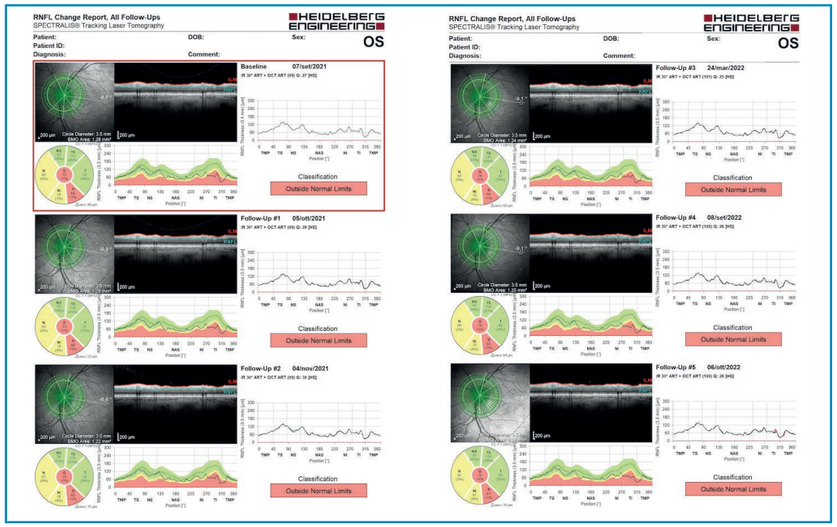

Figure 2
Event Analysis of Retinal Nerve Fiber Layer (RNFL) thickness with Spectralis OCT. Event Analysis of RNFL can be displayed in a report that includes an IR image of the optic nerve head and the protocol scan (e.g., the 3.5 mm circumpapillary scan), the b-scan, the sectorial color-coded analysis, the thickness profile, and the follow-up thickness plot for comparisons with the first baseline test (displayed in the red square), in sequential order. In the follow-up thickness plots, a thinning of the RNFL compared to baseline is flagged in red (see Follow-up #6), whereas an increase in thickness is flagged in green.

Sara Giammaria, Balwantray C Chauhan

Figure 3

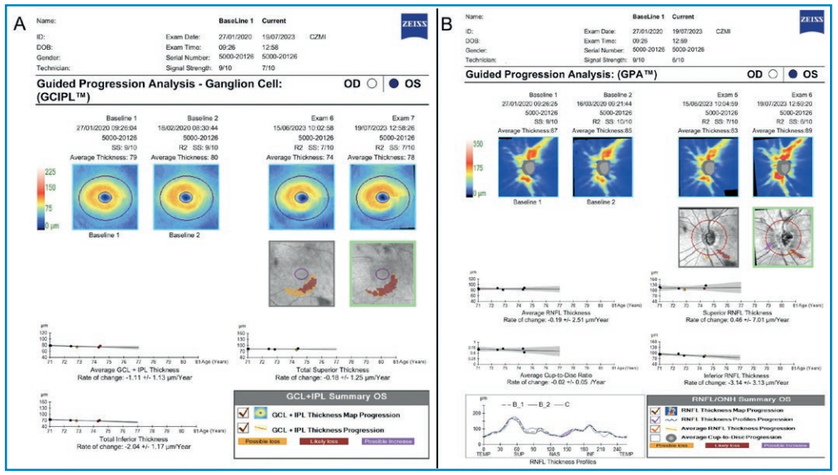

Figure 3
Trend analysis of Ganglion Cell – Inner Plexiform Layer (GCIPL) (A) and Retinal Nerve Fiber Layer (RNFL) and rim parameters (B) with Cirrus OCT. For both parameters, the first two tests are set as baseline for comparison with the following tests. In the upper half of the report, the thickness maps and the deviation maps of the baseline tests and the last two tests are displayed. In the lower half of the report, the thickness change of the global, sectorial thicknesses (e.g., Total Superior and Inferior Thickness of the GCIPL, Superior and Inferior Thickness of the RNFL) and optic nerve head parameter (namely the Average Cup-to-Disc Ratio) are plotted with the regression lines. The corresponding rates of change for each plot are also shown. The RNFL thickness profile of the baseline tests ("B1" and "B2") and the last selected test ("C" – Current) is available in the dedicated report (B). In the maps and the plots, progression is flagged by orange or red, indicating "Possible Loss" (progression detected in one test) and "Likely Loss" (progression detected in two or more tests), respectively, if the change exceeds the test-retest variability. A "Possible Increase" in the measurement is flagged in lavender. In addition, in the Summary Box at the bottom of the report, a color-coded checkmark indicates if the progression has been detected and in which analysis.

Progression with OCT vs Progression with Visual Field (VF)

OCT and VF data provide clinicians with information on glaucoma progression, however these modalities are different expressions of change and not always interchangeable. The different rates of progression between OCT and VF parameters should not be surprising, however, there is increasing evidence demonstrating the mismatch between structural and functional damage, particularly at the macular level.[13] As a result, simultaneous change detection in structural and functional measurements is uncommon and both structural and functional tests should be carefully monitored for the best possible assessment of glaucoma progression. Increasing the number of reliable and good quality tests enables more efficient detection of progression, even in patients who progress at slower rates, and applies to both OCT and VF examinations.[4,5,14]

However, it has also been shown that in real-world settings, the frequency of follow-up visits and VF and OCT testing of glaucoma patients is significantly lower than standard recommendations.[15] Thus, repeating OCT and VF with the recommended timing or performing both tests in the same visit may not be reasonable or feasible for a variety of reasons. Performing OCT and VF tests at alternative visits may delay detection of meaningful progression. In this scenario, clinicians should gauge their available resources (e.g., clinic capacity, testing time, technicians, type of instruments) and patient characteristics (e.g., compliance with the type of testing) and select the technique that can ensure high quality and frequency of testing in order to make the best clinical decisions for the patients.

Figure 4

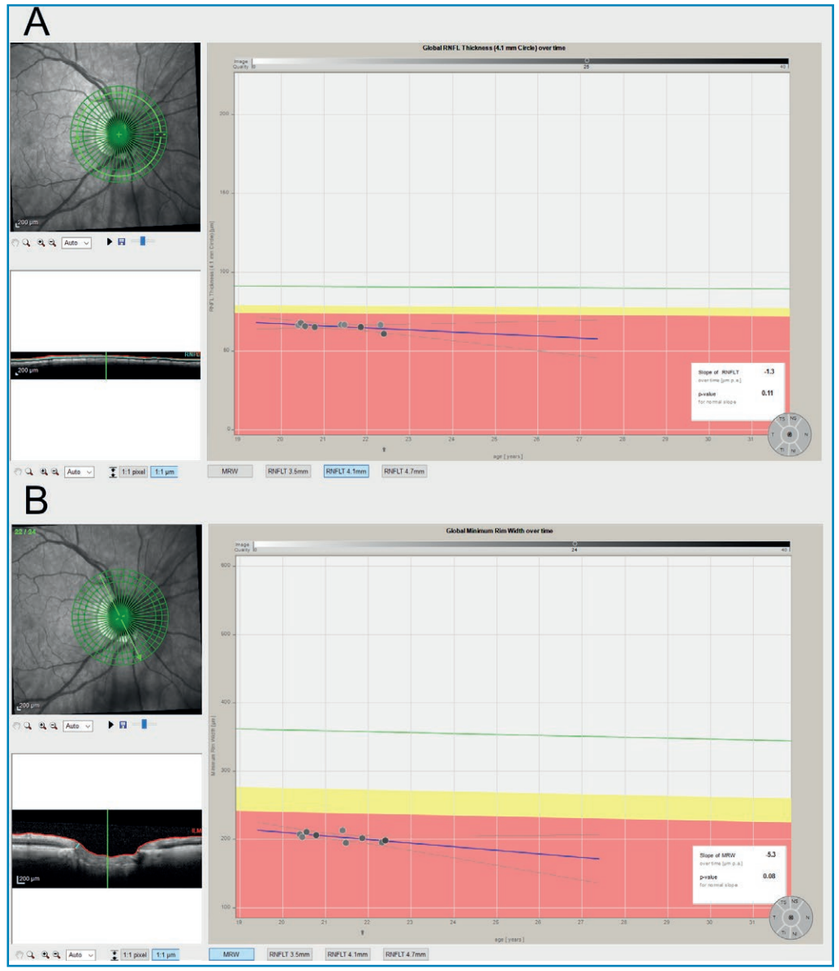

Figure 4
Trend analysis of RNFL thickness (A) and BMO-MRW thickness (B) with Spectralis OCT. For both parameters, the analysis shows in the upper left box the IR image of the optic nerve with the scan protocol superimposed (in green). In the lower left corner, the b-scans of the scan protocol are shown. In the graph on the right, the gray dots represent the thickness of the parameter in relation to the age of the patient at the time of the examination. The regression line of the thickness is depicted in blue, and the confidence intervals are in gray (the slope and its p value are reported in the white box). Background colors of the graph indicate, respectively, the reference values for the 95% (white), <5% (yellow), and <1% (red) of the reference database of the instrument, whereas the green line represents the normal age-related loss.

Conclusions

Currently, although all the OCT parameters show good ability in recognizing progressing glaucoma patients, a single ideal parameter for measuring glaucoma detection in all patients and at all stages of the disease still does not exist. All the available parameters have different dynamic ranges and an integrative approach is recommended to increase sensitivity for detecting change. Most of the devices have been implemented with a combined report, that can be a useful tool for clinicians, not only for improving glaucoma diagnosis but also for monitoring structural progression.

References

1. Chauhan BC, Vianna JR, Sharpe GP, et al. Differential Effects of Aging in the Macular Retinal Layers, Neuroretinal Rim, and Peripapillary Retinal Nerve Fiber Layer. Ophthalmology. 2020;127(2):177-185. doi:10.1016/j.ophtha.2019.09.013
2. Vianna JR, Danthurebandara VM, Sharpe GP, et al. Importance of Normal Aging in Estimating the Rate of Glaucomatous Neuroretinal Rim and Retinal Nerve Fiber Layer Loss. Ophthalmology. 2015;122(12):2392-98. doi:10.1016/j.ophtha.2015.08.020
3. Wu Z, Saunders LJ, Zangwill LM, Daga FB, Crowston JG, Medeiros FA. Impact of Normal Aging and Progression Definitions on the Specificity of Detecting Retinal Nerve Fiber Layer Thinning. Am J Ophthalmol. 2017;181:106-13. doi:10.1016/j.ajo.2017.06.017
4. Bradley C, Hou K, Herbert P, et al. Evidence-Based Guidelines for the Number of Peripapillary OCT Scans Needed to Detect Glaucoma Worsening. Ophthalmology. 2023;130(1):39-47. doi:10.1016/j.ophtha.2022.07.025
5. Mahmoudinezhad G, Moghimi S, Proudfoot JA, et al. Effect of Testing Frequency on the Time to Detect Glaucoma Progression With Optical Coherence Tomography (OCT) and OCT Angiography. Am J Ophthalmol. 2023;245:184-92. doi:10.1016/j.ajo.2022.08.030
6. Shi L, Mohammadi M, Mohammadzadeh V, et al. Comparing Rates of Change in Moderate to Advanced Glaucoma: Retinal Nerve Fiber Layer Versus Bruch Membrane Opening-Minimum Rim Width. Am J Ophthalmol. 2023;253:181-88. doi:10.1016/j.ajo.2023.05.003
7. Park D, Park SP, Na KI. Comparison of retinal nerve fiber layer thickness and Bruch's membrane opening minimum rim width thinning rate in open-angle glaucoma. Sci Rep. 2022;12(1):16069. doi:10.1038/s41598-022-20423-0
8. Leung CKS, Yu M, Weinreb RN, Lai G, Xu G, Lam DSC. Retinal nerve fiber layer imaging with spectral-domain optical coherence tomography: patterns of retinal nerve fiber layer progression. Ophthalmology. 2012;119(9):1858-66. doi:10.1016/j.ophtha.2012.03.044
9. Hammel N, Belghith A, Weinreb RN, Medeiros FA, Mendoza N, Zangwill LM. Comparing the Rates of Retinal Nerve Fiber Layer and Ganglion Cell-Inner Plexiform Layer Loss in Healthy Eyes and in Glaucoma Eyes. Am J Ophthalmol. 2017;178:38-50. doi:10.1016/j.ajo.2017.03.008
10. Lavinsky F, Wu M, Schuman JS, et al. Can Macula and Optic Nerve Head Parameters Detect Glaucoma Progression in Eyes with Advanced Circumpapillary Retinal Nerve Fiber Layer Damage? Ophthalmology. 2018;125(12):1907-12. doi:10.1016/j.ophtha.2018.05.020
11. Shin JW, Song MK, Sung KR. Longitudinal Macular Ganglion Cell-Inner Plexiform Layer Measurements to Detect Glaucoma Progression in High Myopia. Am J Ophthalmol. 2021;223:9-20. doi:10.1016/j.ajo.2020.09.039
12. Shin JW, Sung KR, Park SW. Patterns of Progressive Ganglion Cell-Inner Plexiform Layer Thinning in Glaucoma Detected by OCT. Ophthalmology. 2018;125(10):1515-25. doi:10.1016/j.ophtha.2018.03.052
13. Giammaria S, Sharpe GP, Dyachok O, et al. Elucidating macular structure–function correlations in glaucoma. Sci Rep. 2022;12(1):10621. doi:10.1038/s41598-022-13730-z
14. Chauhan BC, Garway-Heath DF, Goñi FJ, et al. Practical recommendations for measuring rates of visual field change in glaucoma. Br J Ophthalmol. 2008;92(4):569-73. doi:10.1136/bjo.2007.135012
15. Jammal AA, Thompson AC, Mariottoni EB, et al. Rates of Glaucomatous Structural and Functional Change From a Large Clinical Population: The Duke Glaucoma Registry Study. Am J Ophthalmol. 2021;222:238-47. doi:10.1016/j.ajo.2020.05.019

Part I

Chapter 11

OCT in myopic eyes

Antonio Ferreras

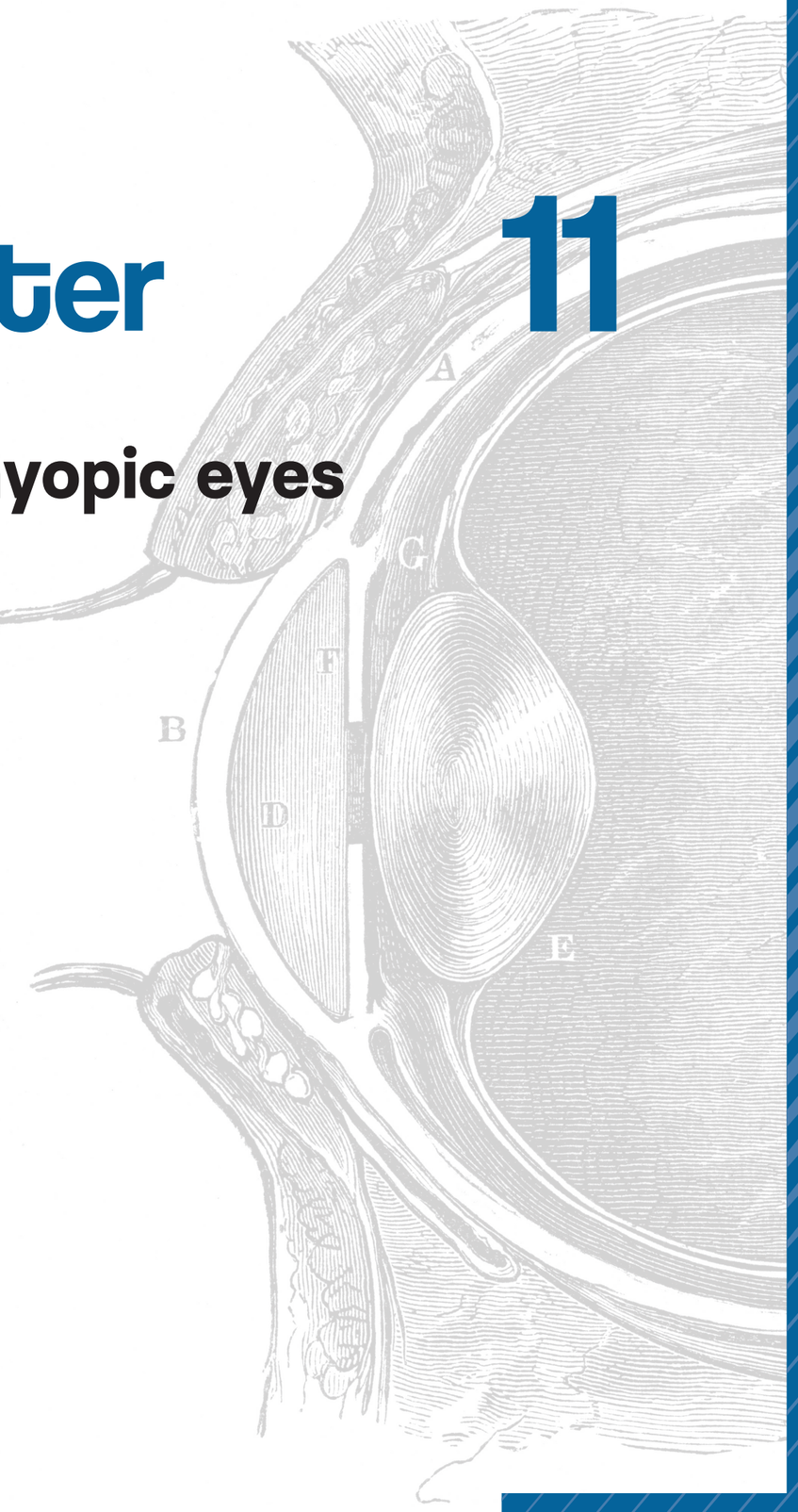

Vertical Section

OCT in myopic eyes

Antonio Ferreras

Miguel Servet university hospital, Zaragoza
University of Zaragoza, Zaragoza (Spain)

Myopia is currently the most common ocular disorder worldwide, and uncorrected refractive errors are the second most frequent cause of blindness.[1,2] Consistent evidence indicates that the prevalence of myopia is increasing globally and could affect 50% of the world population by 2050,[3,4] with vision morbidity becoming a major public health problem.[5] High myopia is usually diagnosed when the refractive error is over -6.00 diopters or the axial length is greater than 26.5mm. This condition represents a major risk factor for different sight-threatening complications, such as glaucoma. Compared with non-myopic eyes, myopic eyes have a two- to three-fold higher risk for primary open-angle glaucoma.[6] Optical coherence tomography (OCT) has become a standard imaging test for assessing the peripapillary retinal nerve fiber layer and evaluating the optic disc characteristics in glaucoma. Nevertheless, the wide variability in normal optic nerve head appearance makes it difficult to obtain accurate information about optic discs with an atypical morphology from imaging devices.

Myopic optic discs are often tilted. Furthermore, the oval-shaped aspect, presence of peripapillary atrophy, shallow cupping, obliquely rotated fibers, pale neuroretinal rim, and retinal nerve layer thinning around the optic nerve head are common characteristics of myopic eyes.[7,8] Consequently, the management of glaucoma with these conditions is complex for clinicians, even with the support of high-definition OCTs or different image analysis tools included in the software for these devices, particularly because the normative databases overall exclude high-myopic individuals and basically comprise measurements of individuals with low refractive errors (Fig. 1). The natural evolution of high myopia is variable; while some cases present only minor changes, others develop pathologic myopia with a significantly modified anatomy. The usual course may include scleral thinning with maximal reduction in the posterior pole (staphyloma); choroidal thinning associated with loss of the choriocapillaris and retinal pigment epithelium; and elongation of the peripapillary scleral flange, while the lamina cribrosa is stretched thin.[9] Because pathologic myopia is a progressive condition, it is frequently not possible to diagnose glaucoma from a single evaluation.

Thus, longitudinal follow-up visits may be necessary to confirm the presence of glaucoma. Moreover, detection of glaucoma progression by distinguishing changes in the evolution of myopia from those produced by glaucomatous damage over time is usually an exigent task. This circumstance applies to all of the most common OCT assessments when evaluating glaucoma: ganglion cell analysis, measurement of the peripapillary retinal nerve fiber layer thickness, and evaluation of the optic nerve head morphology. Hence, joint evaluation of analyses based on different anatomic regions may increase the diagnostic ability to detect glaucoma.[10] Some studies suggest that analysis of the ganglion cell complex (ganglion cell layer plus inner plexiform layer thickness) could have a higher performance in high myopic eyes compared with analysis of the peripapillary

Figure 1
Optical coherence tomography of a young man with high myopia. Thinning of the retinal fiber layer around the optic disc shows a globally reduced profile with defects in the 4 quadrants and at many clock-time positions. Use of this color-coded classification is limited in high myopic eyes due to the absence of specific normative databases.

Figure 1

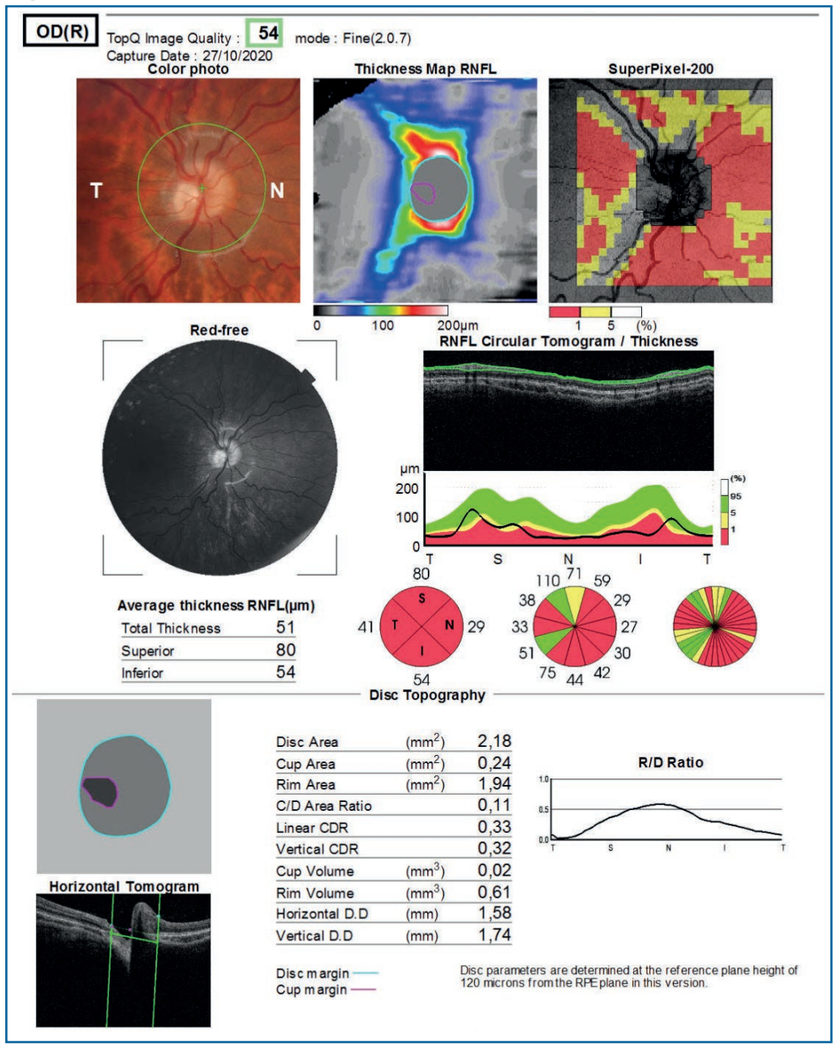

retinal nerve fiber layer thickness parameters. Nonetheless, the presence of a thinner macula or other irregularities associated with high myopia in addition to the lack of a normative database for myopic glaucomatous eyes limits the accuracy of this algorithm in clinical practice.[10,11] The precision of OCT parameters is directly associated with the image quality.[12] Inadequate alignment of the scans with the plane of the examined tissue may lead to significant measurement errors. In high myopic eyes, the axial length, size of the pupil, presence of floaters, tilted discs, steep retinal slopes, areas of atrophy, and status of the retinal pigment epithelium are some factors that can lead to incorrect segmentation of the retinal layers as a result of multiple artifacts (Fig. 2). Besides, image quality is even more critical when evaluating glaucoma progression. Measurement variability is inherent to every single machine, although it differs for each parameter of the same instrument.[13] On one hand, if the variability is high, statistical confidence in detecting small changes over time is low. On the other hand, when the variability is small, small changes can be

Figure 2

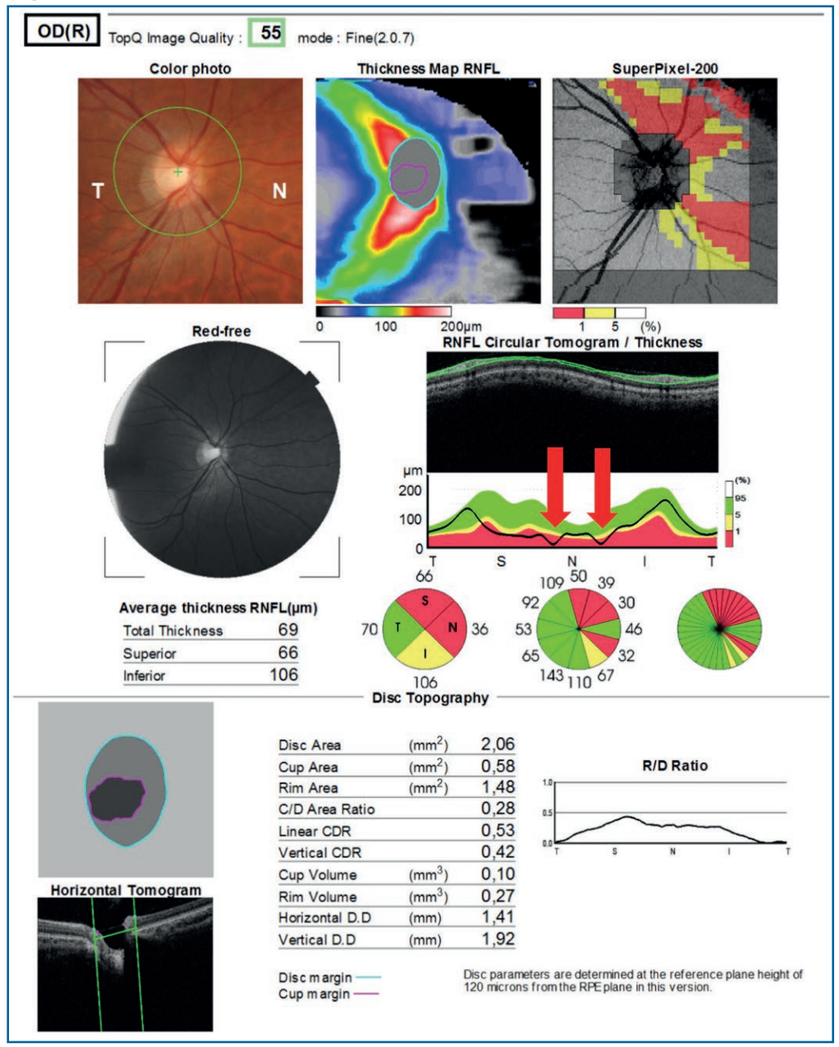

Figure 2
Long axial length eyes are frequently associated with incorrect layer segmentation. The presence of peripapillary atrophy or abnormal retinal pigment epithelium contributes to obtaining erroneous measurements (red arrows). Clinicians should carefully check all the analyses and maps of myopic eyes to identify the presence of artifacts.

identified with confidence. Scanning high myopic eyes with OCT usually results in lower quality images compared with non-myopic eyes and subsequently in higher variability of the measurements and reduced ability to detect true progression. The combination of different diagnostic tests can significantly improve the ability to properly manage glaucoma in myopic eyes. Especially, visual field evaluation is a key assessment that, next to the fundus examination, may help to identify myopic changes detected by OCT that could be confused with those produced by glaucoma (Fig. 3). Although threshold sensitivity tends to decrease in moderate and high myopia, white-on-white perimetry plays a relevant role in diagnosing and monitoring progression in myopic eyes, mainly when the OCT is showing numerous artifacts. Currently, Bruch's membrane opening (BMO) is the reference plane for optic nerve head analysis obtained by OCT. Nevertheless, the margin of Bruch's membrane may be displaced away from the temporal border of the optic nerve head in myopic discs.

Therefore, OCT tends to falsely measure the optic disc area, providing bigger values and potentially false reduction of the neuroretinal rim area and lower peripapillary retinal nerve fiber layer thicknesses.[14] Some studies performed with OCT have shown variations in the morphometric parameters according to the axial length of the ocular globe. BMO and Bruch's membrane shape are related to axial length, while Bruch's membrane deformation is associated with visual field defects and age.[15] Glaucomatous optic nerve head changes in the context of high myopia were characterized by a larger BMO tilt and reduced peripapillary choroidal thickness, but were not related to the severity of glaucoma.[16] Additionally, the patterns of the retinal nerve layer thickness and the BMO-minimum rim width (BMO-MRW) varied with axial length, which should be taken into account when reading OCT images in myopic eyes. Overall, BMO-MRW has good diagnostic ability to detect early glaucoma in myopic individuals.[17] Nonetheless, the performance of this parameter decreased in eyes with a large BMO. Deep learning technology has been used to increase the diagnostic ability of different aspects related to the eye, and glaucoma is one of the most investigated fields. In the past, artificial intelligence has been applied to discriminate between glaucomatous and normal eyes based on the evaluation of fundus photographs.[18] In a recent study, a multimodal model in artificial intelligence was developed based on fundus photographs assessed with OCT to detect glaucoma in populations with a high incidence of myopia, such as the Asian race. The algorithm had a good diagnostic ability for glaucoma and may be suitable for telemedicine in rural areas.[19] Personalized testing strategies and tailored decisions are key to differentiating the changes that physiologically occur over time from those caused by either myopia or glaucoma. Though OCT machines are continuously enhanced, a diagnosis of glaucoma in the setting of high myopia remains challenging. Multimodal assessment, artificial intelligence, and specific normative databases designed for myopic eyes could be useful tools to improve the management of glaucoma in individuals having eyes with a long axial length.[11,14,19]

Figure 3

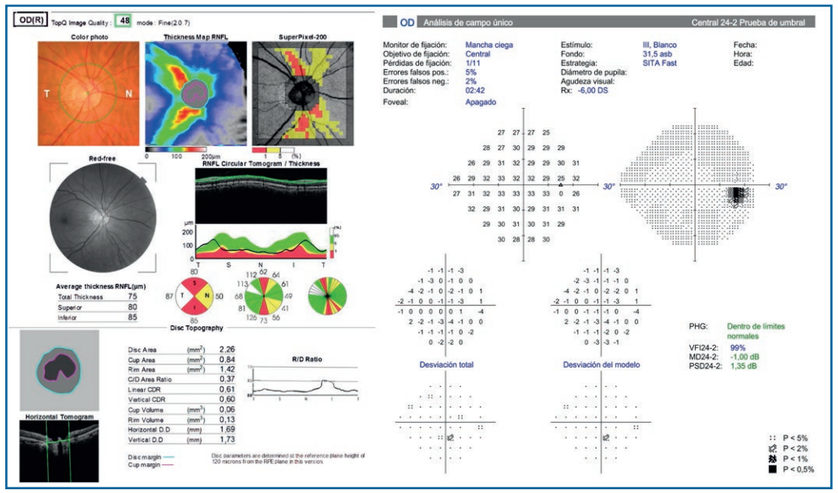

Figure 3
Even when layer segmentation of the peripapillary retinal nerve fiber layer is apparently good, high myopic eyes frequently show a reduction in different sectors. Nevertheless, the normal visual field result confirms that the structural changes are related to myopia.

References

1. Pararajasegaram R. VISION 2020-the right to sight: From strategies to action. Am J Ophthalmol 1999;128:359–60.
2. Bourne RR, Stevens GA, White RA, et al. Causes of vision loss worldwide, 1990-2010: a systematic analysis. The Lancet Global Health 2013;1:e339–49.
3. Williams KM, Bertelsen G, Cumberland P, et al. Increasing prevalence of myopia in Europe and the impact of education. Ophthalmology 2015;122:1489–97.
4. Holden BA, Fricke TR, Wilson DA, et al. Prevalence of myopia and high myopia and temporal trends from 2000 through 2050. Ophthalmology 2016;123:1036-42.
5. Modjtahedi BS, Abbott RL, Fong DS, Lum F, Tan D. Task Force on Myopia. Reducing the Global Burden of Myopia by Delaying the Onset of Myopia and Reducing Myopic Progression in Children: The Academy's Task Force on Myopia. Ophthalmology 2021;128:816–26.
6. Mitchell P, Hourihan F, Sandbach J, Wang JJ. The relationship between glaucoma and myopia: the Blue Mountains Eye Study. Ophthalmology 1999;106(10):2010-5.
7. Kang SH, Hong SW, Im SK, Lee SH, Ahn MD. Effect of myopia on the thickness of the retinal nerve fiber layer measured by Cirrus HD optical coherence tomography. Invest Ophthalmol Vis Sci 2010;51:4075–83.
8. Savini G, Barboni P, Parisi V, Carbonelli M. The influence of axial length on retinal nerve fibre layer thickness and optic disc size measurements by spectral-domain OCT. Br J Ophthalmol 2012;96:57–61.
9. Jonas JB, Xu L. Histological changes of high axial myopia. Eye (Lond) 2014;28:113-17.
10. Shoji T, Nagaoka Y, Sato H, Chihara E. Impact of high myopia on the performance of SD-OCT parameters to detect glaucoma. Graefes Arch Clin Exp Ophthalmol 2012;250:1843–9.
11. Akashi A, Kanamori A, Ueda K, Inoue Y, Yamada Y, Nakamura M. The ability of SD-OCT to differentiate early glaucoma with high myopia from highly myopic controls and nonhighly myopic controls. Invest Ophthalmol Vis Sci 2015;56:6573–80.
12. Sung KR, Wollstein G, Schuman JS, et al. Scan quality effect on glaucoma discrimination by glaucoma imaging devices. Br J Ophthalmol 2009;93:1580–84.
13. Pierro L, Gagliardi M, Luliano L, Ambrosi A, Bandello F. Retinal nerve fiber layer thickness reproducibility using seven different OCT instruments. Invest Ophthalmol Vis Sci 2012;53:5912–20.
14. Tan NYQ, Sng CCA, Jonas JB, Wong TY, Jansonius NM, Ang M. Glaucoma in myopia: diagnostic dilemmas. Br J Ophthalmol 2019;103:1347–55.
15. Lee S, Han SX, Young M, et al. Optic nerve head and peripapillary morphometrics in myopic glaucoma. Invest Ophthalmol Vis Sci 2014;55:4378–93.
16. Rezapour J, Bowd C, Dohleman J, et al. The influence of axial myopia on optic disc characteristics of glaucoma eyes. Sci Rep 2021;11:8854.
17. Park DH, Kook KY, Kang YS, Piao H, Sung MS, Park SW. Clinical utility of Bruch Membrane Opening-Minimum Rim Width for detecting early glaucoma in myopic eyes. J Glaucoma. 2021;30:971–80.
18. Li Z, He Y, Keel S, Meng W, Chang RT, He M. Efficacy of a deep learning system for detecting glaucomatous optic neuropathy based on color fundus photographs. Ophthalmology 2018;125:1199–206.
19. Lim WS, Ho HY, Ho HC, et al. Use of multimodal dataset in AI for detecting glaucoma based on fundus photographs assessed with OCT: focus group study on high prevalence of myopia. BMC Med Imaging 2022;22:206.

Part I

Chapter 12

Integrating structure and function

Dhakshi Muhundhakumar
Ananth Viswanathan

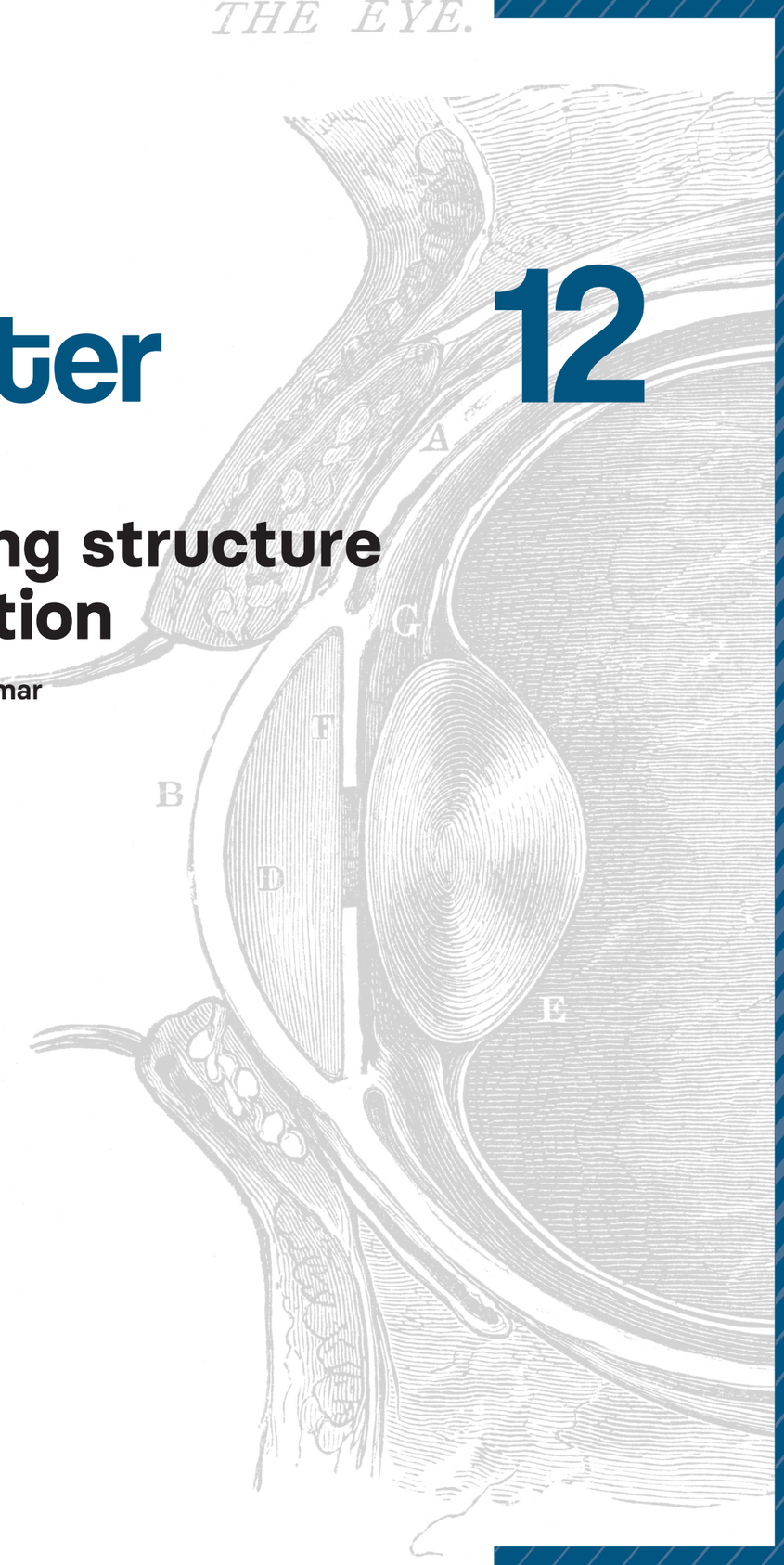

Vertical Section

Integrating structure and function

Dhakshi Muhundhakumar
Ananth Viswanathan

Moorfields Eye Hospital NHSFT, London, UK
UCL Institute of Ophthalmology, London, UK

Introduction

Glaucoma is defined as a group of chronic progressive optic neuropathies that have in common characteristic morphological changes of the optic nerve head (ONH) with associated retinal ganglion cell (RGC) loss and visual field deterioration.[1] Glaucoma specialists strive to correlate these structural and functional changes in the diagnosis, monitoring and decision-making process of glaucoma management. Vast strides have been made in the field of optic nerve and retinal imaging in recent years, with optical coherence tomography (OCT) superseding disc photographs, retinal tomography and other imaging techniques for structural assessment. Meanwhile for assessing function the gold standard remains visual field testing or standard automated perimetry (SAP). The relative importance of structure and function is a topic of ongoing debate amongst glaucoma specialists; these can vary depending on the patient, disease severity, phenotype, instruments used and reliability and reproducibility of the data.

From a clinician's point of view, with glaucoma being initially asymptomatic in the visual domain, it is necessary to tease out what would be most meaningful to the patient in their lifetime. Functional (VF) changes have a direct impact on patients' daily activities (such as driving) but studies have shown that structural changes such as retinal nerve fibre layer (RNFL) thinning can also impact quality of life measures.[2] Ultimately both structure and function as measured clinically are surrogate indices of the same end point in glaucoma - the number of remaining functioning RGCs and their axons. Until sufficiently sophisticated techniques are developed to quantify and assess RGCs in vivo, we continue to rely on these auxiliary parameters. This is a necessary challenge - if structure and function data were perfectly correlated, there wouldn't be the need to assess both in all patients.[3] The astute clinician must learn to use both and balance the information provided from structural and functional tests based on individual patient and technical factors.

Historical understandings of structure and function

The traditional paradigm of thinking is that structural changes occur in early disease and precede functional changes which occur in later disease. This was popularised by Harold Quigley, whose team carried out histological studies on human eyes, compared them with visual field data and reported that "at least 25% to 35% RGC loss is associated with abnormalities in visual field testing."[4] The landmark trial the Ocular Hypertension Treatment Study (OHTS, 2002), which by definition followed pre-glaucomatous patients, found structural progression to be more prevalent in their cohort.[5] In contrast in the Early Manifest Glaucoma Trial (EMGT, 1999) a post hoc analysis by Ohnell et al, found that in glaucomatous eyes with established visual field defects, progression was first noted on visual field testing rather than optic disc photographs.[6] As imaging techniques have

Dhakshi Muhundhakumar, Ananth Viswanathan

grown more sophisticated (such as through the use of OCT) they are able to pick up subtle changes in earlier stages of the disease. Nonetheless the EMGT finding suggests that in eyes with advanced disease, visual function testing may be more informative. Conversely, the fact that perimetric change can precede optic nerve damage is also well documented, and has been demonstrated in OHTS, EMGT and also the European Glaucoma Prevention Study (EPGS) at rates of 35%, 86% and 60% respectively.[7]

Figure 1

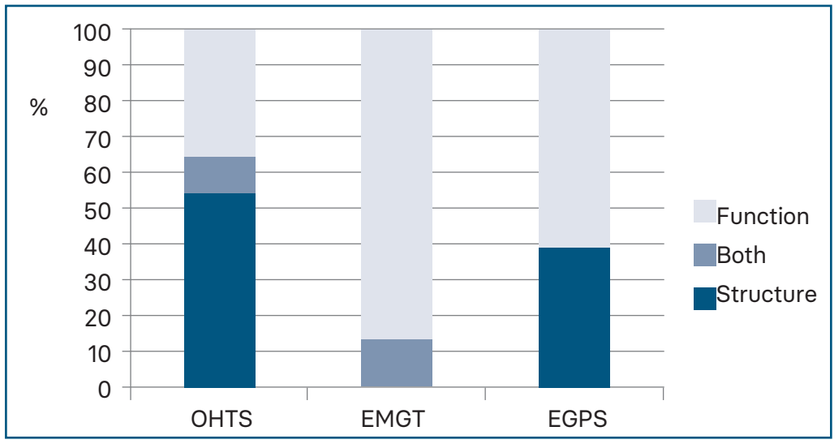

Figure 1
Percentage of patients who had the first detectable glaucomatous change on structural or functional testing or both tests in 3 major clinical trials.[7]

This data demonstrates that Quigley's early assertion of structural change preceding functional change cannot be applied to all patients – instead there are some where both happen contemporaneously and others where perimetric functional change occurs first.[7]

Spatial correlation

Whilst the temporal relationship appears more complex than initially thought, another key aspect of integrating structure and function is establishing the anatomical correspondence of optic nerve rim or RNFL loss with visual field defects. This spatial relationship was elucidated by Garway-Heath et al.[8] They carried out a cross sectional study in 69 patients from the Normal tension glaucoma clinic at Moorfields looking at grayscale photographs showing RNFL defects /prominent bundles and superimposing a scaled Humphrey 24-2 field grid. They were able to assess the relationship of visual field test points with a corresponding RNFL defect and sector of the optic nerve head (ONH). They generated the map illustrated in Figure 2 which is an invaluable resource for clinicians looking for spatial structure function correlation in their patients.

Figure 2

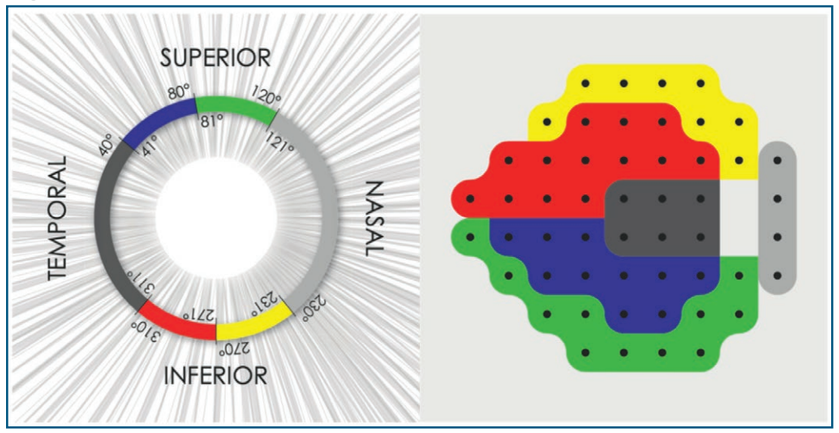

Figure 2
Map representing the relationship between Standard Automated Perimetry visual field sectors and section of the peripapillary OCT scan circle.[9]

The spatial correlations produced by this map are being employed in novel techniques attempting to fuse OCT and VF data from each sector of the optic nerve / visual field grid; Bizios et al have shown that these methods can improve the ability of "artificial neural networks" or ANNs to provide automated glaucoma diagnostics.[9]

Challenges of integrating structure and function

As alluded to above, there are many challenges to overcome in accurately integrating structure and function in glaucoma. The Garway-Heath model[8] represents spatial correspondence in an average eye, but in reality there can be significant variability in the trajectory of RNFL bundles based on the positioning of the ONH with respect to the fovea. Jansonius et al attempted to mathematically model this based on fundus images and found that for a single visual field location the ONH entry point can vary by 20-30 degrees.[10] As mentioned previously, traditional understanding is that in early disease structural change precedes functional change[4] (so-called pre-perimetric glaucoma) due to a "functional reserve" and that in later disease function changes at a greater rate than structure. This relationship was thought to be curvilinear but Garway-Heath et al suggested this apparent relationship could be due to the way in which structure and function are measured.[11] The unit of measurement for structure is linear (RNFL thickness in μm2) versus that for function which is logarithmic (VF decibels or dB in logmar units).[7] The decibels are a non-linear measure – this is demonstrated in Figure 3.[7] Studies have shown that when visual field sensitivity is expressed in linear units (rather than logarithmically), there is a demonstrable linear relationship with ganglion cell density and their activity (pattern electroretinogram or PERG).[11] Therefore rather than a functional reserve and curvilinear relationship, Garway-Heath's

Figure 3
The non-linear relationship between dB units and linear (L-1) metrics of differential light sensitivity for standard automated perimetry.[7] A decline of 2dB from a sensitivity of 32dB is ten-fold greater, on a linear scale, than a decline of 2dB from 22dB.

Figure 3

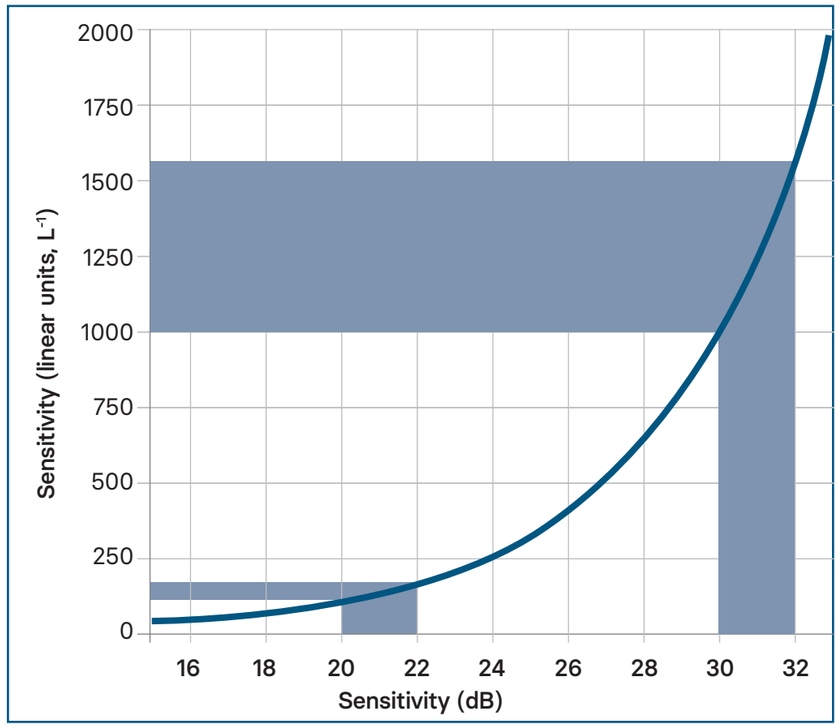

study[11] suggested that when linear measures were compared there is a linear continuous structure function relationship. Various quantitative models exist to relate structure and function in glaucoma. One such model is the Hood-Kardon model[12] which assumes a linear structure function relationship. This model attempts to relate visual field sensitivity in dB with RNFL thickness in µm and has helped demonstrate the existence of a "non-neural structural component." Where visual field sensitivity is non-existent in eyes blind with glaucoma, there is a "floor effect" of the RNFL around 60um thickness where it no longer thins or drops off. This is thought to be accounted for by glial tissue and blood vessels, demonstrating it is possible to have non-existent function with some residual structure remaining.

Another anatomical consideration is the distribution of RGCs across the macula relative to the ONH. The macula contains a very high density of RGCs (up to 33% of total RGCs) although it takes up less than 5% of retinal surface area. The macular region is sparsely sampled with 24-2 visual field testing and yet is known to be affected in mild to moderate glaucoma[13] - therefore in patients where structural change is not corroborated by 24-2 visual field testing it is important to consider 10-2 visual field testing to check macula function more closely. Quigley's assertion of structural change preceding functional change, is further challenged by findings that eyes with normal RGC counts had abnormal visual fields.[7] This could be accounted for by ganglion cells that may appear structurally normal with current imaging techniques, but are in fact "dysfunctional." Where it is possible to measure the functional RGC signals through pattern electroretinograms (PERG) this shows deficits which may not be identified through RNFL thickness measurements alone.[11] Ultimately the most accurate estimates of RGC counts can be achieved by counting cells in vivo and one might expect tighter structure function correlation once this technology is available.

Conclusion

Integrating structure and function in glaucoma continues to pose significant challenges to clinicians. With the evolution of more sophisticated imaging technologies, the challenge simply takes new directions - how can this abundance of data be integrated with existing function data to give clinically meaningful information? Whilst visual field testing has stood the test of time and remains the benchmark for functional assessment, further developments such as increasing sampling points at the macula, mapping visual field test points to distribution of RGCS and stimulus size to match the RGC receptive field, could yield stronger correlations.[7] Other means of further assessing structure and function such as in vivo ganglion cell counts, electrophysiological testing and personalised spatial mapping of RNFL bundles based on the relationship of ONH to fovea, can help provide supplementary information. Whether this can be applied in a high-volume clinical setting is yet to be established.

References

1. European Glaucoma Society Terminology and Guidelines for Glaucoma, 4th Edition - Chapter 2: Classification and terminologySupported by the EGS Foundation: Part 1: Foreword; Introduction; Glossary; Chapter 2 Classification and Terminology. Br J Ophthalmol. 2017;101(5):73-127.
2. Gracitelli CP, Abe RY, Tatham AJ, Rosen PN, Zangwill LM, Boer ER, et al. Association between progressive retinal nerve fiber layer loss and longitudinal change in quality of life in glaucoma. JAMA Ophthalmol. 2015;133(4):384-90.
3. Medeiros FA, Tatham AJ. Structure versus Function in Glaucoma: The Debate That Doesn't Need to Be. Ophthalmology. 22016;123(6):1170-72.
4. Quigley HA, Dunkelberger GR, Green WR. Retinal ganglion cell atrophy correlated with automated perimetry in human eyes with glaucoma. Am J Ophthalmol. 1989;107(5):453-64.
5. Keltner JL, Johnson CA, Anderson DR, Levine RA, Fan J, Cello KE, et al. The association between glaucomatous visual fields and optic nerve head features in the Ocular Hypertension Treatment Study. Ophthalmology. 2006;113(9):1603-12.
6. Öhnell H, Heijl A, Brenner L, Anderson H, Bengtsson B. Structural and Functional Progression in the Early Manifest Glaucoma Trial. Ophthalmology. 2016;123(6):1173-80.
7. Malik R, Swanson WH, Garway-Heath DF. 'Structure-function relationship' in glaucoma: past thinking and current concepts. Clin Exp Ophthalmol. 2012;40(4):369-80.
8. Garway-Heath DF, Poinoosawmy D, Fitzke FW, Hitchings RA. Mapping the visual field to the optic disc in normal tension glaucoma eyes. Ophthalmology. 2000;107(10):1809-15.
9. Bizios D, Heijl A, Bengtsson B. Integration and fusion of standard automated perimetry and optical coherence tomography data for improved automated glaucoma diagnostics. BMC Ophthalmology. 2011;11(1):20.
10. Jansonius NM, Nevalainen J, Selig B, Zangwill LM, Sample PA, Budde WM, et al. A mathematical description of nerve fiber bundle trajectories and their variability in the human retina. Vision Res. 2009;49(17):2157-63.
11. Garway-Heath DF, Holder GE, Fitzke FW, Hitchings RA. Relationship between electrophysiological, psychophysical, and anatomical measurements in glaucoma. Invest Ophthalmol Vis Sci. 2002;43(7):2213-20.
12. Hood DC, Kardon RH. A framework for comparing structural and functional measures of glaucomatous damage. Prog Retin Eye Res. 2007;26(6):688-710.
13. Zhang C, Tatham AJ, Weinreb RN, Zangwill LM, Yang Z, Zhang JZ, et al. Relationship between ganglion cell layer thickness and estimated retinal ganglion cell counts in the glaucomatous macula. Ophthalmology. 2014;121(12):2371-79.

Part I

Chapter 13

Screening, diagnosis and differential diagnosis with optical coherence tomography (OCT)

Panayiota Founti

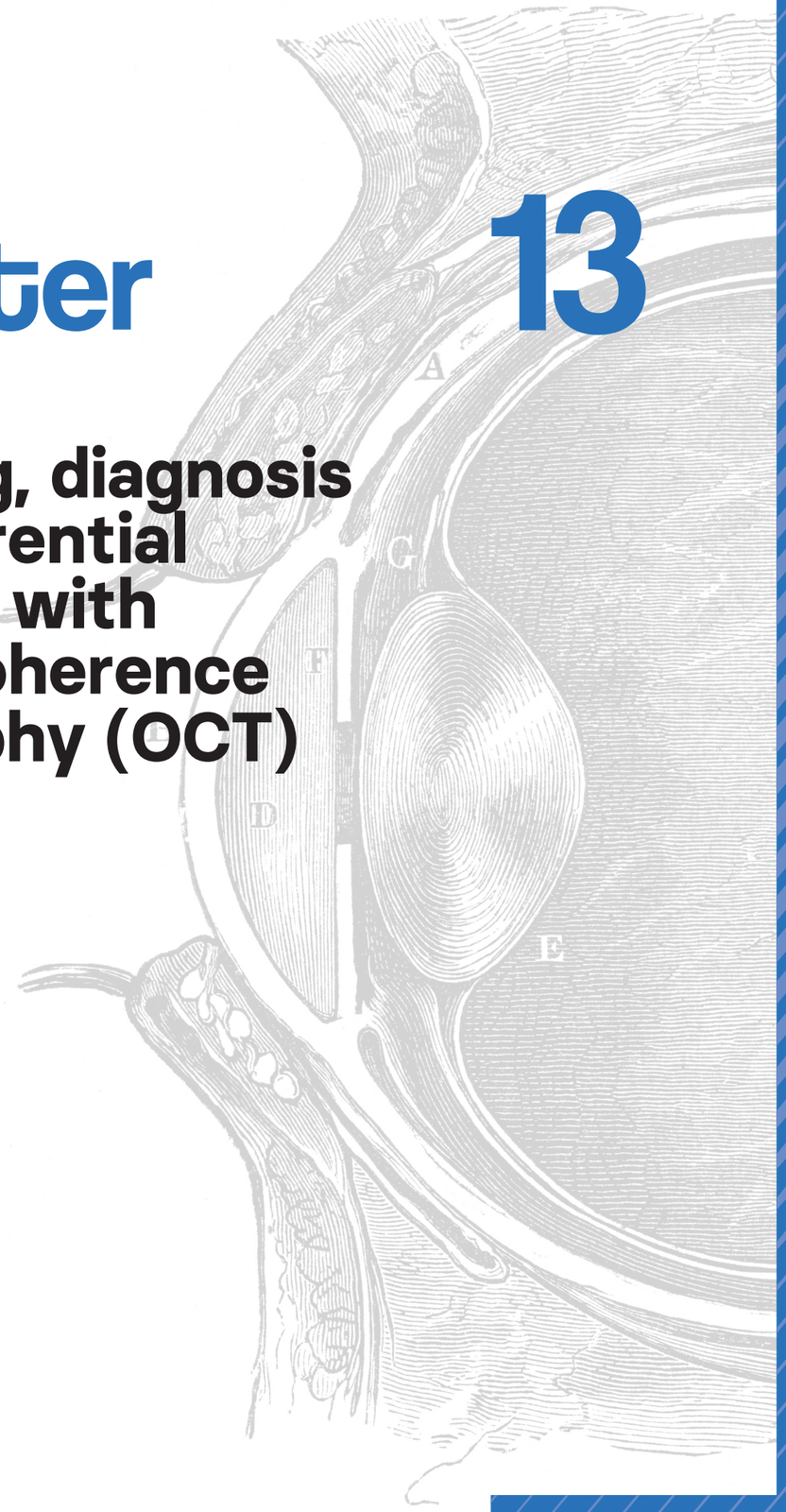

Vertical Section

13
Part I

Screening, diagnosis and differential diagnosis with optical coherence tomography (OCT)

Panayiota Founti

Consultant Ophthalmic Surgeon, Glaucoma Service, Moorfields Eye Hospital
and Honorary Senior Research Associate, UCL Institute of Ophthalmology, London, UK

Spectral domain (SD) OCT has become increasingly important in glaucoma care. As opposed to clinical assessment, which is inherently subjective, imaging with OCT provides an objective assessment of the optic nerve head, the retinal nerve fibre layer (RNFL) and the macula. In addition, it provides anatomical information which extends beyond what can be clinically perceived. Despite the obvious advantages, this powerful technology is not without flaws. Limitations of the built-in normative databases, errors in data acquisition, eye movement, media opacities, segmentation errors by the software can all confound data interpretation. These are being discussed in detail in another section. This chapter focuses on the role of OCT in the screening, diagnosis, and differential diagnosis of glaucoma.

OCT in glaucoma screening

Currently, glaucoma detection relies on opportunistic case finding usually by the general ophthalmologist or the community optometrist, depending on the healthcare setting. With at least 50% of glaucoma cases remaining undiagnosed, population screening represents a major unmet need in the field of glaucoma. Main challenges include the need for highly specific tests to minimise the risk of false positives, but also the relatively low prevalence of the disease, driving the positive predictive value (PPV = the probability of an individual having the disease when the test is positive) of diagnostic modalities low. This also applies to OCT parameters, including those derived from new segmentation software. For example, peripapillary RNFL from the Spectralis (Heidelberg Engineering, Inc., Heidelberg, Germany) has been shown to have 92.5% sensitivity at 80% specificity at discriminating between healthy and early glaucomatous eyes.[1]

With the prevalence of primary open angle glaucoma at 2.5% in those 40-80 years old,[2] the use of RNFL as a diagnostic test would have a PPV of just 11% in the general population. Setting the specificity cut-off at 95% to reduce the proportion of false positives would lead to sensitivity of 87.5% and an improved PPV of 31%, which, however, is still inadequate for population screening. PPV values can increase by increasing the pre-test probability of glaucoma, as in the case of high-risk individuals. In line with the above, an earlier landmark economic evaluation of screening strategies for glaucoma concluded that population screening is not cost-effective, but targeted screening of high-risk groups may be.[3] According to a more recent report from the United States Preventive Services Task Force, there is limited direct evidence on the benefits and costs of screening for glaucoma.[4] Similarly, the United Kingdom National Screening Committee does not recommend screening for glaucoma, because it is not clear if the available tests are accurate enough to use in a screening programme and there is no evidence on how screening would improve disease outcomes.[5]

Screening, diagnosis and differential diagnosis with optical coherence tomography (OCT)

Panayiota Founti

Combining OCT with telemedicine to screen older individuals and incorporating imaging with OCT into broader initiatives for the prevention of blindness may be cost effective options for glaucoma screening. Artificial intelligence (AI) is another powerful tool which may enable glaucoma screening in the future.[6] However, there are several issues to be addressed before AI can be incorporated into clinical care, including the fact that there are no universally accepted criteria for the diagnosis of glaucoma. This creates uncertainty around the ground truth on which an AI model should be trained and validated. In view of this challenge, new methods are being explored for the detection of glaucoma which rely exclusively on OCT.[7] Such an approach could provide the level of standardisation that AI algorithms require. However, it has not been validated yet, nor is it meant to replace the clinical diagnosis of glaucoma for the individual patient, which requires both structural and functional diagnostic tests.

OCT in glaucoma diagnosis

Glaucoma is characterised by neuroretinal rim loss and RNFL loss with related visual field defects.[8] In the context of opportunistic case finding, a thorough clinical examination of the optic disc is of utmost importance, because it is the clinical suspicion of glaucoma on the disc that will prompt the clinician to request additional tests or to initiate a glaucoma referral. From that point on, imaging with OCT can assist in the diagnosis of glaucoma. However, OCT is a classification tool which highlights statistical deviations from a normative database. It cannot provide a clinical diagnosis and, therefore, cannot replace clinical examination and visual field testing.[8] Commercially available SD-OCT devices are similar in their diagnostic accuracy for glaucoma and focus on three ocular structures: the RNFL, the optic nerve head and the macula. The most studied OCT parameter is the RNFL thickness. Imaging of the macula to detect glaucomatous damage is a new approach in glaucoma care and relies on the fact that the macula contains over 30% of the retinal ganglion cells.[9]

Bruch's Membrane opening-minimum rim width (BMO-MRW) is another newly introduced structural marker for the detection of glaucoma.[10] This parameter quantifies the neuroretinal rim from its true anatomic outer border and accounts for its variable orientation. The first step for the effective use of OCT in the diagnosis of glaucoma is a detailed quality assessment of the scans. This will allow the clinician to identify potential errors and artifacts, but also to detect deviations beyond the automatically generated summary statistics. The fundamentals of data interpretation with OCT are being extensively discussed in other sections of this book. The second step is the assessment of the agreement between structure and function ("does the visual field test match the disc?") (Fig. 1 A, B, E). The topographic map that relates different regions of the visual field test to different sectors of the optic nerve head can advise the clinician where to expect the visual field damage, given the disc appearance, and vice versa.[11] The topographic agreement between the glaucomatous damage of the macula and the visual field has also been described.[9] Early glaucomatous damage of the macula in shape and located inferiorly, resulting in a superior arcuate scotoma. The suggested mechanism is that most of the RNFL bundles from the inferior macula project to the inferior quadrant of the disc, which is particularly vulnerable to glaucoma. Conversely, the superior macula projects to the temporal quadrant of the disc, which is relatively less affected. Detecting early glaucomatous damage of the macula in the visual field may require a 10-2 pattern, because the macula is not well-sampled by the 24-2 or 30-2 visual field test (Fig. 1 C, D). The third step is data interpretation in the context of the overall clinical assessment, including patient history, as will be discussed in the following section.

OCT in the differential diagnosis of glaucoma

Imaging with OCT can help the clinician differentiate glaucoma from normal anatomical variations and other disease entities, such as retinal diseases and non-glaucomatous optic neuropathies. In this systematic process imaging with OCT is used in conjunction with the patient history and the rest of the clinical examination. Physiologic large optic disc cups and myopic discs are the most common entities in the differential diagnosis of glaucoma. In the former, the correlation of the cup with the disc size, the presence of a clinically healthy-looking rim and a full visual field should point towards the correct diagnosis. Provided that there is no other ocular pathology, imaging with OCT can provide additional reassurance, with RNFL, macular ganglion cell complex (GCC) and BMO-MRW within the normal range. Conversely, it may be difficult to exclude glaucomatous damage in myopic discs. Data interpretation from OCT in myopia is discussed in another section. While macular GCC has become increasingly important in the diagnosis of glaucoma, its impairment

Figure 1

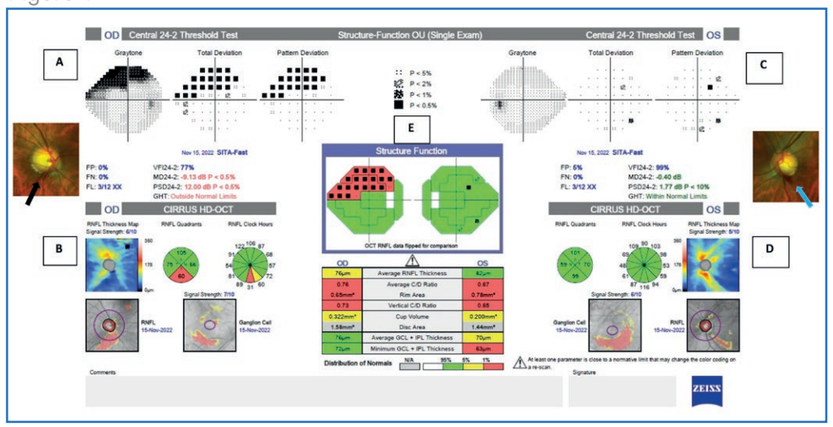

Figure 1
Structure-function correlation in a 53 year old patient with normal tension glaucoma. In the right eye, there is superior visual field loss (A) which is congruous with the optic disc showing inferior neuroretinal rim loss (black arrow). Imaging with optical coherence tomography (OCT) shows an inferior retinal nerve fibre layer (RNFL) defect and an inferior ganglion cell layer (GCL) defect, which are consistent with the clinical impression (B). The structure-function correlation map confirms the tomographic agreement between the visual field findings and the OCT findings. In the left eye, the disc looks glaucomatous, with inferior neuroretinal rim loss and a flame-shamed disc haemorrhage (blue arrow). Imaging with OCT shows a small inferior RNLF defect and an inferior ganglion cell layer defect (D), which are consistent with the clinical impression. Interestingly, the segmentation analysis is within the normal range in all sectors. The visual field test is within the normal range (C). However, in view of the early glaucomatous macular defect (and given that the macula is poorly sampled in the 24-2 visual field), one should request a 10-2 visual field test for the left eye.

is not specific to glaucoma. Several retinal pathologies can lead to GCC loss such as age-related macular degeneration, diabetic retinopathy, myopia and epiretinal membrane. However, in these conditions the GCC loss is either centred around the fovea or of non-specific pattern. Also, macular diseases typically cause reduced visual acuity and metamorphopsia. The visual field almost invariably shows a central scotoma which does not respect the horizontal meridian. Detailed imaging of the macula will usually reveal the corresponding macular pathology. Conversely, retinal vascular occlusions can cause arcuate visual field and RNFL/GCC defects which may be indistinguishable from those observed in glaucoma. Therefore, the differential diagnosis will rely on the patient history, the presence of relevant retinal signs and the non-progressive nature of the OCT and visual field findings. Non-glaucomatous optic neuropathies and neurodegenerative diseases, such as Alzheimer's and Parkinson's disease, can cause RNFL/GCC loss and, therefore, should always be included in the differential diagnosis of glaucoma.[12] In non-glaucomatous optic neuropathies the RNFL loss is typically located temporally and the visual field test shows central or cecocentral scotomas (Fig. 2). Interestingly, BMO-MRW is frequently preserved, despite diffuse RNFL loss. Conversely, optic disc drusen, anterior ischemic optic neuropathy and compressive optic neuropathy can cause RNFL defects which mimic those observed in glaucoma. Also, dominant optic atrophy, Leber hereditary optic neuropathy and compressive optic neuropathy can lead to glaucomatous-like disc excavation. A detailed patient history, the assessment of visual acuity, color vision and pupil reflexes, and the detection of disc pallor are crucial elements in making the correct diagnosis (Table 1).

Figure 2

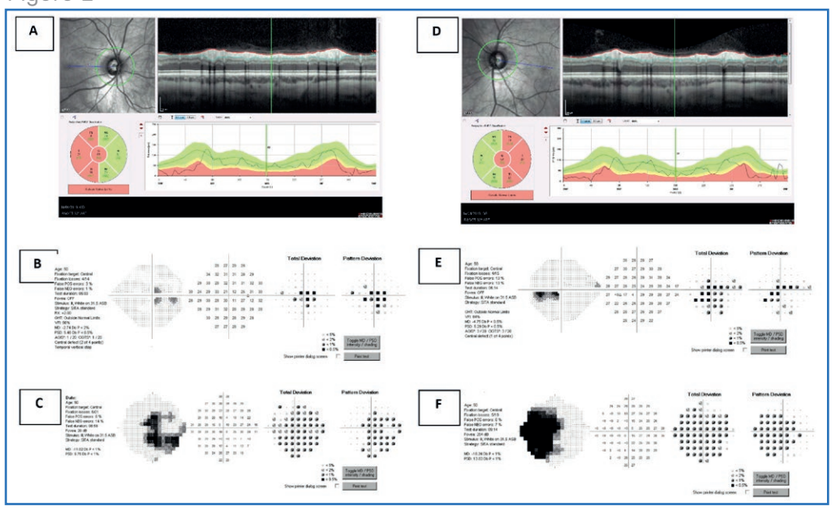

Figure 2
Nutritional optic neuropathy due to B12 deficiency in a 50 year old patient.
Imaging of the optic nerve head shows bilateral temporal RNFL loss (A, D), which is typical of non-glaucomatous optic neuropathies.
The 24-2 visual field shows central/cecocentral scotomas (B, E) which were further assessed with a 10-2 visual field test (C, F).

Table 1

Differential diagnosis of glaucomatous from non-glaucomatous optic neuropathies

Disease entity	Clinical presentation	Optic disc findings	Visual field findings	OCT findings
Optic disc drusen	• Usually asymptomatic	• Pseudopapilledema or subtle elevation of the disc or 'crowded' disc	• Enlargement of the blind spot or generalized constriction • Glaucomatous-like defects	• Glaucomatous-like RNFL loss, usually inferonasally and nasally
Anterior ischemic optic neuropathy	• Unilateral acute vision loss • Dyschromatopsia • RAPD	• Disc oedema (acute phase) • Eventually diffuse or segmental disc atrophy • A small proportion may develop disc excavation	• Altitudinal defect	• Glaucomatous-like RNFL loss (superiorly > inferiorly > temporally > nasally) • Altitudinal GCC loss
Optic neuritis	• Unilateral loss over hours to days • Pain with eye movements (may precede the visual loss by days) • Dyschromatopsia • RAPD	• Normal disc or disc oedema (acute phase) • Eventually disc atrophy (may be subtle)	• Typically, central scotoma but any type of VF loss can be observed	• Temporal RNFL loss • Diffuse GCC loss • Possible RNFL and GCC thinning in patients with MS even without optic neuritis
Dominant optic atrophy	• Bilateral slowly-progressive vision loss starting in the first or second decade of life • Often, family history of vision loss • Dyschromatopsia	• Focal, wedged-shaped temporal disc atrophy or diffuse atrophy • Disc excavation	• Central, centrocecal and paracentral scotomas	• Temporal RNFL loss • Diffuse GCC loss
Leber Hereditary Optic Neuropathy	• Unilateral, slowly-progressive vision loss in the second to fourth decade of life • Second eye involvement is usually weeks to months later (but could be years later) • Unilateral, slowly-progressive vision loss in the second to fourth decade of life • Second eye involvement is usually weeks to months later (but could be years later) • Dyschromatopsia • Family history of vision loss in maternal family members	• Normal or pseudo-edematous optic nerves • Disc atrophy • Disc excavation	• Central or cecocentral scotomas	• Initially temporal RNFL loss, then all four quadrants may be affected • Diffuse GCC loss

Table 1
This table presents common symptoms and signs of the common non-glaucomatous optic neuropathies but is not an exhaustive list.

Table 1 continued

Differential diagnosis of glaucomatous from non-glaucomatous optic neuropathies				
Disease entity	**Clinical presentation**	**Optic disc findings**	**Visual field findings**	**OCT findings**
Toxic/neutritional optic neuropathy **(etiology: alcohol, tobacco, drugs (eg ethambutol), heavy metals, carbon monoxide)**	• Bilateral progressive vision loss, usually starting at the point of fixation • Dyschromatopsia • History of exposure to the corresponding toxin	• Normal disc, disc oedema or hyperemic disc in early detection • Eventually disc atrophy	• Central or cecocentral scotomas with preservation of the peripheral field • Ethambutol may cause bitemporal hemianopsia	• Temporal RNFL loss • Diffuse GCC loss
Compressive optic neuropathy	• Monocular slowly-progressive vision loss • Can be associated with headaches, nausea, vomiting • Dyschromatopsia • RAPD	• Segmental atrophy • Disc excavation	• Glaucomatous-like defects of various extent	• Glaucomatous-like RNFL loss • Diffuse GCC loss
Traumatic optic neuropathy	• Unilateral or bilateral vision loss after blunt or penetrating trauma that cannot be explained by clinical findings • Dyschromatopsia • RAPD • History of trauma	• If anterior, infarction, haemorrhage or central artery retinal occlusion may be detected • If posterior, the disc may be normal • Signs of disc atrophy 3-6 weeks later	• Varies, depending on the extent of the extent of the trauma	• RNFL loss which varies, depending on the extent of the trauma • Diffuse GCC loss

References

1. Pazos M, Dyrda AA, Biarnés M, et al. Diagnostic Accuracy of Spectralis SD OCT Automated Macular Layers Segmentation to Discriminate Normal from Early Glaucomatous Eyes. Ophthalmology. 2017;124(8):1218-28.
2. Tham YC, Li X, Wong TY, Quigley HA, Aung T, Cheng CY. Global prevalence of glaucoma and projections of glaucoma burden through 2040: a systematic review and meta-analysis. Ophthalmology. 2014;121(11):2081-90.
3. Burr JM, Mowatt G, Hernández R, et al. The clinical effectiveness and cost-effectiveness of screening for open angle glaucoma: a systematic review and economic evaluation. Health Technol Assess. 2007;11(41):iii-iv,ix-x:1-190.
4. Chou R, Selph S, Blazina I, et al. Screening for Glaucoma in Adults: Updated Evidence Report and Systematic Review for the US Preventive Services Task Force. Jama. 2022;327(20):1998-2012.
5. Committee UNS. Screening in the UK: making effective recommendations 1 April 2019 to 31 March 2020. https://www.gov.uk/government/publications/uk-national-screening-committee-recommendations-annual-report/screening-in-the-uk-making-effective-recommendations-1-april-2019-to-31-march-2020#:~:text=The%20UK%20NSC%20does%20not%20currently%20recommend%20screening%20for%20glaucoma,use%20in%20a%20screening%20programme. Published 2023. Accessed 14/6/2023.
6. Ting DSW, Pasquale LR, Peng L, et al. Artificial intelligence and deep learning in ophthalmology. Br J Ophthalmol. 2019;103(2):167-75.
7. Hood DC, La Bruna S, Tsamis E, et al. Detecting glaucoma with only OCT: Implications for the clinic, research, screening, and AI development. Prog Retin Eye Res. 2022;90:101052.
8. European Glaucoma Society. Terminology and Guidelines for Glaucoma. 5th Edition. PubliComm, Savona, Italy; 2020.
9. Hood DC, Raza AS, de Moraes CG, Liebmann JM, Ritch R. Glaucomatous damage of the macula. Prog Retin Eye Res. 2013;32:1-21.
10. Chauhan BC, O'Leary N, AlMobarak FA, et al. Enhanced detection of open-angle glaucoma with an anatomically accurate optical coherence tomography-derived neuroretinal rim parameter. Ophthalmology. 2013;120(3):535-43.
11. Garway-Heath DF, Poinoosawmy D, Fitzke FW, Hitchings RA. Mapping the visual field to the optic disc in normal tension glaucoma eyes. Ophthalmology. 2000;107(10):1809-15.
12. Pasol J. Neuro-ophthalmic disease and optical coherence tomography: glaucoma look-alikes. Curr Opin Ophthalmol. 2011;22(2):124-32.

Part I

Chapter 14

Imaging in glaucoma patients with comorbidities

Andreas Katsanos

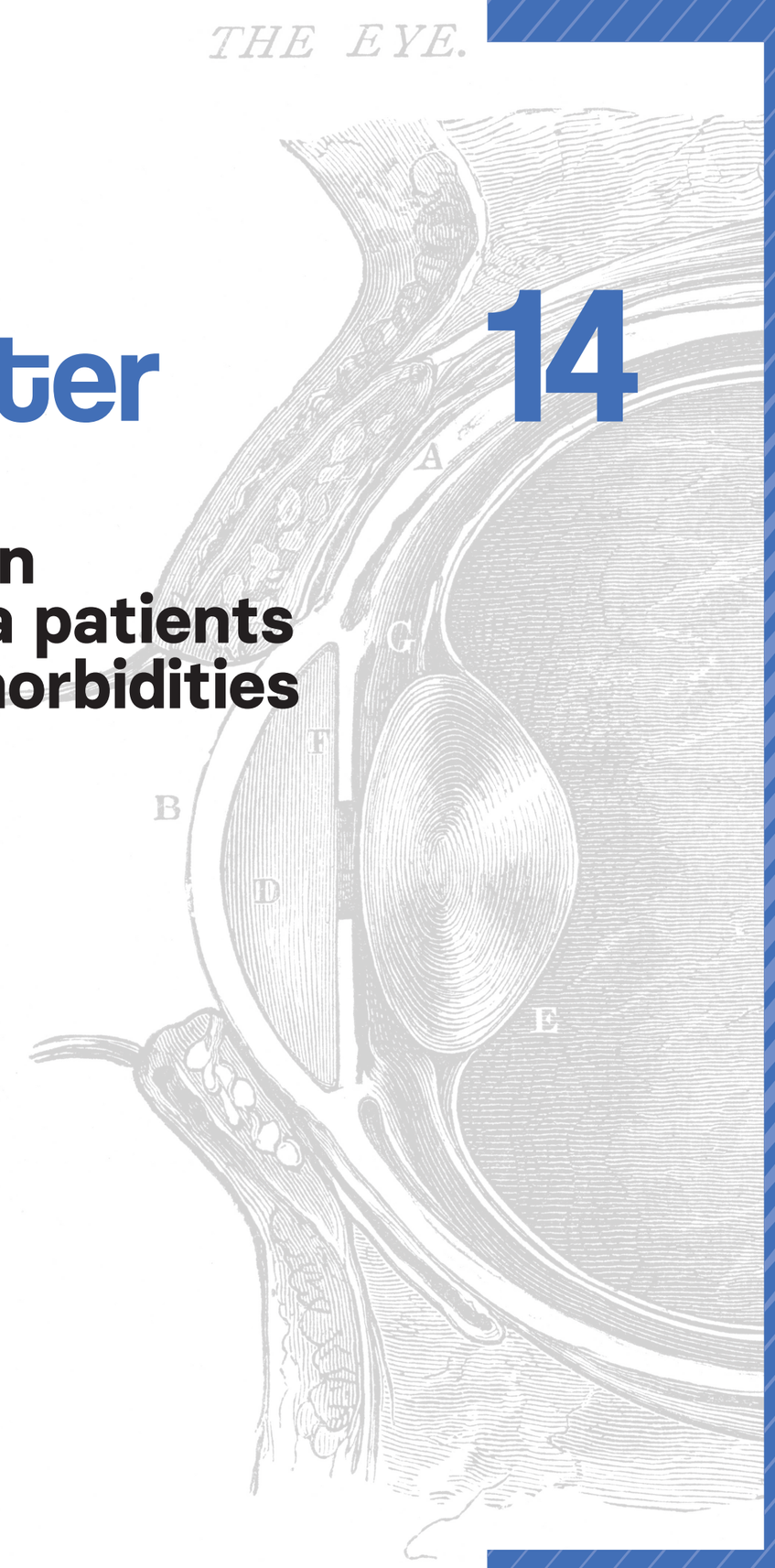

Vertical Section

14
Part I

Imaging in glaucoma patients with comorbidities

Andreas Katsanos

Ophthalmology Department, University of Ioannina, Ioannina, Greece

Using imaging for the evaluation of glaucoma patients who also suffer from other ocular or central nervous system comorbidities can be challenging. Diseases such as age-related macular degeneration (AMD), anterior or posterior ischemic optic neuropathy, or lesions along the optic nerve pathway may affect the imaging modalities used for glaucoma diagnosis or monitoring. In such cases, the cautious interpretation of optical coherence tomography (OCT) scans in the light of the patient's general and ophthalmic history, perimetry results and detailed clinical examination is mandatory.

There is a growing body of evidence supporting the use of macular OCT imaging both for the early detection and long-term monitoring of glaucoma.[1] A recent meta-analysis evaluating 150 studies with 16104 glaucomatous and 11543 control eyes[2] showed that there is a comparable level of diagnostic accuracy in identifying glaucoma using measurements of peripapillary retinal nerve fiber layer (pRNFL), ganglion cell-inner plexiform layer (GCIPL), and ganglion cell complex (GCC) thickness. However, in advanced stages of the disease where a significant proportion of tissue has been lost, the measurements of actual pRNFL thickness and its changes using spectral-domain OCT are less useful due to the existence of a floor effect, beyond which no further thinning can be observed.[3] In such late stages of the disease, a significant portion of GCIPL tissue may remain above the measurement floor, so that GCIPL thickness can be a more meaningful choice than pRNFL thickness for detecting progression.[4] The precise thickness measurement of these retinal layers is based on the detailed and accurate segmentation of the retina in OCT scans, which is a task accomplished automatically by means of inbuilt software algorithms.[5] Unfortunately, segmentation errors can occur quite often in cases with coexistent retinal pathologies. In cases with macular edema or epiretinal membrane, the associated structural changes in the retinal anatomy could cause segmentation errors and inaccuracies in thickness measurements, as both these clinical entities tend to thicken the retina.[6,7] Similar errors might also be observed in patients with outer retina pathologies, like AMD. The presence of large drusen below the retinal pigment epithelium can compress the inner retinal segments, causing a reduction in thickness measurements that could erroneously be interpreted as glaucomatous atrophic changes in the inner retina.[5] On the other hand, this is not observed in eyes with small or medium height drusen, where the retinal layers maintain their shape, and thus, the thickness measurements in such scans can be considered valid.[5] More specifically, it was found that the thickness of the macular GCIPL and the pRNFL are reduced in eyes with dry AMD, and there was a negative correlation between the average

Andreas Katsanos

Figure 1
Large drusen and their effect on inner retina.[5] The correct boundary between the inner plexiform and inner nuclear layer is marked with the white interrupted line. The red line indicates the boundary of the large drusen (marked with arrow in the bottom figure).

Figure 1

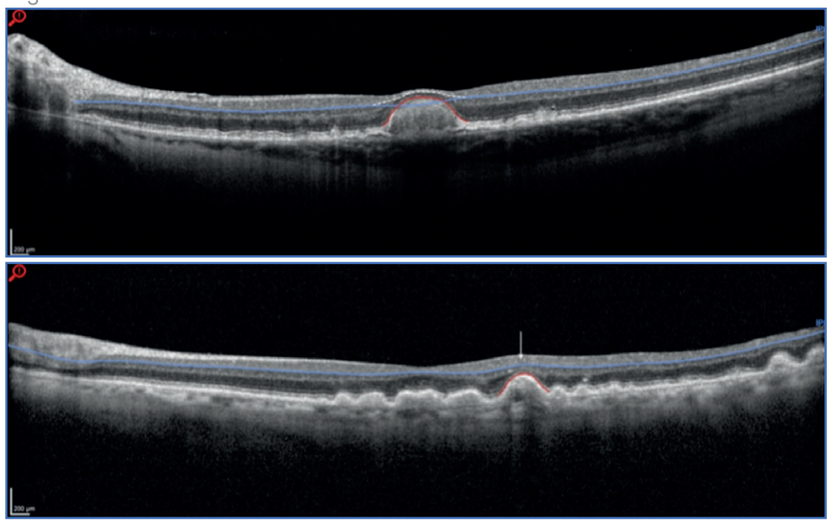

Figure 2
Examples showing prolapse of retinal layers in geographic atrophy.[5] The correct boundary between the inner plexiform and inner nuclear layer is marked with the white interrupted line.

Figure 2

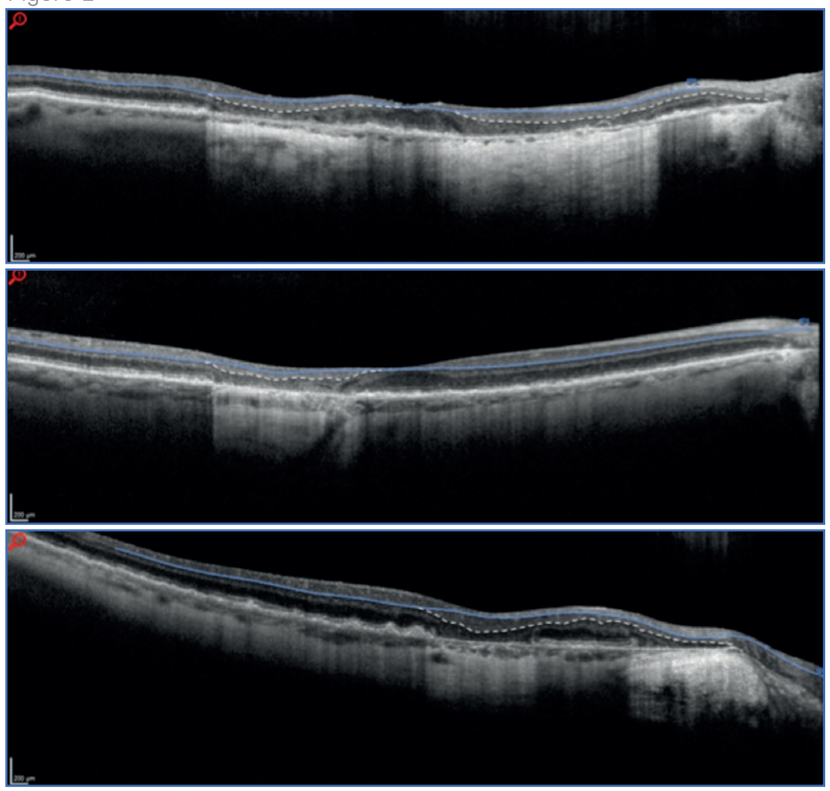

thickness of macula GCIPL and the extent of drusen.[8] Similarly, the thickness of the inner retinal layers can be considerably reduced in AMD patients with extensive geographical atrophy, which can cause posterior retinal prolapse.[5]

In addition to glaucoma, pRNFL thinning can be observed in a range of other optic neuropathies. Distinguishing glaucomatous optic neuropathy (GON) or progression in a patient with established glaucoma from non-glaucomatous neuropathies (NGONs) can be quite challenging. This is especially true when dealing with patients who have a chronic, relatively slow ongoing loss of the optic nerve rim with no sudden visual symptoms and absence of specific history clues. When thinning of the macular GCC or the pRNFL in OCT scans does not correspond to perimetry results or the appearance of the optic disc, the suspicion of non-glaucomatous damage should be high. Ophthalmoscopy clues such as the distribution of neuroretinal tissue, the cup-to-disc ratio, or the extent of optic disc pallor in the remaining neuroretinal rim should be carefully considered. If available, parameters and measurements of the optic nerve head such as pRNFL thickness and Bruch's membrane opening minimum rim width (BMO-MRW), can be utilized to differentiate between these clinical entities.[9] Compared to NGON cases with a similar degree of pRNFL thinning, BMO-MRW serves as an indicator of glaucoma, and more precisely, it has been suggested that the ratio pRNFL/BMO–MRW is diagnostically superior compared to the BMO–MRW alone in discriminating whether the observed optic neuropathy is glaucomatous or non-glaucomatous.[9] The notion that these parameters can be used in order to differentiate glaucomatous from non-glaucomatous damage is based on the anatomical changes that these clinical entities cause in the optic nerve head. Optic discs affected by glaucoma typically develop excavation and narrowing of BMO–MRW before acquiring a pale, atrophic appearance in the final stages. On the other hand, discs with non-glaucomatous optic neuropathies primarily become pale due to the loss of nerve fibers with rare instances of excavation.[9] This typically occurs in the chronic stage of non-arteritic anterior ischemic optic neuropathy (NAION): the loss of pRNFL can be similar to that of glaucomatous eyes, but the optic nerve

Figure 3
Illustration of Bruch's membrane opening (BMO) represented as a dot, the internal limiting membrane (ILM) depicted as a surface line, and Bruch's membrane opening-minimum rim width (BMO-MRW) symbolized by an arrow, which signifies the shortest distance.[10]

Figure 3

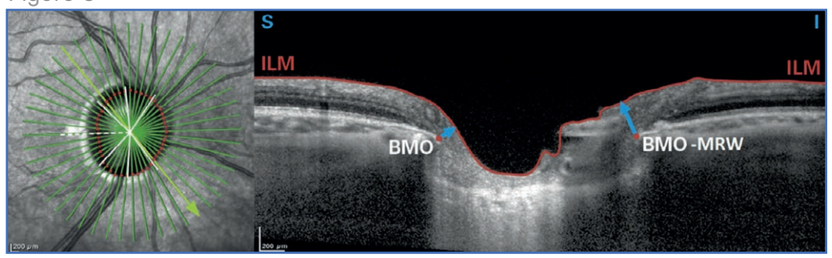

head parameters, such as the BMO-MRW, remain similar to those found in healthy control eyes.[10] This disparity could be helpful in distinguishing between these two different optic neuropathies during the chronic stage of NAION.

Diagnostic confusion can arise in cases with compressive optic neuropathy (CON), as these eyes can exhibit the landmark changes of glaucoma, i.e. cupping and excavation of the optic disc.[11] Distinguishing between CON and normal-tension glaucoma can be especially challenging.[11] It has been shown that compared to open angle glaucoma, CON is much more likely to induce significant thinning in the nasal and temporal sectors of the optic disc. [11] On the other hand, open angle glaucoma is associated with larger cupping and greater cup volume compared to CON.[11] Because the patterns of BMO–MRW changes overlap substantially in these two conditions, relying solely on BMO–MRW measurements is not recommended for distinguishing CON from GON. However, when BMO–MRW is combined with measurements of the pRNFL (i.e. using either the BMO–MRW/pRNFL or the pRNFL/BMO–MRW ratio), the ability to differentiate between these two conditions is increased.[12]

In conclusion, it is essential to consider the possibility of a non-glaucomatous optic neuropathy if unusual patterns of damage on the optic nerve head, such as the selective thinning of temporal or nasal quadrants, are identified on OCT scans. Similarly, discordances between OCT scans and clinical findings, such as thinning of the macular GCC or pRNFL without a glaucomatous-like optic disc appearance, might also raise the suspicion of NGONs. If available, measurements like BMO–MRW, or the ratio between pRNFL and BMO–MRW, along with a detailed fundus examination, comprehensive patient history and perimetry results, could help us to identify true glaucoma damage or progression in cases where other comorbidities pose differential diagnostic challenges.

References

1. Hood DC, Raza AS, de Moraes CG, Liebmann JM, Ritch R. Glaucomatous damage of the macula. Prog Retin Eye Res. 2013;32:1-21.
2. Kansal V, Armstrong JJ, Pintwala R, Hutnik C. Optical coherence tomography for glaucoma diagnosis: An evidence based meta-analysis. PLOS ONE. 2018;13(1):e0190621.
3. Mwanza JC, Budenz DL, Warren JL, Webel AD, Reynolds CE, Barbosa DT, et al. Retinal nerve fibre layer thickness floor and corresponding functional loss in glaucoma. British Journal of Ophthalmology. 2015;99(6):732-37.
4. Hammel N, Belghith A, Weinreb RN, Medeiros FA, Mendoza N, Zangwill LM. Comparing the Rates of Retinal Nerve Fiber Layer and Ganglion Cell–Inner Plexiform Layer Loss in Healthy Eyes and in Glaucoma Eyes. American Journal of Ophthalmology. 2017;178:38-50.
5. Chew L, Mohammadzadeh V, Mohammadi M, Toriz V, Rosa N, Gorin MB, et al. Measurement of the Inner Macular Layers for Monitoring of Glaucoma: Confounding Effects of Age-Related Macular Degeneration. Ophthalmol Glaucoma. 2023;6(1):68-77.
6. De Moura J, Samagaio G, Novo J, Almuina P, Fernández MI, Ortega M. Joint Diabetic Macular Edema Segmentation and Characterization in OCT Images. Journal of Digital Imaging. 2020;33(5):1335-51.
7. Bontzos G, Kabanarou SA, Garnavou-Xirou C, Gkizis I, Kontou E, Triantafyllou D, et al. Segmentation errors and motion artifacts in OCT-A associated with epiretinal membranes. Can J Ophthalmol. 2020;55(4):293-300.
8. Lee EK, Yu HG. Ganglion Cell-Inner Plexiform Layer and Peripapillary Retinal Nerve Fiber Layer Thicknesses in Age-Related Macular Degeneration. Invest Ophthalmol Vis Sci. 2015;56(6):3976-83.
9. Boussion F, Guindolet D, Deschamps R, Lamirel C, Vignal-Clermont C. Retinal Nerve Fiber Layer Thickness/Minimum Rim Width Ratio Differentiates Glaucoma From Other Optic Neuropathies. J Glaucoma. 2023;32(5):435-41.
10. Resch H, Mitsch C, Pereira I, Schwarzhans F, Wasserman L, Hommer A, et al. Optic nerve head morphology in primary open-angle glaucoma and nonarteritic anterior ischaemic optic neuropathy measured with spectral domain optical coherence tomography. Acta Ophthalmol. 2018;96(8):e1018-e24.
11. Danesh-Meyer HV, Yap J, Frampton C, Savino PJ. Differentiation of compressive from glaucomatous optic neuropathy with spectral-domain optical coherence tomography. Ophthalmology. 2014;121(8):1516-23.
12. Andrade TS, Araújo RB, Rocha A, Mello LGM, Cunha LP, Monteiro MLR. Bruch Membrane Opening Minimum Rim Width and Retinal Nerve Fiber Layer Helps Differentiate Compressive Optic Neuropathy From Glaucoma. Am J Ophthalmol. 2022;234:156-65.

Part 2

Chapter 15

Anterior segment. Normal and pathological anatomy

Natalia Porporato

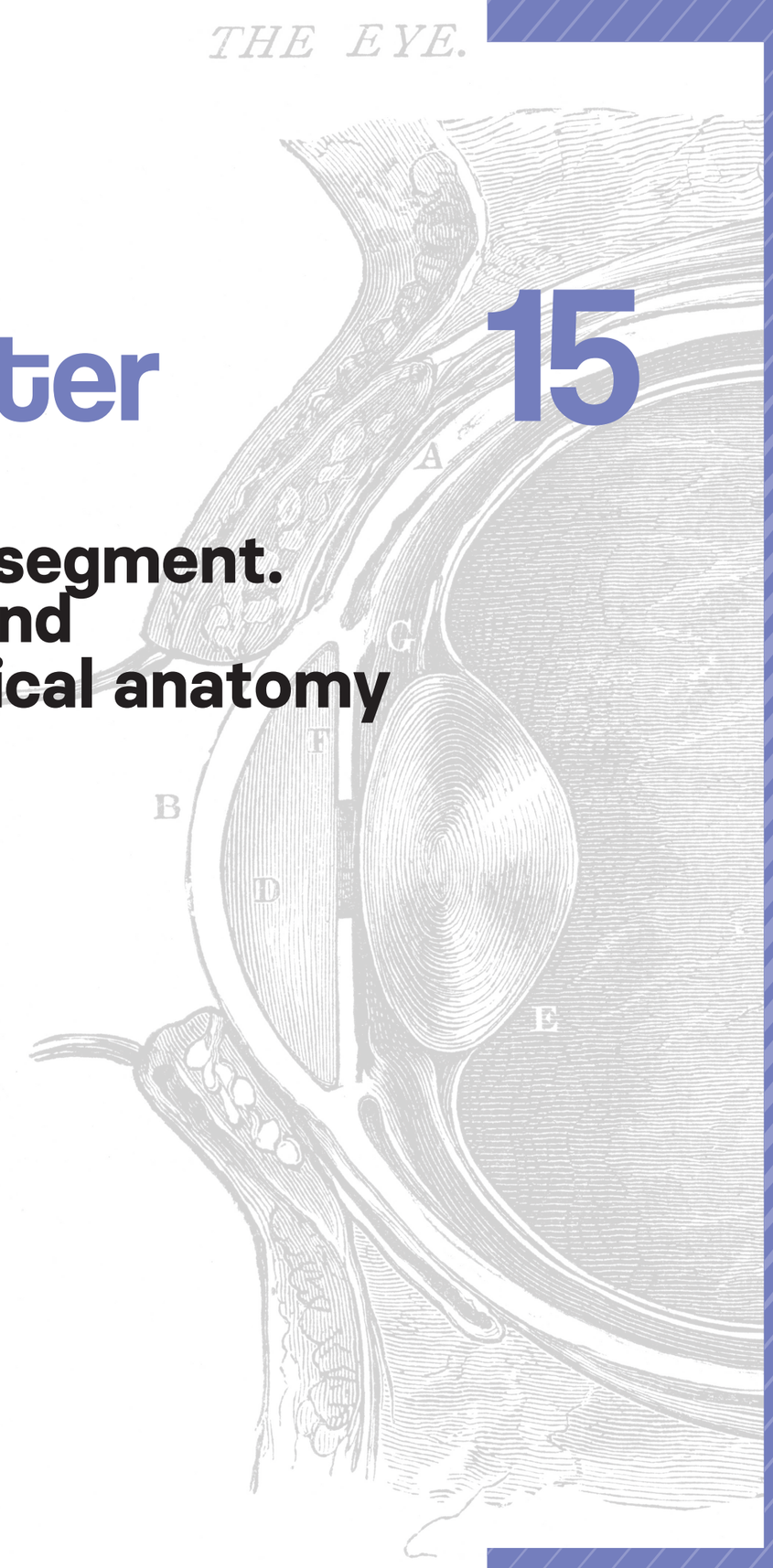

Vertical Section

Anterior segment. Normal and pathological anatomy

Natalia Porporato

Singapore National Eye Centre/Singapore Eye Research Institute

The anterior segment of the eye is a complex region, housing key structures that play a critical role in the homeostasis of the intraocular pressure. Fast and direct non-contact imaging of the anterior segment was possible with the development of the anterior segment optical coherence tomography (AS-OCT). AS-OCT is a high-resolution optically based imaging system that uses low-coherence interferometry to provide images of ocular tissues. AS-OCT has evolved from time-domain to spectral domain systems, with enhanced signal-to-noise ratio, image acquisition speed and resolution. Earlier time-domain devices were limited in the number of cross-sectional scans they could provide, while newer spectral-domain systems are able to scan the whole 360 degrees in a three-dimensional manner (up to 50 000 A-scans per second).[1]

The commercially available AS-OCT devices' wavelength ranges from 840 to 1310 nm, with an axial resolution of approximately 10 µm and a transverse resolution of 30 µm. Figure 1 shows an overview of the different anterior segment parameters that can be estimated from an AS-OCT image. However, one of the biggest limitations of AS-OCT imaging is its inability to image the structures behind the iris. For this reason, ultrasound biomicroscopy (UBM) remains a critical tool for evaluation of the lens zonules and ciliary body. In this chapter, we will delve into the normal and pathological anatomy of anterior segment structures, explore key measurements and parameters crucial for clinical assessment, and consider its relevance in glaucoma management.

Figure 1

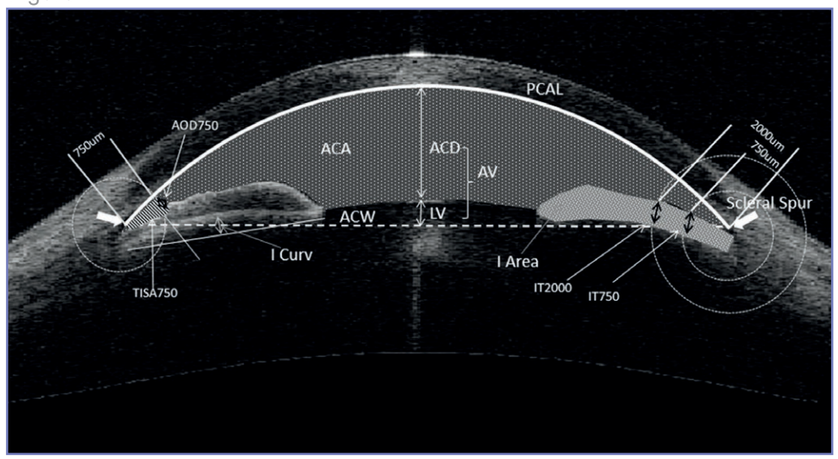

Figure 1
ASOCT image showing the different anterior segment parameters (AOD: anterior opening distance; TISA: trabecular iris space area; I Curv: iris curvature; I Area: iris area; IT iris thickness; ACW: anterior chamber width; ACD: anterior chamber depth; ACA: anterior chamber area; LV: lens vault; AV: anterior vault; PCAL: posterior corneal arc length).

Conjunctiva and Cornea

The conjunctiva is the thin, transparent mucous membrane that covers the front surface of the eye and, at a clinical level, it is divided into palpebral, forniceal and bulbar. The bulbar conjunctiva in AS-OCT imaging is better visualized with raster scan, 12x12 mm of width and 11 mm of scan depth. It is possible to evaluate its thickness and architecture (blood and lymphatic vessels), and plays a major role in the evaluation of post-trabeculectomy bleb. Bleb morphology is an important indicator of bleb function. AS-OCT allows assessment of the internal bleb anatomy (Fig. 2) which may otherwise not be visualized on slit-lamp evaluation such as the bleb height, bleb cavity, bleb and scleral wall thickness, position of the scleral flap, presence or absence of hyporeflective sub-flap space, and, patency or occlusion of the internal ostium.

Good filtration of the aqueous have been shown to be associated with the presence of internal fluid-filled cavities, low reflectivity of the bleb walls, microcysts, and patent internal ostia.[2] The cornea, the clear and outermost layer of the eye, consists of several layers, including the epithelium, stroma, and endothelium, each with distinct functions contributing to its transparency and optical properties. AS-OCT can provide valuable information about the cornea, such as central corneal thickness (CCT). CCT is an important measurement in glaucoma care as individuals with thinner corneas may have a higher risk of developing glaucoma or progressing to more severe stages.[3] Also, thinner corneas can artificially underestimate intraocular pressure readings obtained by tonometry. It worth to highlight that CCT by AS-OCT tends to be about 28 µm thinner than the CCT measured by ultrasound pachymetry.[4]

Anterior chamber and its angle

The anterior chamber in AS-OCT imaging is an optically empty space between the cornea and the irido-lenticular plane. Its angle is defined as the area between the iris and the anterior wall of the trabecular meshwork above the scleral spur. Common parameters used to describe the configuration of the angle include the angle opening distance (AOD), the angle recess area (ARA) and the trabecular-iris space area (TISA). These parameters can be measured at varying intervals anterior to the scleral spur, most frequently at 500 or 750 µm (i.e., AOD500, AOD750). Another valuable parameter is the anterior chamber depth (ACD), that measures the distance between the corneal endothelium to the anterior capsule of the lens. These parameters are possible to calculate with the in-built software of most AS-OCT devices, that can also offer automated detection of the scleral spur. AS-OCT can be used as an adjunct test to gonioscopy for angle closure detection, mechanism assessment and risk stratification.[5,6] In regards of angle closure detection, AS-OCT demonstrated a good agreement with gonioscopy in several hospital and community-based studies.[7]

However, it tends to detect more closed angles compared to gonioscopy,8 with the possible reasons being the inadvertent compression of the cornea leading to spurious opening of the angles and also excessive exposure to light during gonioscopy. The high resolution and scan speed of newer spectral domain AS-OCT devices has also facilitated the measurement of the area and degree of peripheral anterior synechiae (PAS)[9] (Fig. 3). AS-OCT has been useful in elucidating the existence of substantial heterogeneity within angle closure based on both quantitative measurements[10] as well as qualitative categorization of the most likely disease mechanism(s) such as pupil block, plateau iris, thick peripheral iris and large lens. Studies have shown that the outcome of laser peripheral iridotomy and lens extraction differed based on the supposed predominant mechanism.[11] Knowledge of the underlying angle closure mechanism may help predict future changes in the anterior segment parameters. In terms of disease prediction, narrower angles and larger lens

Figure 2
ASOCT image showing peripheral anterior synechiae as obtained with the CASIA SSOCT.

Figure 2

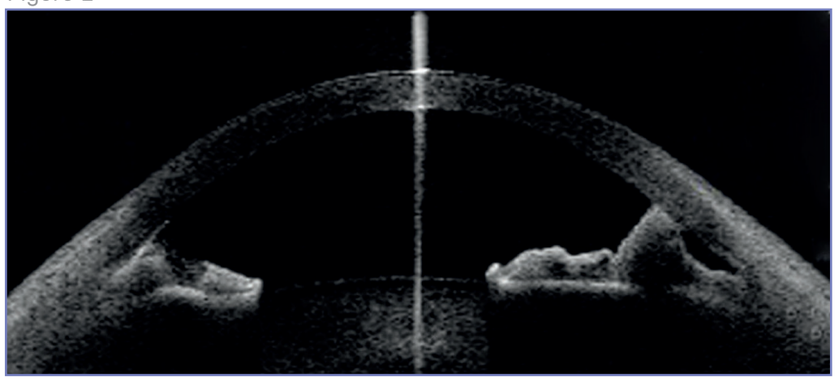

Figure 3

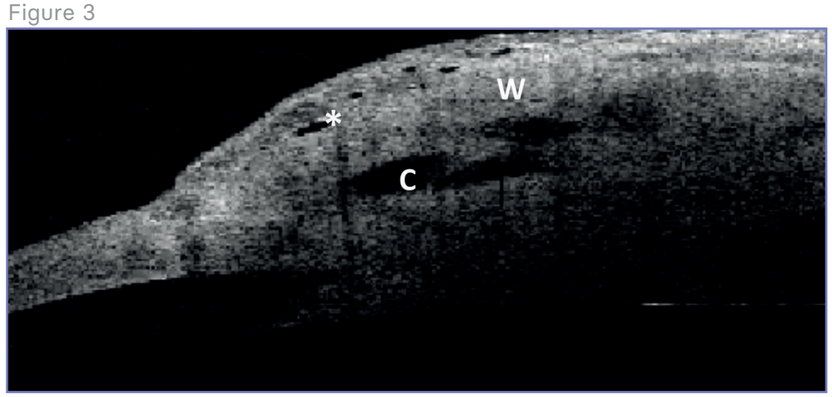

Figure 3
ASOCT image showing the bleb wall (w), cavity (c) and cystic hyporeflective spaces within the wall (*).

vault on AS-OCT has been shown to be predictive of incident gonioscopic angle closure prompting closer monitoring of those with angle closure on AS-OCT.[12,13] Narrower angle and flatter iris have also been shown to be associated with disease progression from primary angle closure suspect to primary angle closure with a moderate diagnostic performance (AUC of 0.73).[6]

Iris and ciliary body

The iris is the most anterior part of the uveal tract and it extends from its relatively thin root in the anterior chamber angle to the pupil. AS-OCT can provide important information about its dynamics and configuration that may impact treatment decisions. It has been shown that angle parameters as measured by AS-OCT are inversely correlated with pupillary diameter in different lighting conditions. In particular, changes in iris volume (IV) and area (IA) in response to pupil dilation independently contributes to angle narrowing when pupillary block is the dominant mechanism.1 AS-OCT can also detect the presence of iris cysts (Fig. 4) or tumors, which may cause secondary glaucoma.

The identification and characterization of these lesions are crucial for diagnosis and treatment planning. The ciliary body comprises the ciliary muscle and ciliary epithelium, arranged anatomically as the pars plana and pars plicata (containing the ciliary processes). Ultrasound biomicroscopy (UBM) is another anterior segment imaging modality that is preferable for visualization of more posterior structures such as the ciliary body, lens zonules and anterior choroidal effusion. It is useful in the evaluation of the presence and extent of weak zonules and lens subluxation (Fig. 5) especially in patients with pseudoexfoliation. It is also preferred over the ASOCT for the diagnosis of plateau iris which is characterized by specific UBM-based features as shown in Figure 6, and for imaging iris pigment epithelial cyst (Fig. 7).

Figure 4

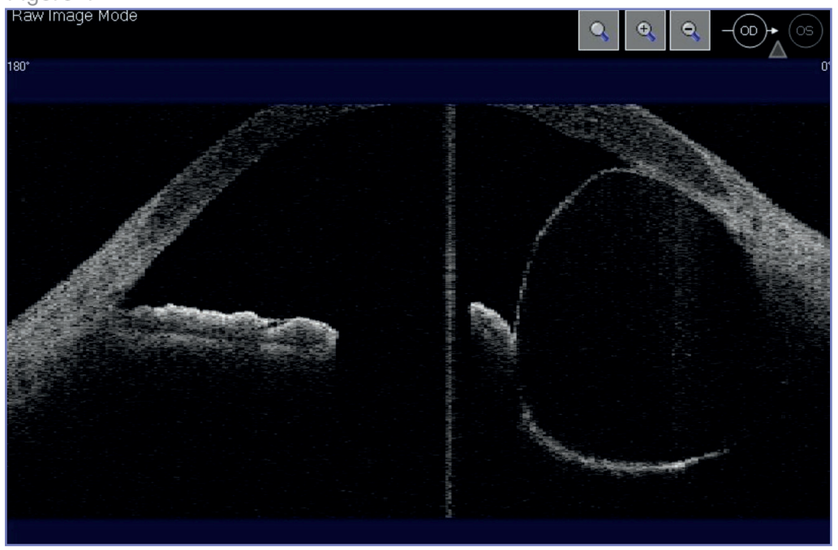

Figure 4
ASOCT image
of a stromal iris cyst.

Figure 5

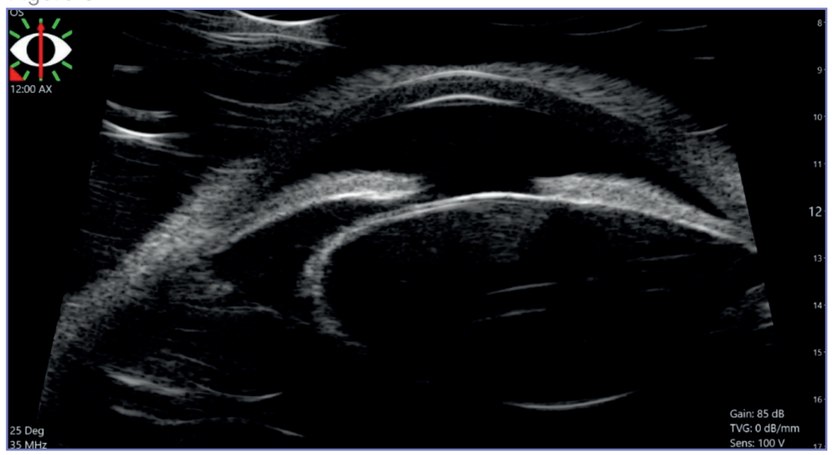

Figure 5
UBM image showing
subluxed lens.

Figure 6

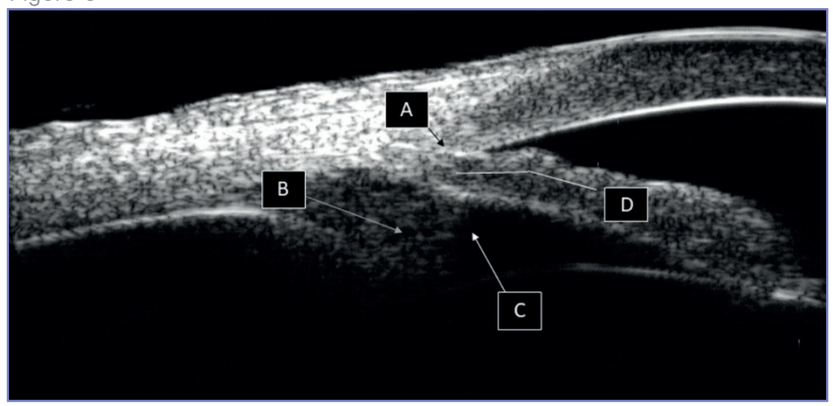

Figure 6
UBM image of a
quadrant of an eye with
plateau iris showing
irido-angle contact (A),
anteriorly directed ciliary
process (B), absent
ciliary sulcus (C), and iris
angulation and flat
iris plane (D).

Figure 7

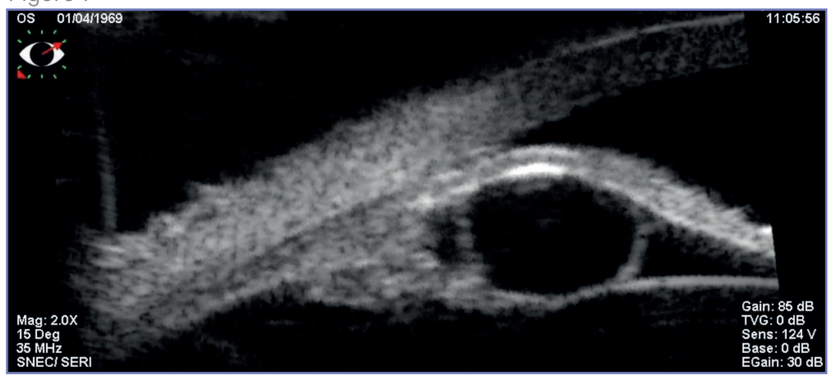

Figure 7
UBM image showing iris
pigment epithelial cyst.

Lens

The lens is a transparent, biconvex structure with an outer acellular capsule. In the unaccommodated state it is about 4mm thick. AS-OCT can provide information about the position and thickness of the lens. In some forms of glaucoma, particularly primary angle-closure glaucoma and lens-related (i.e., phacomorphic) glaucoma, a thicker and more forward displacement of the lens (lens vault or LV) can push the iris against the trabecular meshwork, contributing to the obstruction of the aqueous humor outflow (angle narrowing).[14]

Future directives

Advances in imaging technology may lead to improvements in the acquisition speed, image resolution and depth of penetration of the AS-OCT modalities, while enhancements in computational technology and artificial intelligence (AI) techniques may lead to more efficient classification of AS-OCT scans. These advancements can open more avenues for the role of AS-OCT in the development of personalized management strategies for glaucoma. An example of the applications of AI technology is the automated detection of angle-closure based on the segmentation of anterior segment structures using feature extractions from AS-OCT scans from the 360 degrees of the anterior chamber circumference.[15]

References

1. Porporato N, Baskaran M, Aung T. Role of anterior segment optical coherence tomography in angle-closure disease: a review. Clin Experiment Ophthalmol. 2018;46(2):147-57. doi:10.1111/ceo.13120
2. Singh M, Chew PTK, Friedman DS, et al. Imaging of Trabeculectomy Blebs Using Anterior Segment Optical Coherence Tomography. Ophthalmology. 2007;114(1):47-53. doi:10.1016/j.ophtha.2006.05.078
3. Gordon MO, Beiser JA, Brandt JD, et al. The Ocular Hypertension Treatment Study: Baseline Factors That Predict the Onset of Primary Open-Angle Glaucoma. Arch Ophthalmol. 2002;120(6):714-20. doi:10.1001/archopht.120.6.714
4. Kim HY, Budenz DL, Lee PS, Feuer WJ, Barton K. Comparison of Central Corneal Thickness using Anterior Segment Optical Coherence Tomography vs Ultrasound Pachymetry. Am J Ophthalmol. 2008;145(2):228-32.e1. doi:10.1016/j.ajo.2007.09.030
5. Nolan WP, See JL, Chew PTK, et al. Detection of Primary Angle Closure Using Anterior Segment Optical Coherence Tomography in Asian Eyes. Ophthalmology. 2007;114(1):33-39. doi:10.1016/j.ophtha.2006.05.073
6. Xu BY, Friedman DS, Foster PJ, et al. Ocular Biometric Risk Factors for Progression of Primary Angle Closure Disease: The Zhongshan Angle Closure Prevention Trial. Ophthalmology. Published online October 8, 2021. doi:10.1016/j.ophtha.2021.10.003
7. Porporato N, Baskaran M, Tun TA, et al. Understanding diagnostic disagreement in angle closure assessment between anterior segment optical coherence tomography and gonioscopy. Br J Ophthalmol. Published online September 6, 2019. doi:10.1136/bjophthalmol-2019-314672
8. Sakata LM, Lavanya R, Friedman DS, et al. Comparison of Gonioscopy and Anterior Segment Ocular Coherence Tomography in Detecting Angle Closure in Different Quadrants of the Anterior Chamber Angle. Ophthalmology. 2008;115(5):769-74. doi:10.1016/j.ophtha.2007.06.030
9. Lai I, Mak H, Lai G, Yu M, Lam DSC, Leung CKS. Anterior Chamber Angle Imaging with Swept-Source Optical Coherence Tomography: Measuring Peripheral Anterior Synechia in Glaucoma. Ophthalmology. 2013;120(6):1144-49. doi:10.1016/j.ophtha.2012.12.006
10. Nongpiur ME, Gong T, Lee HK, et al. Subgrouping of Primary Angle-Closure Suspects Based on Anterior Segment Optical Coherence Tomography Parameters. Ophthalmology. 2013;120(12):2525-31. doi:10.1016/j.ophtha.2013.05.028
11. Kwon J, Sung KR, Han S. Long-term Changes in Anterior Segment Characteristics of Eyes With Different Primary Angle-Closure Mechanisms. Am J Ophthalmol. 2018;191:54-63. doi:10.1016/j.ajo.2018.04.005
12. Baskaran M, Iyer JV, Narayanaswamy AK, et al. Anterior Segment Imaging Predicts Incident Gonioscopic Angle Closure. Ophthalmology. 2015;122(12):2380-84. doi:10.1016/j.ophtha.2015.07.030
13. Nongpiur ME, Aboobakar IF, Baskaran M, et al. Association of Baseline Anterior Segment Parameters With the Development of Incident Gonioscopic Angle Closure. JAMA Ophthalmol. 2017;135(3):252-58. doi:10.1001/jamaophthalmol.2016.5847
14. Nongpiur ME, He M, Amerasinghe N, et al. Lens Vault, Thickness, and Position in Chinese Subjects with Angle Closure. Ophthalmology. 2011;118(3):474-79. doi:10.1016/j.ophtha.2010.07.025
15. Porporato N, Tun TA, Baskaran M, et al. Towards "automated gonioscopy": a deep learning algorithm for 360° angle assessment by swept-source optical coherence tomography. Br J Ophthalmol. Published online April 12, 2021:bjophthalmol-2020-318275. doi:10.1136/bjophthalmol-2020-318275

Part 2

Chapter 16

AS-OCT in angle closure

Leopold Schmetterer
Alina Popa Cherecheanu
Munirah Ismail
Jacqueline Chua

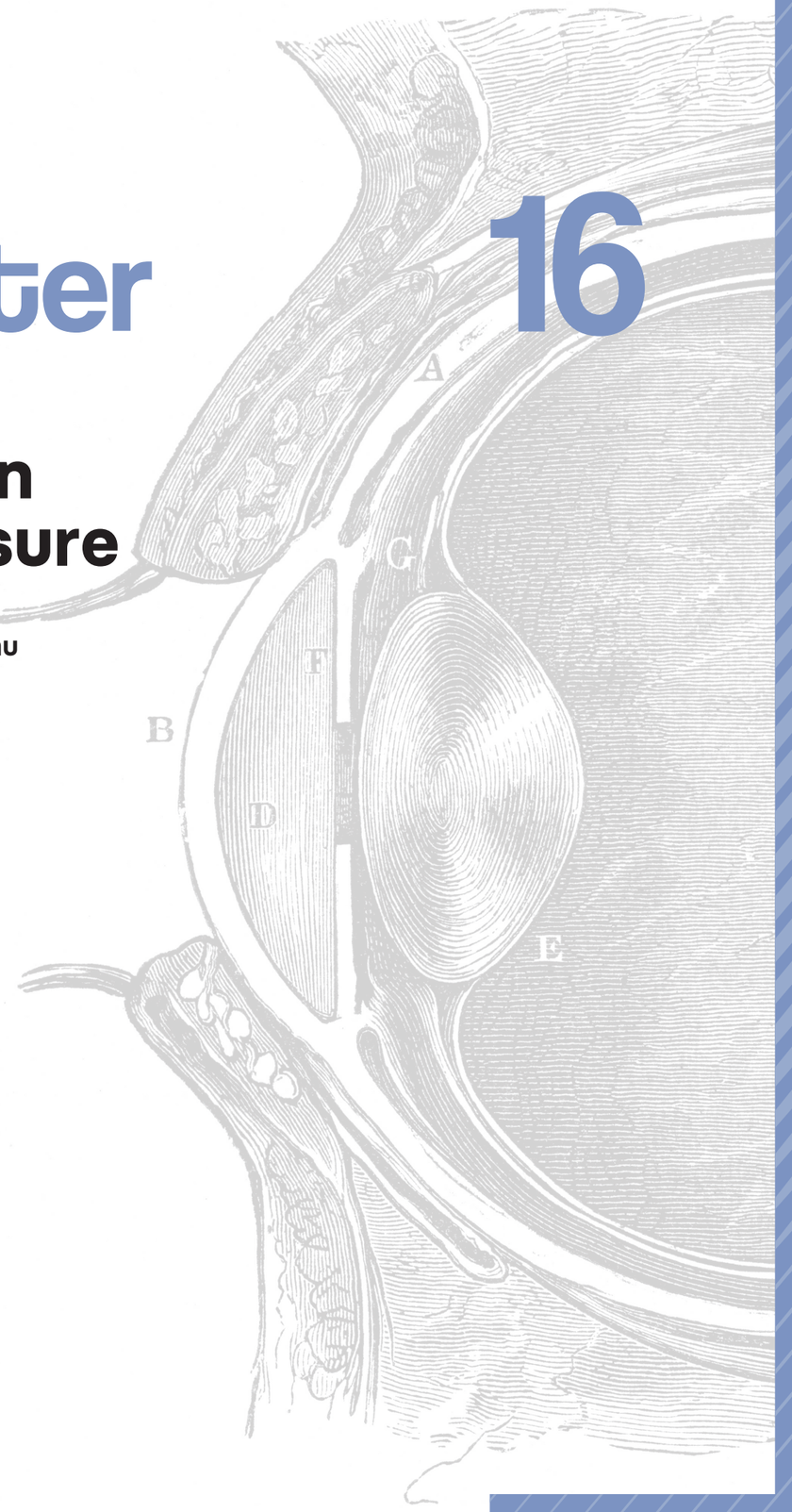

Vertical Section

AS-OCT in angle closure

Leopold Schmetterer, Alina Popa Cherecheanu, Munirah Ismail, Jacqueline Chua

Singapore Eye Research Institute
University of Medicine and Pharmacy „Carol Davila" Bucharest Romania

Imaging of the ocular anterior chamber with anterior segment (AS-) OCT is gaining popularity for the diagnosis, follow-up, and treatment monitoring of angle closure disease. AS-OCT is capable of qualitative and quantitative assessment of anterior chamber angle (ACA), anterior chamber, iris, and lens. Imaging of the AS using OCT has been conducted since the mid-1990s, initially with time-domain OCTs like the Zeiss Stratus OCT. Unlike retinal imaging, which typically utilizes light sources operating at central wavelengths of 840 nm or 1050 nm, AS-OCT can employ light sources at 1300nm due to the minimal light absorption in the vitreous. Longer wavelengths offer the advantage of deeper penetration into the anterior segment due to lower scattering coefficients.[1] Nowadays, various AS-OCT imaging devices are commercially available, using either spectral domain or swept-source configurations. While most of these instruments are designed for retinal use and offer a specific lens for the investigation of the AS, there are stand-alone systems specifically dedicated to AS applications. Angle-closure is defined by AS-OCT as any contact between the iris and the angled wall anterior to the scleral spur. This is in contrast to gonioscopy, where the quadrant is considered open unless the apposition reaches the posterior trabecular meshwork.[2] The identification of the scleral spur is an important landmark in AS-OCT images, but it may not be visible in all cases[3] (Fig. 1). Alternatively, Schwalbe's line (SL) is another landmark that can be identified in OCT images, although, like the scleral spur, it may not be visible in all scans.[4] Parameters that have been used to characterize the anterior chamber angle include the angle opening distance (AOD), the angle recess area (ARA) and the trabecular-iris space area (TISA, Fig. 2).

Figure 1

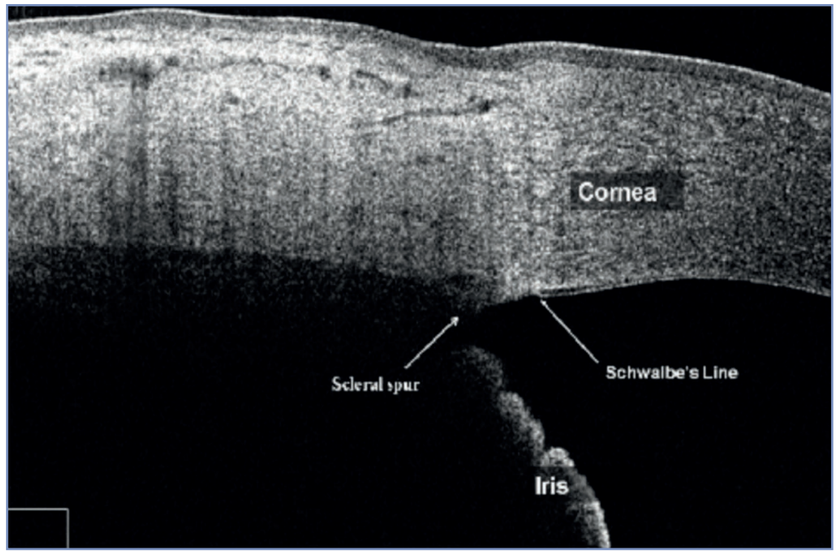

Figure 1
Visualization of scleral spur and Schwalbe's line in anterior segment OCT (reproduced with permission from).[5]

Figure 2
Quantitative analysis with anterior segment optical coherence tomography (OCT) systems.
a: Zhongshan Angle closure Assessment Program for Visante OCT,
b: 360° angle analysis software for Casia swept-source OCT volume scan,
c: Schematic representation of important parameters measured in customised software for Visante OCT: Angle Opening Distance (AOD, measures the perpendicular length between iris anterior surface and trabecular meshwork at a fixed distance), Trabecular Iris Surface Area (TISA, represents the area enclosed by points on scleral spur, iris and trabecular meshwork at a fixed distance), Lens Vault (LV, represents that portion of the lens in anterior chamber beyond the line of scleral spur) and Iris parameters include Iris curvature (ICURV), Iris thickness (IT 2000 at 2000 µm) and Iris Area (IA). (reproduced with permission from).[1]

Figure 2

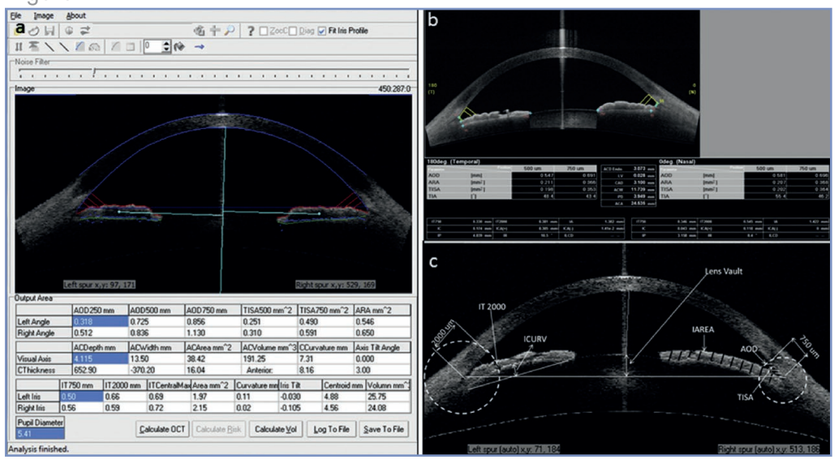

Several studies have compared AS-OCT with gonioscopy for assessing the chamber angle. Qualitative AS OCT (Fig. 3) successfully detected closed angles in 98% of subjects identified through gonioscopy.[6] Furthermore, AS-OCT classified many eyes as closed that were initially found to have open angles via gonioscopy. However, in a community-based setting, AS-OCT showed limited specificity and sensitivity in identifying angle closure, with gonioscopy considered the gold standard.[7] A scoring system based on a combination of six anterior chamber parameters namely, the anterior chamber volume (ACV), anterior chamber width (ACW), iris thickness (IT), IA, anterior chamber area (ACA) and lens vault (LV) outperformed each of the single parameters, with an AUC of 0.94.[8] Although automated algorithms for angle closure using AS OCT have been provided by several vendors, their validation against gonioscopy is limited.[9] Furthermore, while various artificial intelligence based algorithms have been published, they have not been widely tested in external datasets.[10-14] The dynamic study of the chamber angle, particularly in varying light conditions, is an area of significant interest. Ocular biometrics such as iris volume measured under light and dark conditions may improve risk-stratification of patients who have shown future angle closure progression.[15,16] Variations in iris connective tissue and the permeability of the iris stroma to aqueous humour may explain differences in iris volume in angle closure.

Figure 3
Appearance of the chamber angle in open angle and angle-closure glaucoma. The small anterior chamber angle in angle-closure glaucoma is clearly visible. (reproduced with permission from).[9]

Figure 3

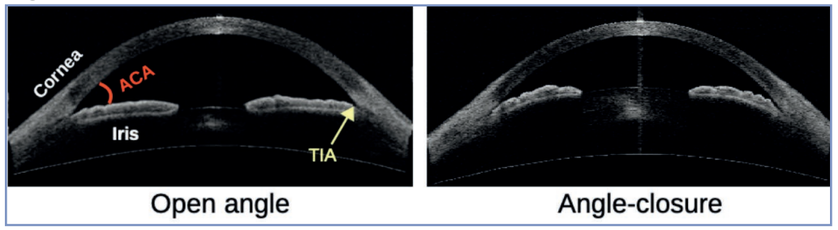

Additionally, the contribution of the lens to angle closure can be studied using parameters such as LV.[17] One challenge of using AS-OCT compared to gonioscopy is the difficulty in visualizing peripheral anterior synechiae (PAS). While some studies have attempted to determine PAS patterns, performance has been suboptimal.[18] Although deep learning systems may improve detection of PAS, results have been moderate at best.[19] Nonetheless, an air-puff dynamic AS-OCT system has recently been shown to detect the presence of PAS.[20] Additionally, AS-OCT images may not easily reveal features such as plateau iris configuration and choroidal effusion. AS-OCT has also been proposed for imaging aqueous outflow channels,[21] including attempts to visualize Schlemm's canal in glaucoma patients.[22-25] However, there has been little agreement among the various devices.[26] Full circumferential morphological analysis of Schlemm's canal in human eyes has only been achieved using non-commercial megahertz swept source OCT.[27] There are other imaging techniques that have been proposed for imaging the chamber angle.[28] These include measurement of anterior chamber depth (ACD) using either Scheimpflug photography or the scanning peripheral ACD analyzer or an estimation of the ACD using the oblique flashlight test and van Herick technique. Recently, an automated gonioscope has been commercialized (NGS-1, NIDEK Co., Gamagori, Japan). This device circumferentially captures a total of 64 images gonioscopic images, covering the entire 360 degrees[29] (Fig. 4). There have been reports of issues with image quality in some studies,[29] while others have reported a high rate of good image quality.[30,31]

Figure 4

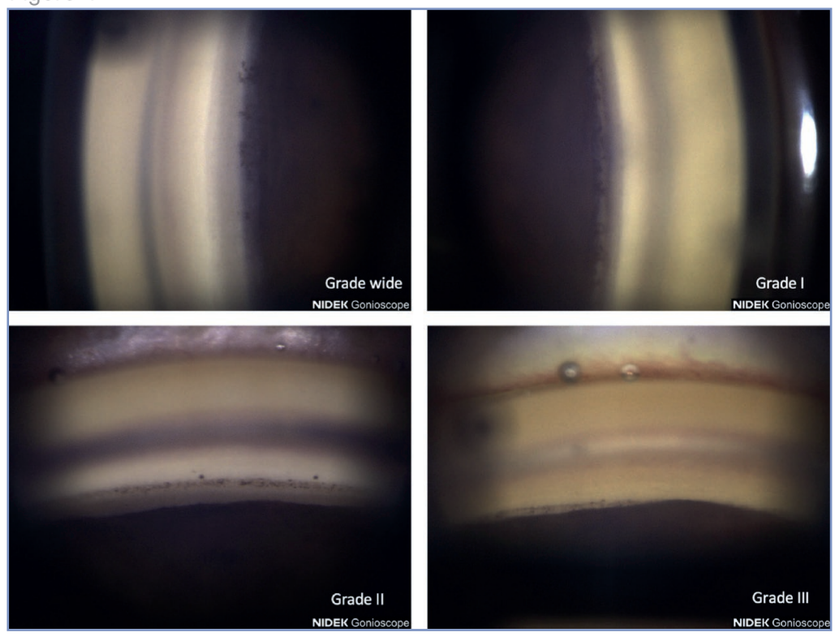

Figure 4
Example images taken by the NGS-1 gonioscope (NIDEK Co, Gamagori, Japan) with angle opening of Scheie grade wide to grade III, respectively. In the Scheie grading system, angles are graded wide if all structures are visible up to the iris root and its attachment to the anterior ciliary body; grade I if all angle structures are visible up to the scleral spur; grade II when angle structures are visible only until the posterior trabecular meshwork (TM); grade III when only the Schwalbe lines and the anterior TM are visible; and, finally, grade IV when no TM can be observed. (reproduced with permission from).[30]

Conclusions

Imaging the chamber angle with OCT has attracted much interest in the recent years. Both qualitative and quantitative measures extracted from these images have been utilized to classify the angle's status. AS OCT can provide diagnostic, mechanistic, and prognostic aid in angle closure eyes. However, few studies have used a longitudinal design for eyes that are imaged using AS-OCT. One paper reported that closed angle, as assessed with AS OCT, was associated with the development of more gonioscopic angle closures at four years.[32] Despite gonioscopy being considered the gold standard in clinical care, there is currently a lack of long-term clinical outcome study to substantiate this claim. Study protocols for such prospective studies have recently been published.[33] The major drawback of gonioscopy in determining angle closure is the use of visible light during examination, which may induce pupil constriction and therefore change angle configuration.

References

1. Ang M, Baskaran M, Werkmeister RM, Chua J, Schmidl D, Aranha dos Santos V, et al. Anterior segment optical coherence tomography. Progress in Retinal and Eye Research. 2018;66:132-56. doi: https://doi.org/10.1016/j.preteyeres.2018.04.002
2. Wright C, Tawfik MA, Waisbourd M, Katz LJ. Primary angle-closure glaucoma: an update. Acta Ophthalmologica. 2016;94(3):217-25. doi: https://doi.org/10.1111/aos.12784
3. Sakata LM, Lavanya R, Friedman DS, Aung HT, Seah SK, Foster PJ, et al. Assessment of the Scleral Spur in Anterior Segment Optical Coherence Tomography Images. Archives of Ophthalmology. 2008;126(2):181-85. doi: 10.1001/archophthalmol.2007.46
4. McKee H, Ye C, Yu M, Liu S, Lam DSC, Leung CKS. Anterior Chamber Angle Imaging With Swept-Source Optical Coherence Tomography: Detecting the Scleral Spur, Schwalbe's Line, and Schlemm's Canal. Journal of Glaucoma. 2013;22(6).
5. Jing T, Marziliano P and Wong H-T, Automatic detection of schwalbe's line in the anterior chamber angle of the eye using HD-OCT images, in Annual International Conference of the IEEE Engineering in Medicine and Biology. 2010:3013-16.
6. Nolan WP, See JL, Chew PTK, Friedman DS, Smith SD, Radhakrishnan S, et al. Detection of Primary Angle Closure Using Anterior Segment Optical Coherence Tomography in Asian Eyes. Ophthalmology. 2008;115(10):1720-27.e2. doi: 10.1016/j.ophtha.2006.05.073
7. Lavanya R, Foster PJ, Sakata LM, Friedman DS, Kashiwagi K, Wong T-Y, et al. Screening for Narrow Angles in the Singapore Population: Evaluation of New Noncontact Screening Methods. Ophthalmology. 2008, 115(10): p. 1720-1727.e2.doi: 10.1016/j.ophtha.2008.03.015
8. Nongpiur ME, Haaland BA, Perera SA, Friedman DS, He M, Sakata LM, et al. Development of a Score and Probability Estimate for Detecting Angle Closure Based on Anterior Segment Optical Coherence Tomography. American Journal of Ophthalmology. 2014;157(1):32-38.e1. doi: 10.1016/j.ajo.2013.09.012
9. Fu H, Xu Y, Lin S, Zhang X, Wong DWK, Liu J, et al. Segmentation and Quantification for Angle-Closure Glaucoma Assessment in Anterior Segment OCT. IEEE Transactions on Medical Imaging. 2017;36(9):1930-38. doi: 10.1109/TMI.2017.2703147
10. Natalia P, Tin AT, Mani B, Damon WKW, Rahat H, Huazhu F, et al. Towards 'automated gonioscopy': a deep learning algorithm for 360° angle assessment by swept-source optical coherence tomography. British Journal of Ophthalmology. 2022, 2022;106(10):1387. doi: 10.1136/bjophthalmol-2020-318275
11. Fu H, Baskaran M, Xu Y, Lin S, Wong DWK, Liu J, et al. A Deep Learning System for Automated Angle-Closure Detection in Anterior Segment Optical Coherence Tomography Images. American Journal of Ophthalmology. 2019;203:37-45. doi: 10.1016/j.ajo.2019.02.028
12. Hao H, Zhao Y, Yan Q, Higashita R, Zhang J, Zhao Y, et al. Angle-closure assessment in anterior segment OCT images via deep learning. Medical Image Analysis. 2021;69:101956. doi: https://doi.org/10.1016/j.media.2021.101956
13. Li W, Chen Q, Jiang C, Shi G, Deng G and Sun X. Automatic Anterior Chamber Angle Classification Using Deep Learning System and Anterior Segment Optical Coherence Tomography Images. Translational Vision Science & Technology. 2021;10(6):19. doi: 10.1167/tvst.10.6.19
14. Jasmeen R, Michael C, Natalia P, Anmol AP, Justin D, Galo Apolo A, et al. Generalisability and performance of an OCT-based deep learning classifier for community-based and hospital-based detection of gonioscopic angle closure. British Journal of Ophthalmology. 2023;107(4):511. doi: 10.1136/bjophthalmol-2021-319470
15. Aptel F, Chiquet C, Beccat S and Denis P. Biometric Evaluation of Anterior Chamber Changes after Physiologic Pupil Dilation Using Pentacam and Anterior Segment Optical Coherence Tomography. Investigative Ophthalmology & Visual Science. 2012;53(7):4005-10. doi: 10.1167/iovs.11-9387
16. Cho A, Xu BY, Friedman DS, Foster PJ, Jiang Y, Pardeshi AA, et al. Role of Static and Dynamic Ocular Biometrics Measured in the Dark and Light as Risk Factors for Angle Closure Progression. American Journal of Ophthalmology. 2023;256:27-34. doi: 10.1016/j.ajo.2023.07.032
17. Nongpiur ME, He M, Amerasinghe N, Friedman DS, Tay W-T, Baskaran M, et al. Lens Vault, Thickness, and Position in Chinese Subjects with Angle Closure. Ophthalmology. 2011;118(3):474-79. doi: 10.1016/j.ophtha.2010.07.025
18. Lai I, Mak H, Lai G, Yu M, Lam DSC and Leung CKS. Anterior Chamber Angle Imaging with Swept-Source Optical Coherence Tomography: Measuring Peripheral Anterior Synechia in Glaucoma. Ophthalmology. 2013;120(6):1144-49. doi: 10.1016/j.ophtha.2012.12.006
19. Yang Y, Wu Y, Guo C, Han Y, Deng M, Lin H, et al. Diagnostic Performance of Deep Learning Classifiers in Measuring Peripheral Anterior Synechia Based on Swept Source Optical Coherence Tomography Images. Frontiers in Medicine. 2022;8. doi: 10.3389/fmed.2021.775711
20. Ye S, Bao C, Chen Y, Shen M, Lu F, Zhang S, et al. Identification of Peripheral Anterior Synechia by Corneal Deformation Using Air-Puff Dynamic Anterior Segment Optical Coherence Tomography. Frontiers in Bioengineering and Biotechnology. 2022;10. doi: 10.3389/fbioe.2022.856531
21. Narayanaswamy A, Thakur S, Nongpiur ME, Schmetterer L, Hong Y-K, Huang AS, et al. Aqueous outflow channels and its lymphatic association: A review. Survey of Ophthalmology. 2022;67(3):659-74. doi: 10.1016/j.survophthal.2021.10.004
22. Pengcheng L, Anum B, Jason LC, Mark PG, Rafael LF, Camila FN, et al. Characteristics and variations of in vivo Schlemm's canal and collector channel microstructures in enhanced-depth imaging optical coherence tomography. British Journal of Ophthalmology. 2017;101(6):808-13. doi: 10.1136/bjophthalmol-2016-309295
23. Jing S, Chen Z, Chen W, Zhang H and Wang J. The 360° circumferential opening of Schlemm's canal in normal individuals detected by enhanced depth imaging optical coherence tomography. Medicine. 2020;99(7):e19187.
24. Ueno Y, Mori H, Kikuchi K, Yamanari M and Oshika T. Visualization of Anterior Chamber Angle Structures With Scattering- and Polarization-Sensitive Anterior Segment Optical Coherence Tomography. Translational Vision Science & Technology. 2021;10(14):29. doi: 10.1167/tvst.10.14.29.
25. Huang H, Tian L, Sun X and Chen Y. En face optical coherence tomography detection of Schlemm's canal in primary open angle glaucoma. Frontiers in Physiology. 2023;14. doi: 10.3389/fphys.2023.1214427
26. Wu X, Tan B, Gan J, Lam AR, Chen Y, Liu X, et al. Evaluation of different OCT systems in quantitative imaging of human Schlemm's canal. Scientific Reports. 2022;12(1):1400. doi: 10.1038/s41598-022-05410-9
27. Yao XA-O, Tan BA-O, Ho Y, Liu XA-O, Wong D, Chua J, et al. Full circumferential morphological analysis of Schlemm's canal in human eyes using megahertz swept source OCT. Biomedical Optics Express. 2021(2156-7085 (Print)): p. 3865-3877.
28. Porporato N, Bell KC, Perera SA and Aung T. Non-optical coherence tomography modalities for assessment of angle closure. Taiwan Journal of Ophthalmology. 2021(2211-5072 (Electronic)):409-14.
29. Teixeira F, Sousa DC, Leal I, Barata A, Neves CM and Pinto LA. Automated gonioscopy photography for iridocorneal angle grading. European Journal of Ophthalmology. 2018;30(1):112-18. doi: 10.1177/1120672118806436
30. Shi Y, Yang X, Marion KM, Francis BA, Sadda SR and Chopra V. Novel and Semiautomated 360-Degree Gonioscopic Anterior Chamber Angle Imaging in Under 60 Seconds. Ophthalmology Glaucoma. 2019;2(4):215-23. doi: https://doi.org/10.1016/j.ogla.2019.04.002
31. Barbour-Hastie C, Deol SS, Peroni A, Gillan S, Trucco E and Tatham AJ. Feasibility of Automated Gonioscopy Imaging in Clinical Practice. Journal of Glaucoma. 2023;32(3):159-64.
32. Baskaran M, Iyer JV, Narayanaswamy AK, He Y, Sakata LM, Wu R, et al. Anterior Segment Imaging Predicts Incident Gonioscopic Angle Closure. Ophthalmology. 2015;122(12):2380-84. doi: 10.1016/j.ophtha.2015.07.030
33. Augusto A-B, John GL, Anthony JK, Paul JF, Gianni V, Mary G, et al. Technologies for the diagnosis of angle closure glaucoma (ACE): protocol of a prospective, multicentre, cross-sectional diagnostic study. BMJ Open. 2023;13(10):e073975. doi: 10.1136/bmjopen-2023-073975

Part 2

Chapter 17

AS-OCT to evaluate glaucoma surgery

Leonardo Mastropasqua
Luca Agnifili

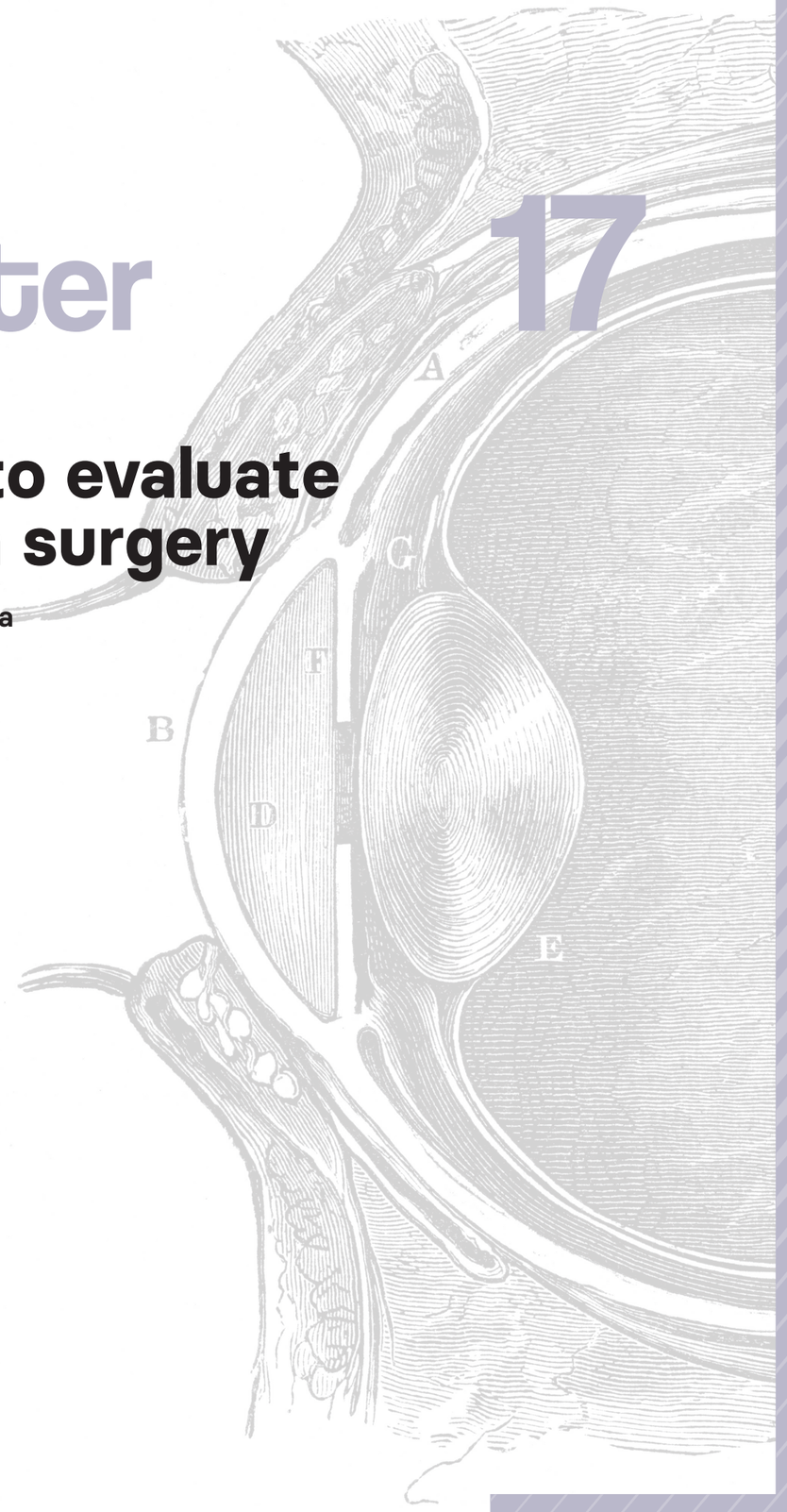

Vertical Section

AS-OCT to evaluate glaucoma surgery

Leonardo Mastropasqua, Luca Agnifili

Ophthalmology Clinic
National High-Tech Center and Excellence Eye Center
University G. d'Annunzio of Chieti-Pescara

Introduction

Anterior segment optical coherence tomography (AS-OCT) is a non-contact, rapid, and in vivo imaging technique that provides cross-sectional images of the anterior segment structures of the eye (Ang et al 2018). Thanks to progressive technological improvements, that increased the speed of capture and the resolution of images, AS-OCT has become a pivotal tool for the assessment of the AS structures in many fields of ophthalmology, including glaucoma. In glaucoma, AS-OCT is mainly utilized to obtain morphological and morphometric data in presence of angle closure, and to assess the aqueous humor (AH) drainage pathways after surgery. In this field, the filtration bleb (FB) functionality evaluation represents the area of primary application (Mastropasqua et al. 2014; Sharma et al 2014). In the last years, AS-OCT is becoming to be utilized also intra-operatively, to guide surgeons, and in the pre-surgical assessment, to recognize predictive biomarkers of filtration failure and to obtain information about the anatomic location of AH channels (Huang et al 2019; Ang et al 2020; Mastropasqua et al 2020).

AS-OCT before glaucoma surgery

The utilization of the AS-OCT before glaucoma surgery represents, to date, a more limited field of application of this imaging tool. However, though initial evidence needs further validations, the available literature suggests that the pre-operative use of AS-OCT may provide some useful information to surgeons.

AS-OCT before glaucoma filtration surgery

A recent AS-OCT study showed that the presence of a thin pre-operative upper bulbar conjunctiva represents a significant risk factor for trabeculectomy failure (Mastropasqua et al 2020). In detail, a thin epithelium and stroma and, thus, reduced values of full conjunctival thickness (FCT), increased the risk of bleb dysfunction at 12 months after surgery. FCT demonstrated as the strongest predictor of surgical outcome, with a relationship of about 8% increased risk of failure for each micron of thinner FCT. Besides conjunctival thickness, also an increased reflectivity of bulbar conjunctiva represented a significant risk factor for failure (Fig. 1). Reasons underlying these results are that a thin conjunctiva shows characteristics unfavorable to the AH percolation, such as a reduced amount of extracellular matrix, a compressed epithelium, but an increased collagen deposition within the stroma. Interesting information are provided also by OCT angiography (OCTA). A recent study found that a poor conjunctival vascularization before surgery was associated with lower IOP values six months after trabeculectomy (Hayek et al 2019). On these bases, an AS-OCT and AS-OCTA evaluation of the bulbar conjunctiva at the site of the upcoming filtration surgery seems providing surgeons some useful data to establish a risk for surgical failure.

Figure 1
Pre-operative conjunctival thickness (black arrows indicate the inner limit of the conjunctival stroma) and reflectivity, and post-operative (12 months) appearance of the filtration bleb. In successful cases (A-C), conjunctiva is thicker and hypo-reflective, with a well evident bleb cavity (asterisk) compared to failure (D-F).

Figure 1

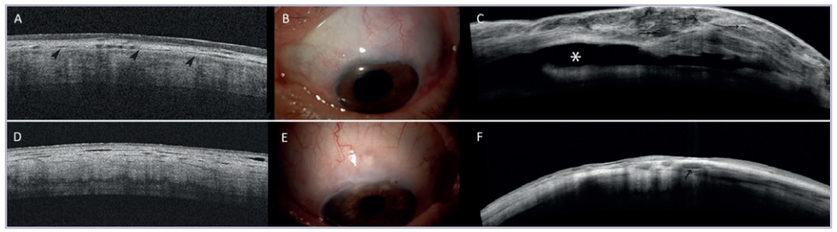

AS-OCT before trabecular bypass surgery

With the aim to reduce intraocular pressure (IOP) in less invasive ways and to promote a faster post-operative recovery, surgical procedures aiming at restoring the physiological AH drainage ability of conventional and unconventional outflow pathways are rapidly growing. These surgeries, which are currently named as minimally invasive glaucoma surgery (MIGS), include a heterogeneous group of IOP lowering devices and procedures. In this field, the application of AS-OCT is related to the surgical planning optimization: in fact, AS-OCT-guided placement of devices may result in an improvement in the IOP control since allow exactly placing MIGS at sites where collector channels are anatomically more represented (Ang et al 2018). This application is clinically feasible since AS-OCT visualizes the entire conventional AH outflow system, from trabecular meshwork (TM) and Schlemm's canal, to collector channels and episcleral veins. This seems to have a huge importance in the final surgical outcome since collector channels present inhomogeneous and segmental patterns around the eye. Because of this, trabecular bypass surgeries have higher success rates when devices are placed toward areas of greater AH flow (Huang et al 2018 and 2019). OCTA also can provide some information before surgery. A recent study performed on patients undergoing TM targeted MIGS found that the success rate of the procedure was significantly higher in eyes presenting a lower pre-operative intrascleral vessel density (VD) (Okamoto et al 2021).

Intra-operative AS-OCT (iAS-OCT)

In the recent years, AS-OCT expanded its application from ambulatory services to operating theater with the aim to assist clinicians during surgical steps (Ang et al 2020). In detail, iAS-OCT may help surgeons to: i) ascertain the scleral incision depth during trabeculectomy (especially in high axial myopia); ii) visualize deeper structures within the bleb during needling, thus allowing targeted release of areas of greater fibrosis; iii) correctly implant tubes within the anterior chamber, especially in presence of opaque cornea; and iv) in visualizing angle structures and facilitating precise implantation of devices or microcatheters during MIGS. Therefore, iAS-OCT has the potential to be exploited in different glaucoma procedures, but especially to facilitate targeted device placement and fine surgical maneuvers in the angles, the sub-conjunctival layer and the suprachoroidal space.

AS-OCT after glaucoma surgery

The post-operative evaluation of patients remains the main field of application of the AS-OCT and AS-OCTA in glaucoma surgery. These platforms can be utilized after all surgical procedures, permitting to assess the AH drainage pathways after MIGS, filtration surgery, and tubes implantation. Overall, AS-OCT may help surgeons in confirming the correct functioning of the new created AH drainage routes, the occurrence of changes in the filtration ability of drainage routes over time, and in diagnosing complications.

AS-OCT after MIGS

Different MIGS procedures can benefit from a post-operative AS-OCT assessment (Kan et al 2022). After iStent Inject surgery, AS-OCT was utilized to confirm the correct location of the implants, to analyze modifications induced by implantation maneuvers to the anterior chamber and iridocorneal angle, and to correlate the placement of the device to surgical outcomes. In patients who underwent canal surgery with Trabectome, AS-OCT was used to evaluate the trabeculotomy size and the effects of trabeculotomy opening size on post-operative IOP. After canaloplasty, AS-OCT confirmed the anatomical success of the procedure, documenting the stretch of the TM and the dilation of the Schlemm's canal (Mastropasqua et al 2012). The application of OCTA after TM targeted MIGS found that in successful cases the deep VDs of episclera and sclera decreased, especially in the sector corresponding to the implant localization. This supports the hypothesis that deep vessels can be involved in the IOP lowering after angle procedures, and that the post-operative VD reductions can be considered as potential biomarkers of favorable response (Gan et al. 2022; Okamoto et al 2022).

AS-OCT after filtration surgery

The post-operative FB evaluation represents the pivotal area of application of AS-OCT and AS-OCTA after glaucoma filtration surgery, either after standard or less invasive approaches. Several studies over the last two decades investigated the FB features with AS-OCT, providing anatomical biomarkers of efficient or poor AH resorption (Mastropasqua et al 2014; Kudsieh et al 2022). AS-OCT permits classifying FBs in favorable (cystic and diffuse) and unfavorable macroscopic patterns (flat and encapsulated) (Leung et al. 2007), with a good correlation with standardized clinical classifications systems (Ciancaglini et al 2008). Even more important, AS-OCT provides several quantitative and qualitative features useful to describe the AH resorption ability of the FB in a deep and comprehensive way. Based on features are represented, clinicians can differentiate a well-functioning FB, which shows a higher total height, a lower fluid-filled cavity height, a hypo-reflective and thick bleb-wall with numerous

hypo-reflective microcystic fluid-filled spaces inside or multiple parallel hypo-reflective layers (striping phenomenon), from failing or failed FBs, which show opposite features (Sacchi et al 2020; Kudsieh et al 2022). From the angiographic side, FBs that show large areas of vessel displacement within the wall, along with a rarefied vascular network are at lower risk of failure and have lower values of post-operative IOP (Mastropasqua et al 2020) (Fig. 2).

Figure 2

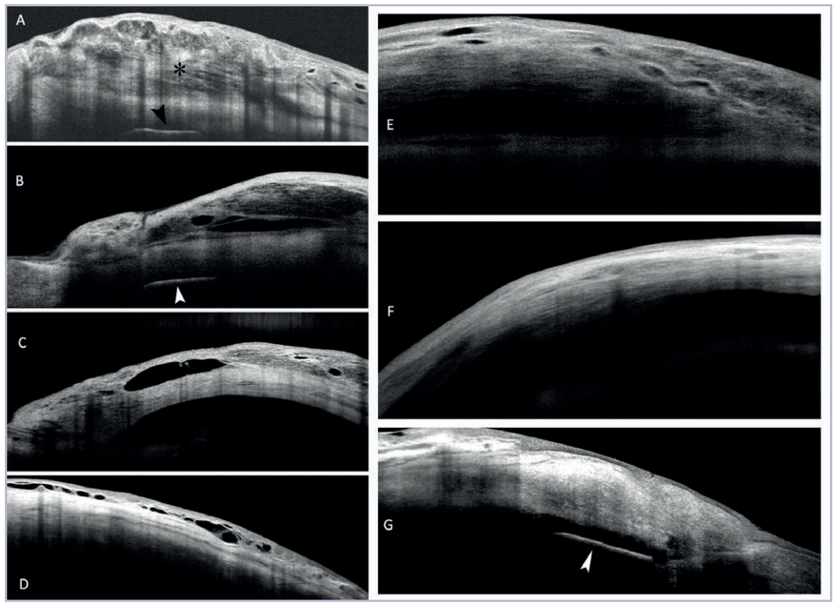

Figure 2
Functioning (A-D) and failed filtration blebs (E-G) after EX-PRESS p200 implantations (arrowheads). Features of hypo-reflective and thick bleb-wall with numerous hypo-reflective microcystic (or macrocystic) fluid-filled spaces inside, and the striping phenomenon (asterisk), are well-evident in successful compared to failed cases.

In clinical practice, the evaluation of these features during follow-up permits revealing fine ultrastructural and angiographic modifications of the FB overtime, which facilitate the detection of failure before it becomes clinically evident. Therefore, especially in challenging cases, in presence of significant pre- and post-operative risk factors for failure, or when complications occur, the AS-OCT analysis of the FB at each follow-up may improve the post-operative management and increase the likelihood of bleb survival.

AS-OCT after tube implantation

AS-OCT provides high-resolution imaging after glaucoma drainage devices implantation. In patients who received a tube, AS-OCT imaging is useful to know the position and patency of the entire tube, the correct position of the intraluminal suture, tube-iris and tube-cornea distances, the tube length within anterior chamber, and to study AH drainage pathways (Sharma et al 2014). This information is crucial especially in presence of opaque cornea that hampers the direct observation of the anterior chamber. In clinical practice, AS-OCT helps clinicians: i) in diagnosing tube lumen obstruction (usually due to accumulation of inflammatory material or blood components); ii) in detecting tube-corneal or tube-iris touch; iii) to suspect endothelial cell loss (based on the tube-corneal distance); iv) in assessing the correct placement of the patch on the tube, or in confirming the scleral patch erosion and the tube extrusion; and v) to study the drainage pathways around the plate and through the bleb-wall (Fig. 3). As well as after standard filtration surgery, AS-OCT provides structural biomarkers of good filtration ability of the bleb, such as that of bleb-wall thickness, which inversely correlates with IOP values, and the bleb-wall reflectivity, which increases in the hypertensive phase as a consequence of tissue remodeling.

Figure 3

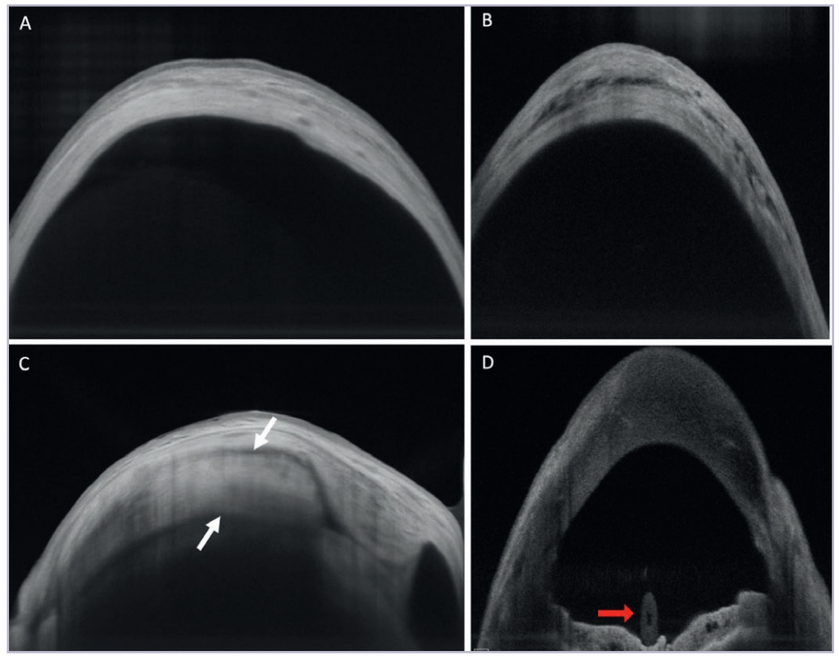

Figure 3
AS-OCT imaging after Paul glaucoma implant surgery. A and B show bleb-wall features around the tube plate, with a dense and hyper-reflective tissue during the hypertensive phase (A), and a spongy appearance indicating fluid outflow six months later (B). Scans shown in C and D depict the correct position of the scleral flap above the tube (white arrows indicate the outer and inner limits of the flap), and confirm the presence of a tube-iris contact, respectively.

Conclusions

AS-OCT represents a useful imaging technology in patients undergoing, or who underwent all surgical procedures for glaucoma. It may significantly help surgeons in different stages of the surgical process: i) pre-operatively, because seems providing predictive markers of failure; ii) intra-operatively, permitting surgeons to be accurate in each surgical step; and iii) post-operatively, permitting to control the AH resorption efficiency during follow-up. However, despite the various indications, currently, the use of this imaging tool can be particularly recommended after filtration surgery to early reveal signs of dysfunctional filtration bleb. The analysis of well recognized structural biomarkers, when carefully investigated during follow-up, could in fact favor the detection of signs of failure in the earliest pre-clinical phases, which is of utmost importance in challenging cases.

References

1. Ang M, Baskaran M, Werkmeister RM, Chua J, Schmidl D, Aranha Dos Santos V, Garhöfer G, Mehta JS, Schmetterer L. Anterior segment optical coherence tomography. Prog Retin Eye Res. 2018;66:132-56.
2. Ang BCH, Lim SY, Dorairaj S. Intra-operative optical coherence tomography in glaucoma surgery-a systematic review. Eye (Lond). 2020;34(1):168-77.
3. Gan J, Sng CCA, Ke M, Chieh CS, Tan B, Schmetterer L, Ang M. Anterior Segment Optical Coherence Tomography Angiography Following Trabecular Bypass Minimally Invasive Glaucoma Surgery. Front Med (Lausanne). 2022;9:830678.
4. Hayek S, Labb. A, Brasnu E, Hamard P, Baudouin C. Optical Coherence Tomography Angiography Evaluation of Conjunctival Vessels During Filtering Surgery. Transl Vis Sci Technol. 2019;8(4):4.
5. Huang AS, Francis BA, Weinreb RN. Structural and functional imaging of aqueous humour outflow: a review. Clin Exp Ophthalmol. 2018;46(2):158-68.
6. Huang AS, Penteado RC, Papoyan V, Voskanyan L, Weinreb RN. Aqueous Angiographic Outflow Improvement after Trabecular Microbypass in Glaucoma Patients. Ophthalmol Glaucoma. 2019;2(1):11-21.
7. Kan JT, Betzler BK, Lim SY, Ang BCH. Anterior segment imaging in minimally invasive glaucoma surgery - A systematic review. Acta Ophthalmol. 2022;100(3):e617-e634.
8. Kudsieh B, Fernández-Vigo JI, Canut Jordana MI, Vila-Arteaga J, Urcola JA, Ruiz Moreno JM, García-Feijóo J, Fernández-Vigo JÁ. Updates on the utility of anterior segment optical coherence tomography in the assessment of filtration blebs after glaucoma surgery. Acta Ophthalmol. 2022;100(1):e29-e37.
9. Leung CK, Yick DW, Kwong YY, Li FC, Leung DY, Mohamed S, Tham CC, Chung-chai C, Lam DS. Analysis of bleb morphology after trabeculectomy with Visante anterior segment optical coherence tomography. Br J Ophthalmol. 2007;91(3):340-44.
10. Mastropasqua L, Agnifili L, Salvetat ML, Ciancaglini M, Fasanella V, Nubile M, Mastropasqua R, Zeppieri M, Brusini P. In vivo analysis of conjunctiva in canaloplasty for glaucoma. Br J Ophthalmol. 2012;96(5):634-39.
11. Mastropasqua R, Fasanella V, Agnifili L, Curcio C, Ciancaglini M, Mastropasqua L. Anterior segment optical coherence tomography imaging of conjunctival filtering blebs after glaucoma surgery. Biomed Res Int. 2014;2014:610623.
12. Mastropasqua R, Brescia L, Di Antonio L, Guarini D, Giattini D, Zuppardi E, Agnifili L. Angiographic biomarkers of filtering bleb function after XEN gel implantation for glaucoma: an optical coherence tomography-angiography study. Acta Ophthalmol. 2020;98(6):e761-e767.
13. Okamoto Y, Akagi T, Kameda T, Suda K, Miyake M, Ikeda HO, Numa S, Kadomoto S, Uji A, Tsujikawa A. Prediction of trabecular meshwork-targeted micro-invasive glaucoma surgery outcomes using anterior segment OCT angiography. 2020;258(8):1763-70.
14. Okamoto Y, Akagi T, Kameda T, Suda K, Miyake M, Ikeda HO, Numa S, Tsujikawa A. Changes in the deep vasculature assessed using anterior segment OCT angiography following trabecular meshwork targeted minimally invasive glaucoma surgery. Sci Rep. 2022;12(1):17187.
15. Sacchi M, Agnifili L, Brescia L, Oddone F, Villani E, Nucci P, Mastropasqua L. Structural imaging of conjunctival filtering blebs in XEN gel implantation and trabeculectomy: a confocal and anterior segment optical coherence tomography study. Graefes Arch Clin Exp Ophthalmol. 2020;258(8):1763-70.
16. Sharma R, Sharma A, Arora T, Sharma S, Sobti A, Jha B, Chaturvedi N, Dada T. Surv Application of anterior segment optical coherence tomography in glaucoma. Survey Ophthalmol. 2014;59(3):311-27.

Part 3

Chapter 18

OCT Angiography

João Barbosa-Breda
Ingeborg Stalmans

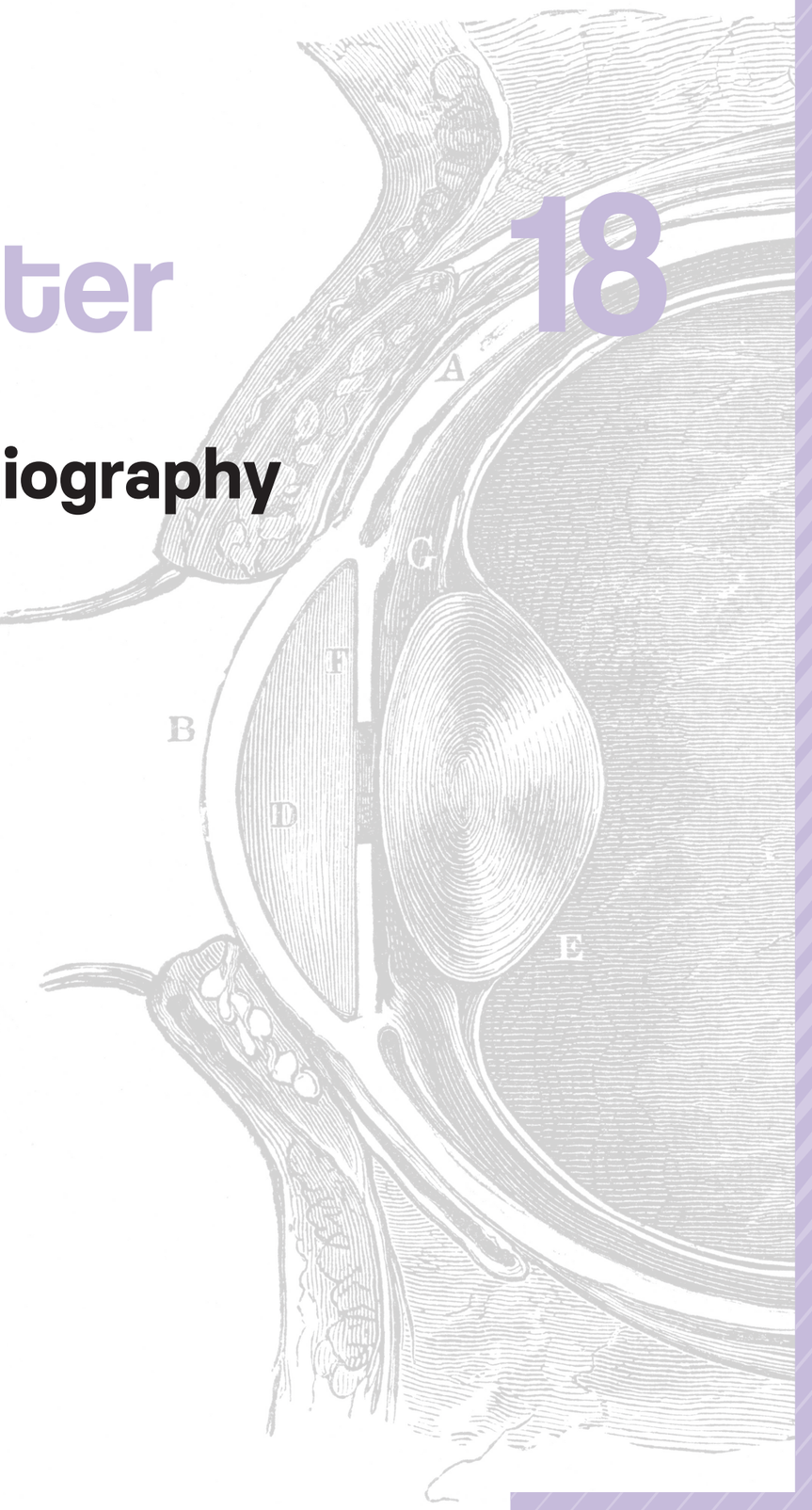

Vertical Section

OCT Angiography

João Barbosa-Breda,[1,2,3] Ingeborg Stalmans[3,4]

[1]Cardiovascular R&D Centre – UnIC@RISE, Department of Surgery and Physiology, Faculty of Medicine of the University of Porto, Porto, Portugal
[2]Department of Ophthalmology, Centro Hospitalar e Universitário São João, Porto, Portugal
[3]KULeuven, Research Group Ophthalmology, Department of Neurosciences, Leuven, Belgium
[4]Department of Ophthalmology, UZ Leuven, Leuven, Belgium

OCT angiography (OCTA) uses the OCT device to repetitively capture B-scans at a fast rate at the same location and identify the features that differ between these scans over time.[1] As such, it is capable of identifying the blood vessels, where moving blood cells appear and disappear between the repeated scans. OCTA has a high resolution, which allows the visualization of the entire vascular network, up to the capillary level, without the need for contrast (unlike fluorescein angiography). Moreover, this technology can provide en-face images at various tissue depths, separating the retinal (superficial, deep, outer/avascular) and choroidal (choriocapillaris, choroidal) layers.

Several manufacturers provide OCTA devices. These devices differ in terms of boundaries of the different vascular beds as well as in their algorithm for image acquisition and automatic analysis, which does not allow direct quantitative comparisons between devices. Some devices provide in-built tools for automatic image quantification while others require post-processing by researchers.

The most used quantitative analysis' parameter is vessel density (% of area occupied by vessels in the area of interest). Additional features have been described in the literature: vessel caliber, vessel perimeter index, vessel tortuosity, foveal avascular zone (FAZ) area and perimeter, FAZ contour irregularity, vessel branching analysis, flow index, choroidal neovascular analysis, and differential artery–vein analysis.[2] However, there is no consensus on the nomenclature used in OCTA features.

Glaucoma has since long been associated with vascular changes which correlate with the location of neuronal loss.[3] It has yet to be defined if a vascular insult precedes neuronal loss or vice-versa. The above-mentioned vascular layers can be evaluated by OCTA in three regions of interest: the macula, the optic nerve head (ONH) and the peripapillary area. Moreover, inside each layer, either the entire image can be studied, or the analysis can be directed to sectors which are more prone to glaucoma-related damage (eg. supero-temporal and infero-temporal in the peripapillary area, hemi-superior or hemi-inferior in the macular region).

The disc-centered images usually have an area of 4.5x4.5 mm and contain peripapillary information (in an annulus around the ONH) and ONH information (inside the ONH). In this location, the layers that have provided the most valuable findings were the superficial layer - often referred to as radial peripapillary capillary (RPC) layer - and the choroidal layer. The macular area is usually covered by 3x3mm and/or 6x6mm scans. The latter seems to detect glaucoma-related alterations more easily since it can capture arcuate defects that are not visible in the smaller 3x3mm.[4] The superficial and deep

retinal layers have been the most studied in the macular area. Automated removal of the large retinal vessels, focusing on the microvascular capillary network, has been proven effective in all regions to improve the correlation with neuro-vascular damage in glaucoma.

Studies have identified a good repeatability and reproducibility for OCTA. The intra-visit coefficient of variation for the peripapillary area (whole area and sectorial) ranged from 2.5% to 6.6%, while for the superficial macular layer it spanned from 3.4% to 5.6%.[5,6] Despite being a reproducible technology, these values are still higher than those identified with OCT. Finally, as has been identified for other glaucoma-related technologies, eyes with glaucoma showed a worse inter-visit repeatability than healthy eyes.[6]

Several OCTA findings have been reported in glaucoma, amongst which a VD reduction in the ONH, the peripapillary and the macular areas.[3] Regarding the peripapillary and macular areas, most findings relate to the superficial layers. In the peripapillary area, the sectors with greatest difference when comparing to healthy eyes were the supero-temporal and infero-temporal,[7] which correspond with the sectors known to be first and foremost affected in glaucoma. Regarding the choriocapillaris layer of the ONH area, zones of microvascular dropout (MvD) have been identified in eyes affected by glaucoma, representing focal areas of complete loss of vascularization within the ONH. These areas correlate well with areas of focal RNFL damage as well as disc haemorrhages (Fig. 1). Eyes with MvD were also found to have a higher rate of progression.[8] Furthermore, lower VD values were observed in eyes with focal lamina cribrosa (LC) defects compared to severity-matched eyes without LC defects. The areas with VD reduction were spatially correlated with the location of the focal LC defect.[9]

Figure 1

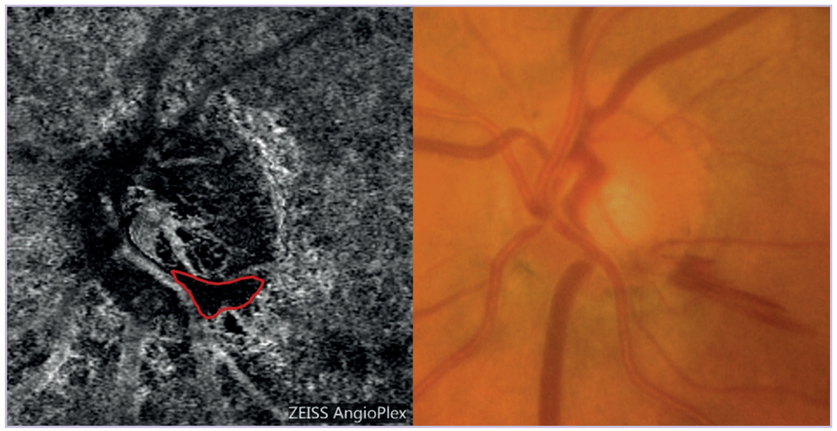

Figure 1
OCT angiography en-face image of the choricapillaris layer with a localized microvascular dropout area (left image, defect delimited with red lines); ONH-centered retinography with a peripapillary hemorrhage at the same location as the microvascular dropout (right image). Images from a glaucoma case.

Figure 2

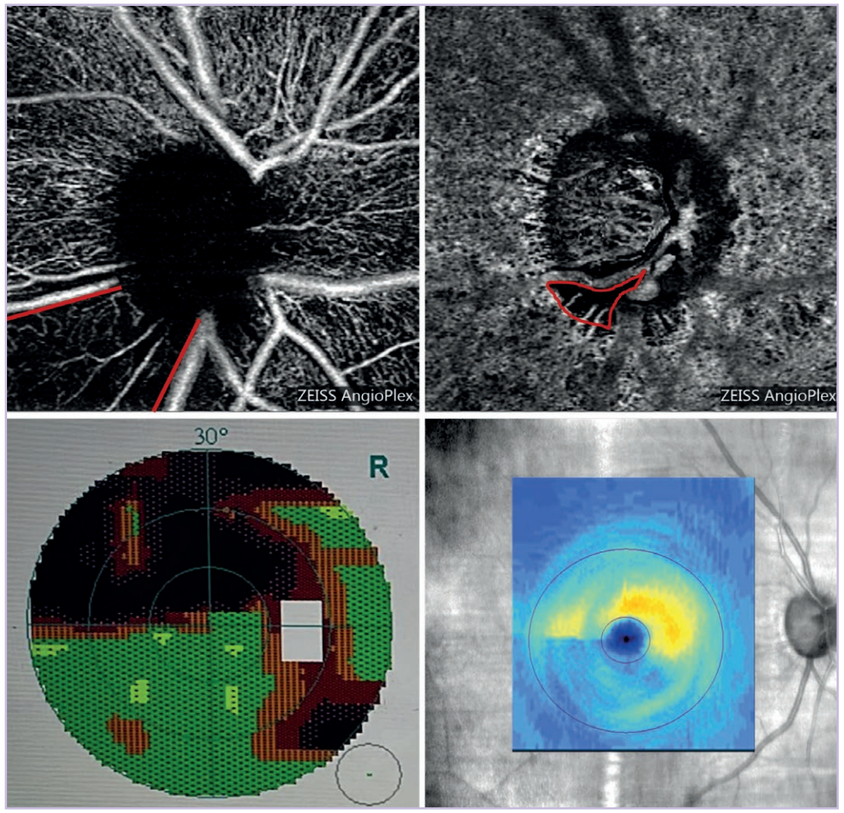

Figure 2
OCT angiography en-face image of the superficial layer showing the radial peripapillary capillary network with a sectoral reduction of vessel density (upper left image, vessel density defect delimited by red lines); OCT angiography en-face image of the choricapillaris layer with a localized microvascular dropout area (upper right image, defect delimited with red lines); visual field showing a deep and almost complete superior arcuate defect (lower left image, Peridata® layout, PeriData Software GmbH); macular ganglion cell thickness map (lower right image) with a profound loss in the inferior half respecting the horizontal midline, which corresponds to the area of severe vessel density reduction and microvascular dropout depicted in the OCT angiography images and the corresponding visual field defect. Images from a glaucoma case.

OCTA findings correlate well with disease severity, with a decreasing VD in worse disease stages.[10] Moreover, OCTA parameters correlate well with OCT and visual field parameters (Fig. 2). In eyes with high myopia and advanced glaucoma (where OCT has limitations due to segmentation artefacts and floor effect) OCTA has shown a stronger correlation with VF parameters than OCT.[11,12] This reduced floor effect in OCTA may be valuable for patients with advanced glaucoma.[11] Regarding the ability to diagnose glaucoma, both OCT and OCTA have shown high values for the area under the receiver operating characteristic curves (AUC) and also high sensitivities at high specificities. Controversial results were published regarding which technology reaches higher values. Of note, the combination of OCT and OCTA achieves better results than each one separately.[13] Moreover, the key to enhance the diagnostic and prognostic yield of OCTA also seems to be combining information from multiple regions and multiple layers. The use of artificial intelligence algorithms to this end

was able to improve the AUC values for glaucoma diagnosis and severity grading.[14] Finally, OCTA is also capable of identifying glaucoma progression,[15] particularly in combination with OCT.[13]

Another frontier in OCTA studies are the so called dynamic or functional studies, where stimuli are applied to induce a vascular response. These stimuli can vary between a flicker light source, a hypoxic challenge or a physical strain test with a hand dynamometer. Dysfunctional vascular behaviour has been observed using OCTA in patients with Diabetes Mellitus without diabetic retinopathy.[16]

Care should be taken when interpreting OCTA findings between and within subjects since several systemic diseases have shown to reduce OCTA VD even in the absence of identifiable ocular disease,[17] including arterial hypertension, diabetes mellitus, coronary artery disease, obstructive sleep apnea. Moreover, non-disease related factors can also influence OCTA values, such as the time of the day (circadian change), exercise, blood pressure, tobacco smoking and systemic medications.[17] There are other potential sources of bias, such as the image quality (a lower signal strength can lead to lower VD values) or a considerable change in intraocular pressure (such as that seen with filtration surgery, which can lead to higher VD values). Changes in software version in the same device can impact automatic segmentation and analysis and should be taken into account. Moreover, projection artefacts, from superficial layers' structures onto deeper layers, can cause interpretation errors. Some devices already have in-built systems to compensate for these artefacts, but there is still room for improvement.

Other improvements could facilitate the usability of OCTA in routine clinical practice. First of all, there is still a need for some harmonization, especially in terms of nomenclature and definitions, such as the boundaries of the studied retinal and choroidal layers. Furthermore, in-built quantitative glaucoma-related metrics of all relevant layers (at least retinal superficial and retinal deep) should be provided, enabling the retrieval of data from sectors that are relevant for glaucoma physicians, such as the Garway-Heath sectors (or similar) in the peripapillary area and the hemifield analysis in the macular region. Currently, many researchers still resort to retina-related sectorial grids, which are not ideal, or in-house built algorithms for post-processing, which lead to heterogeneity in the literature and prevent an accurate aggregation of published data.

Overall, OCTA is a promising tool for glaucoma management, but some barriers still need to be overcome prior to implementation in daily glaucoma routines.

References

1. Jia Y, Tan O, Tokayer J, Potsaid B, Wang Y, Liu JJ, et al. Split-spectrum amplitude-decorrelation angiography with optical coherence tomography. Opt Express. 2012;20(4):4710-25.
2. Yao X, Alam MN, Le D, Toslak D. Quantitative optical coherence tomography angiography: A review. Exp Biol Med (Maywood). 2020;245(4):301-12.
3. Van Melkebeke L, Barbosa-Breda J, Huygens M, Stalmans I. Optical Coherence Tomography Angiography in Glaucoma: A Review. Ophthalmic Res. 2018;1-13.
4. Rao HLR, Riyazuddin M, Dasari S, Puttaiah NK, Pradhan ZS, Weinreb RN, Mansouri K, Webers, CAB. Diagnostic Abilities of the Optical Microangiography Parameters of the 3x3 mm and 6x6 mm Macular Scans in Glaucoma. J Glaucoma. 2018;27(6):496-503.
5. Venugopal JP, Rao HL, Weinreb RN, Pradhan ZS, Dasari S, Riyazuddin M, et al. Repeatability of vessel density measurements of optical coherence tomography angiography in normal and glaucoma eyes. The British journal of ophthalmology. 2018;102(3):352-57.
6. Manalastas PIC, Zangwill LM, Saunders LJ, Mansouri K, Belghith A, Suh MH, et al. Reproducibility of Optical Coherence Tomography Angiography Macular and Optic Nerve Head Vascular Density in Glaucoma and Healthy Eyes. J Glaucoma. 2017;26(10):851-59.
7. Rao HL, Kadambi SV, Weinreb RN, Puttaiah NK, Pradhan ZS, Rao DAS, et al. Diagnostic ability of peripapillary vessel density measurements of optical coherence tomography angiography in primary open-angle and angle-closure glaucoma. Br J Ophthalmol. 2017;101(8):1066-70.
8. Kwon JM, Weinreb RN, Zangwill LM, Suh MH. Parapapillary Deep-Layer Microvasculature Dropout and Visual Field Progression in Glaucoma. American journal of ophthalmology. 2019;200:65-75.
9. Suh MH, Zangwill LM, Manalastas PI, Belghith A, Yarmohammadi A, Medeiros FA, et al. Optical Coherence Tomography Angiography Vessel Density in Glaucomatous Eyes with Focal Lamina Cribrosa Defects. Ophthalmology. 2016;123(11):2309-17.
10. Barbosa-Breda J, Andrade de Jesus D, Van Keer K, Nassiri V, Molenberghs G, Abegão Pinto L, et al. AngioOCT peripapillary microvascular density outperforms standard OCT parameters as a discriminant between different glaucoma severity levels – The Leuven Eye Study. Investigative Ophthalmology & Visual Science. 2018;59(9):4478.
11. Moghimi S, Bowd C, Zangwill LM, Penteado RC, Hasenstab K, Hou H, et al. Measurement Floors and Dynamic Ranges of OCT and OCT Angiography in Glaucoma. Ophthalmology. 2019;126(7):980-88.
12. Shin JW, Kwon J, Lee J, Kook MS. Relationship between vessel density and visual field sensitivity in glaucomatous eyes with high myopia. The British journal of ophthalmology 2018.
13. Kamalipour A, Moghimi S, Khosravi P, Mohammadzadeh V, Nishida T, Micheletti E, et al. Combining Optical Coherence Tomography and Optical Coherence Tomography Angiography Longitudinal Data for the Detection of Visual Field Progression in Glaucoma. American journal of ophthalmology. 2023;246:141-54.
14. Andrade De Jesus D, Sanchez Brea L, Barbosa Breda J, Fokkinga E, Ederveen V, Borren N, et al. OCTA Multilayer and Multisector Peripapillary Microvascular Modeling for Diagnosing and Staging of Glaucoma. Translational vision science & technology. 2020;9(2):58.
15. Miguel A, Silva A, Barbosa-Breda J, Azevedo L, Abdulrahman A, Hereth E, et al. OCT-angiography detects longitudinal microvascular changes in glaucoma: a systematic review. The British journal of ophthalmology. 2021.
16. Sousa DC, Leal I, Moreira S, do Vale S, Silva-Herdade AS, Aguiar P, et al. Retinal Vascular Reactivity in Type 1 Diabetes Patients Without Retinopathy Using Optical Coherence Tomography Angiography. Invest Ophthalmol Vis Sci. 2020;61(6):49.
17. Monteiro-Henriques I, Rocha-Sousa A, Barbosa-Breda J. Optical coherence tomography angiography changes in cardiovascular systemic diseases and risk factors: A Review. Acta ophthalmologica. 2021.

Part 3

Chapter 19

New imaging developments. Visualization of the trabecular meshwork and schlemm's canal

José Ignacio Fernández-Vigo
Noemí Güemes-Villahoz
Jorge Vila-Arteaga
Julián García-Feijóo

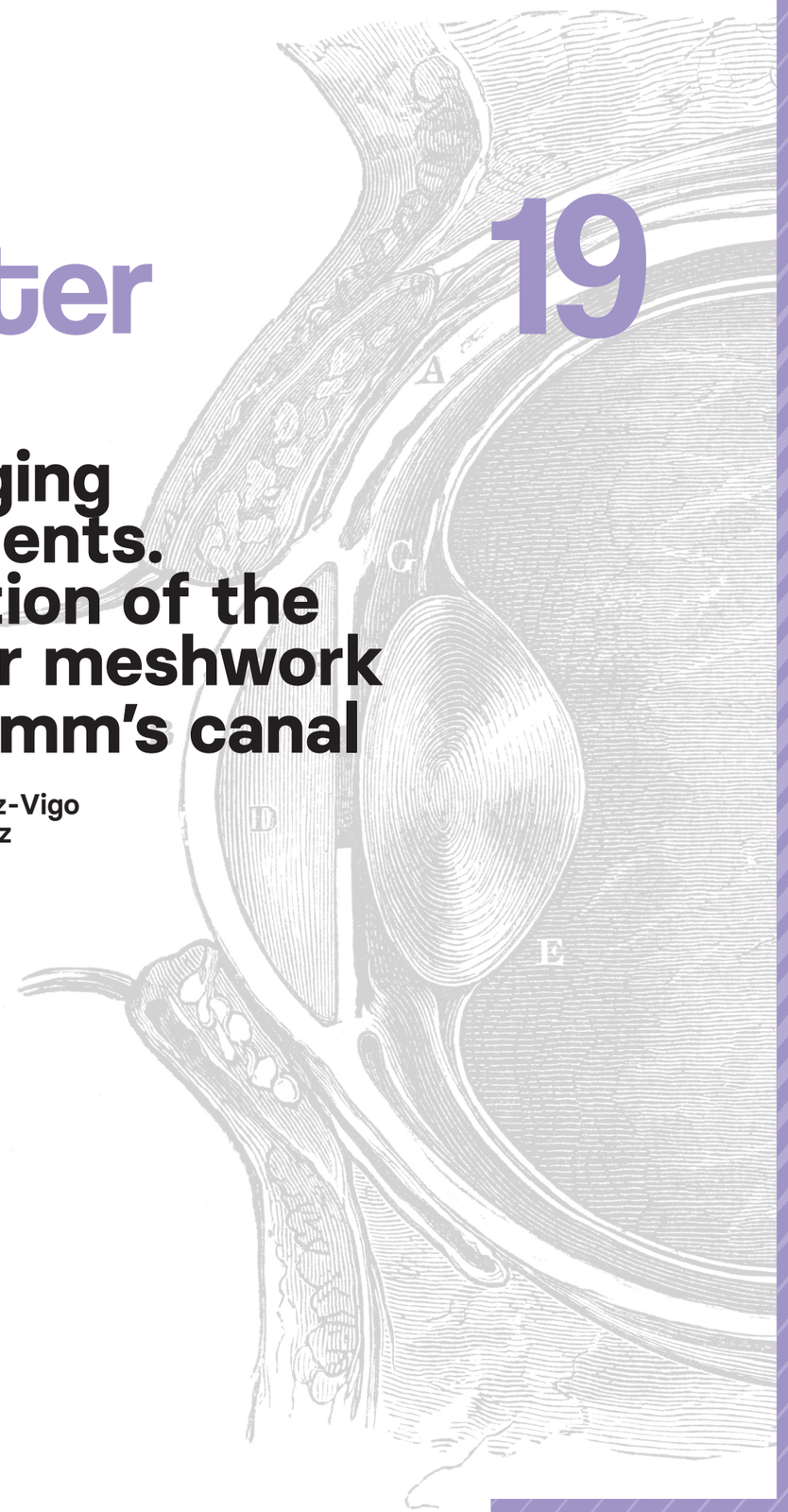

New imaging developments. Visualization of the trabecular meshwork and schlemm's canal

José Ignacio Fernández-Vigo,[1] Noemí Güemes-Villahoz,[1] Jorge Vila-Arteaga,[2] Julián García-Feijóo[1]

[1] Department of Ophthalmology. Hospital Clínico San Carlos-IdSSC. Instituto de Investigaciones Oftalmologicas Ramón Castroviejo. Universidad Complutense. Madrid, Spain
[2] Department of Ophthalmology. Hospital Universitario La Fe. Valencia, Spain

Introduction and OCT imaging

The trabecular meshwork (TM) and Schlemm's canal (SC) are both structures located within the iridocorneal or anterior chamber angle encircling the eye's circumference, which plays a crucial role in regulating the drainage of aqueous humor (AH). The latter flows from the TM into SC and then further into the eye's venous system. Several exploratory imaging techniques are currently available to examine the ACA, with optical coherence tomography (OCT) of the anterior segment considered the gold standard for such examination. AS–OCT is a rapid and non-invasive technique that obtains images of the ocular tissues in vivo.

It is based on the principle of low-coherence interferometry and relies on the backscattering of light as it travels through various tissue structures.[1] AS–OCT technology has evolved, with the transition from time-domain to Fourier-domain or swept-source OCT devices, to provide extremely detailed images that allow the identification and quantification of the angle structures, especially the TM and the SC, in healthy subjects and glaucoma patients, as well as changes following different therapeutic interventions.[2,3] Therefore, this technology has become an essential clinical and research examination tool in different ophthalmology areas, including glaucoma. Some of the main advantages of AS–OCT include the possibility of objectively measuring the angle width, TM and SC size, assessing the angle even in the presence of angular opacities, and exploring pediatric patients or those exhibiting traumatism because it is a noncontact examination.[4] In addition, OCT technology exhibits excellent reproducibility for measuring angle parameters or angle structures using different devices. However, even though various studies have[5] found a good agreement between angle structure dimensions obtained with different OCT devices, absolute values are not interchangeable.

Correlation of AS-OCT with other angle assessment techniques

Gonioscopy

It is classically considered as the reference examination for angle assessment. However, it presents several drawbacks such as being a subjective technique requiring an expert examiner, it is uncomfortable for patients and it does not provide quantitative data, all of which limits its usefulness. On the contrary, the advantages of gonioscopy compared to OCT include direct visualization of angle structures, particularly the TM and its pigmentation degree, dynamic angle evaluation to differentiate apositional from synechial angle closure and the visualization of blood in SC.

Devices based on the Scheimpflug camera

These devices comprise a rotational camera that captures 50 meridional images in under 2 seconds, and are able to produce 3D images and enable angle opening quantification. Compared with OCT, Pentacam tends to overestimate measurements in narrow angles and underestimate them in open angles.[6] However, due to the lower image resolution compared to OCT, it is not possible to assess or measure the TM or SC.

Ultrasound biomicroscopy (UBM)

This is an ecographic technique that utilizes high-frequency ultrasound transducers (50–100 MHz) and has become the reference for studying the posterior chamber and retro-iridian structures. The usefulness of UBM for assessing the angle region includes iris configuration analysis and ciliary body arrangement, cystic angle closure, study of lenses in sulcus, plateau iris as well as for the differential diagnostic of ciliary, angle or iris tumors. The main limitation of this technique is that its resolution does not allow to measure the TM or visualize the SC in a consistent way.

Visualization of the trabecular meshwork and Schlemm's canal

In recent years, several authors have described the ways in which AS–OCT facilitates the identification of angle region structures as well as AH drainage pathways (Fig. 1).[1,7]

Trabecular meshwork (TM)

The trabecular route is responsive to changes in pressure and is prominent in normal physiological conditions, contributing to approximately 90% of AH drainage. Within this pathway, the AH permeates through the TM, a multi-layered porous structure, and enters SC, which is linked to aqueous veins through 25-35 collector channels. From there, the AH is directed into episcleral veins, and subsequently flows into anterior ciliary and superior ophthalmic veins before ultimately reaching the cavernous sinus. Measurements of the TM have been conducted in diverse subjects encompassing various ages and ethnic backgrounds. In 2008, Sarunic et al. obtained the first image thereof using OCT. TM is identified as the hyper-refringent half-moon in the scleral groove, anteriorly limited by Schwalbe's line and posteriorly by the scleral spur. Its identification varies between authors. A key limitation in TM imaging is that, while properly positioned, the ground-truth identity of the OCT signal in the angle including the arc-like hypodensity (interface shadow) has not been firmly established.[7]

Schlemm's canal (SC)

By means of OCT, the SC is seen as a long and narrow hypo-reflective space outside of the TM (Fig. 1). Compared to TM, SC study by AS-OCT is more established with a larger literature. The reason for this is that the fluid-filled SC lumen gives a clear OCT hypo-reflective signal such that it can be easily identified, not unlike blood vessels.[7] Kagemann et al. were the first to identify it through OCT.[8] Hong et al. observed smaller SC sizes in patients with primary open-angle primary glaucoma (POAG) when compared to healthy subjects.[9] Similarly, Imamoglu et al. also observed smaller SC sizes in patients with pseudoexfoliative glaucoma than in healthy subjects.[10] The differences between absolute values of SC size observed by several authors in healthy populations must be noted. This could be due to the use of different OCT devices. In what concerns intraocular pressure (IOP), Hong et al. did not find a correlation with SC area.[9] However, in other studies a correlation has been found between IOP reduction after medical or surgical glaucoma treatment and SC size increase. Accordingly, Chen et al. observed a 90% increase in SC size after instilling travoprost,[11] while Skaat et al. documented a 21% increase in SC area in healthy subjects and 24% SC increase in patients with POAG after instilling pilocarpine.[12] In contrast, IOP elevation has been shown to do the opposite.[7] Recently, Huang and colleagues conducted a compelling research initiative focused on elucidating the drainage routes of AH. Their investigation involved the utilization of AH angiography to delve into the intricate pathways, revealing distinct sectorial, pulsatile, and dynamic patterns. The researchers employed AS-OCT to interpret their findings, effectively delineating the intra-scleral spaces corresponding to the collectors integral to these drainage pathways. The primary aim of this research was to enhance the surgical outcomes of diverse glaucoma techniques by optimizing this newfound understanding. Regarding the primary angle closure disease, trabecular-iris contact (TIC) is the precursor of angle-closure disease (Fig. 1). Appositional closure is the term used to describe potentially reversible contact between the peripheral iris and TM. However, evidence from histological studies suggests that pathologic changes may be produced in subjects who have never had an acute episode of angle closure. These signs appear not only in the areas of

Figure 1

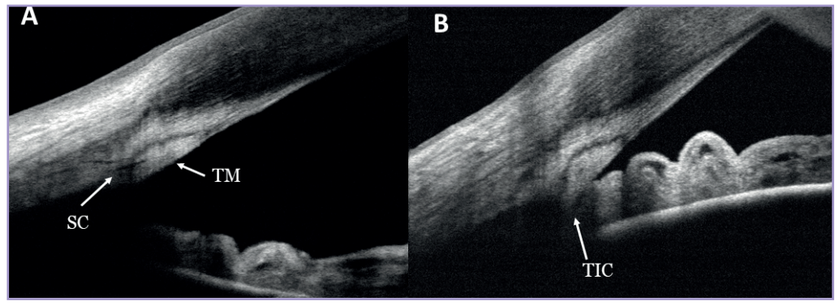

Figure 1
Optical coherence tomography of the anterior chamber angle showing the trabecular meshwork (TM) and the Schlemm's canal in a healthy subject. B) Angle closure with the presence of trabecular-iris contact (TIC).

peripheral anterior synechiae, but also in those of appositional closure. Thus, TIC is an unequivocal pathologic sign. In 2005, Radhakrishnan described the variable trabecular iris contact length (TICL), as a quantifiable parameter to define narrow angles objectively and accurately.[13] In addition, OCT has multiple uses in the study of the different mechanisms of angle closure, the evaluation of changes after a laser peripheral iridotomy or iridoplasty, after cataract surgery, as well as after the implantation of phakic lenses.

AS-OCT Imaging of the TM and SC in Glaucoma Surgery

Glaucoma surgery includes laser, incisional and minimally invasive glaucoma procedures (MIGS). In recent years, different authors have focused on the changes produced by different surgeries on the TM and SC, such as trabeculotomy, viscocanalostomy, trabeculectomy, non-perforating deep sclerectomy or MIGS implants (Figs. 2 and 3). Studies exploring the effects of different glaucoma surgeries on these critical structures have yielded valuable insights. For instance, after trabeculectomy, OCT imaging frequently demonstrates a widening of SC lumen and changes in TM morphology, potentially indicative of enhanced aqueous outflow pathways. In the realm of MIGS, such as trabecular micro-bypass stents, OCT has revealed alterations in the TM adjacent to the stent, suggesting potential remodeling of the AH outflow pathway. Additionally, canaloplasty, a procedure aimed at restoring natural drainage pathways, has shown distinctive canal distension changes on OCT, often illustrating the maintenance or restoration of canal patency. OCT offers invaluable visual evidence of structural modifications, and ongoing research endeavors aim to establish connections between these changes and functional outcomes.

This correlation is crucial for a comprehensive understanding of how surgical interventions impact glaucoma management. As proposed by Huang et al., future directions in this field will likely integrate structural and functional data to deepen our understanding of AH outflow dynamics.[7] Presently, the intricate interplay between structural outflow characteristics and functional measures remains undefined in the anterior segment. As a result, simultaneous investigation of AH outflow structure and function within the same subject and eye emerges as a critical avenue for advancing our comprehension of this complex process. In conclusion, AS–OCT technology has evolved in recent years to provide images enabling the identification and quantification of key angle structures such as TM or SC to determine normal angle anatomy and its alterations or changes after surgery. This could contribute to increasing our knowledge of the physiopathology of glaucoma.

Figure 2

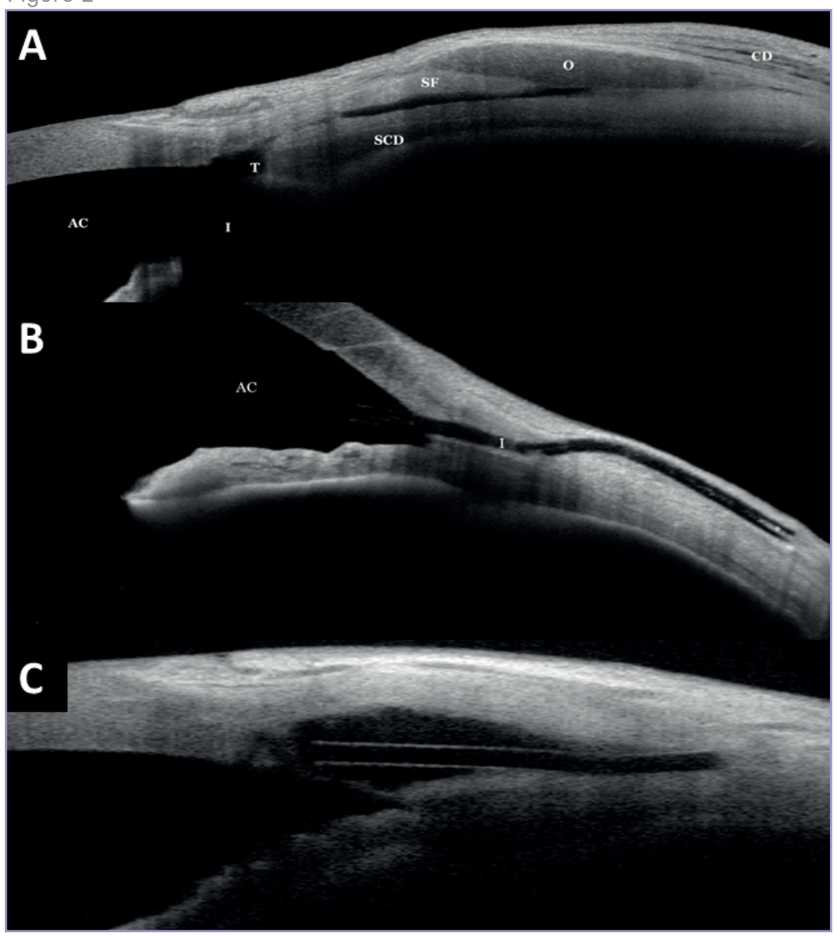

Figure 2
A) Trabeculectomy with Ologen. The drainage pathway is visible from the anterior chamber, below the scleral flap, reaching the Ologen implant. There is extensive posterior diffusion.
A diffuse suprachoroidal filtration can be observed. (I: iridectomy, F: scleral flap, O: Ologen, AC: anterior chamber, T: trabeculectomy, DC: conjunctival drainage, SCD: suprachoroidal drainage).
B) Failed XEN® implant. The path of the implant can be observed through the anterior chamber, intra-scleral, and subconjunctival spaces. At the external ostium, there is subconjunctival material obstructing the outflow of aqueous humor (*). (AC: anterior chamber. I: XEN implant).
C) Non-perforating deep sclerectomy with Esnoper® intra-scleral implant, showing an intact trabeculo-Descemet's membrane and partial aqueous drainage.

Figure 3

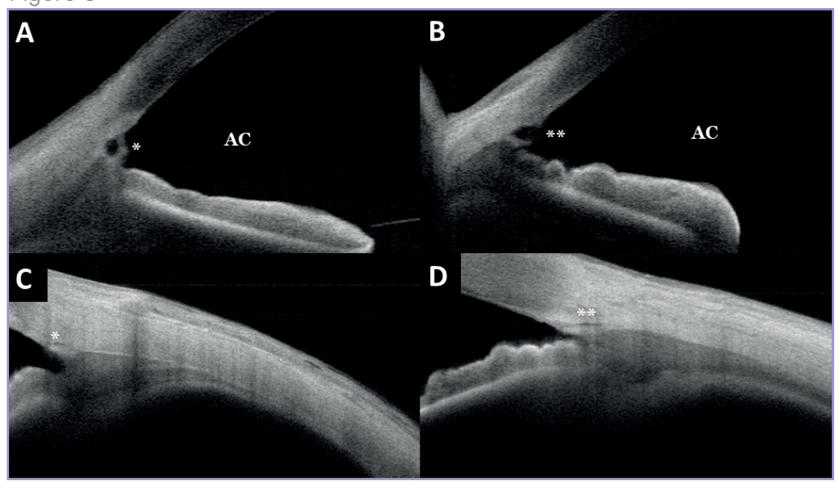

Figure 3
Trabecular Surgery.
A) Schlemm's canal viscodilation (*) performed with OMNI®.
B) Ab interno trabeculotomy (**) performed with Kahook®.
C and D) Different degrees of Schlemm's canal distension post-viscocanaloplasty (mild* and marked** respectively).
AC: anterior chamber.

References

1. Shan J, DeBoer C, Xu BY. Anterior Segment Optical Coherence Tomography: Applications for Clinical Care and Scientific Research. Asia Pac J Ophthalmol (Phila). 2019:10.22608/APO.201910.
2. Fernández-Vigo JI, García-Feijóo J, Martínez-de-la-Casa JM, García-Bella J, Fernández-Vigo JA. Morphometry of the trabecular meshwork in vivo in a healthy population using fourier-domain optical coherence tomography. Investigative Ophthalmol Vis Sci. 2015;56(3):1782-88.
3. Fernández-Vigo JI, De-Pablo-Gómez-De-Liaño L, Fernández-Vigo C, Sánchez-Guillén I, Santos-Bueso E, Martínez-de-la-Casa JM, et al. Quantification of trabecular-iris contact and its prevalence by optical coherence tomography in a healthy Caucasian population. Eur J Ophthalmol. 2017;27(4).
4. Fernández-Vigo JI, De-Pablo-Gómez-De-Liaño L, Fernández-Vigo C, Arcos-Villegas G, Fernández-Pérez C, García-Feijóo J, et al. Anterior Chamber Angle and Trabecular Meshwork Measurements Made by Fourier-domain Optical Coherence Tomography in Healthy White Children. J Glaucoma. 2017;26(9).
5. Fernández-Vigo JI, García-Feijóo J, Martínez-De-La-Casa JM, García-Bella J, Arriola-Villalobos P, Fernández-Pérez C, et al. Fourier domain optical coherence tomography to assess the iridocorneal angle and correlation study in a large Caucasian population. BMC Ophthalmol. 2016;16(1).
6. Fernández-Vigo JI, De-Pablo-Gómez-de-Liaño L, Almorín-Fernández-Vigo I, Fernández-Vigo C, Macarro-Merino A, García-Feijóo J, et al. Agreement between Pentacam and optical coherence tomography in the assessment of iridocorneal angle width in a large healthy population. J Fr Ophtalmol. 2018;41(1):14-20.
7. Huang AS, Francis BA, Weinreb RN. Structural and functional imaging of aqueous humour outflow: a review. Clin Exp Ophthalmol. 2018;46(2):158–68.
8. Kagemann L, Nevins JE, Jan NJ, Wollstein G, Ishikawa H, Kagemann J, et al. Characterisation of Schlemm's canal cross-sectional area. British Journal of Ophthalmology. 2014;98(Suppl 2):ii10–4.
9. Hong J, Xu J, Wei A, Wen W, Chen J, Yu X, et al. Spectral-Domain Optical Coherence Tomographic Assessment of Schlemm's Canal in Chinese Subjects with Primary Open-angle Glaucoma. Ophthalmology. 2013;120(4):709–15.
10. Imamoglu S, Sevim MS, Alpogan O, Ercalik NY, Kumral ET, Pekel G, et al. In vivo biometric evaluation of Schlemm's canal with spectral-domain optical coherence tomography in pseuduexfoliation glaucoma. Acta Ophthalmol. 2016;94(8):e688–92.
11. Chen J, Huang H, Zhang S, Chen X, Sun X. Expansion of Schlemm's Canal by Travoprost in Healthy Subjects Determined by Fourier-Domain Optical Coherence Tomography. Investigative Opthalmology & Visual Science. 2013;54(2):1127.
12. Skaat A, Rosman MS, Chien JL, Mogil RS, Ren R, Liebmann JM, et al. Effect of Pilocarpine Hydrochloride on the Schlemm Canal in Healthy Eyes and Eyes With Open-Angle Glaucoma. JAMA Ophthalmol. 2016;134(9):976.
13. Radhakrishnan S, Goldsmith J, Huang D, Westphal V, Dueker DK, Rollins AM, et al. Comparison of optical coherence tomography and ultrasound biomicroscopy for detection of narrow anterior chamber angles. Arch Ophthalmol. 2005;123(8):1053–59.
14. Kudsieh B, Fernández-Vigo JI, Vila-Arteaga J, Urcola JA, Martínez-de-la-Casa JM, García-Feijóo J, et al. Update on the usefulness of optical coherence tomography in assessing the iridocorneal angle. Arch Soc Esp Oftalmol. 2019;94(10).
15. Kudsieh B, Fernández-Vigo JI, Canut Jordana MI, Vila-Arteaga J, Urcola JA, Ruiz Moreno JM, et al. Updates on the utility of anterior segment optical coherence tomography in the assessment of filtration blebs after glaucoma surgery. Acta Ophthalmol. 2022;100(1):e29–37.

Part 3

Chapter 20

Other functional OCT approaches

Leopold Schmetterer
Munirah Ismail
Jacqueline Chua

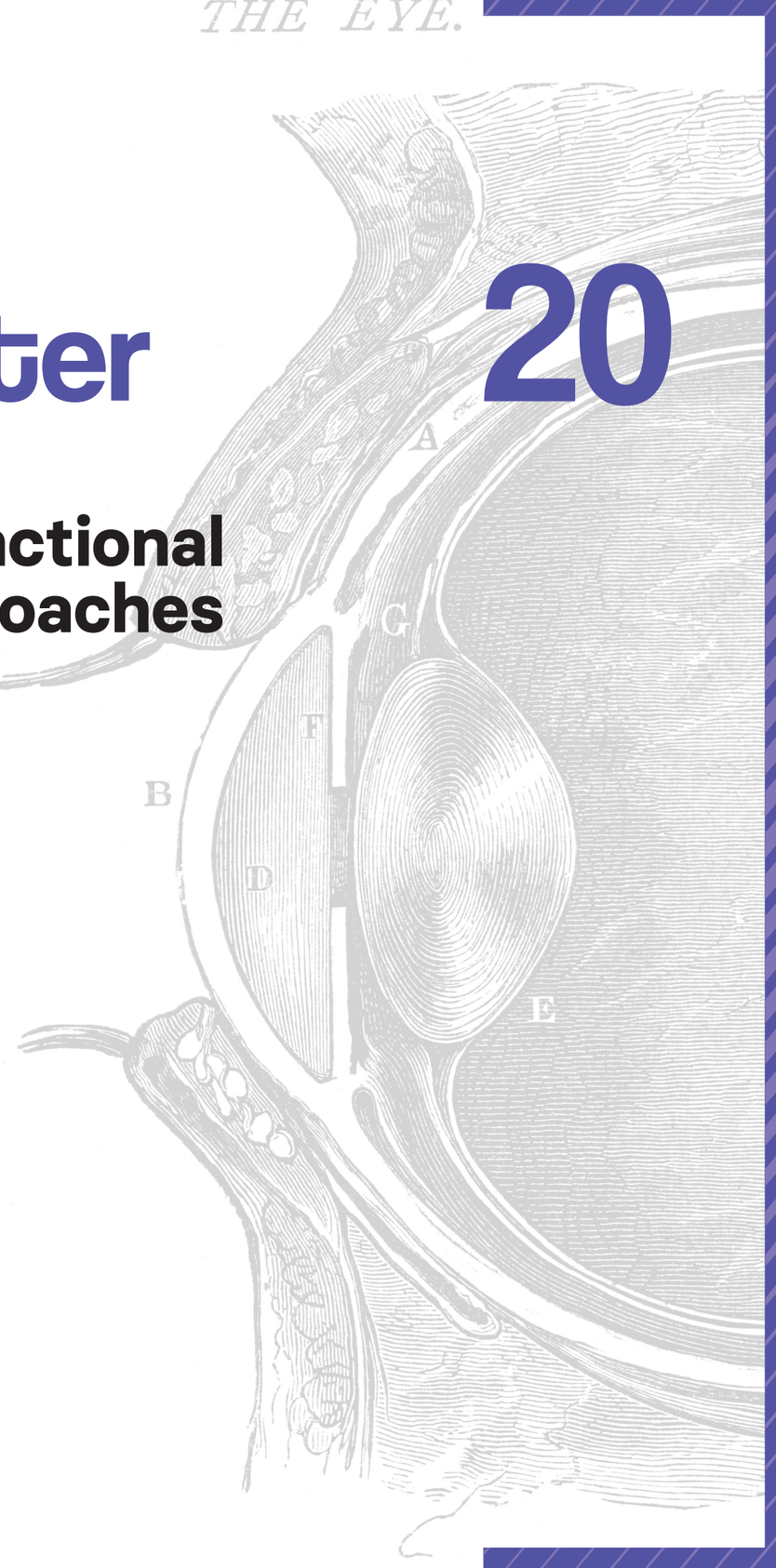

Vertical Section

20
Part 3

Other functional OCT approaches

Leopold Schmetterer, Munirah Ismail, Jacqueline Chua

Singapore Eye Research Institute

OCT angiography stands as the sole functional extension of OCT that has reached commercialization. While several other approaches to extract functional information from OCT exist, they remain at the prototype stage. In the chapter, we will discuss three such techniques, namely Doppler OCT, polarization-sensitive (PS) OCT and optoretinography (ORG).

Doppler OCT

Doppler OCT is a technique closely related to OCT angiography, offering quantification of blood speed and flow in retinal vessels. The history of Doppler OCT started in the mid-1990s when several laboratories introduced techniques to measure the Doppler shift-induced changes in the modulation frequency caused by moving particles.[1-3] Subsequently, techniques were developed based on measuring the phase of the complex OCT signal, applied to both time-domain[4,5] and frequency domain.[6-8] This advancement has enabled the measurement of total retinal blood flow by summing up the Doppler information from each vessel entering the optic nerve head.

Figure 1

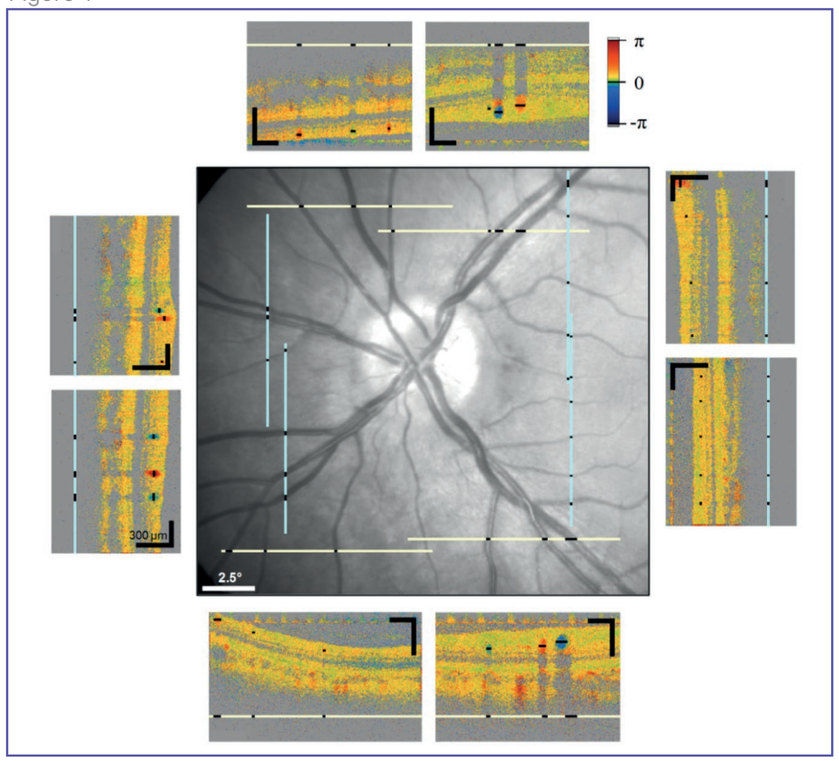

Figure 1
Rectangular scanning pattern around the optic nerve head to measure total retinal blood flow in humans. Scanning positions are denoted by lines in the fundus image, corresponding OCT phase images for each scanning position are presented in the small circumjacent images. Vessel can be clearly identified as red and blue dots in these images, depending on the direction of blood flow and the Doppler angle. Black scale bars correspond to 300µm (reproduced from 13 with permission).

Several approaches have been published on how to extract phase information and the vessel diameters from OCT images including the Doppler angle which is defined as the angle between the incident light beam and the direction of the moving erythrocytes within the vessels.[9-17] However, the current technique is primarily limited to larger retinal arterioles and venules, preventing the quantification of blood flow in small retinal capillaries. A small pilot study discovered reduced retinal blood flow in eyes with glaucoma, correlating with visual field defects.[18] In eyes with damage confined to a single hemifield, retinal blood flow reduction was more pronounced in the affected hemisphere compared to the unaffected hemisphere.[19] Abe and co-workers investigated the area under the curve for distinguishing between glaucomatous and normal eyes using retinal blood flow assessed with Doppler OCT, reporting values of 0.909 and 0.744 for the affected and non-affected hemisphere, respectively.[20] When Doppler OCT is combined with spectroscopy-based measurement of oxygen saturation in retinal vessels, it allows for the calculation of retinal oxygen extraction.[21-24] Two studies have shown that total retinal oxygen extraction is reduced in patients with glaucoma, correlating with structural and functional damage.[25,26] Additionally, reduced total retinal blood flow in glaucomatous eyes is associated with OCT angiography metrics.[27]

Figure 2

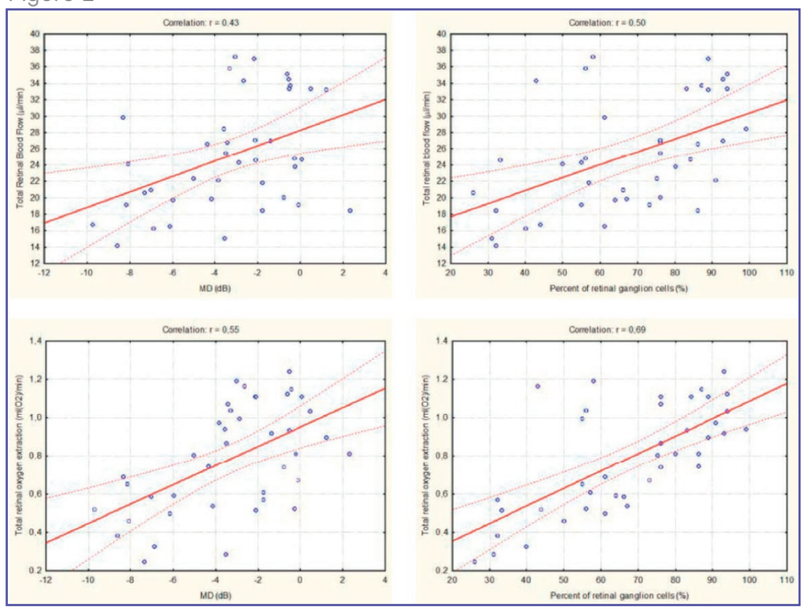

Figure 2
Linear correlation between retinal hemodynamic parameters as measured with Doppler OCT and structural and function damage in patients with primary open-angle glaucoma (reproduced from[26] with permission).

Polarization-sensitive OCT

PS-OCT represents another functional extension of OCT, where contrast in images is achieved through the polarization state of light. Certain tissues can change the polarization state of incident light due to birefringence, diattenuation and/or depolarization. Among these mechanisms, birefringence is particularly significant in tissues such as the corneal stroma, sclera, trabecular meshwork, retinal nerve fiber layer (RNFL), Henle's fiber layer, and fibrotic tissue.[28] Various approaches have been made to measure retinal birefringence

Figure 3

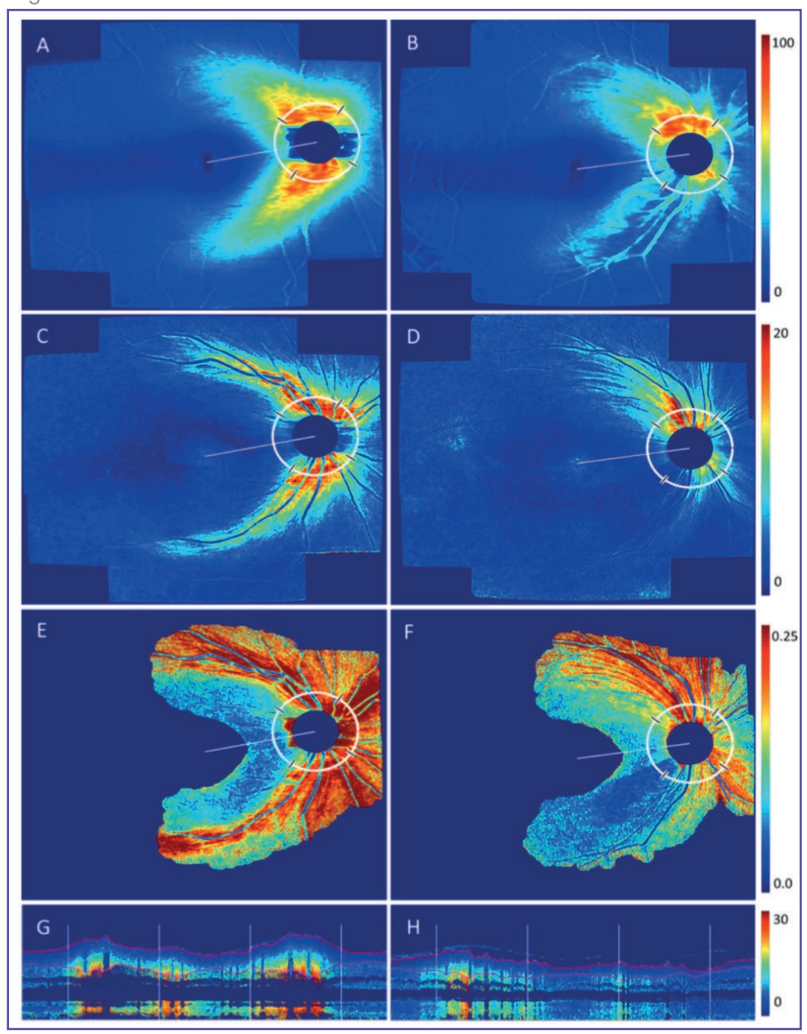

Figure 3
PS-OCT en-face maps of a glaucoma (right column: B, D, F) and an age-matched healthy subject (left column: A, C, E) for nerve fiber layer thickness A–B (µm), retardation C–D (°), and birefringence E–F (°/µm). The virtual circular B-scan plot for retardation (2048 A-scans) is shown in G (healthy) and H (glaucoma). The starting point of the B-scan is the disc-fovea-angle going superiorly (white line between optic-disc center and fovea). The white circle shows the position of the virtual B-scan. Quadrants are separated by small black/white lines (reproduced from[33] with permission).

of the RNFL as an imaging biomarker in glaucoma.[29] The major advantage of PS-OCT over scanning laser polarimetry is that it allows for the depth-resolved measurement of the RNFL, allowing for more detailed and precise imaging of the RNFL.[30-32] Circumpapillary RNFL birefringence is reduced in early glaucoma compared to healthy age-matched controls, suggesting its potential as a biomarker for early-stage disease.[33] Recently, a novel PS-OCT named triple input PS-OCT (TRIPS-OCT) was introduced that showed significant improvements in sensitivity and allowed for imaging of structures as deep as the sclera.[34] Using TRIPS-OCT, it is evident that RNFL birefringence shows little floor effect in advanced glaucoma, making it an attractive device for structural progression monitoring in these high-risk patients.[35]

Optoretinography

ORG represents a promising advancement in retinal imaging, with the potential to replace standard automated perimetry and/or microperimetry in the future.

Figure 4

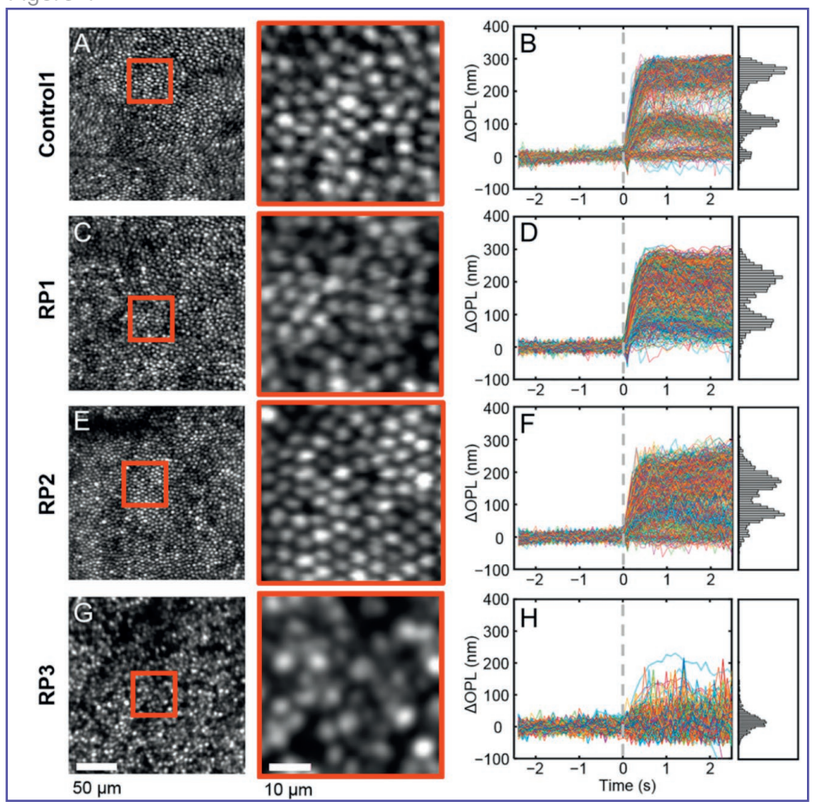

Figure 4
Cone photoreceptor structure and function as measured with adaptive optics optoretinography. En face images of the cone mosaic at 2° eccentricity in one of the controls (A, and B) and three retinitis pigmentosa (RP) subjects: RP1 (C and D), RP2 (E and F), and RP3 (G and H). Magnified views are shown for cones in red boxes. Cone densities are 31,491 (Con- trol1), 22,750 (RP1), 25,258 (RP2), and 14,041 (RP3) cones/mm2. Traces of individual cones' Δ optical path length (OPL) responses to 637-nm stimulus are shown in B, D, F, and H. Traces are randomly color coded, and histograms of peak responses (average ΔOPL from 0.75 to 1.25 s after stimulus) are shown to the right of each plot (reproduced from[40] with permission).

The technique uses either the amplitude or phase of the OCT signal to quantify small changes in neurons induced by light stimuli.[36-38] While the most frequently studied neurons are photoreceptors,[39] ORG has also been explored in pilot studies involving eyes with outer retinal disease.[40,41] Recently, a technique was developed based on a commercial OCT system that quantifies decrease of volume of the subretinal space associated with light adaptation processes of the retina, which may facilitate clinical adaption of such systems.[42,43] While ORG has shown promise in evaluating outer retinal function, its application to inner retinal function is still in its early stages. Signals from the inner retina have been extracted using OCT after visual stimulation, but the extent to which these changes reflect neuronal or vascular changes remains uncertain.[44] Nevertheless, a recent study has introduced a technique to measure nanometer-size changes of the cells within the inner plexiform layer,[45] which may be an interesting biomarker for retinal dysfunction in glaucoma.

Conclusions

Novel functional OCT techniques are emerging as potential sources of important and clinically useful biomarkers in glaucoma. The future will reveal the strength of association between these parameters and glaucomatous damage, as well as their feasibility for early detection and progression monitoring.

Figure 5

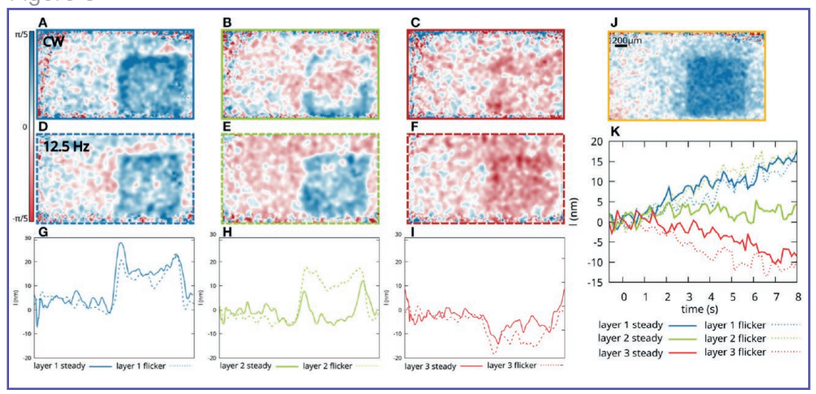

Figure 5
En-face images of the phase changes of three different layers of the inner plexiform layer after 8 s of stimulation with a square-shaped pattern (A-C) or after 8 s stimulation with a 12.5 Hz flickering light (D-F). (G–I) Profile of the optical path length changes after 8 s stimulation. (J) For comparison, phase changes in the photoreceptor OS are shown 0.5 s after the beginning of the stimulation. (K) Corresponding time courses of the optical path length changes averaged over the central part of the stimulated area (reproduced from[45] with permission).

References

1. Chen Z, Milner TE, Srinivas S, Wang X, Malekafzali A, van Gemert MJC, et al. Noninvasive Imaging of In Vivo Blood Flow Velocity Using Optical Doppler Tomography. Optics Letters. 1997;22(14):1119-21. doi: 10.1364/OL.22.001119
2. Izatt JA, Kulkarni MD, Yazdanfar S, Barton JK and Welch AJ. In vivo bidirectional color Doppler flow imaging of picoliter blood volumes using optical coherence tomography. Optics Letters. 1997;22(18):1439-41. doi: 10.1364/OL.22.001439
3. Wang XJ, Milner TE and Nelson JS. Characterization of fluid flow velocity by optical Doppler tomography. Optics Letters. 1995;20(11):1337-39. doi: 10.1364/OL.20.001337
4. Westphal V, Yazdanfar S, Rollins AM and Izatt JA. Real-time, high velocity-resolution color Doppler optical coherence tomography. Optics Letters. 2002;27(1):34-36. doi: 10.1364/OL.27.000034
5. Yazdanfar S, Rollins AM and Izatt JA. In Vivo Imaging of Human Retinal Flow Dynamics by Color Doppler Optical Coherence Tomography. Archives of Ophthalmology. 2003;121(2):235-39. doi: 10.1001/archopht.121.2.235
6. Leitgeb RA, Schmetterer L, Drexler W, Fercher AF, Zawadzki RJ and Bajraszewski T. Real-time assessment of retinal blood flow with ultrafast acquisition by color Doppler Fourier domain optical coherence tomography. Optics Express. 2003;11(23):3116-21. doi: 10.1364/OE.11.003116
7. Leitgeb RA, Schmetterer L, Hitzenberger CK, Fercher AF, Berisha F, Wojtkowski M, et al. Real-time measurement of in vitro flow by Fourier-domain color Doppler optical coherence tomography. Optics Letters. 2004;29(2):171-73. doi: 10.1364/OL.29.000171
8. White BR, Pierce MC, Nassif N, Cense B, Park BH, Tearney GJ, et al. In vivo dynamic human retinal blood flow imaging using ultra-high-speed spectral domain optical Doppler tomography. Optics Express. 2003;11(25):3490-97. doi: 10.1364/OE.11.003490
9. Wang Y, Ii OT and Huang D. In Vivo Retinal Blood Flow Measurement by Fourier-Domain Doppler Optical Coherence Tomography. Investigative Ophthalmology & Visual Science. 2007;48(13):4399.
10. Werkmeister RM, Dragostinoff N, Pircher M, Götzinger E, Hitzenberger CK, Leitgeb RA, et al. Bidirectional Doppler Fourier-domain optical coherence tomography for measurement of absolute flow velocities in human retinal vessels. Optics Letters. 2008;33(24):2967-69. doi: 10.1364/OL.33.002967
11. Yimin W, Bradley AB, Joseph AI, Ou T and David Huang MD. Retinal blood flow measurement by circumpapillary Fourier domain Doppler optical coherence tomography. Journal of Biomedical Optics. 2008;13(6):064003. doi: 10.1117/1.2998480
12. Dai C, Liu X, Zhang HF, Puliafito CA and Jiao S. Absolute Retinal Blood Flow Measurement with a Dual-Beam Doppler Optical Coherence Tomography. Investigative Ophthalmology & Visual Science. 2013:54(13):7998-8003. doi: 10.1167/iovs.13-12318
13. Doblhoff-Dier V, Schmetterer L, Vilser W, Garhöfer G, Gröschl M, Leitgeb RA, et al. Measurement of the total retinal blood flow using dual beam Fourier-domain Doppler optical coherence tomography with orthogonal detection planes. Biomedical Optics Express. 2014;5(2):630-42. doi: 10.1364/BOE.5.000630
14. Ou T, Gangjun L, Liu L, Simon SG, Alex DP, Yali J, et al. En face Doppler total retinal blood flow measurement with 70 kHz spectral optical coherence tomography. Journal of Biomedical Optics. 2015;20(6):066004. doi: 10.1117/1.JBO.20.6.066004
15. Haindl R, Trasischker W, Wartak A, Baumann B, Pircher M and Hitzenberger CK. Total retinal blood flow measurement by three beam Doppler optical coherence tomography. Biomedical Optics Express. 2016;7(2):287-301. doi: 10.1364/BOE.7.000287
16. Pijewska E, Sylwestrzak M, Gorczynska I, Tamborski S, Pawlak MA and Szkulmowski M. Blood flow rate estimation in optic disc capillaries and vessels using Doppler optical coherence tomography with 3D fast phase unwrapping. Biomedical Optics Express. 2020;11(3):1336-53. doi: 10.1364/BOE.382155
17. Szegedi S, Hommer N, Kallab M, Puchner S, Schmidl D, Werkmeister RM, et al. Repeatability and Reproducibility of Total Retinal Blood Flow Measurements Using Bi-Directional Doppler OCT. Translational Vision Science & Technology. 2020;9(7):34-34. doi: 10.1167/tvst.9.7.34.
18. Tan O, Wang Y, Konduru RK, Zhang X, Sadda SR and Huang D. Doppler Optical Coherence Tomography of Retinal Circulation. Journal of Visualized Experiments. 2012;(67):e3524. doi:10.3791/3524
19. Takafumi Y, Youngseok S, Motofumi K, Tomofumi T, Kengo T, Satoshi I, et al. Retinal blood flow reduction in normal-tension glaucoma with single-hemifield damage by Doppler optical coherence tomography. British Journal of Ophthalmology. 2021;105(1):124. doi: 10.1136/bjophthalmol-2019-315616
20. Abe T, Yoshioka T, Song Y, Tani T, Kawai M, Omae T, et al. Glaucoma Diagnostic Performance of Retinal Blood Flow Measurement with Doppler Optical Coherence Tomography. Translational Vision Science & Technology. 2022;11(10):11. doi: 10.1167/tvst.11.10.11
21. Felder AE, Wanek J, Blair NP and Shahidi M. Inner Retinal Oxygen Extraction Fraction in Response to Light Flicker Stimulation in Humans. Investigative Ophthalmology & Visual Science. 2015;56(11):6633-37. doi: 10.1167/iovs.15-17321
22. Werkmeister RM, Schmidl D, Aschinger G, Doblhoff-Dier V, Palkovits S, Wirth M, et al. Retinal oxygen extraction in humans. Scientific Reports. 2015;5(1):15763. doi: 10.1038/srep15763
23. Fondi K, Wozniak PA, Howorka K, Bata AM, Aschinger GC, Popa-Cherecheanu A, et al. Retinal oxygen extraction in individuals with type 1 diabetes with no or mild diabetic retinopathy. Diabetologia. 2017;60(8):1534-40. doi: 10.1007/s00125-017-4309-0
24. Hommer N, Kallab M, Schlatter A, Howorka K, Werkmeister RM, Schmidl D, et al. Retinal Oxygen Metabolism in Patients With Type 2 Diabetes and Different Stages of Diabetic Retinopathy. Diabetes. 2022;71(12):2677-84. doi: 10.2337/db22-0219
25. Aref AA, Maleki S, Tan O, Huang D, Varma R and Shahidi M. Relating Glaucomatous Visual Field Loss to Retinal Oxygen Delivery and Metabolism. Acta Ophthalmologica. 2019;97(7):e968-e972. doi: https://doi.org/10.1111/aos.14120
26. Garhöfer G, Bata AM, Popa-Cherecheanu A, Hommer A, Vass C, Resch H, et al. Retinal Oxygen Extraction in Patients with Primary Open-Angle Glaucoma. International Journal of Molecular Sciences, 2022;23(17):10152. doi: 10.3390/ijms231710152
27. Cano J, Rahimi M, Xu BY, Richter GM, Tan O, Huang D, et al. Relationship Between Macular Vessel Density and Total Retinal Blood Flow in Primary Open-angle Glaucoma. Journal of Glaucoma. 2021;30(8).
28. Pircher M, Hitzenberger CK and Schmidt-Erfurth U. Polarization sensitive optical coherence tomography in the human eye. Progress in Retinal and Eye Research. 2011;30(6):431-51. doi: https://doi.org/10.1016/j.preteyeres.2011.06.003
29. Townsend KA, Wollstein G and Schuman JS. Imaging of the retinal nerve fibre layer for glaucoma. British Journal of Ophthalmology. 2009;93(2):139. doi: 10.1136/bjo.2008.145540
30. Cense B, Chen TC, Park BH, Pierce MC and de Boer JF. In Vivo Depth-Resolved Birefringence Measurements of the Human Retinal Nerve Fiber Layer by Polarization-Sensitive Optical Coherence Tomography. Optics Letters. 2002;27(18):1610-12. doi: 10.1364/OL.27.001610
31. Götzinger E, Pircher M, Baumann B, Hirn C, Vass C and Hitzenberger CK. Analysis of the Origin of Atypical Scanning Laser Polarimetry Patterns by Polarization-Sensitive Optical Coherence Tomography. Investigative Ophthalmology & Visual Science. 2008;49(12):5366-72. doi: 10.1167/iovs.08-2081
32. Götzinger E, Pircher M, Baumann B, Hirn C, Vass C and Hitzenberger CK. Retinal nerve fiber layer birefringence evaluated with polarization sensitive spectral domain OCT and scanning laser polarimetry: A comparison. Journal of Biophotonics. 2008;1(2):129-39. doi: https://doi.org/10.1002/jbio.200710009

33. Steiner S, Schwarzhans F, Desissaire S, Resch H, Fischer G, Pircher M, et al. Birefringent Properties of the Peripapillary Retinal Nerve Fiber Layer in Healthy and Glaucoma Subjects Analyzed by Polarization-Sensitive OCT. Investigative Ophthalmology & Visual Science. 2022;63(12):8. doi: 10.1167/iovs.63.12.8
34. Liu X, Jiang L, Ke M, Sigal IA, Chua J, Hoang QV, et al. Posterior scleral birefringence measured by triple-input polarization-sensitive imaging as a biomarker of myopia progression. Nature Biomedical Engineering. 2023;7(8):986-1000. doi: 10.1038/s41551-023-01062-w
35. Radhakrishnan PR, Wong D, Li C, Yoke JCM, Nongpiur ME, Chong RS, et al. Retinal nerve fiber layer damage assessment in glaucomatous eyes using retinal retardance measured by polarization-sensitive optical coherence tomography (in press). Translational Vision Science & Technology. 2024.
36. Ling T, Boyle KC, Zuckerman V, Flores T, Ramakrishnan C, Deisseroth K, et al. High-speed interferometric imaging reveals dynamics of neuronal deformation during the action potential. Proceedings of the National Academy of Sciences. 2020;117(19):10278-85. doi: 10.1073/pnas.1920039117
37. Boyle KC, Chen ZC, Ling T, Pandiyan VP, Kuchenbecker J, Sabesan R, et al. Mechanisms of Light-Induced Deformations in Photoreceptors. Biophysical Journal. 2020;119(8):1481-88. doi: 10.1016/j.bpj.2020.09.005
38. Kim TH, Ma G, Son T, Yao X. Functional Optical Coherence Tomography for Intrinsic Signal Optoretinography: Recent Developments and Deployment Challenges. Frontiers in Medicine. 2022;9:864824. doi: 10.3389/fmed.2022.864824
39. Ma G, Son T, Kim T-H and Yao X. Functional optoretinography: concurrent OCT monitoring of intrinsic signal amplitude and phase dynamics in human photoreceptors. Biomedical Optics Express. 2021;12(5):2661-69. doi: 10.1364/BOE.423733.
40. Lassoued A, Zhang F, Kurokawa K, Liu Y, Bernucci MT, Crowell JA, et al. Cone photoreceptor dysfunction in retinitis pigmentosa revealed by optoretinography. Proceedings of the National Academy of Sciences. 2021;118(47):e2107444118. doi: 10.1073/pnas.2107444118
41. Maddipatla R, Langlo C, Vienola K, Bartuzel M, Pijewska E, Zawadzki R, et al. Poster Session II: Investigating photoreceptor function in disease-affected retinas using optoretinography. Journal of Vision. 2023, 2023;23(15):63. doi: 10.1167/jov.23.15.63
42. Messner A, Werkmeister RM, Seidel G, Stegmann H, Schmetterer L and Aranha dos Santos V. Light-induced changes of the subretinal space of the temporal retina observed via optical coherence tomography. Scientific Reports. 2019;9(1):13632.doi: 10.1038/s41598-019-50057-8
43. Messner A, Aranha dos Santos V, Stegmann H, Puchner S, Schmidl D, Leitgeb R, et al. Quantification of intrinsic optical signals in the outer human retina using optical coherence tomography. Annals of the New York Academy of Sciences. 2022;1510(1):145-57. doi: https://doi.org/10.1111/nyas.14721.
44. Erchova I, Tumlinson AR, Fergusson J, White N, Drexler W, Sengpiel F, et al. Optophysiological Characterisation of Inner Retina Responses with High-Resolution Optical Coherence Tomography. Scientific Reports. 2018;8(1):1813. doi: 10.1038/s41598-018-19975-x.
45. Pfäffle C, Spahr H, Gercke K, Puyo L, Höhl S, Melenberg D, et al. Phase-Sensitive Measurements of Depth-Dependent Signal Transduction in the Inner Plexiform Layer. Frontiers in Medicine. 2022;9:885187. doi: 10.3389/fmed.2022.885187.

Part 3

Chapter 21

Artificial intelligence using fundus photographs

Ruben Hemelings

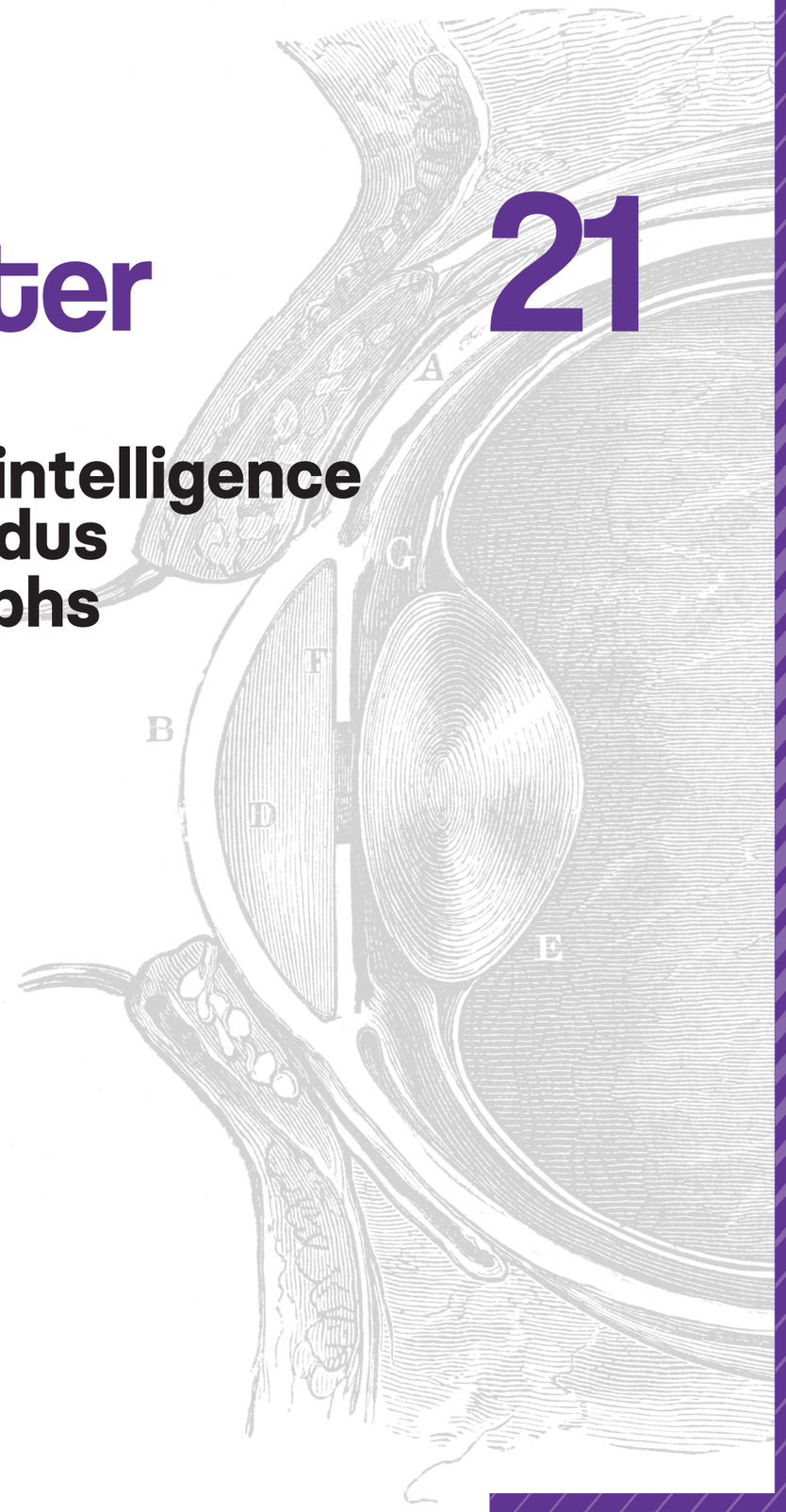

Vertical Section

Artificial intelligence using fundus photographs

Ruben Hemelings

Singapore Eye Research Institute (SERI), Singapore National Eye Centre, Singapore, Singapore
SERI-NTU Advanced Ocular Engineering (STANCE) Programme, Singapore, Singapore
Research Group Ophthalmology, Department of Neurosciences, KU Leuven, Herestraat 49, 3000 Leuven, Belgium

Introduction

In recent years, the application of artificial intelligence (AI) in fundus photography analysis has shown remarkable promise to revolutionize glaucoma care. AI algorithms have the potential to analyze fundus photographs with unprecedented precision and efficiency, leading to improved diagnostic accuracy and enhanced monitoring of disease progression. This chapter delves into the recent developments of this fast-moving field. Fundus photography has long been utilized by ophthalmologists as a non-invasive imaging technique to capture detailed images of the retina, optic nerve head, and surrounding structures. Traditionally, the analysis of these images has relied on subjective interpretations by human experts. However, manual assessment can be limited by inter-observer variability, subjectivity, and the need for specialized expertise. This has paved the way for the application of AI, which has the potential to revolutionize the field of fundus photography analysis.

Deep learning in glaucoma using fundus photographs

Deep Learning (DL), a subset of machine learning inspired by neural networks, has shown remarkable progress since its first success in the 2012 ImageNet competition. In the field of computer vision, DL has reshaped tasks like classification, segmentation (pixel-level classification), and regression. This technology has found its way into medical image analysis, with convolutional neural networks (CNNs) achieving remarkable results on disease detection, and recently vision transformers (ViTs) adding a new dimension to the field. One key advantage of DL is its ability to bypass manual feature extraction. Instead of relying on predefined features, DL models autonomously learn and extract relevant data characteristics for a given task. In glaucoma detection, for instance, traditional approaches required experts to extract metrics like the Vertical Cup-to-Disc Ratio (VCDR) from fundus images, using these metrics to classify cases. With DL, the raw fundus photo, as a pixel array, becomes the input. The DL model learns to identify important features, possibly going beyond VCDR, thereby enhancing glaucoma detection. Convolutional neural networks consist of multiple layers, with a primary focus on convolutional layers that perform mathematical operations. These convolutions help extract both high-level features (like edges) and low-level features (like intricate details) from the input image. Imagine sliding a window with a learnable filter over the image pixels. This filter captures the overlap between the filter and the image at different positions, generating an activation map. These activation maps are then used as input for subsequent layers or mathematical operations like pooling. This process of extracting features and passing them through layers continues for a predetermined number of steps. Vision transformers represent a more recent development that combines transformer models from the domain

of natural language processing with image analysis. Unlike CNNs, which process the entire image uniformly, ViTs split the image into non-overlapping patches for individualized processing. The self-attention mechanism then assigns varying importance to these patches, allowing the model to focus on the most relevant parts (e.g. the optic nerve head in the case of glaucoma). Unlike CNNs, ViTs do not use convolutions, making them a distinct class of DL models.

Figure 1

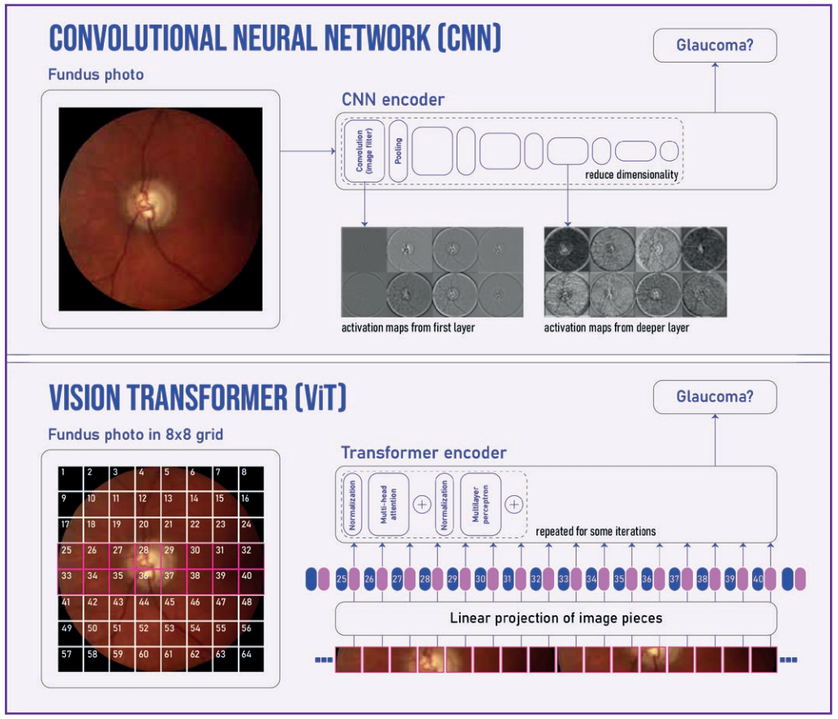

Figure 1
Overview of the two main deep learning architectures in the context of glaucoma detection.

Glaucoma detection from fundus photographs

In the context of diagnostic models, the evaluation metric commonly employed is the "area under the receiver operating characteristic curve," abbreviated as AUC. In diagnostic tasks, this metric serves as a measure of a model's ability to discern the presence of diseases such as glaucoma. In 2015, Chen et al. conducted a pioneering study that utilized DL to develop an automated system for detecting glaucoma based on fundus images.[1] Despite utilizing a relatively shallow network architecture consisting of merely six layers, this model achieved an impressive AUC value of up to 0.89. The input data consisted of color images, each with dimensions of 256 pixels in width, 256 pixels in height, and three color channels. Over subsequent years, advancements in glaucoma detection evolved, driven by the utilization of larger annotated datasets and deeper convolutional neural networks. Another trend was the use of transfer learning that was made possible with the availability of pretrained CNN architectures such as VGG (2014), ResNet (2015), and EfficientNet (2019). In transfer learning, only a select number of layers at the output side would be unfrozen for learning of the glaucoma detection task, with the initial layers pretrained on a general image recognition data set. This strategy reduces the risk of overfitting in small data regimes. Overfitting is the undesired phenomenon when the trained model does not perform well on new data. To ensure a scalable candidate model for deployment in glaucoma detection from fundus photographs, it is imperative that the model demonstrates robust generalization capabilities. This includes the ability to perform well not only on unseen data from the same clinical context (such as the same clinic) but also on diverse datasets sourced from different medical centers. In the domain of CNN-based glaucoma detection from fundus photos, several studies have reported impressively high AUC metrics. However, drawing meaningful comparisons between most studies becomes challenging due to variations in proprietary data sets used for training and testing. These datasets often differ not only in the subjective definition of glaucoma but also in data distribution, making it difficult to establish a fair benchmark.

A pivotal study by Hemelings et al. addressed this issue by achieving excellent performance on a vast dataset of nearly 150,000 fundus images collected from 13 external test sets.[2] Their results show AUC values ranging from 0.85 to 0.99, marking a significant milestone as they fulfill the minimum criteria for a diagnostic test on two population-based sets. Moreover, the work provides a valuable resource by making detection results on 11 publicly available datasets accessible for benchmarking purposes. Other developments in the field have also assessed generalizability.[3] For instance, Fan et al. introduced the use of a ViT model for glaucoma detection, which exhibited superior performance on external testing compared to a CNN.[4] In the challenging ORIGA dataset, their ViT achieved an AUC of 0.73, outperforming the CNN's score of 0.55. Hemelings et al.'s glaucoma risk regression CNN also excelled in external performance, surpassing an AUC of 0.85 on the ORIGA data set.

Structural glaucoma damage from fundus photographs

Next to referable glaucoma detection, there exists research on the use of DL for parameter estimation that quantify structural glaucoma-induced damage from retinal images. The 2019 landmark paper by Medeiros et al. demonstrated that color fundus images contain a lot of glaucoma-related information that is undetectable by human experts.[5] Their group trained and validated a CNN that estimates average RNFL thickness, a parameter derived from OCT software. The resulting regression model was able to

explain almost 70% of the variance in the test set. The BMO-MRW, another OCT parameter that quantifies neuroretinal rim loss, was also modelled shortly after, reporting even lower prediction errors.[5] VCDR values have also been (in)directly estimated from fundus photographs. The traditional approach was to segment both optic cup and disc, and deriving the ratio from the pixel-level classification maps.[6] This provides an extremely insightful approach, as clinicians can review the delineation of optic cup and disc. However, the delineation of the optic cup can be challenging in 2D images as cup depth may be obscured, while disc delineation may be hampered by peripapillary atrophy (PPA) for example. Hence, more recent work has explored the possibility of direct VCDR estimation from fundus photography using a regression CNN.[7,8]
The automated estimation of biomarkers such as RNFL thickness, BMO-MRW, and VCDR from fundus images could be a solution to the high degree of subjectivity in ONH assessment by human experts.

Functional glaucoma damage from fundus photographs

Analogously to the disease path of glaucoma, data-driven CNN modelling of functional parameters quickly followed the first successes of structural damage using retinal images. Global VF metrics such as mean deviation (MD) were able to be retrieved from raw OCT scans and to a lesser degree from color fundus images.[9] This area of research can aid in better understanding the structure-function relationship, and potent models can serve as ersatz solution to estimate visual function in patients who are unable to complete reliable VF exams. However, the author believes that this field will evolve more using OCT imaging, as these devices are (becoming) widely available at glaucoma clinics, and offer more information on the structure-function relationship. A recent study by Hemelings et al. quantified the benefits of circumpapillary OCT rings over a fundus image captured through scanning laser ophthalmoscopy (SLO).[10] Using an OCT-based input decreased the prediction errors on MD and pointwise 24-2 VF estimation by 29% and 14%, respectively.

Glaucoma progression from fundus photographs

Accurate progression monitoring is adamant in glaucoma management, given the disease's neurodegenerative aspect. At each visit, glaucoma experts have to assess the rate of progression, and modify personalized treatment when needed. In (multimodal) glaucoma progression monitoring, recent test results are compared to the baseline established at initial diagnosis. Here, we run into the same challenge as described earlier: the presence of subjectivity and variability in test results induced by multiple sources. There is also not a clear definition for glaucoma progression. However, a progression-focused model can aid to identify progressing patients for intervention and/or predict future progression risk.

Detection of glaucoma progression

The group of Medeiros applied their RNFL thickness estimation model (see section 4) on longitudinal fundus photos and compared the change over time with the OCT-measured change.[11] Next to a Pearson r of 0.76,

Figure 2

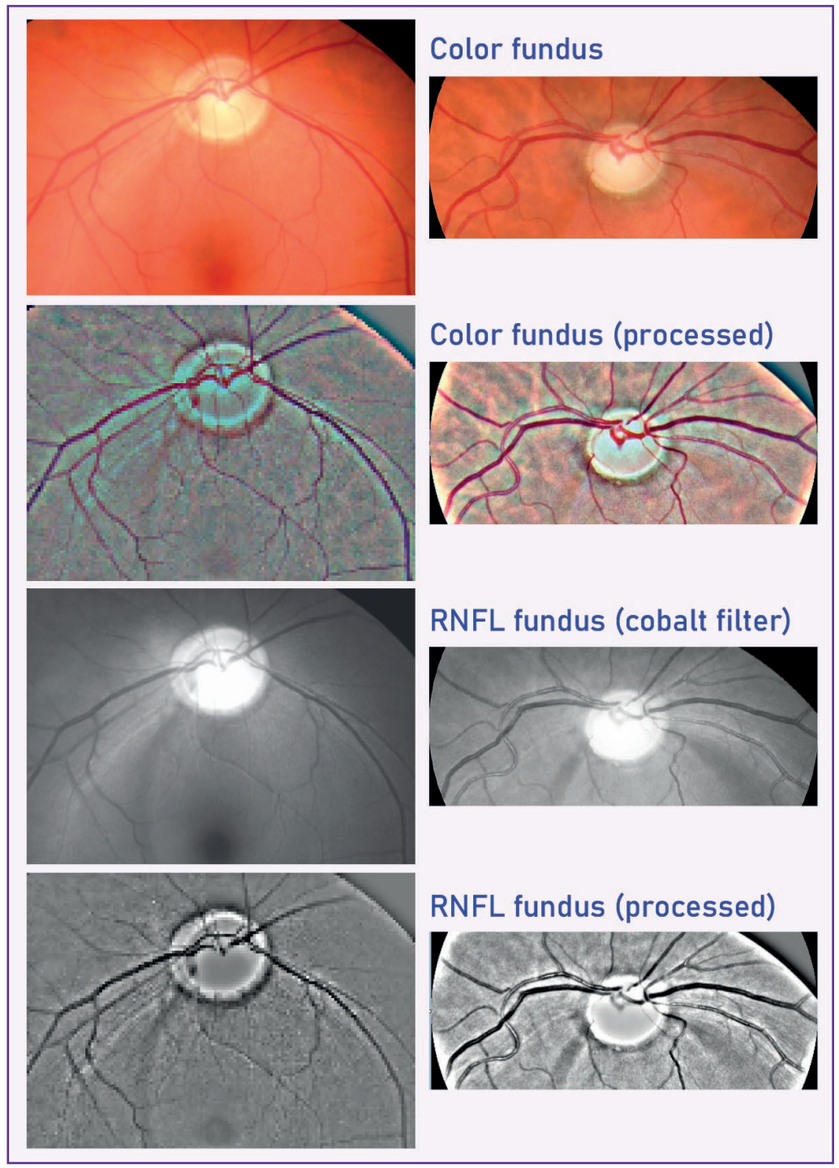

Figure 2
Examples of fundus images photographed at different wavelengths, and post-hoc lighting equalization. Made available by Tays Eye Centre, Tampere University Hospital Finland.

the DL slope was able to obtain an AUC of 0.96 in the detection of fast progressing cases (RNFL loss exceeding 2 µm/year). This is relevant as progression can be quantified from fundus photography using an objective RNFL thickness prediction.

Prediction of glaucoma progression

Recently, research by Li et al. demonstrated the ability of DL to predict future glaucoma progression from a baseline fundus image, with AUC values of 0.89 and 0.87 in two test sets.[12] Progression was defined as at least three visual field locations worsening compared to baseline in two consecutive reliable tests at the 5% level. We believe that the field of glaucoma progression prediction from baseline using AI will advance swiftly in the near future.

Other fundus imaging modalities and image preprocessing

The vast majority of discussed methods have utilized color fundus imaging. Of course, there exist other modalities such as the red-free filter, cobalt blue filter, and previously mentioned SLO. Specialized filters feature a light wavelength that may highlight tissues of interest such as RNFL or PPA. Color fundus images are abundantly available in the field of glaucoma detection and DL, due to (1) its use in spotting disc hemorrhages, and (2) its use in the screening of diabetic retinopathy. Prior to analysis using DL, color fundus images can be processed in such a manner that optimizes the visibility of both rim thinning and RNFL defects, as shown in the example below.

Conclusions

- AI is rapidly advancing glaucoma care by improving the analysis of fundus photographs. Deep learning, in particular CNNs and ViTs, enhances diagnostic accuracy by autonomously extracting key features from images.
- The challenge of generalizability has been addressed by benchmark studies, ensuring reliable model performance on diverse datasets.
- AI extends its impact to quantifying structural and functional glaucoma damage, reducing subjectivity in assessment.
- AI-powered models start to excel at detecting and predicting glaucoma progression from fundus photographs, potentially aiding intervention decisions in the future.

References

1. Chen X, Xu Y, Yan S, Wong DWK, Wong TY, Liu J. Automatic Feature Learning for Glaucoma Detection Based on Deep Learning. In: Navab N, Hornegger J, Wells WM, Frangi AF, eds. Medical Image Computing and Computer-Assisted Intervention – MICCAI 2015. Lecture Notes in Computer Science. Springer International Publishing; 2015:669-77. doi:10.1007/978-3-319-24574-4_80
2. Hemelings R, Elen B, Schuster AK, et al. A generalizable deep learning regression model for automated glaucoma screening from fundus images. Npj Digit Med. 2023;6(1):1-15. doi:10.1038/s41746-023-00857-0
3. De Vente C, Vermeer KA, Jaccard N, et al. AIROGS: Artificial Intelligence for RObust Glaucoma Screening Challenge. Published online February 10, 2023. Accessed September 9, 2023. http://arxiv.org/abs/2302.01738
4. Fan R, Alipour K, Bowd C, et al. Detecting Glaucoma from Fundus Photographs Using Deep Learning without Convolutions. Ophthalmol Sci. 2023;3(1):100233. doi:10.1016/j.xops.2022.100233
5. Medeiros FA, Jammal AA, Thompson AC. From Machine to Machine: An OCT-trained Deep Learning Algorithm for Objective Quantification of Glaucomatous Damage in Fundus Photographs. Ophthalmology. 2019;126(4):513-21. doi:10.1016/j.ophtha.2018.12.033
6. Fu H, Cheng J, Xu Y, Wong DWK, Liu J, Cao X. Joint Optic Disc and Cup Segmentation Based on Multi-Label Deep Network and Polar Transformation. IEEE Trans Med Imaging. 2018;37(7):1597-1605. doi:10.1109/TMI.2018.2791488
7. Hemelings R, Elen B, Barbosa-Breda J, Blaschko MB, De Boever P, Stalmans I. Deep learning on fundus images detects glaucoma beyond the optic disc. Sci Rep. 2021;11(1):20313. doi:10.1038/s41598-021-99605-1
8. Alipanahi B, Hormozdiari F, Behsaz B, et al. Large-scale machine-learning-based phenotyping significantly improves genomic discovery for optic nerve head morphology. Am J Hum Genet. 2021;108(7):1217-30. doi:10.1016/j.ajhg.2021.05.004
9. Lee J, Kim YW, Ha A, et al. Estimating visual field loss from monoscopic optic disc photography using deep learning model. Sci Rep. 2020;10(1):21052. doi:10.1038/s41598-020-78144-1
10. Hemelings R, Elen B, Barbosa-Breda J, et al. Pointwise Visual Field Estimation From Optical Coherence Tomography in Glaucoma Using Deep Learning. Transl Vis Sci Technol. 2022;11(8):22. doi:10.1167/tvst.11.8.22
11. Medeiros FA, Jammal AA, Mariottoni EB. Detection of Progressive Glaucomatous Optic Nerve Damage on Fundus Photographs with Deep Learning. Ophthalmology. 2021;128(3):383-92. doi:10.1016/j.ophtha.2020.07.045
12. Li F, Su Y, Lin F, et al. A deep-learning system predicts glaucoma incidence and progression using retinal photographs. J Clin Invest. 2022;132(11):e157968. doi:10.1172/JCI157968

Part 3

Chapter 22

OCT and Telemedicine

Alfonso Anton

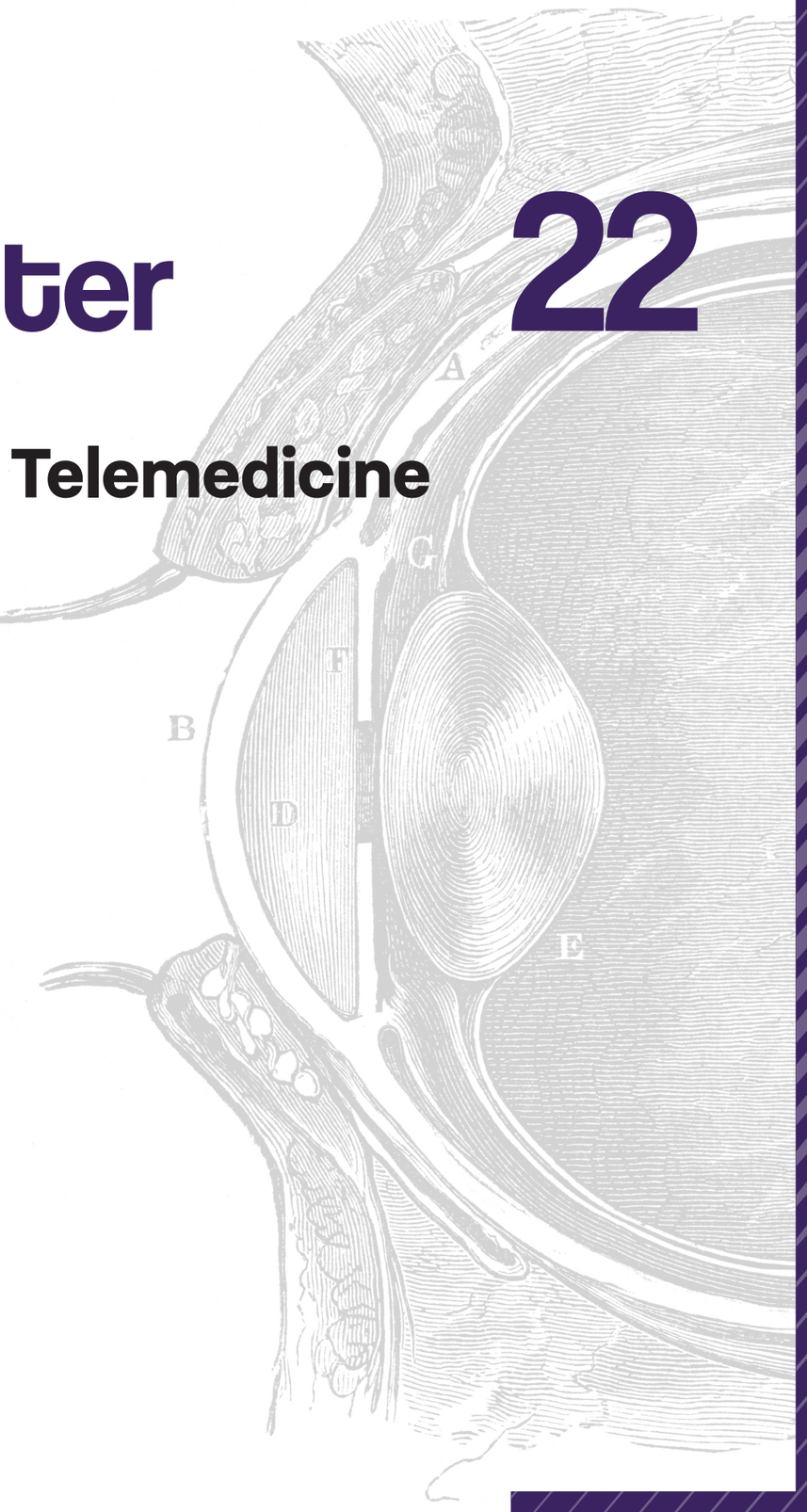

Vertical Section

22
Part 3

OCT and Telemedicine

Alfonso Anton

Universitat Internacional de Catalunya
Institut Catalá de Retina, Barcelona, Spain

OCT images have become the standard and most frequently performed images in any glaucoma clinic. EGS Guidelines[1] indicate that optic nerve and nerve fiber layer images should not replace clinical examination or visual fields, but that they are widely performed to assist in glaucoma diagnosis and follow up. OCT images offer significant advantages for the management of glaucoma but also have certain limitations that have to be considered, both will be reviewed in the next few pages. There are solid advantages of OCT that make this technology especially suitable for telehealth services in glaucoma. In first place, OCT offers objective evaluation of structural damage with a very short acquisition time. In second place, results are compared with a normative database offering an automatic classification. In third place, the diagnostic precision for glaucoma detection has been widely proven to be more than adequate in case-control studies[2,3] and acceptable, but more limited, in screening settings.[4,5] In fourth place, OCT imaging takes few seconds and it is feasible to obtain good quality images in population-based studies in over 95% of cases.[4,6] In fifth place, inter-observer agreement of OCT images interpretation tends to be better than that of fundus photographs.[6] Finally, OCT images, in combination with photographs and intraocular pressure measurements (IOP) and telemedicine, maybe cost-effective for the detection of glaucoma, as sown in a population-based screening setting, aim at high risk population, using telemedicine.[7] At present, OCT images have already been used in telemedicine for the detection and follow-up of glaucoma and for the evaluation of the irido-corneal angle.

Detection

Few studies have evaluated the application, usefulness costs and effectiveness of OCT to detect glaucoma through telemedicine. Grau et al[8] used IOP and OCT images to screen over 900 healthy volunteers and found epiretinal membrane in 1%, glaucoma in 1%, vitelliform maculopathy in 0,5% age related maculopathy in 0,5% and diabetic retinopathy in 0.2% of the sample. A metanalysis on the screening capabilities of teleglaucoma estimated a sensitivity of 0.83, a specificity of 0.79, a cost per patient screened of 922$, a cost per glaucoma detected of 1098$, a positive likelihood ratio (PLR) of a positive screening of 3.97, and a negative likelihood ratio (NLR) of 0.21. Since the PLR was clearly over 1 and the NLR was under 1, the first is significantly associated with glaucoma and the last with the absence of glaucoma.[9] OCT was used in only one of 45 studies included in the metanalysis in this study published in 2014, but undoubtedly the proportion of screening studies and programs including OCT images has increased since then. Thomas et al[10] applied a glaucoma screening program in Alberta (Canada) and found that tele-glaucoma (including OCT images) was more sensitive (86%), less specific (78%) and more cost effective than the presential clinic with a cost of 27,460$ per quality adjusted life year (QALY)

gained. Our group also found detection of glaucoma with OCT, photographs (Figs. 1 and 2) and telemedicine useful (sensitivity 86 to 69%, specificity 82 to 94%) and cost effective with a cost of 12,214€/QALY gained[7], compared with opportunistic detection. Nevertheless, one small study (n=256) performed in the Veteran Affairs Health System in 2015[11] did not find any benefit to the diagnostic accuracy of a telemedicine detection-program when OCT images and results were added to the clinical information available to the evaluator.

Follow up

Virtual glaucoma clinics are becoming more frequent in certain environments, and most publications describe them based on IOP, photographs and visual fields.[12] Modjtahedi et al[13] designed a telemedicine follow-up program for low-risk glaucoma-suspects using visual acuity, IOP and OCT images. Most participants (92%) attended the 1-year and 2-year visits, five patients (2.5%) met criteria for referral to ophthalmologist and over 80% thought (100 participants filled in a questionnaire) that the program was extremely or quite helpful, convenient and professional. The benefits and limitations (see above and below) of OCT information and clinical usefulness in glaucoma follow up should be very similar to those in presential clinics.

Irido-Corneal Angle Assessment

Phu et al evaluated the interobserver and intertest agreement for the remote assessment of the irido-corneal angle with photographs and with anterior segment OCT.[14] Only moderate agreement (Kappa 0,3 to 0,5) was found between instruments and observers, and no differences were found in the degree of agreement between the two tests and ground truth. A tendency to an underestimation of the angle grade, with remote evaluation of images, was detected.

Figure 1

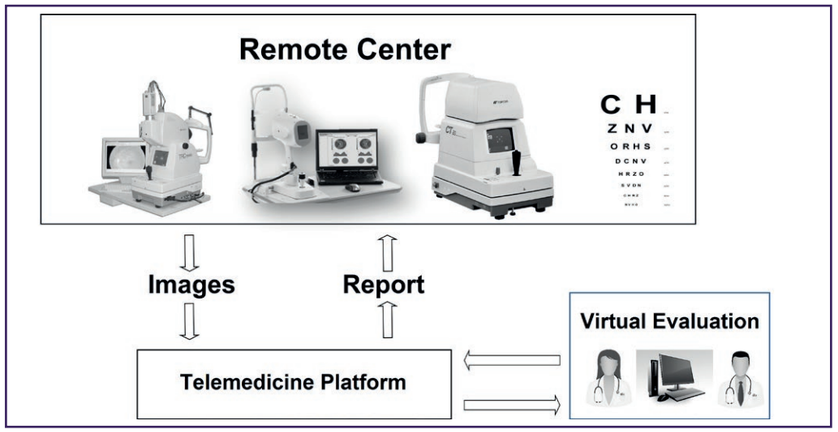

Figure 1
Telemedicine Screening Program Scheme. Examination (IOP, OCT, fundus photographs) were obtained at remote centre (Primary Care Centre) by optometrists or nurses, data and images were uploaded to the telemedicine platform, and they were evaluated remotely, in a deferred basis, by ophthalmologists.

Figure 2

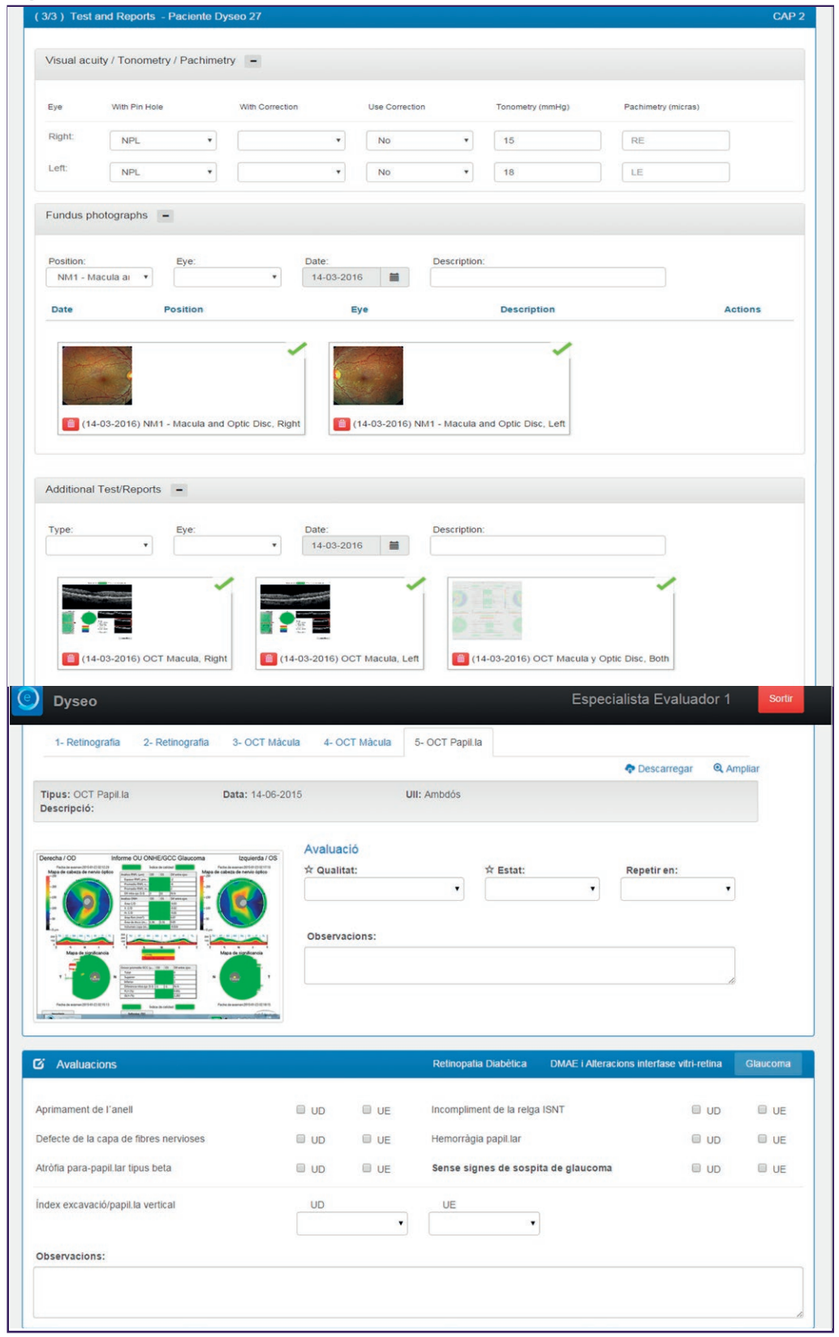

Figure 2
Telemedicine platform software. Evaluators had remote access to all data and images (2.A) and were asked to evaluate quality and usefulness of images, to look for a list of pathological signs in the images and to give a global classification of the images (2.B). The figure shows several screens of the telemedicine platform used.

Alfonso Anton

Limitations

Among the several limitations of OCT usage, in presential and in telemedicine clinics, the most important are the following. In first place, OCT always gives results but artifacts; false positive and false negative classifications may lead to wrong clinical conclusions if not adequately interpreted. Specificities of around 80%, with only one study over 90%, are clearly not optimal for screening purposes in large populations at risk. In second place, OCT images include a limited size normative database with incomplete representation of all ethnic origins. In third place, case control studies are undoubtedly imperfect to evaluate any diagnostic device if it is meant to be used in a screening setting, since accuracy could be over-estimated. In fourth place, the continuous change in OCT technology may preclude long term follow up of a chronic life lasting disease. Many times, last version of OCT cannot directly compare the data from new images with that from older images from a previous version of the device. Finally, OCT images add costs (instrument, image acquisition, image interpretation...) to any screening or follow-up program. It is also important to underline that adequate and methodic interpretation of OCT results, by the clinician, is mandatory before making any clinical decision and that correlation between OCT images and visual field results is only moderate[1]. An adequate interpretation of OCT print outs should consider image quality, rule out artifacts, and take into account physiological thinning of nerve fiber layer, ganglion cell layer or neuro-retinal rim. All of them are key factors for making solid clinical decisions using OCT information. In summary, OCT images maybe useful in tele-glaucoma for detection, follow-up and to evaluate angle characteristics since they offer objective quantitative data on structural damage. Nevertheless, solid evidenced-based data on the added value to examinations without OCT is limited, it adds certain costs and adequate interpretation of the results is always needed. The author subjectively estimates that OCT will expand its usage in teleglaucoma and hopes that ongoing studies will offer new solid data in the near future.

References

1. Spaeth GL. European Glaucoma Society Terminology and Guidelines for Glaucoma, 5th Edition. Br. J. Ophthalmol. 2021;105:1-169. doi:10.1136/BJOPHTHALMOL-2021-EGSGUIDELINES.
2. Michelassi M, Lucenteforte E, Oddone F, Brazzelli M, Parravano M, Franchi S, Ng SM, Virgili G. Optic Nerve Head and Fibre Layer Imaging for Diagnosing Glaucoma. Cochrane database Syst. Rev. 2015. doi:10.1002/14651858. CD008803.PUB2
3. Fallon M, Valero O, Pazos M, Antón A. Diagnostic Accuracy of Imaging Devices in Glaucoma: A Meta-Analysis. Surv. Ophthalmol. 2017;62:446-61.
4. Anton A, Nolivos K, Pazos M, Fatti G, Ayala ME, Martínez-Prats E, Peral O, Poposki V, Tsiroukis E, Morilla-Grasa A, et al. Diagnostic Accuracy and Detection Rate of Glaucoma Screening with Optic Disk Photos, Optical Coherence Tomography Images, and Telemedicine. J. Clin. 2021;11. doi:10.3390/jcm11010216
5. Koh V, Tham YC, Cheung CY, Mani B, Wong TY, Aung T, Cheng CY. Diagnostic Accuracy of Macular Ganglion Cell-Inner Plexiform Layer Thickness for Glaucoma Detection in a Population-Based Study: Comparison with Optic Nerve Head Imaging Parameters. 2018. doi:10.1371/journal.pone.0199134
6. Anton A, Nolivos K, Pazos M, Fatti G, Herranz A, Ayala-Fuentes ME, Martínez-Prats E, Peral O, Vega-Lopez Z, Monleon-Getino A, et al. Interobserver and Intertest Agreement in Telemglaucoma Screening with Optic Disk Photos Ancoherence Tomography. J. Clin. Med. 2021;10:1-13. doi:10.3390/jcm10153337
7. Anton A, Serrano D, Nolivos K, Fatti G, Zmuc N, Crespo C, Monleon-Getino T, Sotelo K, Morilla A, García V, et al. Cost-Effectiveness of Screening for Open Angle Glaucoma Compared With Opportunistic Case Finding. J. Glaucoma. 2023;32:72-79. doi:10.1097/ IJG.0000000000002132
8. Grau E, Horn F, Nixdorff U, Michelson G. OCT and IOP Findings in a Healthy Worker Cohort: Results from a Teleophthalmic Study in Occupational Medicine. Graefes Arch. Clin. Exp. Ophthalmol. 2019;257:2571-78. doi:10.1007/S00417-019-04457-1
9. Thomas SM, Jeyaraman M, Hodge WG, Hutnik C, Costella J, Malvankar-Mehta, MS. The Effectiveness of Teleglaucoma versus In-Patient Examination for Glaucoma Screening: A Systematic Review and Meta-Analysis. PLoS One 2014;9:1-24. doi:10.1371/journal.pone.0113779
10. Open Access Citation, Thomas S, Hodge W, Malvankar-Mehta M. The Cost-Effectiveness Analysis of Teleglaucoma Screening Device. PLoS One 2015;10:137913. doi:10.1371/journal.pone.0137913
11. Maa AY, McCord S, Lu X, Janjua R, Howell AV, Hunt KJ, Medert CM, Giangiacomo A, Lynch, MG. The Impact of OCT on Diagnostic Accuracy of the Technology-Based Eye Care Services Protocol: Part II of the Technology-Based Eye Care Services Compare Trial. Ophthalmology 2020;127:544-49. doi:10.1016/J.OPHTHA.2019.10.025
12. Wright HR, Diamond JP. Service Innovation in Glaucoma Management: Using a Web-Based Electronic Patient Record to Facilitate Virtual Specialist Supervision of a Shared Care Glaucoma Programme. Br. J. Ophthalmol. 2015;99:313-17. doi:10.1136/BJOPHTHALMOL-2014-305588 Two-Year Outcomes of a Pilot Glaucoma Suspect Telemedicine Monitoring Program. Clin. Ophthalmol. 2018;12:2095-2102. doi:10.2147/OPTH.S171263
13. Modjtahedi BS, Chu K, Luong TQ, Hsu C, Mattox C, Lee PP, Nakla ML, Fong DS. Two-Year Outcomes of a Pilot Glaucoma Suspect Telemedicine Monitoring Program. Clin. Ophthalmol. 2018;12:2095-2102. doi:10.2147/OPTH.S171263
14. Phu J, Wang H, Khou V, Zhang S, Kalloniatis M. Remote Grading of the Anterior Chamber Angle Using Goniophotographs and Optical Coherence Tomography: Implications for Telemedicine or Virtual Clinics. Transl. Vis. Sci. Technol. 2019;8(5):16. doi:10.1167/TVST.8.5.16

Glaucoma Imaging Note

Vertical Section of the Eye.

ISBN: 979-12-80718-23-5